Nanoparticle toxicokinetics in the nose an assessment of risk

Kumar, Abhinav

Awarding institution:
King's College London

Title: Nanoparticle toxicokinetics in the nose
an assessment of risk

Author: Abhinav Kumar

Nanoparticle toxicokinetics in the nose: an assessment of risk

Abhinav Kumar

A thesis submitted for the degree of
Doctor of Philosophy

King's College London

Department of Pharmacy
King's College London

August 2012

Abstract

In recent years there has been a dramatic increase in the number of nanomaterials being developed, thus increasing the need for hazard assessment methods beyond the capacity of toxicological screening methods using animals. Current *in vitro* assays have a number of shortcomings, which were addressed in this thesis. These include: (i) high dependence on immortalized cell lines, (ii) inaccurate dosimetry descriptors, (iii) poor robustness of assay systems, and (iv) hyperoxic culture conditions. A method for harvesting viable human nasal epithelial cells using a washout technique was developed to provide squamous epithelial cells for use in culture assays. However, poor proliferation of these cells *in vitro* limited their use in toxicological assays. A particokinetic model was developed to relate the 'delivered dose', i.e. the number of nanoparticles reaching immortalized airway cell layers by gravitational force and diffusional mechanisms, to toxicological endpoints measured *in vitro*. This model was applied to a panel of rigorously characterized nanoparticles (CuO, TiO_2, polystyrene and in-house manufactured lipid nanocapsules) and the results provided compelling evidence that the delivered dose is a more appropriate dose descriptor for cell-based toxicity assays than the widely used nominal dose, as it reflects the number of particles (or their equivalent surface area) available to interact with the cell layer over a given exposure time. The results were confirmed in two airway epithelial cell lines RPMI 2650 and A549 after 6 and 24 h using two standard toxicological end-points. However, when cells were cultured in normoxic (for the respiratory tract) oxygen concentration, 13%, as opposed to the standard culture conditions of 21% they were found to be more responsive to nanoparticle exposure in terms of both production of reactive oxygen species and reduced cell viability. This suggests that standard incubation conditions of 21% oxygen provide a baseline of oxidative stress within a cell culture system that induces adaptive mechanisms and reduces their sensitivity to materials that exert adverse effects through oxidative stress.

Declaration

The work in this thesis is based on research carried out in the Institute of Pharmaceutical Science, School of Biomedical Sciences, King's College London, UK.

No part of this thesis has been submitted elsewhere for any other degree or qualification and it is all my own work unless referenced to the contrary in the text.

Publications & conference presentations

Papers

1. Jones MC, Kumar A, Spina D, Forbes B, Page C, Dailey LA. *In vivo* Safety and Particokinetics of Inhaled Nanomedicines. *J Drug Deliv Sci Tech 2011; 21:339-346.*
2. Khanbeigi RA, Kumar A, Sadouki F, Lorenz C, Forbes B, Dailey LA, Collins H. The Delivered Dose: Applying Particokinetics to *In vitro* Investigations of Nanoparticle Internalization by Macrophages. *J Control Release 2012.*
3. Silva AC, Kumar A, Wild W, Ferreira D, Santos D, Forbes B. Long-Term Stability; Biocompatibility and Oral Delivery Potential of Risperidone-Loaded Solid Lipid Nanoparticles. *International Journal of Pharmaceutics.*
4. Kumar A, Swedrowska M, Siow RCM, Mann GE, Mudway I, Merolla L, Fletcher S, Dailey LA, Forbes B. Standard Atmospheric (21% oxygen) Culture Conditions Promote Adaptations that Mask Toxicity in Cell-based Nanotoxicity Assays. *Nano Letters (In Preparation)*
5. Kumar A, Jones MC, Lorenz C, Mudway I, Forbes, B, Dailey LA. Particokinetic Modelling is Essential to Compare *In Vitro* Cytotoxicity of Soft vs Inorganic Nanomaterials. *(In Preparation)*

Conference presentations

1. Kumar A, Swedrowska M, Siow RCM, Mann GE, Mudway I, Merolla L, Fletcher S, Dailey LA, Forbes B. Normoxic culture conditions are requisite for cell-based nanotoxicity assays. NanoFormulation, Barcelona, 2012 (Invited flash presentation)
2. Khanbeigi RA, Kumar A, Sadouki F, Lorenz C, Forbes B, Collins H, Dailey LA. The delivered dose: applying particokinetics to *in vitro* investigations of nanoparticle internalization by macrophages. NanoFormulation, Barcelona, 2012 (Invited flash presentation)
3. Kumar A, Bicer EM, Mudway I, Merolla L, Fletcher S, Dailey LA, Forbes B. Dosimetry *in vitro:* an under appreciated risk?. NanoFormulation, Singapore, 2011. (Invited presentation)
4. Kumar A, Parisini I, Mudway I, Merolla L, Fletcher S, Dailey LA, Forbes B. Inhaled nanoparticle toxicity assay optimization: dose, size and oxidative potential. Drug Delivery to Lungs, Edinburgh, 2010. (Invited presentation)
5. Forbes B, Cao Minh QA, Evrard B, Kumar A, Dailey LA. *In vitro* safety assessment of inhaled products using respiratory epithelial cells. Respiratory Drug Delivery 12: 615-618 (2010)

Acknowledgments

I am very grateful to Dr. Ben Forbes, Dr. Ian Mudway and Dr. Lea Ann Dailey, who supervised me during my PhD and for everything I learned from them during this time.

I would like to especially thank them for being always available and helpful, and letting me take responsibility for my project. I very much appreciate, that they encouraged me to become an independent researcher. I would also like to thank all my collaborators – Dr. Chris Lorenz, Prof. Giovanni Mann and Dr. Richard Siow for helping me in carrying out all the research.

I acknowledge the Dorothy-Hodgkin Post-Graduate Award (in collaboration with Unilever Pvt. Ltd.) for funding this project and the Institute of Pharmaceutical Science for giving me an extra 6-month studentship.

All the work would not have been possible without some of the wonderful interns (Irene, Cindy, Alvin, Kasia and Magda) or as enjoyable without the great friends (Anna, Thomas and Gian) around me, who made my life in and outside the university an unforgettable time. I am very grateful to Franziska Bode and my family for all their support they gave me in every possible way they could to keep me constantly motivated.

Table of Contents

Table of Figures

Table of Tables

List of commonly used abbreviations

NP - nanoparticle

CCM - cell culture medium

FBS - fetal bovine serum

RTLF - respiratory tract lining fluid

CuO - copper oxide

TiO_2 – titanium dioxide

PS 50 - polystyrene 50 nm

PS 200 - polystyrene 200 nm

LNC 50 – lipid nanocapsule 50 nm

LNC 150 – lipid nanocapsule 150 nm

LDH assay – lactate dehydrogenase assay

MTT assay – metabolic activity assay

ROS - reactive oxygen species

GSH - glutathione

PMN - polymorphonucleocyte

Chapter 1

Introduction

1.1 Nanotechnology: Reality and Future

"There's plenty of room at the bottom" – stated Richard Feyman (1) in his grand vision presented in a lecture at Caltech in 1959. From modern day iPods and cars, there have already been revolutionary advances in the field of nanotechnology such as the development of low cost water purifier using silver nanoparticles by Tata Swach® (2). Nanotechnologies incorporate materials composed of particles that have by definition at least one dimension in a size range between one and one hundred nanometers (3). The promise of nanotechnology lies in the development of new materials with unique properties and unique capabilities. The successful development of nanomedicines such as Doxil® (doxorubicin-encapsulated stealth liposomes), Abraxane® (paclitaxel-encapsulated albumin nanoparticles; Abraxis BioScience Ltd.), and Elan's NanoCrystal technology (Rapamune®, Emend®, TriCor®, Megace®ES and Invega®Sustenna™) provides examples of products at the forefront of a projected nanomedicine boom (4). According to one estimate, global research and development investment in nanotechnologies exceeded $18 billion in 2008 and the value of products utilizing nanotechnologies has been projected to exceed $3 trillion by 2015 (Lux Research 2009) (5). Nanomaterials are already incorporated into a wide variety of industrial products and processes, such as semiconductors, electronics, catalysts, sunscreens, food, clothing, cosmetics, medicines etc. According to the Nanotechnology Consumer Products Inventory, more than 600 self-claimed nanotechnology products are currently being produced by 322 companies in 20 countries (6).

1.2 Nanotoxicology: A New Discipline

The diversity and increasing number of applications of manufactured and engineered nanomaterials carries with it a potential for human exposure to

nanomaterials. Unintentional exposure to engineered nanomaterials may take the form of emissions into air from transport vehicles, power plants, occupational settings and consumer goods and the primary exposure routes are via inhalation and dermal exposure (7). Intentional exposure can also occur when nanomaterials are used in medical applications (major exposure routes include parenteral, dermal, oral and pulmonary) as well as in food additives (ingestion).

Historically, the most extensive and well-documented research on the health impacts of nanoparticle exposure have come from the mining industry and air pollution research. In both fields, a significant body of evidence has been accumulated showing that the inhalation of nanoparticles, regardless of whether they are derived from aerosolised dusts or emissions from combustion processes, can lead not only to a wide variety of progressive lung diseases, such as silicosis or asbestosis (8), but also are implicated in cardiovascular effects (9-11) and increases in population morbidity and mortality rates (12, 13). The evidence that inhalation exposure to nanoparticles can have a negative impact on human health has prompted research into the health impacts of other types of nanomaterials, especially those engineered for specific purposes, such as incorporation in consumer products. Exposure scenarios to engineered nanomaterials will differ greatly and will depend upon the production method, nanomaterial composition, bulk material composition, product use and lifecycle. Therefore, currently exposure is to likely be restricted to the workplace, particularly research laboratories; start-up companies; pilot production facilities; and operations where engineered nanomaterials are processed, used, disposed, or recycled (14). However, as the number of products containing nanomaterials increases, it is important to understand how human exposure to engineered nanomaterials may occur and what the possible health impacts may be.

Over the past 20 years, concerns about the safety of engineered NP have been further expressed by scientists and governmental organizations (3, 15-18). As research began to focus on the potential risk associated with NP, the term ‘nanotoxicology’ was formalized in an editorial in *Occupational and Environmental Medicine* by Donaldson *et al.* (19) –

> *“NP [nanoparticles] have greater potential to travel through the organism than other materials or larger particles. The various*

interactions of NP with fluids, cells, and tissues need to be considered, starting at the portal of entry and then via a range of possible pathways towards target organs. The potential for significant biological response at each of these sites requires investigation. In addition, at the site of final retention in the target organ(s), NP may trigger mediators which then may activate inflammatory or immunological responses. Importantly, NP may also enter the blood or the central nervous system, where they have the potential to directly affect cardiac and cerebral functions. We therefore propose that a new subcategory of toxicology—namely nanotoxicology—be defined to address gaps in knowledge and to specifically address the special problems likely to be caused by nanoparticles."

Due to the significant detrimental impacts of certain types of inhaled nanomaterials (e.g. silicosis and development of lung cancer or increased adverse health effects after exposure to air pollution (8, 12, 13, 20)), the inhalation route of nanoparticle exposure has been of greatest concern and the most widely studied. Thus, new engineered nanomaterials are now in most cases evaluated for their impact on the respiratory tract in addition to other relevant exposure routes. The effect of nanoparticles on the respiratory tract is measured both at a whole organism level (e.g. *in vivo* studies) and at a cellular level (e.g. *in vitro* studies). The following sections will provide a more detailed account of evidence of respiratory toxicity after pulmonary exposure to nanomaterials both *in vivo* and *in vitro*, thus also introducing the most common methodologies used in nanotoxicology research (Section 1.3). This will be followed by a detailed description of the primary mechanisms of nanotoxicity in the respiratory tract, as identified to date (Section 1.4). Finally, a perspective on the challenges of future nanomaterial safety testing will be given in light of the increasing number of nanomaterials being generated for a larger number of applications. This will incorporate a discussion on the potential for developing *in vitro* nanotoxicity assays which are predictive of *in vivo* nanotoxicity outcomes. The current state-of-the-art in *in vitro* nanotoxicity will be presented along with a number of recognised flaws in these systems (Section 1.5). The overall aim of this thesis has been to investigate identified flaws in *in vitro* nanotoxicity testing and provide recommendations for

assay improvement which will enhance the usefulness of such assays for future implementation in routine nanomaterial safety testing (Section 1.6).

1.3 How do inhaled nanoparticles result in lung toxicity?

When NPs deposit in the respiratory tract, the site of deposition and the nature of the NPs will determine both the fate of the particles and the response of the lung. Particles deposited in the upper airways are cleared by the mucociliary escalator, which is an efficient system and has been suggested to be valid for NPs (21). Kreyling *et al*. (21) studied the translocation of ultrafine (15 and 80 nm) insoluble iridium particles from the lung. The authors observed that both particles were cleared predominantly from the peripheral lung via thoracic airways to the larynx into the GI tract and feces one day after inhalation. The authors noted that iridium particle translocation to liver or spleen was minimal. However, in another study by Oberdorster *et al.* (22) significant amounts of ultrafine carbon particles (25 nm) were found to have translocated to the liver after whole body exposure of rats. Therefore, one cannot exclude adverse health effects in secondary target tissues that are not evolved to deal with particles compared to tissues of the respiratory tract. When particles enter the deep lung, the clearance is facilitated primarily by alveolar macrophage (AM) phagocytosis and to a lesser extent by epithelial cell uptake. Successful particle phagocytosis by AM has been linked to chemotactic attraction of AM to the site of particle deposition (23). This is followed by a gradual movement of the macrophages with internalized particles toward the mucociliary escalator.

Experimental data indicates that there is significant size dependent effect on this clearance mechanism. For example, in several studies rats were exposed to different sized iridium particles of 15-20 nm, 80 nm and polystyrene particles of 0.5 µm, 3 µm and 10 µm (24-27). Twenty four hours later the lungs were repeatedly lavaged and it was observed that approximately 80% of the 0.5-, 3- and 10- µm particles were retrieved within the macrophages where as only 20% of nanosized 15–20-nm and 80-nm particles could be recovered from the cellular component of the lavage. In effect, approximately 80% of the NP <100 nm were retained in the lung after exhaustive lavage. This may indicate that the nanoparticles were not phagocytised by macrophages and entered the epithelial cells or had translocated to

the interstitium (28). It is thought that, due to the inefficiency of macrophage clearance, NP< 100nm in diameter may accumulate in the lung after deposition, leading to inflammation and eventually fibrotic changes (29).

In the study by Ferrin *et al.* (30) rats were exposed, via inhalation, to both NP (21 nm diameter) and fine (250 nm diameter) TiO_2 particles, as well as intratracheally instilled with TiO_2 particles of various sizes (12, 21, 230 and 250 nm in diameter) over a period of 12 weeks. Examination of the effects of treatment with each particle size was then performed over a 70-week post-exposure period. It was demonstrated that TiO_2 NPs promoted an acute inflammatory response following both intratracheal instillation and sub-chronic inhalation techniques compared to the larger particles (230 and 250 nm). The inflammation observed in exposure animals was subsequently found to reduce to control levels post-exposure (64 weeks), with a noted decrease (from peak levels) in the number of neutrophils present in the lung at this time. NPs were also found to remain within the lung longer (501 days) than fine particles (174 days). The prolonged retention of TiO_2 NPs in the lung was suggested to be an effect of the finding that at equivalent masses, NPs were able to translocate to the pulmonary interstitium more efficiently than the larger TiO_2 particles. It was suggested that the translocation of NPs to the interstitium was due to the smaller particles (12 and 21 nm) not being taken up by alveolar macrophages and undergoing clearance from the alveoli via uptake by alveolar type-1 epithelial cells instead. In addition to this, it was found that an increased dose (increased number of particles and decreased particle size) promoted movement of particles within the pulmonary system. It was also observed that the number of particles present, particle size, delivered dose and the delivered dose rate also had an effect on the translocation process. The authors concluded that the observed inflammation was due to rat lung exposure to NPs, impaired lung clearance and NP redistribution.

In a subsequent publication, these findings were supported by Oberdorster et *al.* (25) who showed increased levels of inflammation to be present in the alveolar space of rats after instillation with 500 μg TiO_2 NPs (20 nm) over 24 h, compared to TiO_2 fine particles (250 nm) at the same mass dose. The author further suggested that the increased inflammatory response to acute NP exposure could not be explained fully by the movement of particles to the interstitium but could be related to the larger surface area of the particles and their interaction with alveolar macrophages and

interstitial cells. These two studies challenged the long held assumption that response to particulate exposure could be understood in terms of chemical composition and suggested unusual biological activity associated with NPs. The two studies prompted increased interest into the effects of NPs on the lung, as well as the possible health effects that exposure to NPs might pose to respiratory system.

Further studies have demonstrated that inspiration of nanoparticles could cause acute inflammation, progressive fibrosis, granulomas and functional respiratory deficiencies. A study by Hamilton *et al.* (31) of carbon nanoparticles exposure through intranasal route in BALB/c murine model showed that nanoparticles significantly exacerbated airway hyperresponsiveness as measured by the whole body plethysmography and caused an influx of macrophages in the lungs measured by lung lavage differential cell count. *In vitro* assays on the alveolar macrophages isolated from the mice gave evidence of nanoparticle presence in the plasma membranes of the cells as seen in the transmission electron microscopy images and altered the alveolar macrophage cellular function of antigen presentation, as well as subsequent cytokine production in response to the antigen. It is theoretically possible that long term exposure to engineered nanoparticles may cause serious damage to humans as well as animals.

A recent report on the clinical toxicity in humans due to long term exposure to nanoparticles has been reported by Song *et al.* (32). Seven patients working in the same department of a printing plant were admitted to a hospital in Beijing, China. The patients presented the symptoms of shortness of breath, pleural effusion and pericardial effusion. At the hospital the patients underwent a variety of procedures including drainage of pleural effusions, bronshoscopic examinations with BAL, transbronchial lung biopsy, transmission electron microscopy of the pleura, pleural fluid and lung tissue. The analysis of the particles collected from the workplace using electron microscopy showed that the particles were ~ 30 nm in diameter. Examination of BAL fluid showed decreased macrophages, increased lymphocytes, and elevated neutrophils in 5 of the 7 patients. Lung biopsies in all the patients showed swollen and widened alveolar septums, pulmonary fibrosis and aggregation of phagocytes and inflammatroy cells. TEM imaging of the lung tissue showed nanoparticles to be lodged in the cytoplasm and caryoplasm of the pulmonary epithelial cells. Thus this study raises concern that exposure to some nanoparticles may be related to damage of

human lungs. The possible pathways for clearance of insoluble particles deposited in the pulmonary region are illustrated in Figure 1-1.

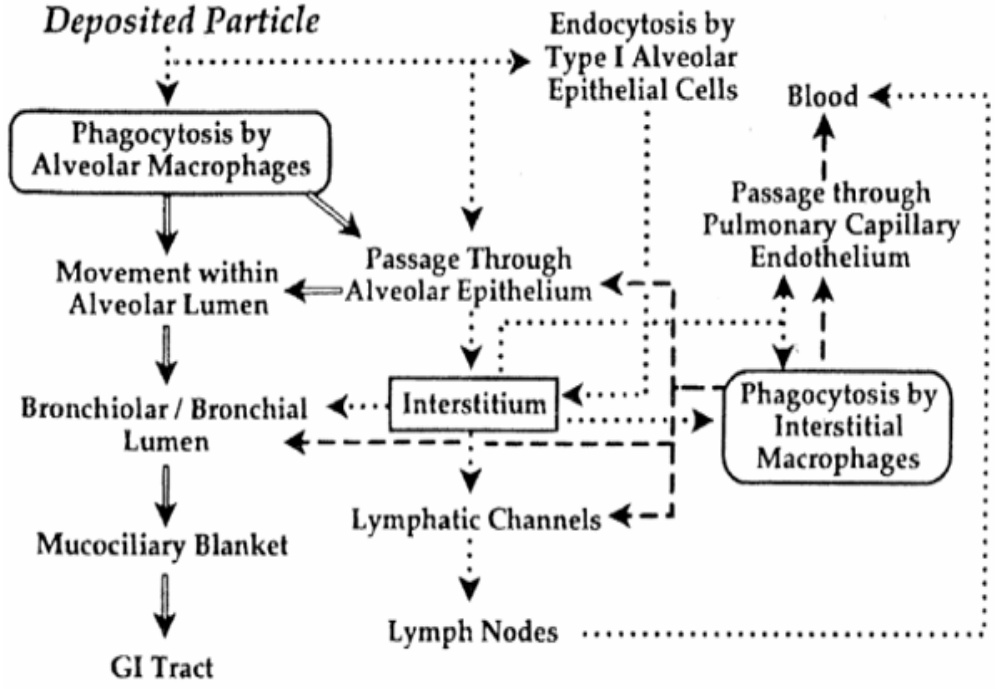

Figure 1-1: Clearance pathways for insoluble particles deposited in the pulmonary region (33).

The reduction in particle size and increase in specific surface area that accompanies formation of nanoparticles (NP), gives the NP quite different physicochemical properties as compared to the bulk material of identical chemical composition such as surface reactivity, improved solubility etc. This emergence of unique properties at nanoscale can be illustrated by taking the example of water as in Table 1-1. If 1 kg of water were in particles of 1 nm, 1 µm or 1 mm and the density of water at 25°C is 997 kg/m^3 then the particle number, surface area and surface energy would change according to Table 1-1.

Table 1-1: Changes in particle number, surface area and surface energy of water particles with change in diameter from 1 nm to 1 mm.

Diameter	Particle number (N)	Total surface area A_{total}= N x $4\pi r^2$ (m^2)	Surface energy S = 0.072 x A_{total} (J)
1 nm	2×10^{24}	6×10^{6}	4×10^{5}
1 µm	2×10^{15}	6×10^{3}	4×10^{2}
1 mm	2×10^{6}	6×10^{0}	4×10^{-1}

In agreement with the collision theory in chemistry, a high collision probability of particles due to large number of particles would lead to high reactivity. Hence, it is understandable that the biological behavior of NPs become dramatically different to bulk material of identical chemical composition.

1.4 Mechanisms of NP toxicity in the respiratory tract

1.4.1 Generation of reactive oxygen species (ROS)

1.4.1.1 Mechanisms by which NP may induce ROS production

Reactive oxygen species (ROS) is a term used to describe a range of species including both oxygen radicals and non-radical derivatives of molecular oxygen. Free radicals and ROS are produced naturally within the body, for example during metabolism and by phagocytic cells for purposes of host defence (34). The enhanced surface reactivity of nanoparticles and their related ability to increase oxidative stress is one of the principal mechanisms hypothesized to drive both nanoparticle-induced inflammation and cellular damage (35-38). NP can react with molecular oxygen present in biological fluid either by energy transfer reactions such as those occurring under the influence of light in the presence of appropriate photosensitizers, or by electron transfer i.e. by reduction (39). NP may act as photosensitizers, causing the production of both singlet oxygen and superoxide from ground state molecular oxygen under the influence of light.

It was demonstrated that irradiated (photoactivated) TiO_2, a constituent of NP employed for dermatological and cosmetic purposes, could stimulate the formation of singlet oxygen and superoxide (40). Furthermore, it has been shown that the ability of NPs to trigger generation of reactive oxygen species (ROS) is greater than that of larger micron-sized particles in biological systems. In a study by Li *et al.* (41) coarse (2.5-10 µm), fine (< 2.5 µm), and ultrafine (< 0.1 µm) particulate matter were examined for the potential to induce oxidative stress in RAW 264.7 murine macrophage cell line and BEAS-2B transformed human bronchial epithelial cell line. The authors measured production of ROS by measurement of hemeoxygenase-1 and glutathione depletion in the cells. The results indicated that ultrafine particle was more potent in generation of ROS than fine or coarse particles. This size differential

with respect to ROS generation and toxicity may be explained by the significant increase in the surface area and therefore surface reactivity of the NPs with decreasing particle size (28, 42).

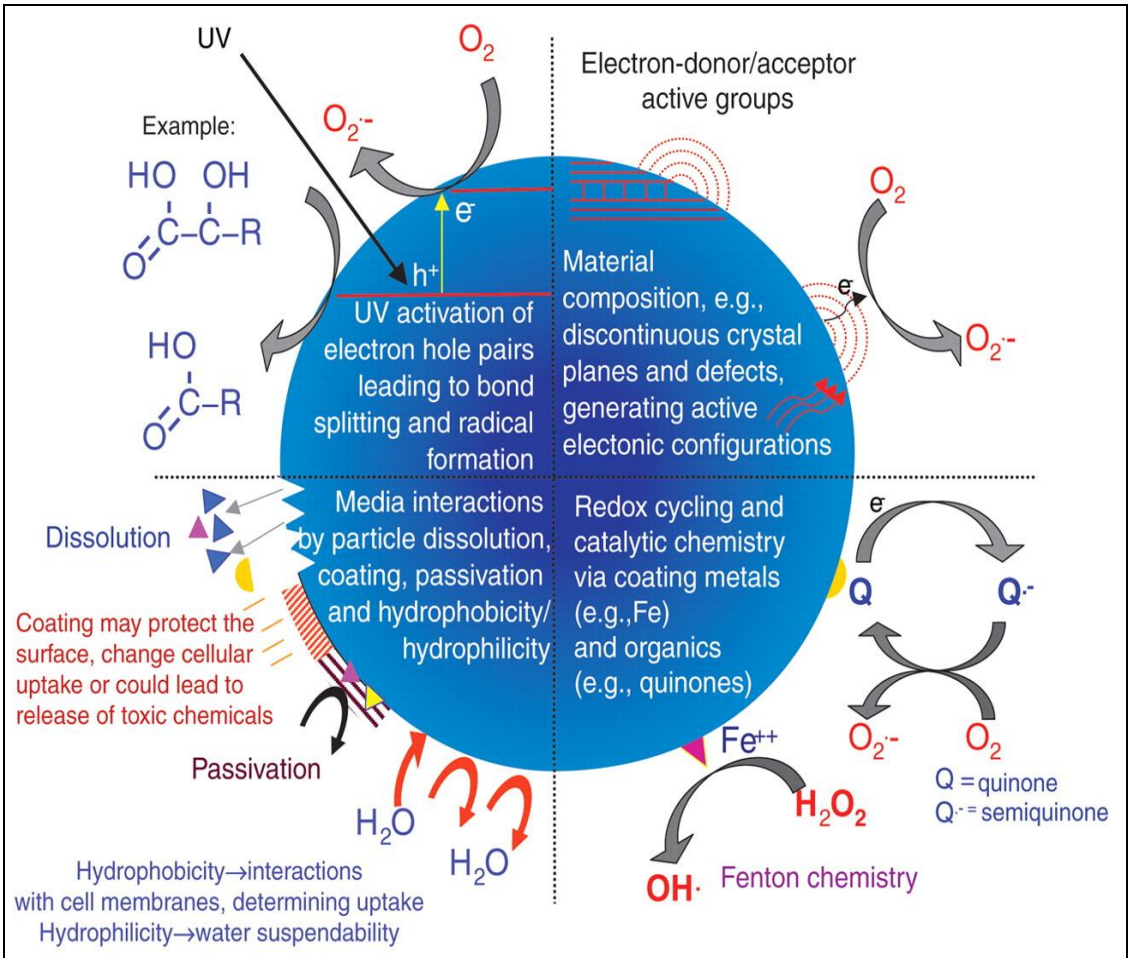

Figure 1-2: Possible mechanisms by which nanomaterials interact with biological tissue. Examples illustrate the importance of material composition, electronic structure, bonded surface species (e.g., metal-containing), surface coatings (active or passive), and solubility, including the contribution of surface species and coatings and interactions with other environmental factors (e.g., UV activation). Image reproduced from Nel *et al.* (42).

1.4.1.2 ROS production stimulates an inflammatory response and cell death

A model for NP-induced oxidative stress has been proposed under which cells undergo a hierarchy of responses: Upregulation of antioxidant defences (Tier I), inflammation (Tier II) and cell death (Tier III) (Figure 1-3).

Figure 1-3 illustrates a number of genes known to be up-regulated in these adaptive responses, under the regulation of Nrf2 and AP-1, including glutathione S-

transferase and heme oxygenase-1. Further oxidative stress causes a decrease in the cellular GSH/GSSH ratio leading to the transcription of genes under the regulation of NFκB to produce mediators such as pro-inflammatory cytokines and inducible nitric oxide (Tier II responses). Further oxidative stress leads to cell arrest and induction of cell death, either by apoptosis or necrosis (Tier III).

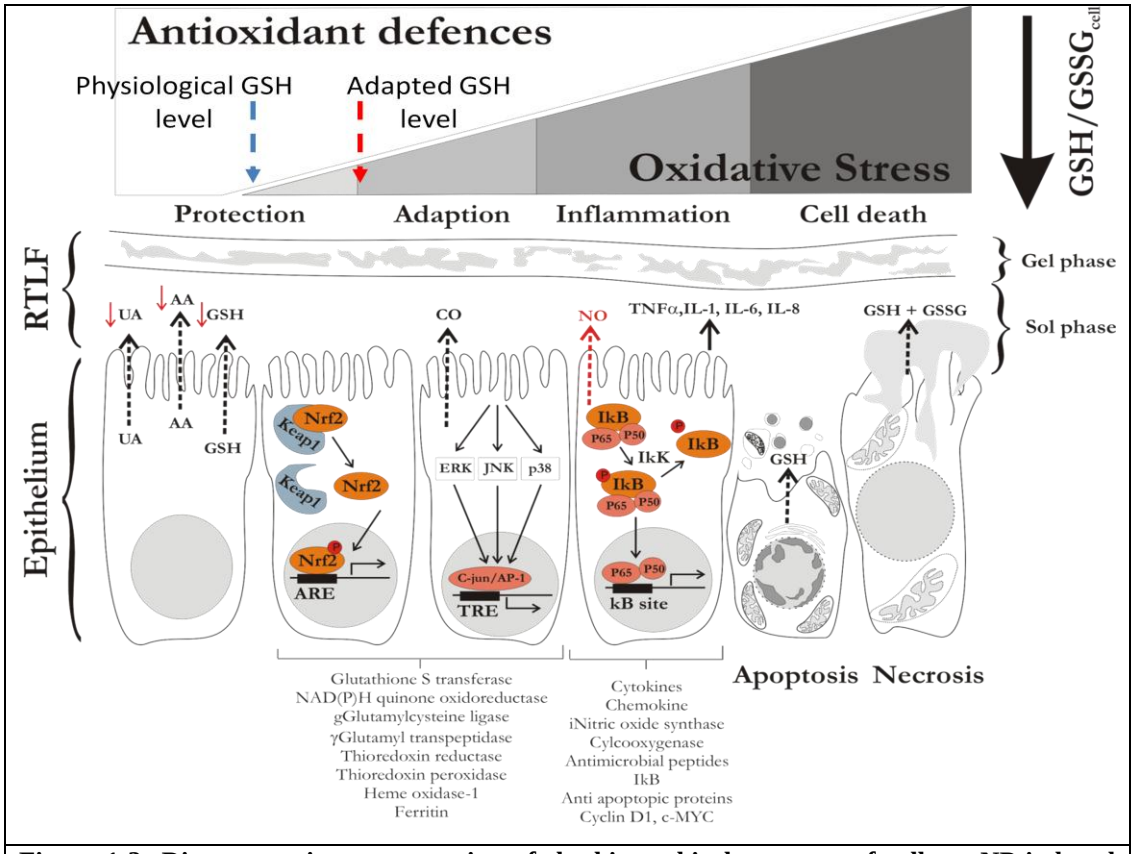

Figure 1-3: Diagrammatic representation of the hierarchical response of cells to NP-induced oxidative stress at the air-lung interface. This diagram is modified from the model proposed by Nel *et al.* (38, 43), to include the influence of the antioxidant defences within the respiratory tract lining fluids which overlay the epithelium. In this modified model the initial defence against NP-induced oxidative stress resides within the respiratory tract lining fluid (RTLFs), initially characterised by acute early losses of ascorbate (AA), urate (UA) and glutathione (GSH). When these defences are overwhelmed the underlying cells employ adaptive strategies to deal with the oxidative stress (Tier I responses). The figure illustrates a number of genes known to be up-regulated in these adaptive responses. Image reproduced with permission from Dr. Ian Mudway.

Tier I. The human body has a number of natural antioxidant defence systems to protect us against NP-derived ROS. Antioxidant enzymes include superoxide dismutases (SOD) (44), which are present in almost all aerobic cells and in

extracellular fluids, catalases which are localized to peroxisomes in most eukaryotic cells (45) and peroxiredoxins. These enzymes are responsible for the conversion of superoxide radical and hydrogen peroxide to water and oxygen (46) as shown in Figure 1-4. Under oxidative stress there is overexpression of the antioxidant enzymes mediated through Jun Kinase, AP-1 or NF-κB which attenuates the oxidative stress and helps in restoring the oxy-homeostasis (47). Further, small molecule antioxidants such as uric acid, ascorbic acid, vitamin E and glutathione help to remove ROS. However, when the amount of ROS generated overwhelms the body's natural antioxidant defences it leads to a state of oxidative stress.

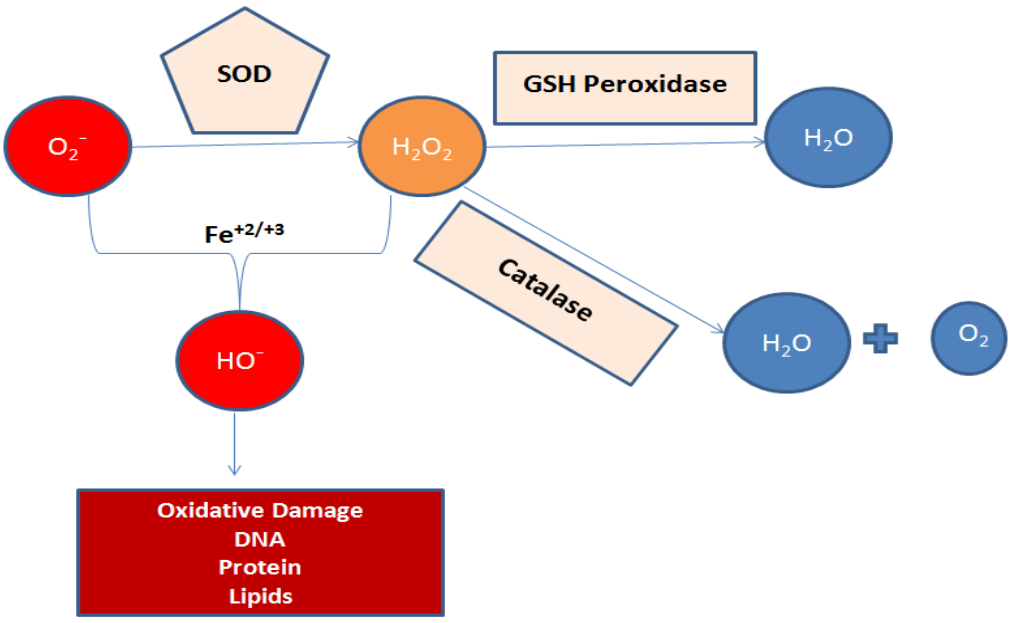

Figure 1-4: Activity of antioxidant enzymes under the presence of oxidative stress in the form of oxide radical.

Glutathione is one of the most important antioxidants abundantly present in cells and biological fluids throughout the body. Glutathione is present as GSH in its reduced formed and this reacts with ROS to form oxidized glutathione, GSSG. The body rapidly converts GSSG back to GSH using NADPH (reduced nicotinamide adenine dinucleotide phosphate) as a reducing agent. The ratio of GSH/GSSG is often used as an indicator of oxidative stress. However, the GSSG concentration in reality is very low and difficult to detect. This problem is further complicated by the fact that cells will actively convert GSSG to GSH as a protective mechanism thereby

decreasing the ability to detect GSSG *in vitro*. It is therefore common to measure GSH nmol/mg protein to express oxidative stress.

Other markers of oxidative stress include measurement of lipid peroxidase and levels of mRNA expression for oxidative stress dependent genes, such as heme oxygenase-1 (HO-1). The stratified response commences with HO-1 expression when the GSH/GSSG ratio is minimally disturbed, proceeds to Jun kinase activation at intermediary levels of oxidative stress, and culminates in cellular toxicity at high oxidative stress levels (41). The significance of Jun kinase (JNK) activation is the transcriptional activation of cytokine, chemokine, and adhesion receptor promoters. These products play a role in the proinflammatory effects of PM in the lung and possibly also the cardiovascular system (48). The JNK activation leads to induction of AP-1-dependent target genes involved in cell proliferation, cell death, inflammation, and DNA repair (49). Inflammation occurs via the induction of redox sensitive pathways such as the mitogen activated protein kinase (MAPK) cascade and the nuclear factor kappa –B (NFk-B) pathway (42). These pathways are thought to act in a synergistic manner to upregulate the expression of pro-inflammatory cytokines, chemokines and adhesion molecules which have all been shown to contribute to the induction of inflammation (50). Induction of cytotoxic pathways are thought to involve the programmed release of apoptotic mediators such as cytochrome C from the mitochondria (42). The continued oxidative stress leads to the transcription of genes under the regulation of NFκB to produce mediators such as pro-inflammatory cytokines and inducible nitric oxide.

Tier II. Oxidation of cellular glutathione leads to activation of transcription factors, NFκB and activator protein-1 (AP-1), which leads to the production of pro-inflammatory cytokines such as TNF-α, IL6 and IL-8 (51, 52). Study of oxidative effects on cultured macrophages has shown that the generation of ROS (37) leads to antioxidant depletion (37, 41), generation of pro and anti-inflammatory lipid mediators (53, 54) and expression of pro-inflammatory cytokines such as TNF-α (55), IL-6 and IL-8 (56).

The role of oxidative stress in the control of the pro-inflammatory cytokine TNF-α was investigated by Brown *et al.* (57) in rat macrophages. The authors found that after exposure to ultrafine carbon black (14 nm) the macrophages showed a dose dependent increase of TNF-α where as for fine carbon black (260 nm) no such effect

was observed. The expression of TNF-α was inhibited by pre-treatment of cells with 5 mM of the thiol antioxidant, Nacystelin, which indicated a role for ROS mediated mechanism in the activation of this cytokine. The authors also incubated peripheral human blood monocytes with the carbon black particles (14 nm) and found a significant increase (30%) in nuclear localisation of both the p5 and the p65 subunit of NFκ-B using a fluorescent staining technique. However, upon pre-incubation of monocytes with vitamin E analogue trolox and Nacystelin inhibition of nanoparticle induced nuclear translocation of NFκ-B was observed thus implicating ROS in the induction of NFκ-B.

An example of NP-induced transcription factor activation was also provided by Xia *et al.*, who conducted a series of experiments exposing RAW 264.7 mouse monocyte derived macrophages to ultrafine particles (UFP collected in the Los Angeles basin through the use of particle concentrator technology), carbon black (CB), titanium dioxide (TiO_2), fullerol, polystyrene (PS), amine substituted polystyrene (PS-NH_2) and carboxyl substituted polystyrene (PS-COOH) and then measured intracellular ROS generation, glutathione depletion, induction of HO-1, induction of JNK and TNF-α (58). The size of the UFP, CB, TiO_2, fullerol, PS, PS-NH_2 and PS-COOH particles in cell culture medium was reported as 1778, 154, 175, 106, 90, 527 and 82 nm respectively. The measurement of intracellular ROS showed that only UFP, fullerol and PS-NH_2 showed a significant increase in ROS production as measured by dichlorofluorescein diacetate (DCFH-DA). Pre-treatment of cells with the thiol antioxidant, *N*-acetylcysteine (NAC), significantly suppressed ROS production in the presence of UFP. Cellular thiol was measured by thiol-interactive fluorescent dye, monobromobimane. UFP and PS-NH_2 showed a dose dependent decline in monobromobimane fluorescence whereas CB, TiO_2, fullerol PS and PS-COOH had no effect. Using an immunoblotting approach to assess HO-1 expression the authors found that both UFP and PS-NH_2 particles elicit a response, while fullerol, CB, TiO_2, and other PS nanoparticles were ineffective. HO-1 is an example of a phase II enzyme that mediates antioxidant, antiinflammatory, and cytoprotective effects and is useful as a marker for particle-induced oxidative stress. The induction of HO-1 expression was suppressed by pre-treatment of cells with NAC thus showing role of ROS in induction of HO-1. Among the NP's tested only UFP's were capable of JNK

activation and TNF-α production. The production of TNF-α was suppressed in the presence of NAC thus confirming the role of oxidative stress.

Tier III. The mitochondrial membrane lipids, proteins and nucleic acids are subjected to ROS attack and prone to oxidative damage (59). It is hypothesised that oxidant accumulation results in early alterations in steady-state mRNA levels of two mitochondrially encoded components of mitochondrial enzymes, cytochrome c oxidase subunit III (COIII) and NADH dehydrogenase subunit 5 (ND5), in a dose-related fashion (59). The decreased expression of COIII and ND5 triggers and effects later cell death (59). Tier III responses towards NP-induced toxicity include the activation of apoptosis (i.e. programmed cell death) through mitochondrial injury, nuclear DNA damage and also necrotic cell death. A possible mechanism for mitochondria damage was hypothesised by Wang *et al*. (60) who used gold nanorod of 55 nm length and 13 nm width on A549 cells and studied the uptake and selective accumulation of the nanorods in A549 mitochondria. The authors found using acridine orange stain, a probe to study lysosomal integrity that there was a significant change in lysosomal membrane potential after internalization of gold nanorods. This disruption of lysosome caused the release of nanorods in the cytosol which was partly translocated to mitochondria verified using TEM to observe the presence of gold nanorods in the mitochondria. The Figure 1-5 illustrates the proposed mechanism of the fate and effect of gold nanorod on A549 cells. Further the authors used mitochondrion specific JC-1 dye to show that gold nanorods after 24 h exposure induced mitochondrial damage in A549 cells.

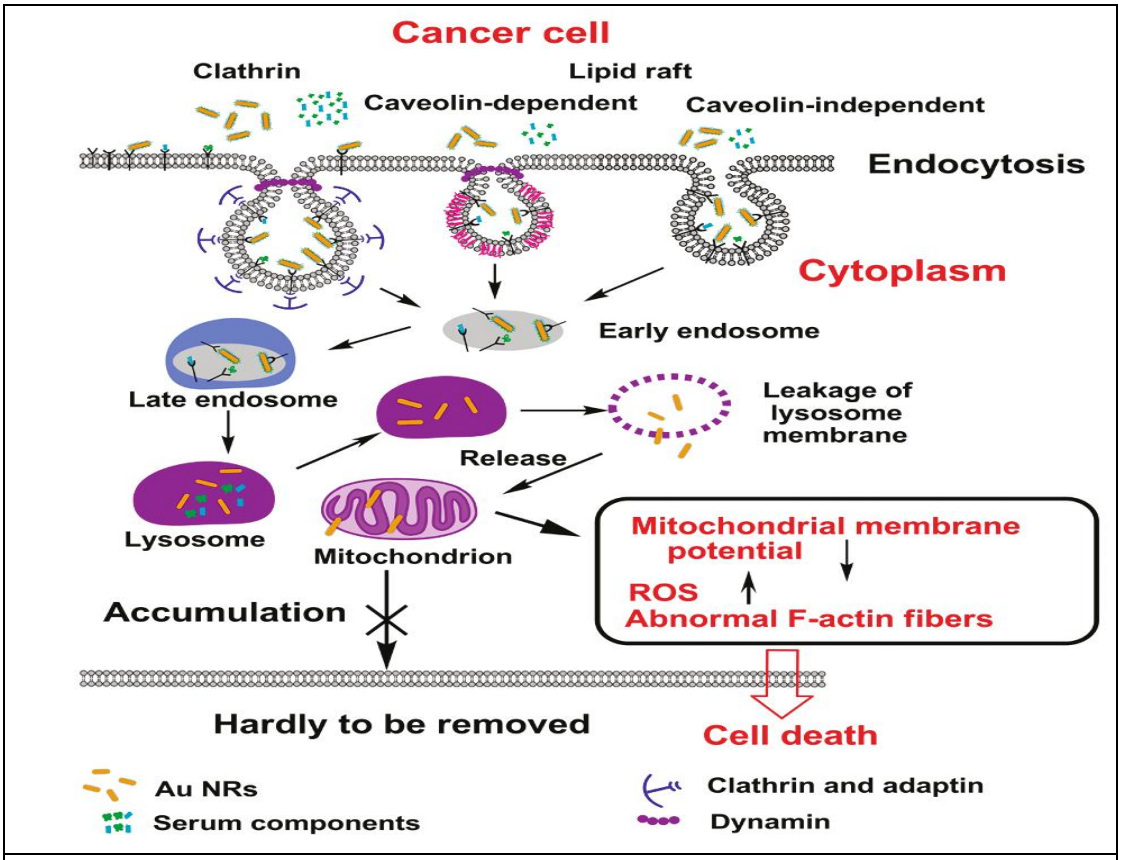

Figure 1-5: Fate and effect of gold nanorods in A549 cells (60).

In the study by Xia *et al*. (58) the mitochondrial membrane potential (MMP) was measured as a marker for perturbation of mitochondrial function. The fluorescence of a mitochondrial dye, DiOC6 was tracked by flow cytometry. Decrease in mitochondrial membrane potential led to the release of dye and decrease in fluorescence as seen during the treatment with UFP (within an hour) and PS (after >6 h incubation). In another study by George *et al*. (61) $[Ca^{2+}]_i$ flux, MMP and propidium iodide uptake was assessed on BEAS-2B and RAW 267.4 cell lines as markers of Tier III responses after incubation with quantum dots (443 nm), zinc oxide (45 nm), platinum (173 nm), silicon dioxide (528 nm), gold (29 nm), silver (110 nm) and aluminium dioxide (57 nm) NP. These particle sizes were reported in bronchial epithelial growth medium supplemented with growth factors and 2 mg/ml bovine serum albumin but no serum. However, in 10% v/v serum supplemented Dulbecco's modified Eagle's medium the authors reported the particle size of quantum dots (48.5 nm), zinc oxide (24.2 nm), platinum (28.6 nm), silicon dioxide (341.5 nm), gold (21.9 nm), silver (77.2 nm) and aluminium dioxide (25.8 nm).The authors ranked the quantum dot and zinc oxide NP as more toxic than other NPs tested based on the

lowering of MMP, increased $[Ca^{2+}]_i$ flux and increased propidium iodide uptake. However, it must be noted that the quantum dots used by the authors had size in cell culture medium which was not in the quantum dot size range of 1 to 10 nm. The supplier (Sigma-Aldrich) reported the size of quantum dots as 6.5 nm dispered in toluene. The particle size measured in cell culture medium might be indicative of the quantum dot aggregation.

1.4.2 Other mechanisms of NP toxicity

Some NPs cause toxicity by what's called a "Trojan horse" mechanism. Once a metal-containing nanoparticle has penetrated a cell, metal ions can leach from the particle and generate ROS in the cell interior. The work by Limbach *et al*. (62), Park *et al*. (63) and Lubick *et al*. (64) demonstrated that easily solubleparticles such as cobalt, manganese and silver NPs could efficiently enter the cells by a Trojan horse-type mechanism which provoked higher oxidative stress if compared to reference cultures exposed to aqueous solutions of the same metals.

Another possible mechanism of action for the toxicity of NPs includes injury of epithelial tissues/cells. Ruenraroengsak *et al*. (65) have shown that positively charged amine modified polystyrene latex NP of 50 and 100 nm when exposed to alveolar epithelial type 1 like-cells (TT-1) caused severe damage and holes on the cell membranes. The authors performed live cell imaging using hopping probe ion conductance microscopy after exposing the TT-1 cells to NP's for 4 h.

1.5 Traditional assessment of risk *in vivo* and the need for predictive *in vitro* nanotoxicology

One of the primary drivers for the growth in nanotoxicology research is the rapid expansion of engineered nanomaterials designed for use in consumer products. The use of laboratory animals provides an alternative to testing of NPs on human beings, however the resultant data is often difficult to extrapolate to humans due to significant species-dependent differences in airway architecture and dimensions, breathing patterns, as well as respiratory tract cell populations (66) (67). Another disadvantage of the whole animal model is the large number of animals and quantities

of nanomaterials required for toxicology assessment (68) which leads to an increase in the cost of research.

According to the Project on Emerging Nanotechnologies, there are currently more than 1300 consumer products that incorporate nanomaterials and this number is expected to grow to 10^4 materials within a decade (6). Thus, the rate of expansion must be considered when deciding what constitutes an appropriate toxicological paradigm so as to avoid the conundrum of the chemical industry, where among the >40 000 industrial chemicals, fewer than 1000 have undergone toxicity testing. One of the major factors contributing to this backlog is the high cost and length of time to complete even a single toxicological screen through animal testing. The traditional approach of using whole animal exposure models to assess the safety of all nanomaterials via all exposure routes will not be feasible given the rapid rate of development in the materials science sector (69, 70). Instead, the development of predictive *in vitro* models of nanotoxicology based on robust paradigms linking nanoparticle (NP) physicochemical properties and *in vivo* outcomes is the way forward.

It has been demonstrated that toxicity testing carried out using the conventional cell culture techniques show little correlation to the results obtained from *in vivo* testing (71, 72). Sayes and co-workers (71) assessed the pulmonary toxicity of five different particle types -carbonyl ion (CI), crystalline silica (CS), amorphous silica (AS), nano-zinc oxide (NZnO), and fine-zinc oxide (FZnO) using both *in vivo* and *in vitro* assessments. The authors exposed rats to the above mentioned particles by intratracheal instillation and measured the *in vivo* LDH level and PMN recruitment in BAL after 24 h, 1 week, 1 month and 3 months. The authors also cultured immortalized rat L2 lung epithelial cells, primary rat lung alveolar macrophages and coculture of rat lung epithelial cells and lung alveolar macrophage and exposed them to the particles and measured LDH release, production of inflammatory mediators (MIP-2) and cytokine production (TNF-α and IL-6) after 1h, 4 h, 24 h and 48 h. The study was designed to assess the capacity of *in vitro* screening studies to predict *in vivo* pulmonary toxicity of the particle types tested in rats. Results of *in vivo* pulmonary toxicity studies demonstrated that CI did not produce any LDH or PMN recruitment. CS caused a significant increase in the production of LDH and PMN recruitment and this was sustained over the 3 month period. AS caused a

significant increase in production of LDH and PMN recruitment at 24 h but was this was reversible after a week. NZnO caused a significant increase in LDH release and PMN recruitment and this was resolved only after a week. FZnO did not cause an increase in LDH release but caused a significant increase in PMN recruitment which was resolved after a week. *In vitro* cytotoxicity testing showed that in L2 cell line all the five particles tested caused LDH release but none of them showed MIP-2, TNF-α or IL-6 production. In macrophages only CI and CS caused LDH release, AS and CS caused the production of MIP-2 and none of the particles caused the production of TNF-α or IL-6. In cocultures all the particles except CI caused the release of LDH, AS and CS caused the production of MIP-2, AS caused the production of TNF-α and CS, AS and NZnO caused the production of IL-6. These results were inconsistent with the findings of *in vivo* study which found CS, NZnO, FZnO to cause LDH release and PMN recruitment. Therefore the authors concluded that under the conditions of this study, the results of *in vivo* and *in vitro* cytotoxicity and inflammatory cell measurements demonstrated little correlation.

Faux *et al.* (73) exposed A549 cells to a range of nanoparticles (ultrafine carbon black, ultrafine titanium dioxide, fine carbon black, fine titanium dioxide, barium sulphate and DQ12 quarth) and measured cytotoxicity in terms of LDH release, oxidative stress in terms of GSH depletion and inflammation in terms of IL-8 (mRNA and protein). When the IL-8 mRNA result was plotted against particle surface area dose/surface area of culture dish (cm^2/cm^2) there was an approximate common threshold at 1 cm^2/cm^2. For IL-8 protein release the threshold appeared to be between 1 (for most of the particles tested) and 10 cm^2/cm^2 (for carbon black). This *in vitro* data was compared to *in vivo* data of PMN levels in BAL fluids of rats exposed to ultrafine TiO_2, fine TiO_2 and $BaSO_4$ generated by Tran *et al*. (74) and Oberdorester *et al*. (75). The PMN levels were plotted against particle surface area/surface area of rat lung (cm^2/cm^2). The authors found that *in vitro* and *in vivo* dose-response curves were similar and the threshold dose *in vivo* was about 1 cm^2/cm^2 (Figure 1-6).

***In vitro* dose-response curve**	***In vivo* dose response curve**
a 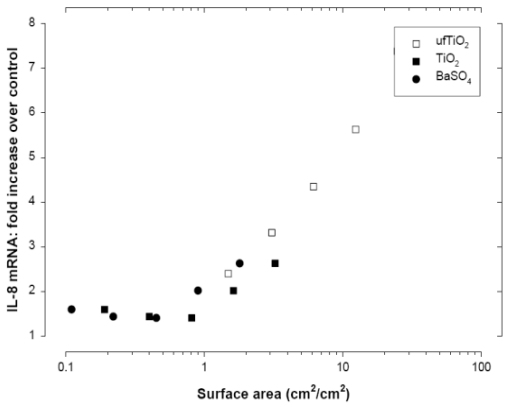	b 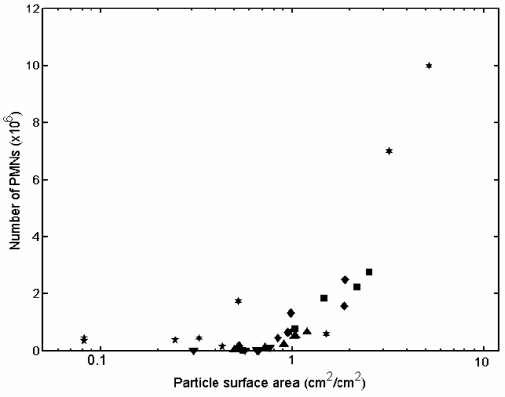

Figure 1-6: Dose-response curve, (a) *in vitro* (b) *in vivo*. Slopes of the dose-response relationship after exposure to ultrafine TiO_2, fine TiO_2 and $BaSO_4$. The threshold dose identified in each dataset appears to be approximately the same dose of particulate surface area per unit surface area of epithelial cells (1 cm^2/cm^2). The graph has been reproduced from Faux *et al.* (73).

In another recently published study George and co-workers (61) demonstrated the correlation between *in vitro* and *in vivo* results using a high throughput screening technique. They screened seven commercially available particles using two different airway cells BEAS-2B and RAW 264.7 (murine derived macrophage cell line) and used calcium ion flux (calcium ions can activate NFκ-B (76)), mitochondrial depolarization, mitochondrial superoxide generation and propidium iodide uptake (nuclear dye that fluoresces red and enters cells showing compromised membrane integrity) as toxicity endpoints. The multidimensional data set generated by primary high throughput screening (HTS) analysis included 4032 data points (2 cell lines × 4 cytotoxicity responses × 8 time points × 7 NPs × 9 doses). The authors further used self-organising maps (SOM) analysis to project the HTS data set onto a two-dimensional display wherein the spatial distribution of the different NPs at given concentrations provided a qualitative indicator of the degree of similarities or differences between materials that generated one or more of the cellular response outcomes.

The authors used a zebrafish (*Danio rerio*) model for screening NP toxicity *in vivo*. It must be noted that although zebrafish model qualifies as a system for chemical and NP toxicity, it is not a model for *in vivo* respiratory nanotoxicology. Zebrafish

embryos were exposed to NP suspensions at 4 h post-fertilization (hpf) and were assessed for toxicity every 24 h, starting at 24 hpf and continuing for a 120 h observation period. Toxicity end points involved scoring of hatching rates, mortality rates, cardiac rate, and the appearance of abnormal morphological features (*e.g.*, pericardial/yolk sac edema, large/small yolk, short tail, body length, bent spine, *etc*. The authors then compared the hazard ranking from HTS *in* vitro experiments and *in vivo* zebrafish embryos and upon comparison they observed a strong correlation between *in vitro* and *in vivo* data hazard ranking although there was a difference in species. Thus, this study demonstrated that through the use of an integrated cellular response pathway for screening, advanced *in silico* data analysis tools, and zebrafish embryo screening, it was possible to develop a predictive toxicological paradigm for NP hazard assessment. However, this study does not demonstrate the ability to predict NP toxicity in the human lung.

The examples cited above should be viewed as snapshots, which shows that there is a considerable debate about how to proceed with nanomaterial toxicity testing in terms of physicochemical characterization of NP, toxicological endpoints to screen for, as well as the balance of use between *in vitro* vs. *in vivo* testing methods (77-80). A recent report by National Academy of Science, *Toxicity Testing in the 21st Century* (81) has set forth a vision of paradigm shift needed in toxicity screening of NP. The vision rests fundamentally on a comprehensive suite of high-throughput *in vitro* assays in human cells and cell lines enabling us to identify and evaluate the perturbations of toxicity pathways. Clearly, there are a number of scientific challenges to be met before implementing this vision.

1.5.1 Limitations of *in vitro* nanotoxicology assays and thesis aims

Major limitations of *in vitro* studies, such as 1) the use of cell lines single cell types in culture that differ in response to cells in the body, 2) the lack of relevant NP characterisation (this is also a limitation for *in vivo* assays), or 3) unrealistic exposure conditions must be considered.

1.5.1.1 Shortcomings of immortalised cells and cell monocultures

Hypothesis 1: If nasal epithelial cell harvesting depends on the lavage technique, then optimizing this technique will increase the quality (yield, % epithelial cells, viability) of th recovered cells.

Physiological relevance comes into question in the first case, as immortalized cell lines often exhibit more rapid division, differential gene expression patterns and higher endocytosis/phagocytosis rates compared to their *in vivo* counterparts. An *in vivo* scenario in which only a single cell type interacts with the NPs is unrealistic as organ systems are diverse in their cellular makeup, and different cell types often participate in coordinated responses. Recent work focusing on the lung, for example, has demonstrated how cultured epithelial cells, macrophages, and dendritic cells cooperate in nanoparticle trafficking, and that uptake into the cells is enhanced *in vitro* with co-cultured cells in comparison to monocultures (82). Increasingly, the use of primary cells use is urged, but the isolation of these cells, yield, maintenance and the problem with attachment to the plate surface makes the process tedious and expensive. Another limitation with the methods used for establishing primary human cell culture systems is the difficulty in obtaining primary cells from the donors as the procedure is often highly invasive. Also, with this collection method, the cell pool originates from a limited number of individuals so inter-individual variations of response are difficult to obtain. On top of this, unlike immortalized cell lines, primary cells do not survive for a long time. This means that there is a need for frequent cell donation and this reduces the usefulness of the *in vitro* models developed so far. This creates a problem for scaling up high throughput toxicology assays using primary human epithelial cells.

Thesis Aim 1:

The first aim of this project was to develop a primary human nasal epithelial cell culture model using a non-invasive technique for harvesting cells. The rationale for this subsection of the project was to evaluate whether a primary human nasal epithelial cell culture model could be established which would address some of the shortcomings listed above, especially in terms of ease of access and non-invasiveness of the procedure. Chapter 2 of this thesis provides an in-depth description of the methodology and results of this component of the study.

1.5.1.2 Insufficient nanoparticle characterisation

Hypothesis 2: If *in vitro* nanotoxicity outcomes are related to particle properties then information about the key particle characteristics will affect the assay interpretation.

What happens to NPs once they are synthesised? Do they retain the same characteristics as the manufactured state even after they come in contact with *in vitro* cell culture medium which usually contains biomolecules such as proteins? Physico-chemical characterization of NPs is paramount in order to correlate biological/toxicological responses with these properties (83). For example, in a study about oxidative damage caused by TiO_2 particles on BEAS-2B cells by Gurr *et al.* (84) it was concluded that oxidative and genotoxic potential of nanoparticulate forms of TiO_2 was superior to that of their larger counterparts. The authors exposed BEAS-2B cells to 10, 20 and 200 nm anatase TiO_2 NPs. The results showed that 10 and 20 nm NPs in the absence of photoactivation induced oxidative DNA damage, lipid peroxidation, and micronuclei formation, and increased hydrogen peroxide and nitric oxide production in BEAS-2B cells, whereas 200 nm particles did not induce any oxidative damage in the absence of photoactivation. The authors concluded that the smaller the particle, the higher potency it had to induce oxidative stress in the absence of photoactivation. However, there was no particle characterization study done. The authors only mentioned that TiO_2 NPs had an approximate size of 200 nm in from the information supplied by the manufacturers. However, particles seldom retain their 'original' size in dry state when they are put in cell culture medium. In fact, Murdock *et al.* (85) have shown that the size of 10 nm and 16 nm TiO_2 particles in medium without serum was 1790 nm and 1810 nm as measured by dynamic light scattering. This size was similar to the size of 100 nm TiO_2 particles in medium without serum which was found to be 2500 nm. This agglomeration in biologically relevant medium raises concern about concluding size or surface area dependent toxicity *in vitro* based on particle size measurement either as supplied by manufacturer or measurement in dry state (EM) or measurement in PBS. These are just few examples to demonstrate the importance of particle characterization in correct interpretation of toxicology data obtained from *in vitro* studies.

In an article titled 'How meaningful are the results of nanotoxicity studies in the absence of adequate material characterization?' by Warheit *et al*. (86) the importance of particle characterization in the interpretation of nanotoxicity data

obtained from *in vitro* or *in vivo* studies has been further highlighted. The author raised an important issue with regard to particle characterization data either being reported as supplied by the manufacturer without cross checking or being reported as size in dry phase or non-biologically relevant medium. As most of the reported studies with nanoparticles have been conducted under *in vitro* cell culture conditions (i.e., in the wet phase) wherein the physicochemical characteristics of the particles, including particle size, are likely to change from the "just received" (i.e., dry phase) or size in PBS this limits the interpretation of cell-nanoparticle interaction data. The author concluded that for *in vitro* toxicity studies, particle size, size distribution, particle morphology, particle composition, surface area, surface chemistry, and particle reactivity in solution are important factors which need to be accurately characterized as prerequisites for implementing nanoparticle toxicity studies.

Thesis Aim 2:

The second aim of this project was to characterise rigorously a panel of nanoparticles spanning a range of physicochemical properties in various biological environments (e.g. cell culture media, respiratory tract lining fluid). The rationale for this subsection of the project was to avoid problems associated with a lack of particle characterisation as highlighted above which should enable robust correlations between particle properties and *in vitro* cytotoxicity results. Chapters 3, 4 and 5 of this thesis provide an in-depth description of the methodology and results of this component of the study.

1.5.1.3 Shortcomings of current *in vitro* dosimetry

Hypothesis 3: If delivered dose (as opposed to administered dose) is determined by sedimentation and diffusion then adjusting for the effects of these processes will help in estimation of the delivered dose.

An important question in nanotoxicology relates to the selection of doses, both for *in vitro* and *in vivo* studies. Many studies are driven by a desire to demonstrate an effect and to determine underlying mechanisms, which is most easily achieved with high NP doses. These doses may never be reached under realistic exposure conditions at the primary point of entry or in secondary organs (87). *In vitro* studies of NP applications and toxicity rely on our ability to quantify the interactions between

nanoparticles and cells. In a typical *in vitro* experiment, cells are immobilized at the bottom of a culture plate or on a substrate placed at the bottom of a culture plate, and incubated with a suspension of nanoparticles. The nanoparticles are assumed to be well-dispersed in the culture medium so the concentration of nanoparticles at the cell surface is assumed to be the same as that of the initial bulk concentration. However, particles in suspension are not only under the effect of gravity, but also undergo diffusion caused by Brownian motion, which means that experimental conditions such as nanoparticle size, density, concentration, aggregation, and particle incubation time will dictate the number of particles in the suspension which will reach the cells during a given *in vitro* experiment. Limbach *et al*. (88) Hinderliter *et al*. (89) and Teeguarden *et al*. (90) have highlighted the importance of distinguishing the administered and delivered doses of nanoparticles *in vitro*. The administered dose is defined as the mass, particle number or particle surface area per volume of cell culture medium. In contrast, the delivered dose is defined as the mass, particle number or particle surface area that reaches the cell monolayer (expressed either as monolayer surface area or total cell protein) during the experiment. The delivered dose, therefore, takes into account not only initial particle concentration, but also colloidal behavior and nanoparticle exposure time, making it a more accurate description of effective nanoparticle dose *in vitro*.

The relevance of the delivered dose becomes especially important when comparing *in vitro* studies of nanoparticles with very different properties and when developing predictive models of nanoparticle toxicity. Limbach *et al.* (88) measured the uptake of 25-50 nm cerium oxide nanoparticles and compared it to the uptake of 250-500 nm cerium oxide nanoparticles in human lung fibroblasts. After exposing the cells to NPs for different times the cells were dried and elemental analysis was performed for quantification of NP uptake. They found the uptake by fibroblasts of 25-50 nm cerium oxide NP was lower as compared to uptake of 250-500 nm cerium oxide NP. The cellular dose of 25 nm ceria oxide nanoparticles correlated extremely well with the predicted delivered dose (based on Stokes'-Einstein diffusion), while the cellular dose of larger particles (320 nm) was lower than the predicted delivered dose (hypothesized to be primarily sedimentation-dependent) (88). Teeguarden *et al.* (90) extended this analysis to theoretically show that colloidal behaviour not only affected uptake, but might also affect relative toxicity. Their model analyses the colloidal

behaviour of the particles whereby the fractions of the administered dose calculated to sediment and diffuse towards the cell layer were summated to obtain a single delivered dose value for any given set of experimental conditions. The authors reanalyzed data for lactate dehydrogenase release *post-hoc* from a study by Hussain *et al*. (91) who had reported the cytotoxicity (EC_{50} value) for various nanoparticles (1000 nm cadmium oxide NP (CdO), 15 and 100 nm silver NP (Ag) and 30 and 150 nm molybdenum trioxide NP (MoO_3) on rat BRL 3A liver cells). Teeguarden *et al.* were able to show that the EC_{50} values reported (normalized to the administered dose) were 150-1200 fold higher than the values obtained when the results were normalized *post hoc* to the derived delivered dose according to the Teeguarden model. In a further paper, the same authors refined the Teeguarden model and modelled the effect of sedimentation and diffusion on a particle in the liquid suspension using Matlab® to develop a particokinetic model which became known as the *In Vitro* Sedimentation, Diffusion and Dosimetry model or ISDD (89).

Thesis Aim 3:

The third aim of this project was to develop a user-friendly particokinetics program based on that of Teeguarden *et al.* (90) to calculate the delivered dose of nanoparticles used in all cytotoxicity experiments. The rationale for this subsection of the project was to provide a means to account for colloidal behaviour of nanoparticles in cytotoxicity data through use of delivered dose instead of administered dose values. Chapter 3 describes the development of this model using Excel as a user-friendly programming format and the validation of the resulting calculated delivered dose values against experimental data and ISDD (89). In Chapter 4, *in vitro* cytotoxicity data was generated for a panel of well-characterised nanoparticles with very different physicochemical properties. Using the particokinetics programme developed in Chapter 3, the results were normalised to both the administered and delivered doses and compared.

1.5.1.4 Measuring oxidative stress *in vitro* under hyperoxic culture conditions

Hypothesis 4: If cells adapt to hyperoxic environment (21% oxygen) then cells at normoxia (13 % oxygen physiological oxygen level at alveioli) will be more physiologically relevant.

The enhanced surface reactivity of NP and their related ability to generate oxidative stress is one of the principal mechanisms hypothesized to drive both NP-induced inflammation and cellular damage (reviewed by (35, 36)). Based on this paradigm, cell cultures in which reactive oxygen species (ROS) production and the generation of oxidative stress can be quantified are regarded as valid assay systems for comparing the toxicity of manufactured or ambient NP (35, 36, 38, 43, 58). A hierarchical model for NP-induced oxidative stress has been proposed in Section 1.4, in which cells undergo graded or tiered responses in response to increased insults: Tier 1) upregulation of adaptive antioxidant defences, Tier 2) inflammation and Tier 3) cell death (Fig 1; (38, 43, 58)). What has been overlooked, however, is the fact that standard cell culture practices use atmospheric oxygen (i.e. 150 mm Hg, ~21%, O_2) concentrations that constitutes a hyperoxic environment. With the exception of the cornea, epidermis and respiratory tract epithelial layer, cells *in vivo* typically experience 1-10 mmHg oxygen pressure (equating to ~ 1-5% O_2). In the respiratory tract, small airway epithelial cells and alveolar cells experience approximately 100 mm Hg oxygen (~ 13% O_2) (92). Despite this, most mammalian cells are cultured using 21% O_2, which promotes increased intracellular production of ROS (93, 94). Cultured cells that fail to adapt to this oxidative environment fail to thrive, thus leaving only cells that have adopted an adaptive phenotype (94-97). Cellular adaptation to the oxidative stress, sometimes termed 'culture shock', involves enhancement of antioxidant defenses (e.g. upregulation of superoxide dimustases, increased glutathione (GSH) synthesis etc.), downregulation of ROS-generating enzymes (e.g. cytochrome *c* oxidase (98)) or alteration of cellular targets of oxidative damage (replacement of fumarase A and B with fumarase C in *E. Coli (99)* and loss of aconitase in primates (100)). Logically, this process of adaptation may be anticipated to mute oxidative responses in cells cultured using 21% O_2, thereby masking NP toxicity when measured using oxidative stress-related endpoints and making such systems poor predictors of *in vivo* toxicity outcomes.

Thesis Aim 4:

The final aim of this project was to assess the impact of cultivating cells at atmospheric (21%) vs. physiological (13%) oxygen (O_2) on the results of standard cytotoxicity assays. The rationale for this subsection of the project was to determine

whether hyperoxia (i.e. 21% O_2) will induce adaptive changes to the cellular state which will ultimately render cultured cells less sensitive to nanoparticle challenge. Chapter 5 describes the methodology and results of this component of the study.

Taken together, the aims of this thesis address selected, but important limitations of *in vitro* nanoparticle toxicity assessment and explore methodological parameters which may be optimised to improve the data generated by such assays. The following chapters provide robust data generated by methods which incorporate state-of-the-art recommendations for nanotoxicity studies. The findings will 1) contribute to existing knowledge regarding the evaluation of primary nasal cell cultures, 2) verify the importance of robust particle characterisation procedures, 3) demonstrate why *in vitro* cell culture studies should all be normalised to the delivered dose value and 4) provide new insights into the impact of culture conditions on cytotoxicity outcomes.

Chapter 2

A benign methodology for establishing primary human nasal cell cultures

2.1 Introduction

The respiratory system represents a major portal of entry for xenobiotics into the body, whether they are intentionally administered as in the case of drugs and anesthetics, or inadvertently taken in by the inhalation of ambient air polluted with materials from a wide variety of sources. Nasal inhalation is a major route of entry into the body for airborne pollutants, including diesel exhaust particles, dust, pollen and nanoparticles used in sprays for both household use and drug delivery. It has been reported that upper size limit for nasal inhalation of airborne particles in calm air is 135 µm (101). Since a large proportion of pollutants exist in the nano-range up to 50 µm (such as pollen), this means that significant particles deposition can occur in the nasal cavity (102). The nasal cavity may provide a port of entry to systemic circulation, and particles which are deposited in the nasal cavity might stimulate airway epithelial cells to secrete pro-inflammatory cytokines.

2.1.1 Anatomy and physiology of the nose

The nose is the uppermost portion of the human respiratory system, located in the middle of the face and the internal structure lies above the roof of the mouth. The shape of the nose is determined by the ethmoid bone and the bony median septum, which consists mostly of cartilage and divides the nasal cavity into two non-connected parts. While the anterior part of the nasal cavity opens to the face through the nostril, the nasal cavity extends posteriorly to the nasopharynx (103).

The nasal cavity consists of the vestibule, olfactory and the respiratory regions. The vestibule consists of the region just inside the nostrils with an area of about 0.6 cm^2. The second region is the olfactory region, situated in the roof of the

nasal cavity and covers approximately 3-5% of the total nasal area of 150 cm^2 in man. The respiratory region constitutes the remainder of the nasal cavity and accounts for 94% of the nasal cavity. It is separated from the vestibule by the atrium and possesses lateral walls dividing it into three sections: The superior, the middle and the inferior nasal turbinates (Figure 2-1).

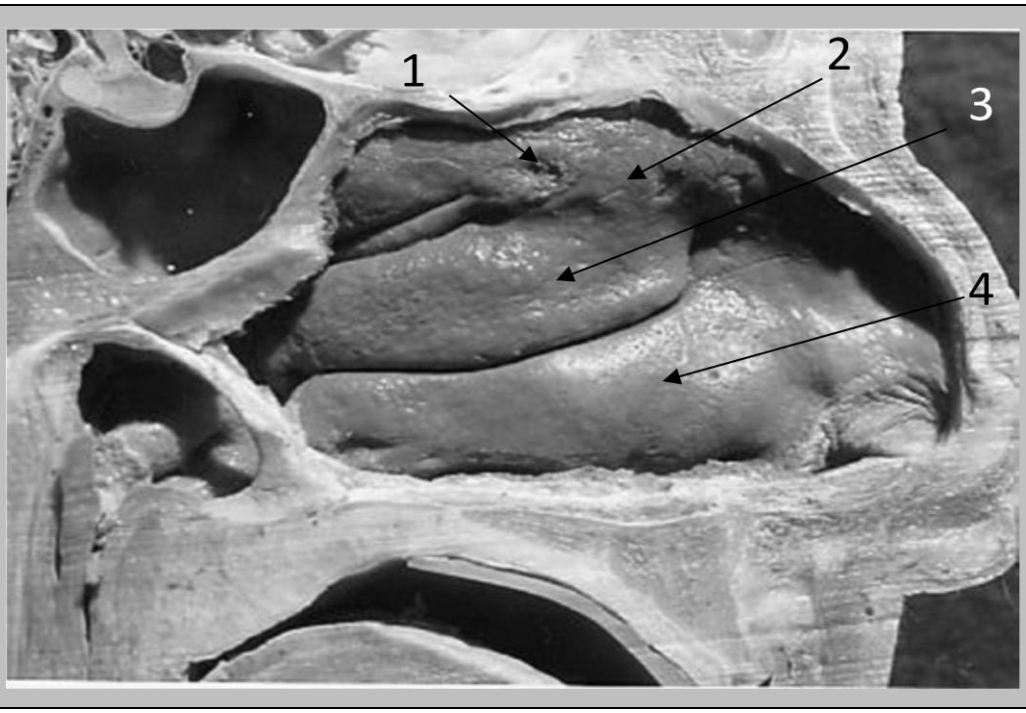

Figure 2-1: Lateral section of the nasal cavity (adapted from reference (104)), showing the extensive respiratory region (the turbinate and the olfactory region). 1: olfactory region, 2: superior turbinate, 3: middle turbinate, 4: inferior turbinate.

The presence of these turbinates creates turbulent airflow through the nasal passages which ensures a good contact between the inhaled air and the mucosal surface (105). The epithelial cells in the nasal vestibule are stratified, squamous and keratinized with sebaceous glands. Due to its nature, the nasal vestibule is very resistant to dehydration and can withstand noxious environmental substances. The atrium is a transitional epithelial region with stratified, squamous cells anteriorly and pseudostratified columnar cells with microvilli posteriorly (105). The respiratory region is covered with pseudostratified columnar epithelial cells interspersed with goblet cells, seromucus ducts and the openings of subepithelial seromucus glands. Furthermore, many of these cells possess actively beating cilia and microvilli. These cilia are 4-6 microns long and their thin projections beat with a frequency of 1000

strokes per minute. Each ciliated cell contains about 100 cilia, while both ciliated and nonciliated cells possess about 300 microvilli each. The mucus flow rate in the respiratory region is in the order of 5 mm per min and hence the mucus layer is renewed every 15-20 min (103).

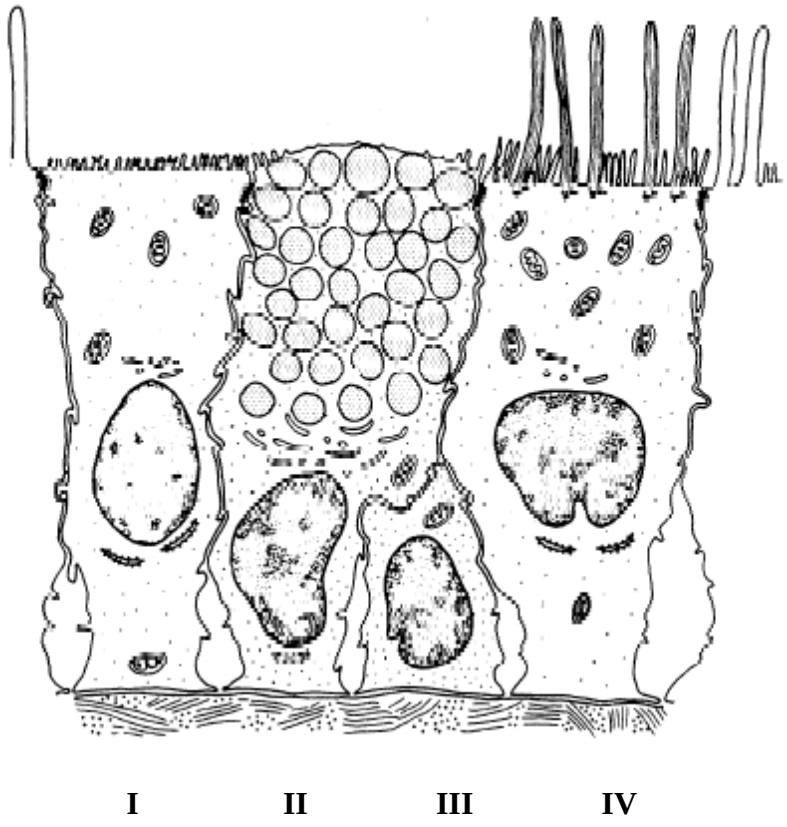

Figure 2-2: Diagrammatic representation of the cell types of the nasal mucosa as seen by transmission electron microscopy adapted from reference (106) showing (I) non ciliated columnar cell, (II) goblet cell with mucus granules, (III) basal cell, (IV) cilliated columnar cell. The epithelium is covered by a 5-10 µm mucus layer (not shown).

The nasal secretions consist mainly of heterogeneous secretory products originating from the goblet cells and submucosal glands, with additional contributions from lacrimal fluid and the vascular region. Together these secretions form a distinct two-layer airway lining fluid. The main function of the mucus is to mediate the interactions between the epithelial cells and their environment via processes such as lubrication, maintaining water balance and entrapment of particles, including bacteria and viruses (103). Approximately 1.5 to 2 L of mucus is secreted daily within the

nasal cavity (107). It is continuously cleared by cilia, which extend through the periciliary fluid and hook the mucus layer with their tips to transport it towards the nasopharynx. The coordination of cilia motility is controlled by neural innervations, chemical pacemaking and hormonal stimulation and the effects of ions such as calcium and potassium (107).

The nasal cavity has an essential protective function that it filters, warms and humidifies the inhaled air before it reaches lower airways. Any inhaled particles or microorganisms are trapped by the hairs in the nasal vestibule or by the mucus layer covering the respiratory area of the nasal cavity (103). Due to the mucociliary clearance mechanism, the mucus layer will gradually carry deposited particles to the back of the throat, down the oesophagus and further into the gastrointestinal tract (107). The nasal mucosa also has some metabolic capacity that aids the conversion of endogenous materials into compounds that are more easily eliminated (104, 106).

2.1.2 Particle deposition within human nasal airways

Historically within the field of toxicology the nose has garnered little attention as a target for nanoparticle toxicity studies. In addition to their role in olfaction, the nasal passages provide some protection to the lower respiratory tract by filtering the inspired air. However, little importance has been given to it as a portal of entry of environmental toxins and its role in particle capture and removal. Knowledge regarding particle deposition processes in the nasal cavity is important in both aerosol therapy and inhalation toxicology.

Aerosol deposition in the nasal cavity has been investigated by a number of researchers. Cheng and co-workers (108) measured the total deposition of submicron aerosols (5–200 nm) in a nasal cast at constant flow rates between 4 and 50 L/min. The deposition efficiency increased with decreasing particle size and flow rate, indicating that diffusion was the dominant mechanism. Cheng and co-workers (109) also measured submicron particles ranging from 4 to 150 nm at constant flow rates of 10 and 20 L/min in 10 volunteers. The net deposition efficiency of 4, 8 and 20 nm particles varied greatly, although as the following numbers show, particle size had more of an influence on deposition rate than air flow: 32-65% (4 nm particles @ 10 L/min) compared to 26-60% (4 nm particles @ 20 L/min) 18-49% (8 nm particles @

10 L/min) compared to 14-43% (8 nm particles @ 20 L/min), and 8-36% (20 nm particles @ 10 L/min compared to 6-29% (20 nm particles @ 20 L/min). The deposition efficiencies of 150 nm particles were less than 10% for both flow rates in eight out of ten volunteers.

2.1.3 Local particle deposition pattern in the nose

Although the above study shows that particles do deposit in the nasal cavity, it lacks information about detailed local deposition patterns, which is very important in studies of aerosol therapy and inhalation toxicology. Wang and co-workers (110) compared the deposition pattern of micron and nano-sized particles in a realistic nasal cavity. The nasal cavity model used by Wang and co-workers was divided into ten separate sections named Zone 1-10 for analysis of local deposition pattern.

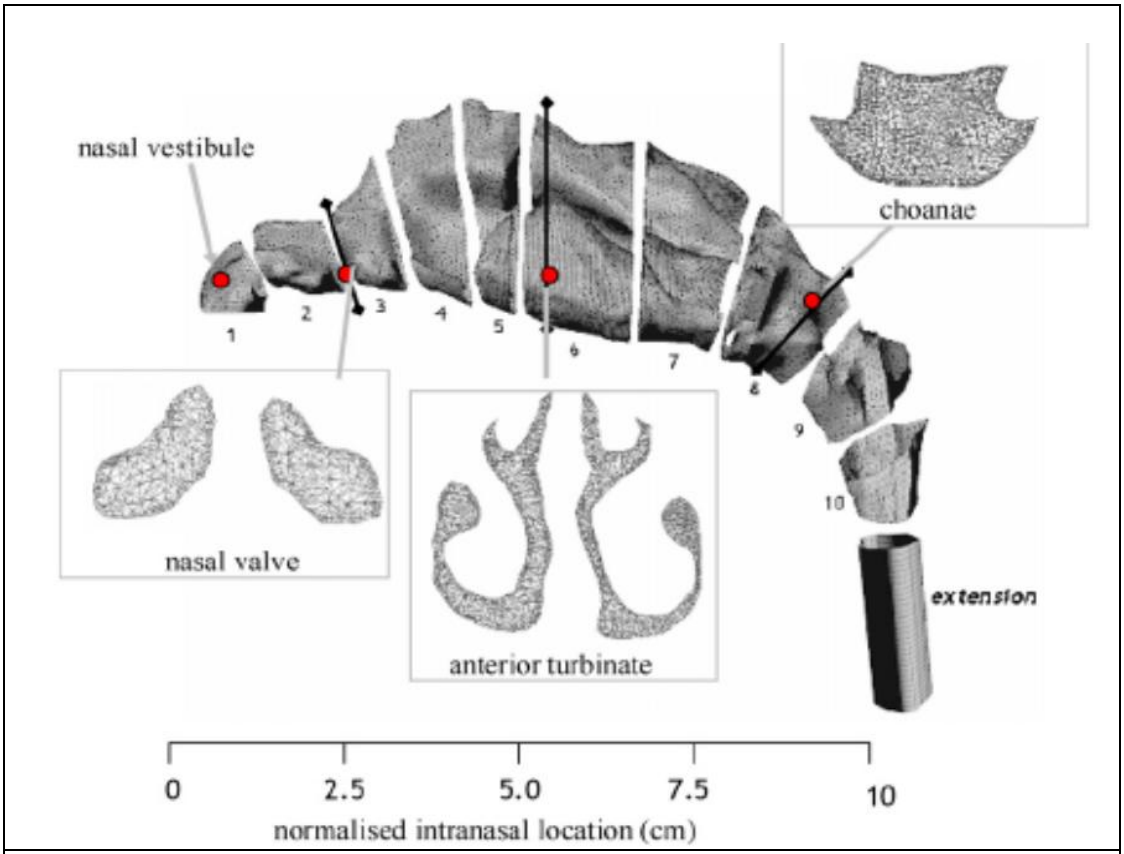

Figure 2-3: Nasal cavity model used by Wang and co-workers (10).

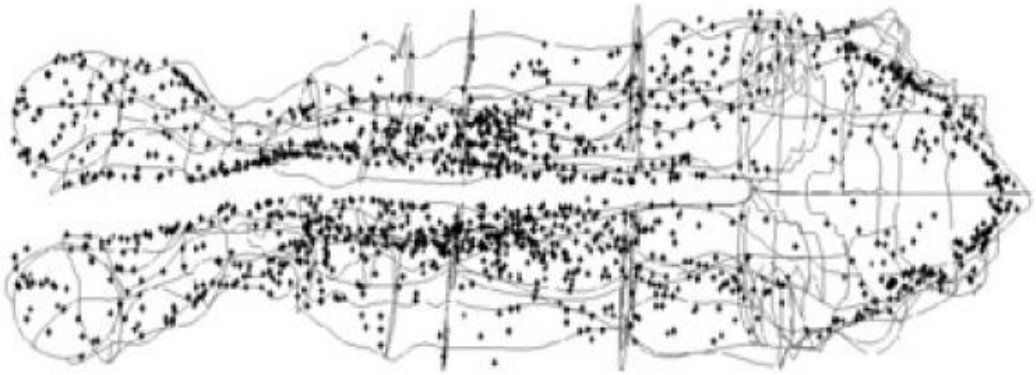

Figure 2-4: Local deposition pattern of 1 nm particles inhaled at a density of 1000 kg/m^3 showing even deposition in each zone (as defined in Figure 2-3). Deposition efficiency is 80%. The image and data are reproduced from reference (10)

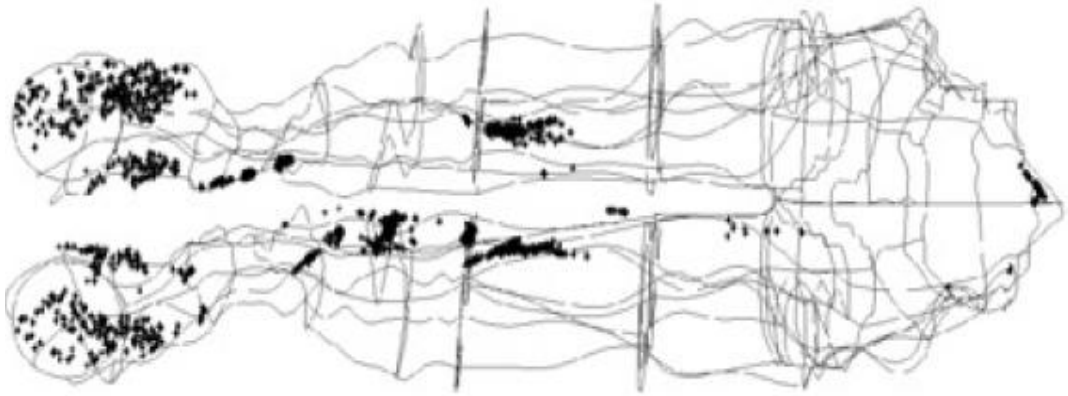

Figure 2-5: Local deposition pattern of 22 µm particles inhaled at a density of 1000 kg/m^3 showing maximum deposition in Zone 2 (as defined in Figure 2-3), which is the anterior region of the nose. Deposition efficiency is 80%. The image and data are reproduced from reference (10).

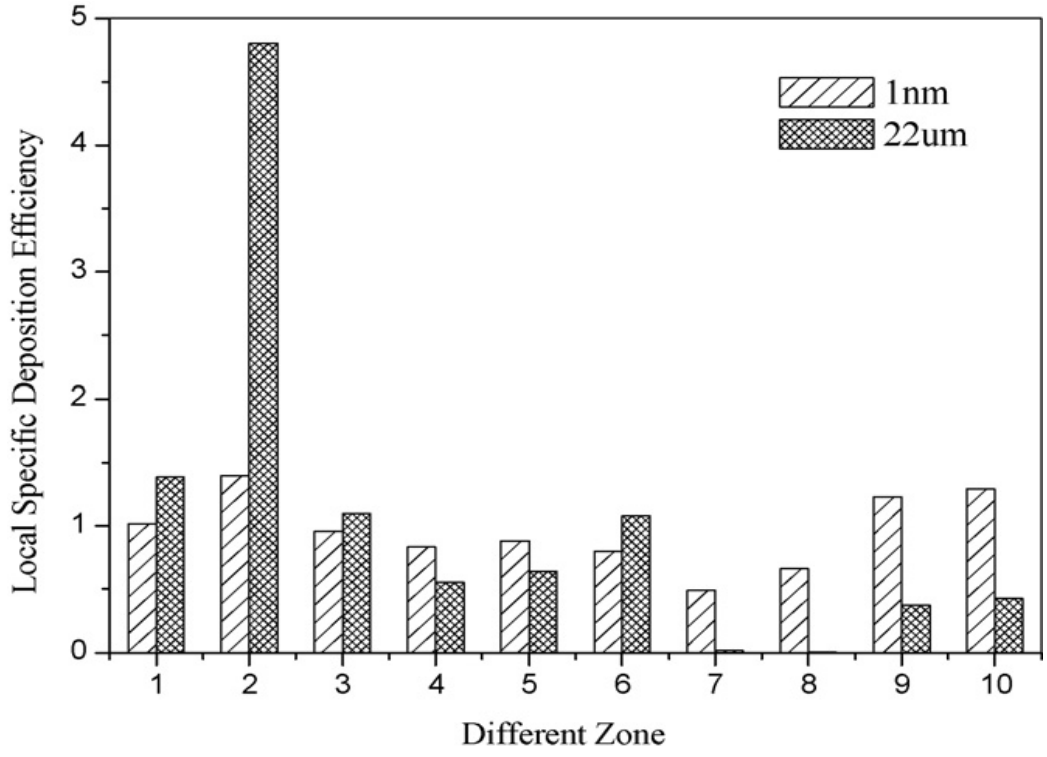

Figure 2-6: Deposition patterns of 1 nm and 22 µm particles in different zones as defined in Figure 2-3. The image and data are reproduced from reference (10)

This study shows that particle diameter has significant effect on deposition patterns for both micron sized particles and submicron sized particles. The major regions of deposition of micron sized particles were found to be the nasal valve and the middle septum parts in the nasal turbinate, while for submicron sized particles there was a uniform distribution of deposited particles. This means that there is a uniform and significant particle deposition in of the submicron sized particles inhaled by human beings in the nasal cavity. The upper turbinate of the human nose contains the olfactory epithelium which serves as an important barrier between the nose and the olfactory bulb. Particles which get deposited in this region can be taken up by the olfactory system and get into the olfactory bulb.

2.1.4 Nose to brain translocation of particles

Evidence that nose to brain transport for solid particles takes place in man is steadily accumulating. In a review by Sunderman (111) the deposition of heavy metals in the olfactory region of the brain was highlighted amongst the workers

occupationally exposed to nickel or cadmium containing dusts in alkaline battery factory, nickel refineries and cadmium industries. At the autopsy of one such worker Badder (112) observed bright yellow staining of the olfactory bulbs, which suggested that cadmium entered the brain via the olfactory pathway. Studies in monkeys with intranasally instilled gold ultrafine particles (UFPs; <100 nm) and in rats with inhaled carbon UFPs suggested that solid UFPs deposited in the nose travel along the olfactory nerve to the olfactory bulb. Elder and co-workers (113) exposed groups of rats to manganese oxide ultra fine particles (30 nm). They analyzed manganese concentrations in lung, liver, olfactory bulb, and other brain regions, and performed gene and protein analyses. After 12 days of exposure with both nostrils patent, Mn concentrations in the olfactory bulb increased 3.5-fold, whereas lung Mn concentrations doubled. There were also increases in striatum, frontal cortex, and cerebellum. Lung lavage analysis showed no indications of lung inflammation, whereas increases in olfactory bulb tumor necrosis factor-alpha mRNA (approximately 8-fold) and tumor necrosis factor-alpha protein (approximately 30-fold) were found after 11 days of exposure and, to a lesser degree, in other brain regions with increased Mn levels. Macrophage inflammatory protein-2, glial fibrillary acidic protein, and neuronal cell adhesion molecule mRNA was also increased in olfactory bulb. They concluded that the olfactory neuronal pathway is efficient for translocating inhaled Mn oxide as solid UFPs to the central nervous system and that this can result in inflammatory changes.

2.1.5 Nasal epithelium damage due to particles

In another study cytological damage to the nasal epithelium of residents of a heavily polluted city was analyzed as compared to residents of less polluted city. In total 20 residents from each city were studied after environmental (non-deliberate) exposure to polluted air containing ozone and PM_{10}. Nasal scrapings were taken from the subjects at different time intervals during a month. In total, four scrapings of the nasal epithelium were taken from each subject. Control subjects from the less polluted city showed no cytological alterations in 30% cases and in the remaining 70% of the cases only mild or moderate inflammation could be seen. In contrast all the residents

of heavily polluted city showed moderate to severe inflammation. This study showed concluded that exposure to inhaled pollutants damages the nasal epithelial cells (114).

2.1.6 Animal models

The above studies provide evidence that particles deposit in the nose, where they may exert an adverse effect on the nasal epithelium and possibly be taken up via the olfactory route. At the same time, because of an increased interest in the development and use of nanoparticles for drug delivery applications, concerns about their toxicity must be addressed. Experiments performed on human subjects are limited due to the invasive nature of the procedures such as turbinectomy, corrective surgery of the nasal septum or simply an elective surgery and dangers associated with toxic aerosols. The use of laboratory animals provide a surrogate for human studies; however, the resultant data is often falsely extrapolated due to species-dependent differences in airway dimensions, breathing characteristics (66), architecture of the upper airway and in the surface epithelial population of the mucosal tissue lining the nasal passages. (67). Other disadvantages of the whole animal model are the large number of animals and quantities of material required (68) which leads to an increase in the cost of research and loss of animal lives.

2.1.7 *In vitro* models

Due to the above-mentioned disadvantages there is tremendous pressure to find non-animal alternative testing strategies. The development of an appropriate human nasal epithelial cell culture would provide a promising system to enable early stage predictions of nasal drug transport, metabolism and toxicity in humans. The human origin of cells would be of greater clinical relevance compared to studies performed with animal models of different species. The use of *in vitro* cultures of nasal epithelial cells in pharmacological and toxicological studies also has several advantages: (i) more standardized systems due to control of the experimental conditions; (ii) rapid evaluation of permeability, metabolism and toxicity; (iii) *in vitro* exposure of human cells to compounds that could not be investigated in humans *in vivo*, allowing an understanding of the mechanism of drug transport, metabolism and toxicity as well as the evaluation of the strategies for their modulation; (iv) limiting

the number of experimental animals and amount of research compound required in the screening phase (115, 116). Cell culture systems and excised nasal mucosae provide meaningful *in vitro* models to study the toxic potential of nanoparticles on the nasal epithelium. Table 1 below gives the summary of primary human nasal epithelial cell cultures developed to date for transport, metabolism and toxicity studies.

In the studies described in Table 2-1, it has been shown that human nasal primary cultures show the potential for the study of nasal drug absorption, metabolism and toxicity. It can also be seen that groups working in this domain have used a large variety of culture media for establishing the primary cell cultures. It is still not conclusive as to which medium is best suited for the culturing of primary human nasal cells.

Cell lines derived from carcinomas of epithelial origin with their extended lifespan, improved proliferation and homogeneity may relieve some of the limitations of the primary cell cultures. The nasal cell lines most often used in these studies are RPMI 2650, BT and NAS 2BL. BT is derived from normal bovine turbinates and NAS 2BL is derived from a rat nasal squamous carcinoma. The RPMI 2650 has been derived from a human nasal anaplastic squamous cell carcinoma of the nasal septum. In culture, RPMI 2650 cells form clusters composed of round and slightly flattened cells or show a tendency to spread. RPMI 2650 do not form monolayers and do not express goblet and ciliated cells (68, 115, 116). This makes RPMI 2650 cell cultures unsuitable for the evaluation of nasal transport. They can be used for metabolism and toxicity studies, although results should be interpreted with caution.

Table 2-1: Summary of primary human nasal epithelial cell cultures reported in the literature

Ref.	Method of obtaining cells	Number of speci-mens	Nature of growth surface	Culture medium	TEER value (Ω cm^2)	Meta-bolism studies	Cytokine release	ALI**	Other Information
(68)	Surgery	N/A	Poly(ethylene-tere-phthalate)	DMEM, supplemented with 1% nonessential amino acids, 1% glutamine, 10% FCS	N/A	✓	×	✓	Seeding density: 10^5-10^6 cells cm^2 Monolayer formed
(117)	Surgery	N/A	Collagen-coated	DIF-1000 Seromed medium supplemented with EGF (15µg/l), hydrocortisone (725 µg/l), retinoic acid (30µg/l), insulin (10mg/l), transferring (10mg/l), BSA (8mg/l)	N/A	×	✓ IL-1 IL-6	✓	Ciliary beat frequency evaluated
(118)	Surgery	N/A	Poly(ethylene-tere-phthalate)	DMEM, 1% nonessencial aminoacids, 1% glutamine, 10% FCS	665±124	✓	×	✓	Transport and metabolism of peptide drugs studied
(119)	Surgery	N/A	Rat tail collagen	DMEM-F12 (1:1) supplemented with Ultroser G (2%), choleratoxin (10ng/ml)	N/A	×	×	×	Ciliary beat frequency evaluated
(120)	Surgery	8	Three collagen substrata tested	DMEM-F12 (1:1) supplemented with Ultroser G (2%), choleratoxin (10ng/ml)	200-650 (Days 2-10)	×	×	✓	MTT, LDH, CBF studies performed

* Table 2-1 continued on next page

Ref.	Method of obtaining cells	Number of speci-mens	Nature of growth surface	Culture medium	TEER value (Ω cm^2)	Meta-bolism studies	Cytokine release	ALI**	Other Information
(121)	Surgery	N/A	No coating	BEGM in apical and DMEM supplemented with 1% nonessential aminoacids, 1% L-glutamine, 10% FBS, and 1ng/ml EGF	800-1200	×	×	×	LCC on Transwells
(122)	Surgery	N/A	Human placenta Type IV Collagen	1:1 mixture of BEGM and DMEM/F-12 supplemented with insulin (5µg/ml), epinephrine (0.5 µg/ml), triiodothyronine(6.5ng/ml), Tranferrin(10 µg/ml) human EGF(0.5ng/ml) bovine pituitary extract(0.13mg/ml), BSA(1.5 µg/ml)	Varied between donors range 1700 to 2800	×	✓	✓	LDH, Quantification of phagocytosis, Intercellular ROS, Analysis of ICAM-I surface expression Cells exposed to particles
(123)	Nasal brushing after anesthesia	N/A	Type 1 rat-tail collagen	BEGM	N/A	×	✓	×	
(124)	Nasal brushing	15	Type 1 rat-tail collagen	20% FCS for the first 2 days and then serum free media	N/A	×	✓	×	

List of abbreviations: HNE: Human nasal epithelial cells, ALI = Air-liquid interface, DMEM = Dulbecco's modified eagle medium, DMEM/F-12 = Dulbecco's modified eagle medium containing Ham's nutrient, BEGM = Bronchial epithelial growth medium, FCS = Fetal calf serum, EGF = Epidermal growth factor, BSA = Bovine serum albumin, N/A = not available, ✓ = performed, × = not perfomred

2.1.8 Disadvantages of present models

These cell culture systems listed in Table 2-1 represent the epithelium of the middle or superior turbinate area (Figure 2-3) of the nasal cavity. From the local deposition pattern of micro and nano-sized particles we know that a vast majority of particles are also deposited in the nasal valve comprising of Zones 1 and 2 (Figure 2-4, 2-5 and 2-6). Another limitation with the methods used for establishing a primary human nasal cell culture system is the difficulty in obtaining primary cells from the donors as the donor has to undergo painful traumatic method of nasal biopsy, brushing or scraping. These methods are not donor-friendly and rely on the availability of patients being treated for endonasal surgery for donation. Also, with this collection method, the cell pool originates from a limited number of individuals so inter-individual variations of response cannot be assessed. On top of this, unlike immortalized cell lines, primary cells do not survive for a long time. This means that there is a need for frequent cell donation and this reduces the utility of the *in vitro* models developed so far. Since the methods used for obtaining the primary human nasal cells are traumatic, this creates a problem of scaling up the primary human nasal epithelial cell model.

In this regard the proposed method to be developed in this current research is a simple, atraumatic method for obtaining nasal epithelial cells. This method is nonsurgical and is well tolerated; it requires no anesthesia and permits repeated isolation from the same source.

2.1.9 Aim

The aim of this work is to isolate human nasal epithelial cells, characterize them and establish cell culture conditions and evaluate the suitability of this technique to provide a primary cell culture system for particle transport and toxicological studies.

2.2 Materials and Methods

2.2.1 Materials

Nasal spraying devices were obtained from Apoteket Production & Labaratory (Goteborg, Sweden). Dulbecco's Modified Eagle Medium containing Ham's nutrient (DMEM), trypsin-EDTA (2.5 g/l trypsin, 0.5 g/l EDTA), fetal bovine serum (FBS), L-glutamine (200 mM), penicillin-streptomycin solution (100x), trypan blue solution (0.4%) and May-Grunwald Giemsa (MGG) solutions were purchased from Sigma-Aldrich (Poole, UK). LHC basal medium and bovine serum albumin were purchased from BioSource International (Camarillo, CA, USA). Type I bovine collagen was purchased from BD Labs. Tissue culture plastic-wares were purchased from Costar (High Wicombe, UK). Phosphate buffered saline tablets were purchased from Oxoid (Basingstoke, UK).

2.2.2 Methods

2.2.2.1 Study Population

The present study was approved by the Biomedical & Health Sciences, Dentistry, Medicine and Physical Sciences & Engineering Research Ethics Sub-Committee, King's College, London (REC Reference Number: **BDM/08/09-82**) and written informed consent was obtained from all volunteers. Multiple nasal lavaging was performed on 25 volunteers. The mean age and standard deviation (SD) of study volunteers was 29 ± 9 years and 10 females and 15 male subjects were included in the study. Volunteers with (i) nasal infection or disease, (ii) taking nasal medicine, (iii) below 18 years old were excluded from the study.

2.2.2.2 Nasal lavage procedure and treatment of recovered fluid

Nasal lavage (NL) samples were collected according to the method of Harder *et al.* (125) with some modifications. Briefly, 10 x 0.1 ml aliquots of phosphate buffered saline (PBS) were sprayed into the nose, with the material draining from the nose and collected in a sterile glass beaker after each 1 mL was sprayed. This spray and collection procedure was repeated five times into each nostril, *i.e.* a total volume of 5 mL per nostril. Throughout the procedure the glass beaker with the pooled nasal

lavage was kept on ice. After the lavage was completed the recovered liquid was filtered through a sterile 100 µm-pore nylon filter to remove mucus and cell aggregates before centrifugation at 400 x *g* for 15 minutes at 4°C to pellet the cell fraction.

The cell-free supernatant obtained by this procedure was measured using a graduated 10 mL plastic pipette, was removed and discarded. The cells from each individual were either 1) re-suspended in 100 µL cell culture medium for seeding in a 96 well plate, 2) re-suspended in 100 µL cell culture medium for cell counting using a Haemocytometer or 3) were re-suspended in 300 µL of cell culture media for staining with May-Grunwald Giemsa and subsequent microscopic evaluation.

2.2.2.3 Viable Cell Count

Trypan blue dye (0.4%) (100 µL) was mixed with 100 µL re-suspended cells. The total cell count and viable cell count was performed using a haemocytometer and the viability of the cells was assessed by Trypan blue dye exclusion assay. This assay is based on the principle that live cells possess intact cell membranes that exclude certain dyes such as Trypan blue, eosin or propidium, whereas dead cells do not; thus a dead cell will have a blue cytoplasm and a viable cell will have a clear cytoplasm. The cells are examined visually to determine whether cells take up or exclude dye and the cell number is calculated according to Equation 2-1:

$$\text{Cell count} = \text{Average cell count} \times \text{dilution factor} \times 10^4$$

Equation 2-1

Where, average cell count was the sum of cells counted in the four quadrants of Haemocytometer divided by four and the dilution factor was the volume of cell suspension plus the volume of Trypan Blue added to the cell suspension divided by the volume of cell suspension.

2.2.2.4 Differential cell staining for microscopic examination of nasal lavage

For differential cell counting, cells were re-suspended in 300 µL of cell culture medium. Serial dilutions (1:2, 1:3, 1:4) of the re-suspended cells were prepared using fresh cell culture medium. 200 µL of cell suspension from each of the serial dilutions was added to a Cytospin apparatus and the cells were deposited onto a microscope

slide by centrifugation at 450 rpm for 5 min. After the cells had air-dried, they were incubated for 5 min with May-Grunwald solution diluted with methanol (2:1). The slides were then washed with tap water for 1 min and incubated for 15 min with Giemsa solution diluted in distilled water (1:9). After a final rinse with tap water for 1-2 min, the slides were dried at room temperature and observed under the microscope.

2.2.2.5 Optimisation of lavage and culture methods

The experimental design for establishing a primary human nasal cell culture followed a general methodology of performing nasal lavage, filtration of lavage, centrifugation of collected lavage at 400*g* for 15 min, removal of cell-free supernatant, re-suspension of pelleted cells in cell culture medium and then seeding of cells into a 96-well cell culture plate. The plate was kept in a sterile, humidified incubator maintained at 37ºC and 5% CO_2 / 95% air and cells were cultured until confluent. The cell culture medium was changed every 24-48 h.

Phase I Effect of seeding volume

The diagram in Figure 2-7 illustrates the first set of experiments, termed Phase I experiments, investigating the effect of cell seeding volume on cell confluency at 96 h post seeding. Due to a limited amount of cells gathered from each lavage, a cell count was not performed before plating. Instead, all cells from the lavage were suspended in either 100µl of CCM1 (SV1), 300 µl of CCM1 (SV2) or 500 µl of CCM1 (SV3). The composition of CCM1 is listed below in Table 2-3. After seeding, the cell culture medium was changed every 24 h and the number of cells present in the well were observed under the microscope at t = 96 h after seeding to see which seeding density gave better multiplication and growth of cells.

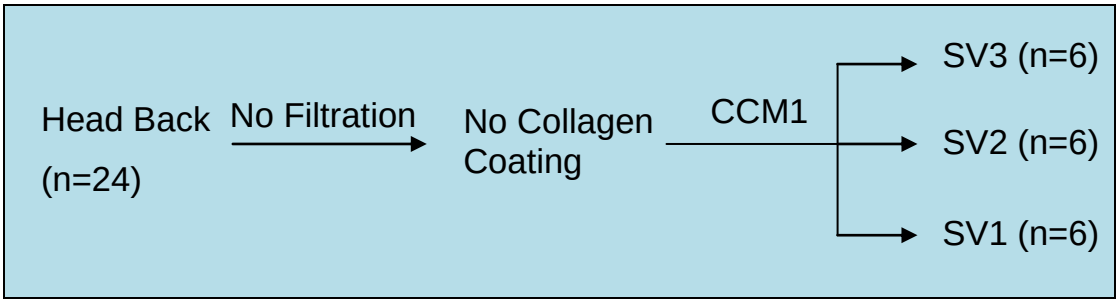

Figure 2-7: Diagram of the design for experiments in Phase I experiments.*SV: Seeding Volume, CCM: Cell culture medium;

Phase II Effect of cell culture medium

Having arrived at suitable seeding density value a further study was carried out to determine the effects of collagen coating and cell culture medium composition on adherence of cells at 96 hours post seeding. The diagram in Figure 2-8 illustrates the second set of experiments, termed Phase II experiments. Cells from the lavage were suspended in 100 µl of either CCM1 or CCM2 and seeded onto collagen-coated plates as described below. The compositions of CCM1 and CCM2 are listed below in Table 2-3. The cell culture medium was changed every 24 h and the confluency of cells was evaluated qualitatively under the microscope at t=96 h after seeding.

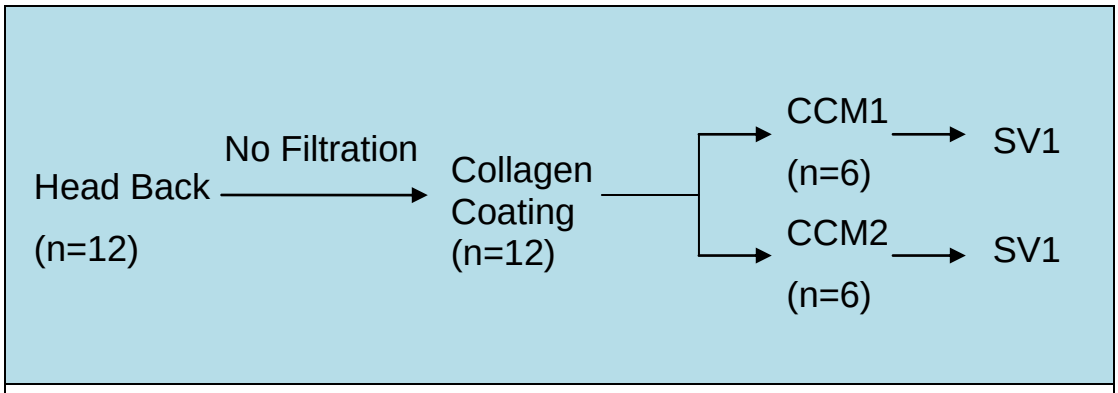

Figure 2-8: Diagram of the design for experiments in Phase II experiments.

Phase III Effect of lavage technique

From the previous two studies it was concluded that SV1, collagen coating and CCM2 gave better results in terms of cell growth and adherence after t = 96 h post seeding. A third group of experiments was carried out to evaluate a new method of nasal lavage to determine its effect on the volume of lavage collected, total number of cells collected, the proportion of viable cells collected and cell confluency at t=96 h. Further, the filtration of the nasal lavage was investigated to determine whether it had an effect on the contamination rate of the cultured cells. The diagram in Figure 2-9 illustrates the third set of experiments, termed Phase III experiments. The procedures are described in more detail below. However, all cells harvested in this experimental group were resuspended in 100 µl of CCM2 and seeded onto collagen-coated plates. The cell culture medium was changed every 24 h and the confluency of cells was evaluated qualitatively under the microscope at t = 96 h after seeding.

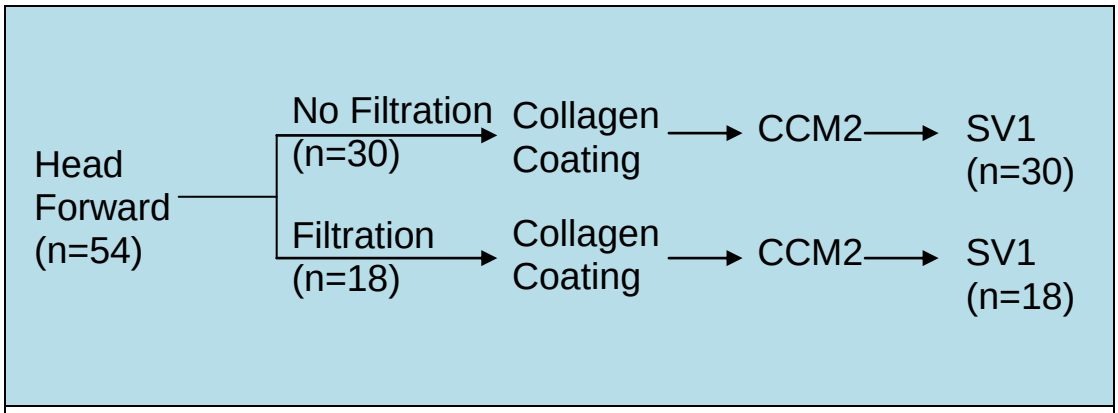

Figure 2-9: Diagram of the design for experiments in Phase III experiments.

The system was optimised in three phases. In Phases I-III the following variables were optimised (Table-2-2).

Table 2-2: Independent variables affecting cell culture and their dependent variables

Variable #	Independent Variable Description	Dependent Variable Description
Variable 1	Head back vs. Head forward	1. Volume of lavage 2. Cell count
Variable 2	Filtration vs. Non-filtration	1. Microscopic observation of nasal debris vs. no debris 2. Contamination rate
Variable 3	Collagen coating vs. No-collagen	1. Microscopic observation of cell attachment 2. Confluency at 96 h
Variable 4	CCM1 vs. CCM2	1. Confluency at 96 h 2. Viability at 96 h
Variable 5	Seeding volume	1. Confluence at 96 h

***CCM: Cell Culture Medium**

Variable # 1: Nasal lavage technique

Head back: In this method, the volunteer was asked to tilt their head back at ~30 degrees, press one nostril closed and self-administer the PBS spray to the open nostril. During the spraying process the patient was asked neither to breathe nor swallow. After 10 metered aliquots of ~ 0.1 mL were sprayed into the nostril the volunteer was asked to tilt their head forward and allow the fluid to drip into a sterile beaker glass. This process was repeated as described in 3.2.2. for both nostrils.

Head forward: In this method, the volunteer was asked to tilt their head forward, press one nostril closed and whilst taking a deep breath spray the PBS into the open nostril. The intake of breath whilst spraying creates a negative pressure which prevents the PBS from dripping out of the nostril. After 10 metered aliquots were administered, the fluid was collected in a beaker glass as described in 3.2.2.

Variable # 2: Filtration of nasal lavage fluid

In phases I-II, collected lavage samples were processed immediately without a filtration step. During phase III experiments, the collected lavage fluid was passed through a nylon filter by pouring the lavage on a nylon filter with a pore size.of 100 µm to remove nasal debris and reduce contamination upon culturing.

Variable # 3: Collagen coating of growth surface

The cell-support materials and coatings most commonly used for culturing human nasal epithelial cells can be seen in Table 2-1. Collagen coating has been used by a number of research groups to enhance the attachment of cells.

In phase I cells were seeded directly onto plastic tissue culture 96 well plates. In phases II and III plates were coated by preparing a solution containing 17.6 mL of Laboratory of Human Carcinogenesis (LHC) basal medium of Lechner and LaVeck (126), 2.0 mL of bovine serum albumin suspended in double distilled water at a concentration of 1 mg/ml and 0.4 mL of collagen I suspended in double distilled water at a concentration of 2.9 mg/ml. Collagen coating solution (100 µl) was then added to each well of the 96-well plate. The plate was stored in an incubator at 37°C overnight. After incubation, all the coating solution was removed from each well and the plate was allowed to dry under aseptic conditions for at least one hour.

Variable # 4: Cell culture medium

The medium and its supplements are primary factors affecting the viability, proliferation and differentiation of the cells in culture. A wide range of cell culture media and medium supplements have been used in culturing of primary human nasal epithelial cells (Table 2-1). Since no preference for a particular medium composition can be derived from Table 2-1, two simple media were chosen initially for practical and economic reasons. The primary difference lies in the quantity of fetal bovine calf serum used in each medium. Table 2-3 summarises each of the components.

Table 2-3: Contents of cell culture medium used		
	Cell Culture Medium 1 (CCM1)	Cell Culture Medium 2 (CCM2)
Name	Dulbecco's Modified Eagle Medium containing Ham's nutrient (DMEM/F12)	Dulbecco's Modified Eagle Medium containing Ham's nutrient (DMEM/F12)
Supplements	Fetal bovine serum (FBS) **10%** L-Glutamine 1% Non-essential amino acids 1% Penicillin-Streptomycin solution	Fetal bovine serum (FBS) **20%** L-Glutamine 1% Non-essential amino acids 1% Penicillin-Streptomycin solution

Variable # 5: Cell seeding volume

Seeding volumes: After lavage, the centrifuged cells were re-suspended in different volumes either 100 µl (SV1), 300 µl (SV2) or 500 µl (SV3) of cell culture medium immediately before seeding. Cell multiplication was evaluated after 96 h by qualitative assessment of the area covered by the cells in each well using microscopy.

2.3 Results

2.3.1 Nasal lavage

The lavage procedure took about 5 min to complete. In total 90 nasal lavages were performed on a volunteer population of 25 subjects. Of these 36 lavages were performed according to the Head Back technique and 54 were performed according to the Head Forward technique. The mean age and standard deviation of study was 29 ± 9 years. There were 10 females and 15 male subjects. There was no pain or discomfort experienced by any volunteer. There was no bleeding observed in any volunteer although red blood cells were observed in 18 lavage samples after centrifugation.

2.3.2 Lavage collection and cell viability

The mean volume of lavage fluid collected, total cell count and cell viability data from each lavage technique is compiled in Table 2-4.

Table 2-4: Nasal lavage volumes and cell counts according to each lavage technique. Values listed are the mean ± SD.

Lavage Technique	n	Lavage fluid volume (ml)	Number of cells collected	Number of viable cells	% Viability
Head Back	18	4.0 ± 0.4	157941 ± 47311	76212 ± 28968	47.5 ± 6.5
Head Forward	48	5.3 ± 0.3*	238595 ± 57148*	128156 ± 43503*	53.0 ± 7.0

***There is a significant difference in the volume of lavage collected, total cell count and the viable cell count between the Head Back technique and Head Forward technique with P<0.001 for all three variables.**

As it can be seen from Table 2-4, the Head Back lavage technique led to a loss of sprayed PBS as some quantity always hit the back of the throat and was swallowed. The Head Forward technique led to a better recovery of lavage fluid, with a fairly consistent volume of lavage of 5-6 mL collected each time. The number of cells collected by the Head Forward technique was also higher, while the percentage of viable cells collected by each method was equivalent between 40-60%.

2.3.3 Differential cell staining for microscopic examination of nasala lavage

MGG staining was performed and cells identified by their structure as epithelial cells, neutrophils, eosinophils, lymphocytes, basophils, mast cells and erythrocytes. MGG staining was performed in 6 samples from phase III which filtered and all the samples showed the presence of a substantial amount of epithelial cells in the lavage fluid (Figure 2-10 A). In some cases, neutrophils could be seen under the microscope after MGG staining (Figure 2-10-B).

The Figure 2-10 below shows microscopic images of MGG-stained cytospin preparations of fresh nasal lavage as observed under Olympus X50 microscope at 200X magnification.

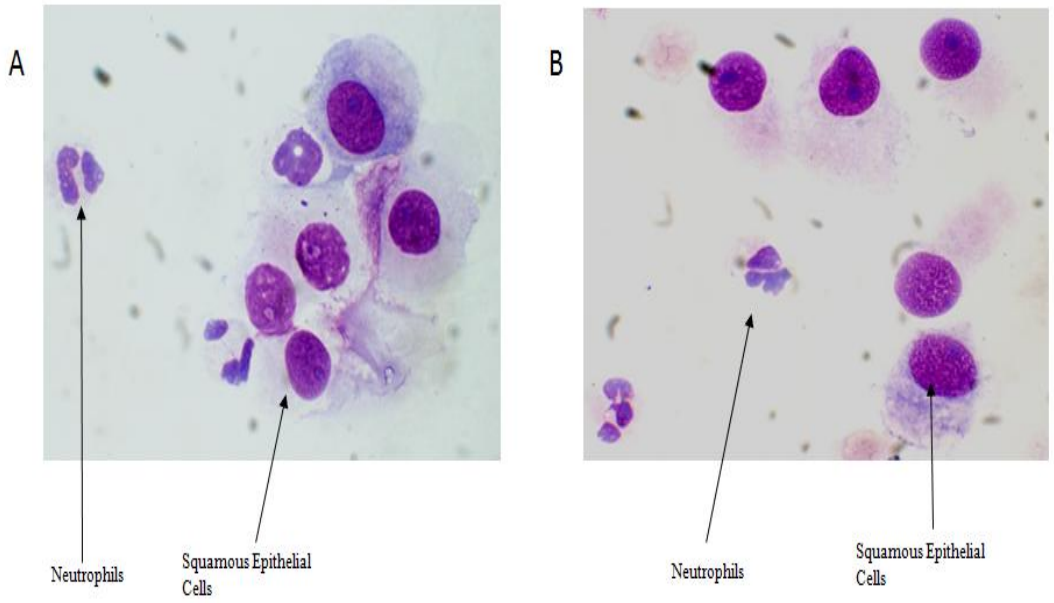

Figure 2-10: MGG-stained nasal lavage sample showing presence of squamous epithelial cells, red blood cells and neutrophils. Samples were observed under observed under Olympus X50 microscope at 200X magnification.

The differential count of MCG-stained cell samples (filtered and using head forward nasal lavage technique) showed that 90% of the cells were epithelial in nature (Table 2-5).

Table 2-5: Differential count performed on cells recovered from the nasal cavity of human volunteers by draining lavage fluid after administration of 10 ml PBS by nasal spray

Volunteer ID	Lavage fluid (mL)	Total Cells (x 10^5)	Viable Cells (%)	% cells recovered		
				Epithelial	Neutrophil	Macro-phage
1	6	2.5	41	97	3	0
2	5	3.2	49.5	86	14	0
3	6	4	39.3	72	28	0
4	5.5	3.3	61.2	94	3	3
5	6.5	1.8	48.5	94	6	0
6	5.5	2.5	49.3	93	7	0
Mean	**5.8**	**2.8**	**48.1**	**89.3**	**10.2**	**0.5**
sd	**0.5**	**0.7**	**7.8**	**9.2**	**9.6**	**1.2**

2.3.4 Optimization of lavage and culture methods

A summary of results for Phases I-III of the study to establish cell harvesting and culturing conditions is provided in Table 2-6. In Phase I it was determined qualitatively that a lower seeding volume (and thus a higher seeding density) led to better cell adherence, although cells did not grow to confluency during this experimental phase. In Phase II, a similar qualitative assessment of cell growth suggested that collagen coating of the growth surface led to better cell adherence and multiplication. This study also showed that cell culture medium two was better for cell multiplication, although confluency was not achieved. In Phase III it was determined that the Head Forward lavage technique resulted in the recovery of a significantly larger volume of nasal lavage fluid (Table 2-4) and a significantly greater number of collected nasal cells. In a further innovation, it was shown in Phase III that filtration of the lavage fluid reduced nasal debris, although it was not eliminated completely. This step was shown to significantly reduce the number of cultures that developed microbial contamination compared to unfiltered cultures. Confluence of cells in phase III was not achieved either and attempts to passage cells when seeded at confluence failed.

Table 2-6: Compiled results from phase I – III of the cell harvesting and culture conditions optimisation experiments.

Variable 1	Outcome		Variable 2	Outcome		Variable 3	Outcome	Variable 4	Outcome	Variable 5	Outcome
Lavage technique	Volume (ml)	Cell Count	Filtration	Debris	# of contaminated cultures	Collagen coating	Cell attachment	Medium	Con-fluency	Seeding Volume	Con-fluency
Phase I Experiments											
Head back (n=18)	4.0 ± 0.4	158000 ± 47300	No Filtration (n=18)	18/18 (100%)	11/18 (61%)	Not coated (n=18)	3/18 (17%)	CCM1 (n=18)	0/18 (0%)	SV3 (n=6)	0/6 (0%)
										SV2 (n=6)	0/6 (0%)
										SV1 (n=6)	0/6 (0%)
Result: Seeding Density 1 showed better multiplication of cells at t=96 hrs although confluency was not reached at 96 h											
Phase II Experiments											
Head back (n=12)	n.d.	n.d.	No Filtration (n=12)	12/12 (100%)	8/12 (66%)	Coated (n=6)	4/6 (67%)	CCM1 (n=6)	0/6 (0%)	SV1 (n=6)	0/6 (0%)
						Coated (n=6)	5/6 (83%)	CCM2 (n=6)	0/6 (0%)	SV1 (n=6)	0/6 (0%)
Result: Coated surface showed better cell adherence and CCM2 showed better cell multiplication at t=96 hrs though confluence was not reached											
Phase III Experiments											
Head forward (n=48)	5.3 ± 0.3	238600 ± 57000	No Filtration (n=30)	30/30 (100%)	18/30 (60%)	Coated (n=30)	26/30 (86%)	CCM2 (n=30)	3/30 (10%)	SV1 (n=30)	3/30 (10%)
			Filtration (n=18)	18/18 (100%)	8/18 (44%)	Coated (n=18)	16/18 (88%)	CCM2 (n=18)	2/18 (11%)	SV1 (n=18)	2/18 (11%)
Result: Filtration leads to reduction in the amount of debris in the seeded cells, reduces contamination rate but complete debris removal was not possible using 100 µm nylon filters. *CCM = cell culture medium, SV = seeding volume.											

2.4 Discussion

This study aimed to optimise and characterise a primary nasal epithelial cell culture system involving atraumatic collection of nasal cells. Nasal cells or tissue sampled from the nasal cavity may originate from four different domains (127): (i) the vestibular area, covered by a stratified, keratinized and squamous epithelium including strong hairs which filter particles; (ii) the atrium, representing an intermediate zone lined with transitional epithelium, squamous at the anterior part and with microvilli at the posterior part; (iii) the three turbinates located on the lateral nasal walls and (iv) the olfactory epithelium which is above the medium turbinate consisting of specialized olfactory cells.

Fundamentally, there are three different groups of technique to sample nasal epithelial material for the development of human nasal primary cell culture systems, i.e. atraumatic methods, traumatic methods and post mortem biopsy (115). Main advantages of the traumatic method and the post mortem method is usually the high number of cells harvested. The major disadvantage is that traumatic sampling can rarely be repeated. As primary cell culture passaging is limited to a maximum of about three subsequent passages (128) per sample repeated sampling from the same subject and from the same area may be required.

Some of the atraumatic methods can meet this requirement. Pipkorn and Karlsson (129, 130) gave an overview on the atraumatic methods used for obtaining specimens from the nasal mucosa. Such techniques include nasal smears, blow secretion, nasal lavage, scraping from nasal mucosa, brush techniques and imprints. These techniques are easy to perform but suffer from the low amount of cells obtained which might be insufficient to allow the culture of confluent cell layers. By utilizing a fairly large volume for nasal lavage which covers a large surface area it is feasible to harvest between 10^5 and 10^6 cells per sampling (129, 130). Thus the nasal lavage technique may provide enough cells for cell culturing but the shortcomings of these methods are: an exact sampling site can not be standardized and mainly superficial cells are obtained (115).

For the successful development of a primary cell culture model in general many factors have to be considered, namely method of procuring the cells, seeding density, support membrane (e.g. polyester, collagen and polycarbonate membranes),

medium composition (to improve cell growth and differentiation), feeding regimen, culture time, cell heterogeneity, cell viability, reproducibility and costs involved. No specific approach in the culturing of primary human nasal epithelial cells is generally superior to another, and the method selection depends on the scientific goal of the study (131).

The pre-optimization studies performed showed the importance of each variable. Studies to optimize the technique developed in this chapter showed that:

Lavage Technique: Different methods have been proposed to perform nasal lavage (132-135). The number of cells obtained may be low depending on the method used for nasal lavage (135, 136). The analysis of cells obtained by nasal lavage presents some problems such as mucus aggregates or broken cells interfering in the assessment of total and differential cell counts and this might lead to misrepresentation of results. The results in Table 2-4 indicate that the lavage technique is extremely important in determining not only the volume of recovered lavage fluid, but also the total number of cells collected. Interestingly, the percentage of viable cells did not significantly differ according to the lavage method and ranged between 47% and 52%, irrespective of the lavage technique used. These results are in good agreement with results obtained by Prat and co-workers (137, 137, 138). They analysed cells obtained by nasal lavage by instilling 5 ml of sterile saline solution in each nostril with the subject's head tilted backwards at a 30º angle. They reported an average total cell count of $1.27 \times 10^5 \pm 0.41 \times 10^5$ cells/ml (compared to $1.58 \times 10^5 \pm 0.47 \times 10^5$ cells/ml in this study using a similar technique). Although they did not report the viable cell count, they observed that cell viability was low and ranged between 60% and 70%. The total number of cells increased considerably when using the head forward technique (Table 2-4; $P<0.001$). This can be explained by the fact that with the head tilted backwards a proportion of PBS was lost from the nose to the back of the throat. This is reflected by the difference in the volume of lavage collected by the two different methods employed (Table 2-4; $P<0.001$).

Prat and coworkers also reported that their nasal lavage samples contained 70 ± 7 % epithelial cells, 26 ± 7% neutrophils and 0.56 ± 0.3% eosinophils. In this study, microscopic examination of the nasal lavage fluid, using MGG staining to differentiate the cell types, confirmed the presence of epithelial cells and neutrophils. However, eosinophils were not detected in any of the samples investigated in this

study. Differential cell count performed on the 6 samples (filterd) stained using MGG staining technique showed that 90% of the cells were epithelial in nature and 10% were neutrophils (Table 2-5).

Filtration: Mosler and co-workers (124) performed a microbiological investigation on samples of nasal epithelial cells obtained by brushing technique. They cultured the aliquots of the centrifuged medium on horse blood and chocolate blood agar and identified *S. aureus, S. pmeumoniae, H. Influenza, streptococci, staphylococci, Neisseria species and Corynebacterium species.* The pre-optimization study showed that filtration of the lavage sample before centrifugation leads to a cleaner debris free sample and reduces the chances of contamination. It can be seen from the results in Table 2-6 that the percentage of contamination came down to 44% (n=18) from 60% (n=30). This can be attributed to the fact that filtration helped in removing mucus aggregates and other nasal debris in the nasal lavage which may contain the infection causing organisms. The presence of bacteria in nasal mucus was analyzed by Park and co-workers (139). They sampled mucus from 36 individuals and found that only 6 were sterile while the remaining 30 were non-sterile. This finding suggests that filtration will play a very important role in reducing the chances of contamination. In this study a 100 µm pore size nylon filter was used but we were not able to remove all the debris. Other groups (120, 140) have used 60-70 µm pore size nylon filters. Reducing the pore size of the nylon filter might further help in reduction of nasal debris. This hypothesis needs to be analyzed further.

Collagen coating: Dissociated nasal epithelial cells have been grown on plastic tissue culture dishes, glass or plastic cover slips, microporous inorganic membranes, collagen treated culture dishes and inorganic membranes, collagen matrices, floating collagen gels and full collagen membranes. The type of surface on which the cells grow influences the preservation of specific phenotypic characteristics (141) and the development of specialized epithelial functions such as barrier formation and vectorial transport of solutes (142). In this study, we also showed the importance of collagen coating which can be explained by the fact that being a part of the lamina propria, collagen may improve cell attachment efficiency (128, 143), cell proliferation (128), and cell differentiation (144). On the other hand Werner and Kissel (68) found no differences in cell growth and proliferation between untreated and collagen treated supports. This may be difficult to explain knowing the

fact that nasal epithelial cells which do not have hemidesmosomes and attach to the basement membrane only by cell-adhesion molecules like laminin and fibronectin (106). In this study the use of collagen I showed better attachment of cells which can be explained by the fact that the respiratory basement membrane is composed of mainly collagen fibres (106). Consequently, biological matrix such as collagen is important to obtain a stable and reproducible nasal culture system.

Cell culture medium: The medium and its supplements are primary factors affecting the viability, proliferation and differentiation of cells in culture. A wide range of cell culture medium and medium supplements has been used in human nasal epithelial cell cultures (Table 2-1). The media that been proven to be the best for culturing of freshly isolated human nasal epithelial cells are; Dulbecco's modified Eagle's medium (DMEM); Ham's F-12; Bronchial epithelial growth medium (BEGM); and the 1:1 mixtures of DMEM:Ham's F-12 and BEGM:DMEM. Results from the study by Mattinger and co-workers (145) indicate that BEGM medium with added supplements provided optimal conditions for growth, expansion, viability and morphology of primary human nasal epithelial cells and their passages. From the abundance of information on cell culture medium suitable for primary human nasal cell culture (Table 2-1) it cannot be concluded which medium is best suited. Therefore, for this study we started with the use of a very simple cell culture medium for practical and economic reasons. Wu and co-workers (128) identified three substances improving the *in-vitro* culture of human nasal epithelial cells: hydrocortisone, cholera toxin, T3 and epidermal cell growth supplement. Insulin was also identified to be critical for multiplication of cells.

Insulin initiates its action by binding to a glycoprotein receptor (insulin receptor) on the surface of the cell. Binding to this receptor generates a signal that eventually results in insulin's action on glucose, lipid and protein metabolism. The growth-promoting effects of insulin appear to occur through activation of receptors for the family of related insulin-like growth factors (IGFs) (146-149). In cell culture, insulin is a component of serum-free media formulations for all primary cells and cell lines so far examined. In addition to the stimulation of cell growth, classical insulin responses such as increased fatty acid and glycogen synthesis are seen in serum-free medium.

Four agents known to increase the level of cellular cAMP by different means (cholera toxin, dibutyryl cAMP, methyl isobutyl xanthine and isoproterenol) increase the growth of colonies of cultured human epidermal cells and of keratinocytes derived from other stratified squamous epithelia. This effect is due to an increase in the overall rate of cell proliferation in the colonies. The increased proliferation in the presence of the toxin is associated with an increased proportion of small cells known to include the multiplying fraction. The use of the toxin makes the cultivation of keratinocytes from epidermis and other stratified squamous epithelia much easier and prolongs the culture life of the cells (150).

As it can be seen from Table 2-1, a number of research groups have used serum-free culture medium which offers several advantages as compared to serum-supplemented culture medium. Serum-free culture medium does not have any qualitative or quantitative variabilities of the additives caused by serum and the microbiological contaminations can be omitted (145). Furthermore they found that supplementation with epinephrine caused increased viability, short population doubling time and increased passages. They also found that use of epidermal growth factor and bovine pituitary extract increased the viability. The essential and synergistic effects of EGF with insulin on human keratinocyte spreading and proliferation have been described by other authors (151, 152). This may be attributed to the fact that insulin or insulin like growth factor I (IGF-I) increase cell surface EGF receptors and this effect in part may be responsible for the synergism (153).

Heme toxicity: Some of the lavage samples collected showed the presence of red blood cells. This was more often seen during the dry summer season when the nose was dry. Nasal drying is a common cause of nose bleeds. In the cases where RBC was present in the lavage collected, epithelial cell growth could not be seen as the lysis of RBC leads to the release of free heme in the cell culture medium which might be toxic for cells. Iron-derived reactive oxygen species (ROS) are implicated in the pathogenesis of numerous vascular disorders including atherosclerosis, microangiopathic hemolytic anemia, and vasculitis and reperfusion injury. One abundant source of redox-active iron is heme released from intracellular heme proteins. Free heme damages lipid, protein, and DNA through the generation of ROS. Heme and heme proteins have been implicated in a variety of toxic effects through oxidation of lipid (154-158). Heme in the aqueous phase frequently

aggregates in the membrane and promotes oxidation, which leads to the enhancement of permeability and membrane disorder. Oxidation of membrane components may promote cell lysis and death (159, 160). The red blood cells could be removed by changing the cell culture medium at t=6 h after seeding based on the hypothesis that RBC and epithelial cells would have differential adherence rates.

Seeding density: From the literature review (Table 2-1) it can be seen that most of the research groups cultured the primary human nasal epithelial cells on air-liquid interface. It has also been reported that cells were seeded at 20,000 to 35,000 cells per cm^2 at ALI by Auger and co-workers (122) and they reported confluent monolayer formation. Other research groups have generally seeded the cells at a higher seeding density of 10^5-10^6 cells/cm^2. Mosler and co-workers (124) used brushing technique to collect nasal epithelial cell samples from infants and they found that a minimum seeding density of 50,000 viable cells/cm^2 was necessary for successful culturing of cells. The seeding density according to the head forward technique of nasal lavage ranges between 30,000 to 80,000 viable cells/cm^2.

2.5 Conclusion

A procedure was established for the atraumatic collection of nasal epithelial cells. These cells morphologically appear to be squamous epithelial cells in nature. These cells can be cultured to confluence but not passaged. However, this method will require further adaptations and verifications (especially characteristics of the cell type) before it can be successfully used as a model for studying nanoparticle toxicity in the nose.

This model offers the opportunity to investigate an important question: to what extent do inhaled nanoparticles cause inflammation to the nasal epithelium**.** This model potentially provides the opportunity of scaling up the data from results based on 8 to 10 individuals at the maximum (Table 2-1) to a statistically significant number of human beings. However, to grown the cells successfully further modifications are required to the culturing technique. Although primary human nasal cells are readily obtained, the capacity offered by this system to perform extensive *in vitro* toxicity is currently much less than that of immortalised cell lines, which are utilised in subsequent chapters.

Chapter 3

Particle kinetics in assay systems: Delivered dose

3.1 Introduction

Our interest in identifying, understanding, and addressing potential risks to human health and the environment due to NPs has increased because of the rapid expansion of engineered nanomaterials designed for use in consumer products. To understand these risks, controlled laboratory toxicology experiments are conducted on a variety of biological systems ranging from simple cell culture systems to more complex animal or human models. The usual aim of these experiments is to obtain biologically relevant information which might help in predicting potentially harmful effect in human beings upon exposure to nanomaterials. When cell culture models are used in the laboratory for toxicological experiments it would be ideal to use doses of NP which reflect particle deposition in the human respiratory tract (which may or may not be possible depending on the analytical technique used) for a more robust extrapolation of results from *in vitro* experiments to *in vivo* experiments. However, NPs in cell culture medium are in a dynamic state where they are settling, diffusing, aggregating based upon the NP properties and the characteristics of the medium (88). This affects their transport to the cells which makes the definition of dose for NP in an *in vitro* system more complicated (88, 90). The aim of this chapter is to understand the colloidal behaviour of NP in suspension and improve the understanding of NP dose in an *in vitro* system.

3.1.1 Dosimetry

The search for the appropriate dose metric for evaluating biological effects of NPs has been central to addressing the toxicity of nanomaterials. Oberdorster (161) highlights three areas which are significant in understanding nanomaterial toxicity compared with that of macroscale materials and/or constituent chemicals: dose,

biokinetics, and the significance of physicochemical properties. Evidence has emerged that, for some materials, the use of mass concentration alone as a dose metric can obscure associations between the material and biological behaviour (161), as can be seen from Figure 3-1. Other authors have highlighted the use of surface area as an appropriate dose metric (162-164).

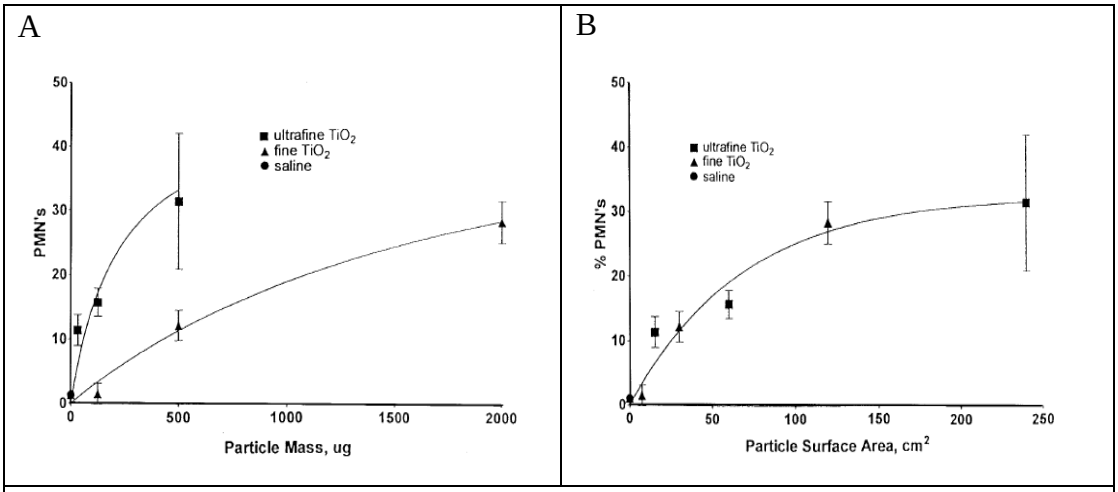

Figure 3-1: Dose response relationship for instilled ultrafine (20 nm primary particle size) and fine (250 nm primary particle size) titanium dioxide particles 24 h after intratracheal instillation in rats. (A) Correlation between particle mass and lavaged polymorphonuclear neutrophils (PMN's) and (B) correlation between instilled particle surface area and lavaged PMN's. Figure reproduced from Oberdorester *et al.* (165, 166).

However, Wittmaack *et al.* (167) challenged the findings of Oberdorester *et al.* (165, 166) and Stoeger *et al.* (164) by recalculating the data presented by the authors and suggesting that particle number rather than surface area is a more suitable dose metric for evaluating dose-response relationships for particle-induced inflammation particularly for differently prepared carbon nanoparticles. The discussion of appropriate dose metric *in vitro* was started by Limbach *et al.* (168) who debated that uptake of oxide NPs by human lung fibroblast cells were affected by particle size, density and agglomeration state and due to diffusion and gravitational settling of particles this would impact delivery of particles to cell monolayers. Figure 3-2 shows the three ways which people have generally used to quote dose – one is nominal dose in terms of mass, surface area or particle number which basically is the amount of particles put on the system, second is the delivered

dose which is basically the amount of NPs actually reaching the cells and third is the cellular dose which is the amount of NPs internalized by the cells.

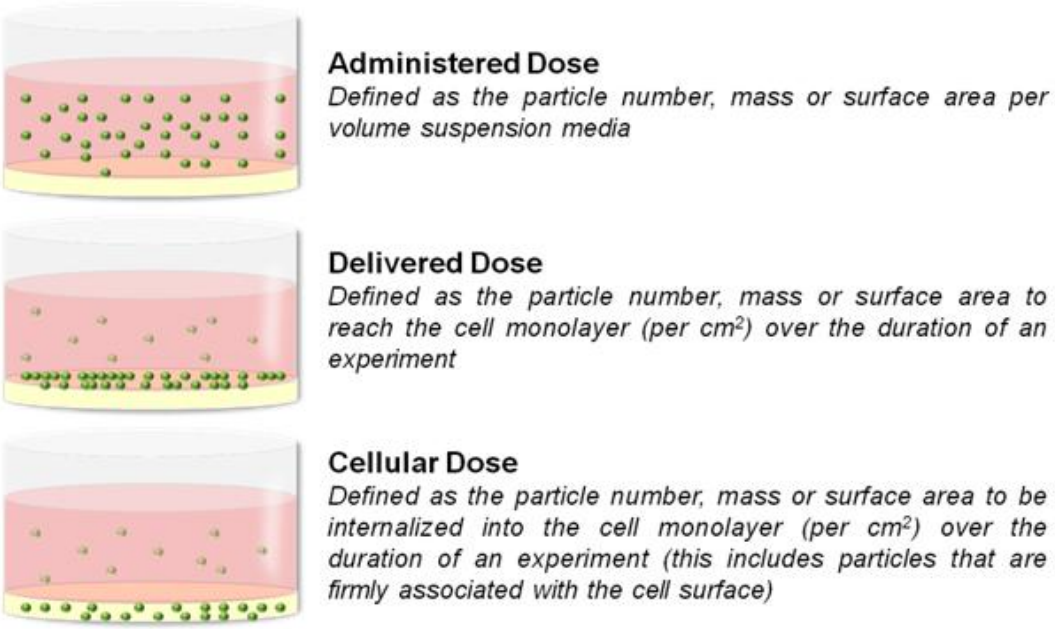

Figure 3-2: Definitions of dose metrics for accurate assessment of *in vitro* particle-cell interactions (Khanbeigi *et al*. (169))

In a typical *in vitro* experiment, cells are immobilized at the bottom of a culture plate or on a substrate placed at the bottom of a culture plate, and incubated with a suspension of NPs. The NPs are assumed to be well-dispersed in the culture medium so the concentration of NPs at the cell surface is assumed to be the same as that of the initial bulk concentration. However, particles in suspension are not only under the effect of gravity but also undergo diffusional movements (driven by both Brownian motion and regional concentration gradients), which means that not all the particles in the suspension will reach the cells.

Limbach *et al.* (88) and Teeguarden *et al.* (90) have identified discrepancies between the amount of a material introduced to *in vitro* cell cultures, i.e. the administered dose, and the amount of material cells are able to interact with after a given exposure time, i.e. the delivered dose. As particles form a dynamic concentration gradient within the suspension medium, there are indications that over short incubation periods actual doses of material interacting with cells may be orders of magnitude lower than assumed. Limbach *et al.* (88) measured the cellular dose of internalized 25-50 nm cerium oxide nanoparticles and compared it to the cellular dose of 250-500

nm cerium oxide nanoparticles in human lung fibroblasts. Separately, they calculated the delivered dose by assuming that small particles reached the cell layer by diffusion only and larger particles reached the cell layer via sedimentation. They then compared their predicted delivered dose values with measured cellular doses (i.e. after exposing the cells to the NPs for different exposure times, the cells were dried and elemental analysis was performed for quantification of NP uptake). The cellular dose of 25 nm ceria oxide nanoparticles correlated extremely well with the predicted delivered dose (based on Stokes'-Einstein diffusion). A number of mechanisms explain the effective internalization of these relatively small particles (especially at low particle doses). One such mechanism is the endocytic pathways with small vesicle structures, which is an especially prevalent pathway in fibroblast cells (170) and can be found during calveolae-mediated endocytosis (vesicle size 60-80 nm) (171). On the contrary, particles of large sizes (320 nm) are excluded from these pathways and therefore show a limited uptake rate compared to small particles. This results in discrepancies between the delivered vs cellular dose (88).

In the case of small or low density particles, diffusion-limited transport dominates whereas for large or high density particles, the transport is mainly driven by gravitational settling. The results of Limbach *et al.* indicate that the computed delivered dose values are realistic for particles of different sizes, densities and agglomerate states (88). Using the same mathematical model, Teeguarden *et al.* (90) theoretically showed that the process of particle transport not only affected the particle uptake but also the relative toxicity. In the study, Teeguarden *et al.* calculated separate values for particles that reach the cell layer by either sedimentation (gravity) or diffusion (Brownian motion) and summated the two values to obtain delivered does for a given experiment. Teeguarden *et al.* (90) then re-analyzed published data of lactate dehydrogenase release from a study by Hussain *et al.* (91), who had reported the cytotoxicity (EC_{50} value) for various nanoparticles (1000 nm cadmium oxide NP (CdO), 15 and 100 nm silver NP (Ag) and 30 and 150 nm molybdenum trioxide NP (MoO_3)) on rat BRL 3A liver cells. The analysis by Teeguarden provided EC_{50} values as normalized to the delivered dose of particles (0.005 to 0.66 cm^2/ml). The post hoc analysis contrasted dramatically with the EC_{50} value range calculated by Hussain *et al.* (0.005 to 89.3 cm^2/ml), who normalized their results to the administered surface area dose (Table 3:1).

The purpose of the Teeguarden *et al*. study was to highlight the discrepancy in the administered surface area dose and transport adjusted (delivered) surface area dose. The study shows the relevance of normalizing *in vitro* results to the delivered dose when reporting the cytotoxicity data. The consequence of reporting data normalised to the administered dose is that artificially high values may be reported, biasing the results of efficacy and safety studies.

Table 3:1: Recalculation of EC_{50} values by Teeguarden *et al.* (90) after taking into account the particle transport.

Particle Type	EC_{50} Administered Surface Area Dose (Hussain *et al.* (91)) (cm^2/ml)	EC_{50} Particle Transport Adjusted Dose (Teeguarden *et al.* (90)) (cm^2/ml)
CdO-1000 nm	0.005	0.005
Ag 100-nm	1.37	0.02
Ag 15-nm	19.0	0.272
MoO_3 150-nm	21.3	0.262
MoO_3 30-nm	89.4	0.663

Hinderliter *et al.* (89) further refined the study by Teeguarden *et al.* (90). The improved model is based on a parabolic partial differentiation equation (Equation 1), which was independently developed by both Smoluchowski (172) and Mason and Weaver (173). The equation (Equation 3-1) calculates the particle movement through a fluid (i.e. towards the cell layer) under a set of defined boundary conditions. The resulting particokinetic model by Hinderliter became known as the *In Vitro* Sedimentation, Diffusion and Dosimetry model or ISDD (89). The improved model calculates both sedimentation and diffusion simultaneously for the same particle and therefore excludes the drawback of the model by Teeguarden *et al*. (90) of potentially counting particles twice in the delivered dose calculation. Using the ISDD model, Hinderliter *et al.* (89) theoretically demonstrate the dramatic effects of altering not only nanoparticle composition, density, incubation time and particle size distribution, but also the influence of different cell culture medium volumes and agglomerate fractal densities.

$$\frac{dn}{dt} = D\frac{\partial^2 n}{\partial x^2} - V\frac{\partial n}{\partial x}$$

Equation 3-1

Where:

- *n*: particle concentration (number or mass/mL)
- *t*: time (s)
- *D*: Stokes-Einstein diffusion rate (m^2s)
- *x*: distance travelled (m)
- *V*: Stoke's sedimentation velocity (ms^{-1})

The focus of the studies presented is based on the theoretical aspects of the colloidal behaviour in a suspension, however provide limited *in vitro* cell culture data to demonstrate a robust use of the model in practice. In addition, particokinetic modelling in drug delivery and nanotoxicity research has not been explored and may prove a useful technique in assessing the safety of NPs with regards to *in vitro-in vivo* correlation. Further the ISDD model developed above requires expensive programming platform Matlab® to calculate delivered dose value.

Thus the aim of this work was to develop an easy-to-use model taking into consideration the non-agglomerate particle size polydispersity.

3.1.2 *Theory of sedimentation and diffusion*

In contrast to soluble chemicals, particles can settle, diffuse and aggregate in fluids. It is thus important to understand their physical behaviour in fluids to understand the dynamics of dosing. Nanoparticles in suspension are under the influence of gravity and undergo diffusion which is the net migration of particles from regions of high to low concentration (Figure 3-3). To understand the dynamics of particle transport in fluids a simple model describing particle sedimentation and particle flux is derived.

A video by Clift *et al.* (174) of live imaging of J774.A1 cells treated with fluorescently labelled polystyrene nanoparticles of 20 and 200 nm for 60 min clearly demonstrates the gravitational and diffusional influenced movement of NPs. The forces acting on a particle in suspension are illustrated in Figure 3-4.

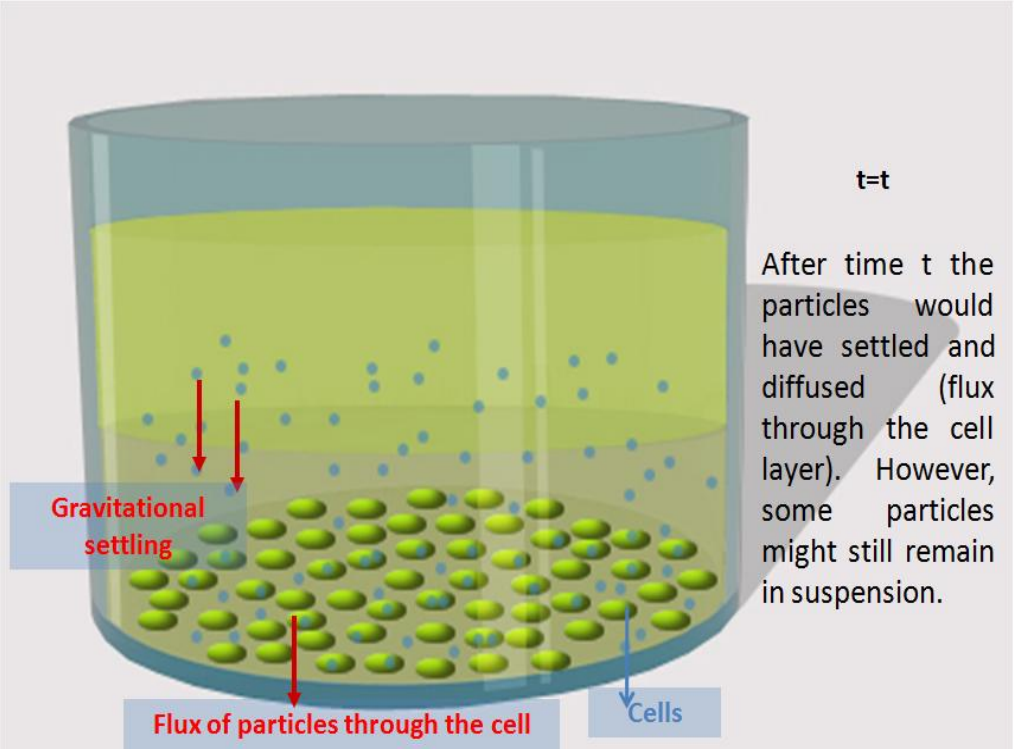

Figure 3-3: Diagramatic summary of nanoparticle behavior in suspension in traditionally used *in vitro* toxicity testing experimental setup. Nanoparticles in suspension are under the influence of gravity and diffuse from regions of high concentration to low concentration. The colloidal behavior of the particle suspension will have an important impact on the effective dose of particles to interact with cells and elicit a response (e.g. internalization, membrane damage, inflammatory response, cytotoxicity, etc.).

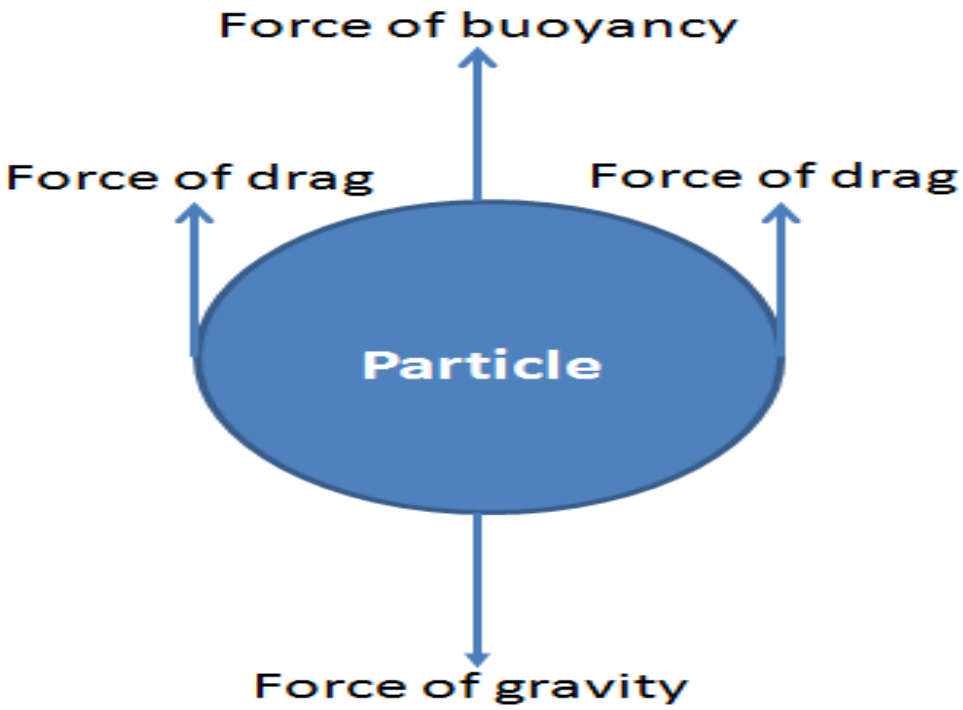

Figure 3-4: Illustration of forces acting on a particle in suspension.

Gravitational Settling: Gravitational settling can be determined by the balance of forces acting on a particle in suspension. The forces which act on the particle in suspension are buoyancy and drag forces resisting the movement of the particle under the influence of gravity as illustrated in Figure 3-4.

The gravitational force acting on the particle is a function of its mass which is dependent upon the density and the size of the particle. Buoyancy is equal to the mass of fluid medium displaced which is equivalent to the volume of the particle (size) and the density of the fluid medium. The only other force remaining is drag force which is dependent upon the size of the particle, the viscosity of the fluid and the particle velocity. Terminal velocity or settling velocity is reached when there is a steady-state situation where this velocity becomes constant. This terminal velocity can be derived using Stoke's law:

$$V_s = \frac{2(\rho_s - \rho_m)gr^2}{9\mu}$$

Equation 3-2

Where:

- V_s is the particle's settling velocity (m s^{-1}),
- g is the gravitational acceleration (m s^{-2}),

- ρ_s is the mass density of the particles (kg m^{-3}),
- $\rho_m$is the mass density of the fluid (kg m^{-3}),
- μ is the fluid's viscosity (kg m^{-1} s^{-1}),
- *r* is the radius of the particle (m).

Diffusional Motion: Diffusion is the random movement of particles from regions of higher concentration to regions of lower concentration (Figure 3-3). There is no net transport by diffusion when a system is at equilibrium. However, in an *in vitro* cell culture setup the cells internalize the particles thus making them unavailable in the suspension. This creates a concentration gradient at the medium layer immediately above the cells which drives the diffusion process. This transport process can be represented by Fick's second law:

$$\frac{\partial c}{\partial t} = \frac{D\partial^2 c}{\partial z^2}$$

Equation 3-3

Where:

- *c* is the particle's concentration (kg m^{-3}),
- *D* is the diffusion coefficient (m^2 s^{-1})
- *t* is the time (s)
- *z* is the spatial coordinate (from bottom to top of the culture well) (m).

The diffusion coefficient *D* of a small particle can be derived using the Stokes-Einstein equation:

$$D = \frac{RT}{N6\pi\mu r}$$

Equation 3-4

Where:

- *R* is the gas constant (8.314 J K^{-1} mol^{-1}),
- *T* is the temperature (K)
- *N* is the Avogadro's number
- μ is the fluid's viscosity (kg m^{-1} s^{-1}),
- *r* is the radius of the particle (m).

Further the Equation 3-4 and Equation 3-4 mathematically relate the sedimentation velocity and diffusion coefficient both to the hydrodynamic radius of the particle. Thus, prior to modelling the particle behaviour in suspension it is essential to characterize the particle size in the relevant medium. In the ISDD model the authors utilized the equations developed by Smoluchoski (172) and Mason and Weaver (173) to understand the behaviour of small articles settling in fluid and using Matlab® to solve the Equation 3-1 the authors calculated the predicted deposited dose.

3.2 Aims and objectives

The aim of this chapter was to develop an Excel program for the calculation of delivered dose based on Stoke's law of sedimentation and Fick's second law (describing diffusion), and to verify output of this model by comparing it to the ISDD model developed by Hinderliter *et al.* (89). Further, the delivered dose values produced by the Excel model will be compared with experimental data from Khanbeigi *et al.* measuring uptake of 50, 100, 200, 700 and 1000 nm polystyrene beads by murine macrophages (J774.1).

3.3 Materials and methods

3.3.1 Materials

Microsoft Excel® (2010) and Matlab® (7.4.0)

3.3.2 Methods

3.3.2.1 Theoretical elements of the particokinetics program developed

Calculating the number of particles reaching the bottom of the well due to gravitational settling

For the purpose of developing the program, we must know the shape and dimension of the vessel in which the particles diffuse. Typically cells are cultured in tissue culture plates which are cylindrical in nature as illustrated in Figure 3-5.

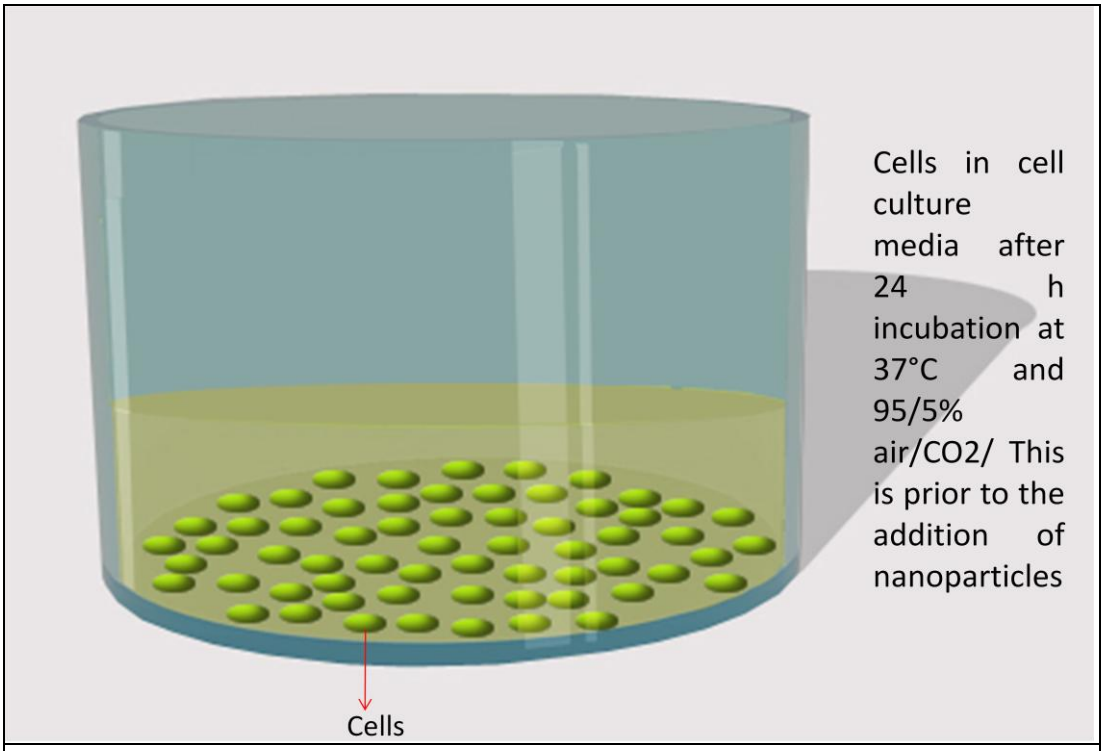

Figure 3-5: Typical cell culture plate which is cylindrical in nature and cells are at the bottom of the well.

After culturing the cells for 24 h in the incubator, equal volumes of NP suspension prepared in the same media in which the cells were cultured are added to the cells. At this time point (t = 0 h) the particles are assumed to be homogeneously distributed through the medium (Figure 3-6).

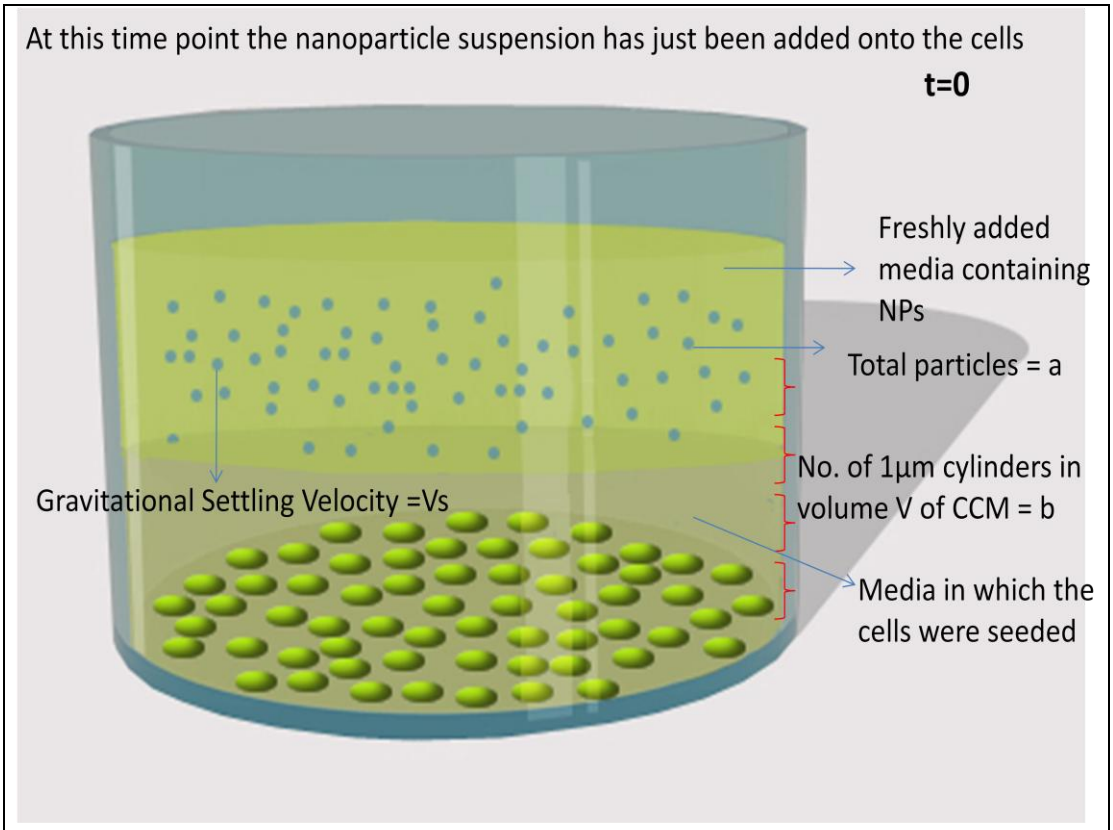

Figure 3-6: Calculation of particles reaching the bottom of the well by gravitational settling.

To calculate the number of particles reaching the cells by sedimentation we divide the total volume occupied by the cell culture medium into cylinders which are 1 µm high and have the same surface area as that of the tissue culture plate. Let's say the total number of such cylinders is 'b'. Since we have assumed homogeneous distribution of particles we can calculate the number of particles contained in each of these 1 µm high cylinders by dividing the total number of particles 'a' by the total number of cylinders 'b'. Now we can calculate the total distance travelled 'l' (m) by a given particle by multiplying the gravitational settling velocity Vs (m/s) with exposure time of the experiment 't' (s) . In the end, the total number of particles reaching the cell layer would be equal to the number particles contained in all 1 µm-thick cylinders that can be contained within a height equal to the maximum distance a particle with a given size may sediment i.e. 'l' (m). So the number of particles reaching the bottom of the well can be calculated by Equation 3-5.

$$Nsed = \frac{2(\rho_s - \rho_m)gr^2}{9\mu} * \frac{a}{b} * t$$

Equation 3-5

Calculating the number of particles reaching the bottom of the well due to diffusion

For calculation of the rate of diffusion, particles were assumed to diffuse in the liquid toward the cells in one dimension (top to bottom of the culture well). This is a reasonable assumption because diffusion is a concentration-driven phenomenon. Under the experimental conditions we have assumed uniform distribution of particles in each of the 1 μm cylinders (Figure 3-6). The only direction where concentration gradient exists is along the z- axis as particle internalization by cells at the bottom of the plate maintain constant sink conditions. However, along the x-axis and y-axis there is no concentration gradient (due to uniform particle distribution) so there will be no diffusion along these axes. Net diffusional movement driven by Brownian motion is regarded as zero in this model, due to the fact that Brownian motion occurs in all directions and therefore cancels itself out. This concentration gradient-driven transport process can be represented by Fick's second law (Equation 3-3):

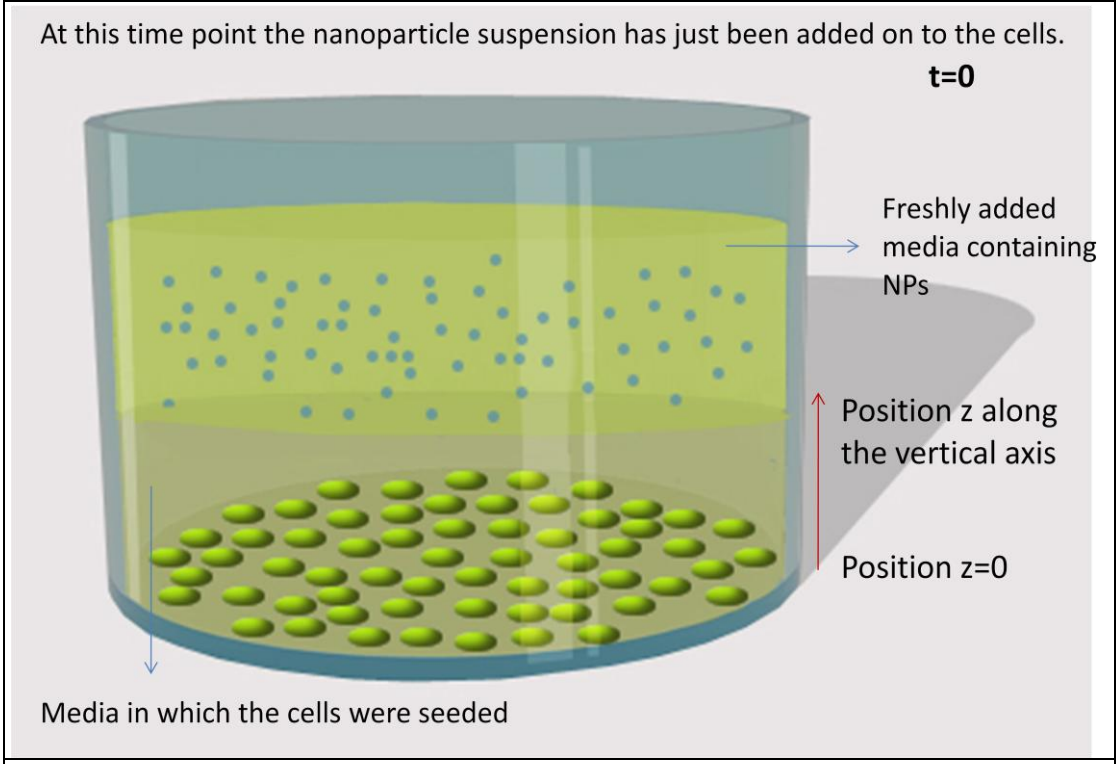

Figure 3-7: Typical cell culture plate which is cylindrical in nature and cells are at the bottom of the well. The particles are added at t = 0 h.

At time point (t=0) the particle suspension has just been added to the well. This means that the particle concentration throughout the media at any position (i.e. any given z along the vertical axis) is the initial concentration of particles ($C_{initial}$) (Figure 3-7).

Equation 3-3 was solved according to the method by Cussler *et al*. (175). To solve Fick's second law of diffusion the authors applied the following experimental boundary conditions which are based on an assumption of very short contact time:

Assumption: t+Δt reflects the assumption of very short contact times. At such early time points, the particles barely have a chance to diffuse through a given cross sectional area and reach the cell monolayer surface (defined as the interface; position z = 0).

Therefore, at time point t+Δt, we assume that particles didn't have a chance to diffuse. So the concentration at position z=0 would still be 0 and at any other given position z (z = ∞) would be equal to the initial concentration of particles $C_{initial}$.

$$t=0, \text{ all } z: C=C_{initial}$$
$$t+\Delta t, z=0: C=0$$
$$t+\Delta t, z=\infty: C=C_{initial}$$

Using the above boundary conditions, Cussler (175) provided the solution for Equation 3-3 to derive the flux *j* (kg m^{-2} s^{-1}) across the interface (z=0):

$$j = \int_0^t \sqrt{\frac{D}{\pi t}}(0 - Cinitial)$$

Equation 3-6

After the exposure period (t = t) some particles would have reached the cells while others might still be suspended in the media (Figure 3-8).

After calculating the number of particles reaching the bottom of the well by sedimentation and diffusion using Equations 3-5 and 3-6, respectively, we can calculate the total number of particles reaching the bottom of the well by adding the two values. A similar approach was taken by Teeguarden *et al*. (90) but they used a

different equation to calculate the time required to diffuse a given distance in one dimension (Equation 4 in the paper).

Total particles reaching the bottom of the well = *Nsed* + *Ndiff*

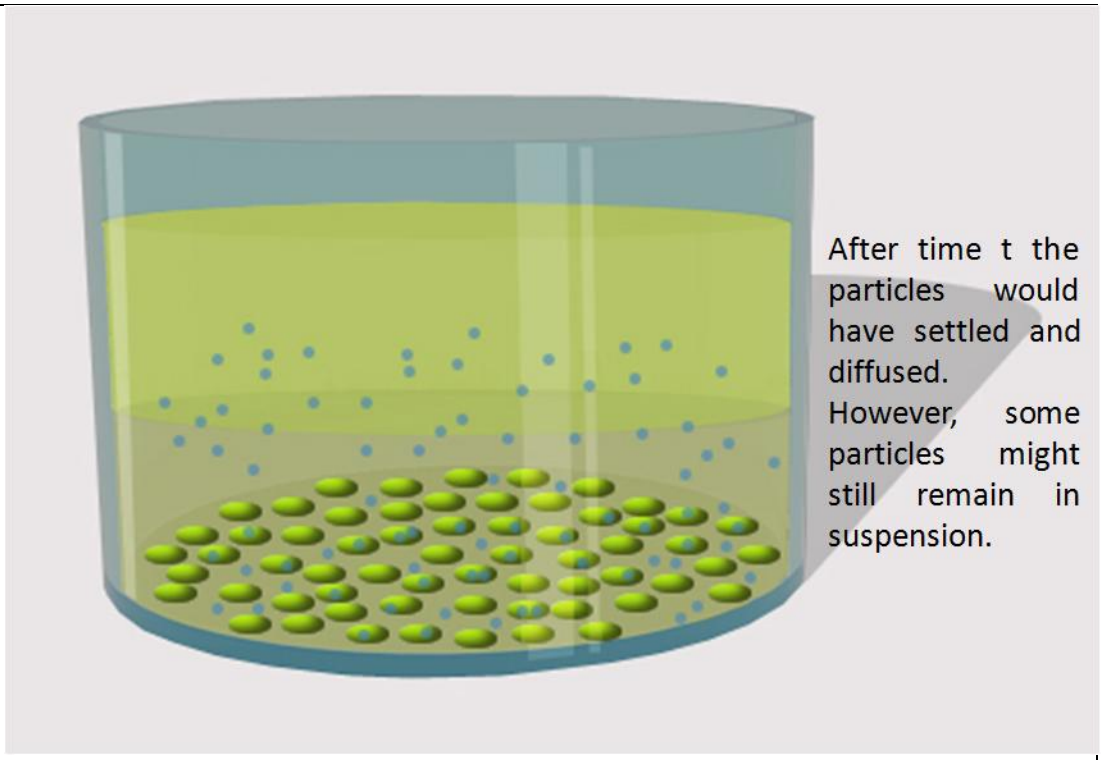

Figure 3-8: Illustration to show the situation after the exposure period t (h) where some particles would have reached the bottom of the well and others would still be suspended in the medium.

3.3.2.2 ISDD model

The Matlab® code for the ISDD model was kindly provided by Justin G. Teeguarden (Biological Sciences Division, Pacific Northwest National Laboratory, Richland, WA, USA). The cell culture experiments were performed in 24-well plate with 200 µl of cell culture medium at 37°C. Dynamic viscosity of the cell culture medium was 0.736 mPa.s. The following variables were input into the ISDD model for calculating the delivered dose: Mean particle size (nm) = measured HD in $DMEM/FBS_{10\%}$; administered dose (µg/mL); and incubation time (h).

3.3.2.3 Cell culture medium and particle size characterization

All experimental work reported in this chapter was performed by Raha Ahmad Khanbeigi. The experimental conditions are described in detail here to

provide sufficient information to understand the verification and validation of the particokinetics model developed in this chapter.

The viscosity of the cell culture medium supplemented with 10% FBS ($CCM_{FBS10\%}$) was measured at 37°C using an AMVn Automated Micro Viscometer (Anton Parr). Briefly, the samples were loaded into the microcapillary and the viscosity was determined according to Höppler's falling ball principle.

The polystyrene particles were characterized in two different media – water and cell culture medium with 10% serum ($CCM_{FBS10\%}$). The hydrodynamic diameters (HD) of fluorescent labelled polystyrene beads at particle sizes of 50, 100, 200, 700 and 1000 nm were measured using photon correlation spectroscopy (Nanosizer, Malvern Instruments, UK) at a scattering angle of 173°. Suspensions (2 mL) of each particle size were prepared in purified water (to verify manufacturer data) or DMEM without phenol red supplemented with 10% (v/v) FBS,1% sodium pyruvate, 1% penicillin/ streptomycin, 1% HEPES buffer and 1% L-glutamine (DMEM /$FBS_{10\%}$) at a concentration of $8.5x10^9$, $2.1x10^9$, $5.3x10^8$, $4.1x10^7$ and $2.1x10^7$ particles/200 µL for 50, 100, 200, 700, 1000 nm particles, respectively. The instrument parameters used for measurements in cell culture media were: Refractive index of particles=1.590, refractive index of DMEM /$FBS_{10\%}$ = 1.337 (176), temperature = 37°C, dynamic viscosity of DMEM/$FBS_{10\%}$ = $0.738x10^{-3}$ Pa s. The suspensions were incubated for 4 hours at 37°C with particle size measurements taken every 15 minutes.

3.3.2.4 Macrophage cell culture

J774.1 murine macrophage-like cells were cultured in DMEM supplemented with 10% fetal calf serum (FCS), 100 µM sodium pyruvate, 100 µg/mL penicillin/ streptomycin, 100 µM HEPES buffer and 100 µM L-glutamine. (FCS was obtained from Gibco and all other supplements from Lonza). Cells were passaged twice weekly by scraping cells and splitting 1:10.

3.3.2.5 Polystyrene nanoparticle uptake by macrophages

J774A.1 cells were seeded in 24-well plates at a density of $1x10^6$ cells/well and incubated overnight in cell culture medium (DMEM supplemented with 10%

(vol/vol) FBS, 1% sodium pyruvate, 1% penicillin/ streptomycin, 1% HEPES buffer and 1% L-glutamine) in a humidified 5% CO_2 incubator at 37°C. For treatment, the cell culture medium was removed and replenished with 200 μL fresh cell culture medium containing different concentrations of polystyrene beads (i.e. administration doses) according to the selected experimental conditions chosen for each particle size. To ensure uniform mixing, all latex bead suspensions were mixed vigorously prior to addition to cells. Negative controls comprised of cells treated with 200 μl fresh cell culture medium were included in all experiments. Depending on the selected experimental conditions, plates were incubated for 0.25, 0.5, 1 or 4 h, after which the medium was removed, cells were washed three times with PBS (37°C) and the plate was left exactly 18 h at room temperature to air dry under light exclusion. The dried monolayer was dissolved in 1mL N-methyl-pyrrolidone/ 25 mM Tris buffered saline pH 8.1 (1:3) and fluorescence was measured as described below. The number of latex beads associated with the cell monolayer was calculated from the corresponding calibration curve. For each exposure time and concentration the experiment was repeated six times using cell passage numbers 3-20.

To determine the amount of particles taken up by macrophages, calibration curves were produced for each particle size, showing number of particles in suspension against the fluorescence measured. The cells for the uptake experiment were dissolved in 500μL N-methylpyrrolidone/25mM Tris Buffer Saline pH 8.1 (3:1), and after scraping were transferred to a 1.5mL microcentrifuge tube. This was repeated twice so that the final volume of liquid collected was 1000 μL. The fluorescence in 1mL of the collected cell lysate was measured (Cary Eclipse Fluorescence Spectrophotometer-Varian) using a quartz cuvette (104F-QS 10mm) at excitation maxima of 468nm and emission maxima of 508nm (PMT = high (800 V), slit width of 5).

3.4 Results

3.4.1 Cell culture medium and particle characterization

The viscosity of cell culture medium at 37 °C was found to be 0.736 ± 0.002 mPa.s. Unmodified polystyrene beads were shown to remain stable in size over the duration of the four hour experimental period when suspended in $DMEM/FBS_{10\%}$

and incubated at 37°C (Figure 3-9); reproduced from (169)). However, a look at the particle size distribution data (Figure 3-10) showed that all the particles with the exception of PS 200 nm had a very wide particle distribution (PDI>0.2).

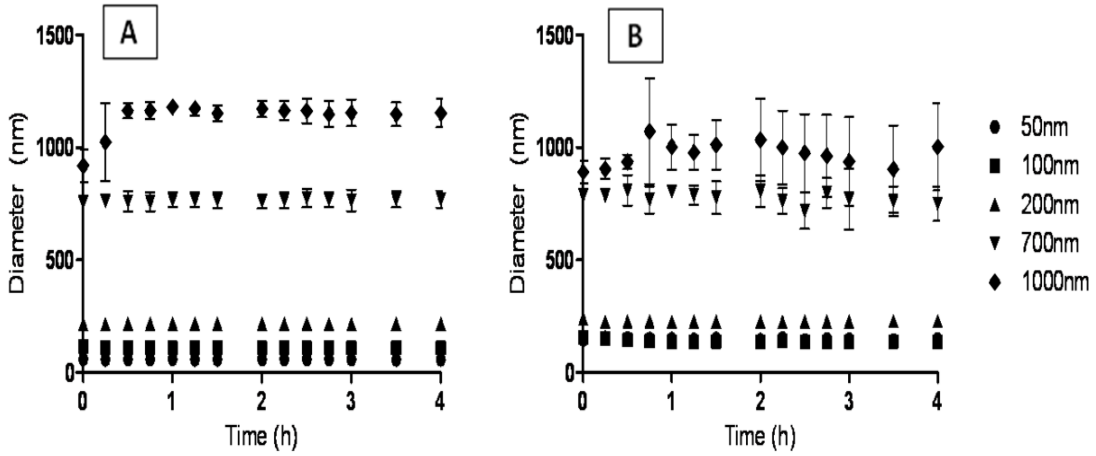

Size (manu-facturer)	HD in water (nm) (PDI)	HD in DMEM/FCS$_{10\%}$ (nm) (PDI)	ZP in water(mV)	ZP in DMEM/FCS$_{10\%}$ (nm)	Endotoxin Content (EU/mL)
50nm	59.0±2.7 (0.03±0.14)	149.3±3.6 (0.48±0.16)	-32.3±2.1	-17.0±0.6	0.09±0.01
100 nm	110.33±2.5 (0.01±0.01)	140.0±5.8 (0.36±0.35)	-27.7±1.3	-18.03±1.3	0.12±0.00
200 nm	216.9±3.0 (0.02±0.01)	228.1±3.3 (0.13±0.01)	-29.3±0.6	-18.6±0.5	0.13±0.05
700 nm	765.5±30.1 (0.12±0.09)	778.3±25.0 (0.40±0.09)	-31.3±0.8	-18.6±0.8	0.06±0.00
1000nm	1134.4±89.3 (0.49±0.38)	972.6±52.8 (0.39±0.16)	-34.5±3.3	-19.2±0.8	0.11±0.01

Figure 3-9: Top panel: Particle size measurements of polystyrene beads in ultrapure water (A) and DMEM/FBS10% (B) over 4 h. The table includes HD values measured at the 4h time point, zeta potential and endotoxin content. All values listed represent the mean ± SD of n=3 experiments. Figure reproduced from Khanbeigi *et al.* (169).

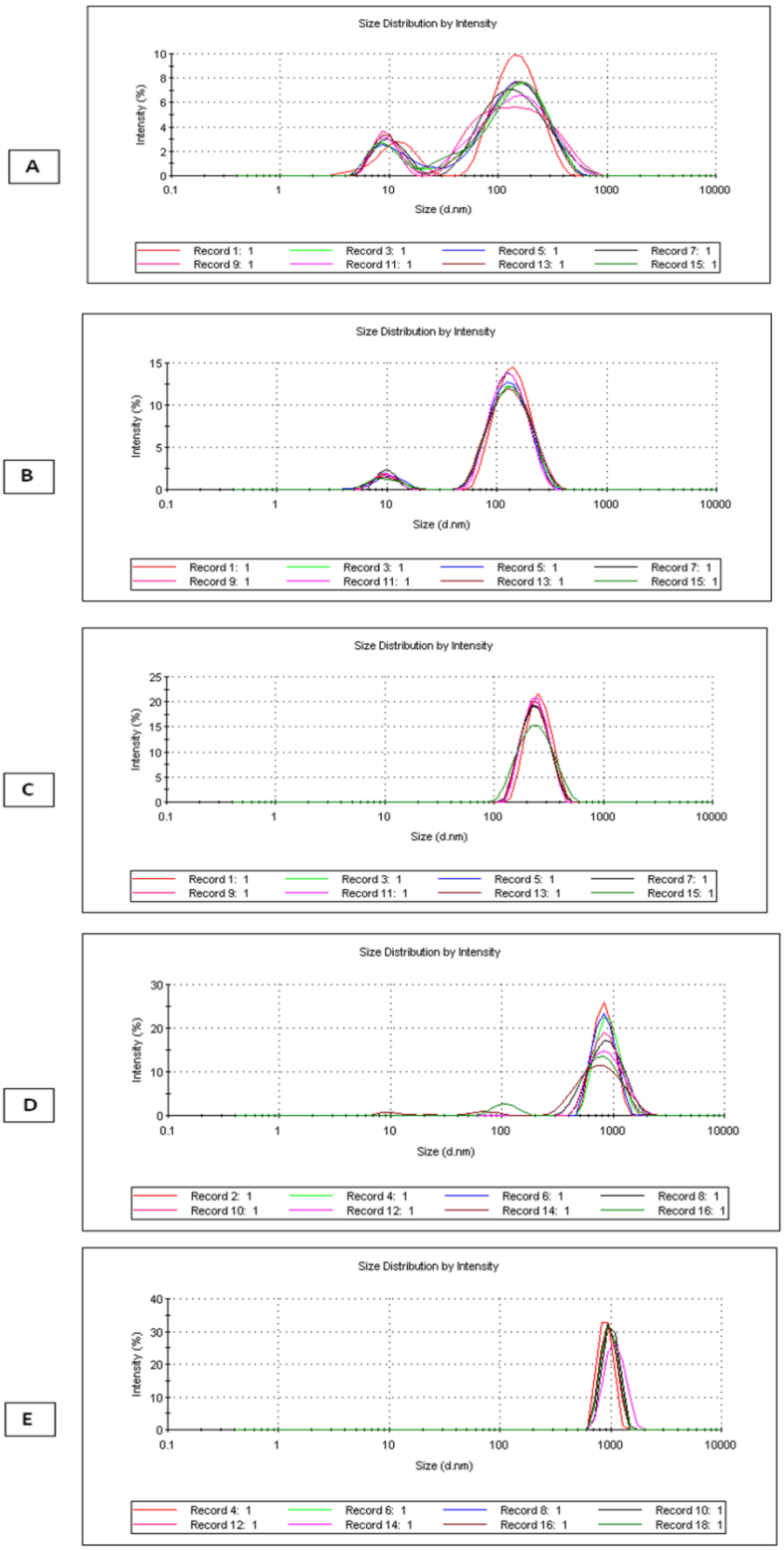

Figure 3-10: Examples of hydrodynamic diameter (intensity) distribution of polystyrene particles in DMEM/FBS$_{10\%}$ (A) 50nm , (B) 100nm, (C) 200nm, (D) 700nm, (E) 1000nm. The measurements were taken every half an hour over 4h and traces are representative of n=3 individual experiments. Figure reproduced from Khanbeigi *et al.* (169).

3.4.2 Comparison of Excel®- and ISDD-derived delivered dose values and experimentally derived cellular doses

A comparison of the Excel®-based (abbreviated as EXCEL) and ISDD-derived delivered dose values was carried out for polystyrene beads of 50, 100, 200, 700 and 1000 nm particles after 4 h exposure to the macrophages (Figure 3-11). It can be seen that the EXCEL predicted delivered dose values had very little discrepence from the ISDD predicted delivered dose values. The error bars on the EXCEL model represents the variance in the frequency distribution data obtained from particle sizing experiment conducted three times. The size of the error bars represent the polydispersity index of the particles so for PS 50, 700 and 1000 nm we get large error bars which confirms with the large PDI (>0.4) observed during particle characterization (Figure 3-9). Further, the contribution of sedimentation and diffusion separately to the total delivered dose has been plotted which shows that for PS particles less than or equal to 200 nm the transport is diffusion dominated whereas for PS 700 and 1000 nm the transport is sedimentation dominated.

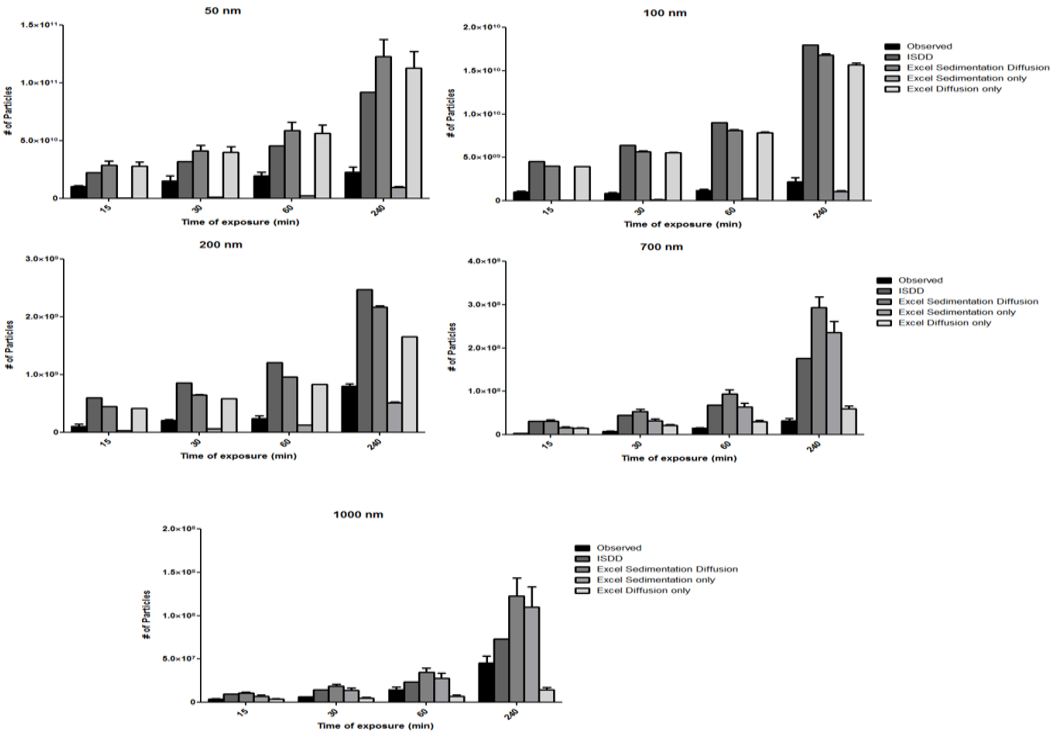

Figure 3-11: The measured cellular dose (particle #/cm^2) versus predicted delivered doses (particle #/cm^2) from the EXCEL (sedimentation + diffusion), EXCEL (sedimentation only), EXCEL (diffusion only) and ISDD models after exposing non-activated J774A.1 macrophages for 15 min to 240 min to 50, 100, 200, 700 and 1000 nm PS beads. The data for measured cellular dose has been taken from Khanbeigi *et al.* (169).

The Table 3:2 shows that the comparison of EXCEL model prediction for the delivered dose - sedimentation + diffusion, sedimentation only and diffusion only as percentage of ISDD predicted delivered dose values. It shows that the EXCEL model prediction shows little discrepancy from the ISDD predicted values. However, if we were to take into consideration only sedimentation or only diffusion then the EXCEL model would either underpredict (PS 50, 100 and 200 nm) or overpredicted (PS 700 and 1000 nm) the deposited dose.

Table 3:2: The EXCEL predicted delivered dose value as percentage of ISDD predicted values for PS 50, 100, 200 and 1000 nm particles over the 4 h period.

Particle Type	EXCEL (Sedimentation + Diffusion) % of ISDD	EXCEL (Sedimentation only) % of ISDD	EXCEL (Diffusion only) % of ISDD
PS 50	129.63	5.65	123.98
PS 100	90.08	3.07	87.01
PS 200	79.34	10.97	68.37
PS 700	130.30	87.72	42.99
PS 1000	139.90	109.25	30.99

3.5 Discussion

The aim of this study was to develop an EXCEL model as a quick and easy tool to calculate administered dose values for a corresponding delivered dose. The EXCEL-based platform offers greater flexibility and ease of access in comparison to the ISDD model which is run through Matlab®, a program which is expensive and unfamiliar to many biologists. However, the development of each model requires certain assumptions and these may explain the deviation between the EXCEL and ISDD model. As mentioned earlier in the introduction both the models take into account only the downward vector of diffusion. This is a reasonable assumption because diffusion is concentration driven phenomenon. Under the experimental conditions we have assumed uniform distribution of particles in each of the 1 μm cylinders (Figure 3-6). The only direction where concentration gradient exists is along the z- axis as the cells at the bottom of the plate act as a constant sink condition. However, along the x-axis and y-axis there is no concentration gradient (due to uniform particle distribution) so there will be no diffusion along these axes. We can also ignore the advective force as under normal cell culture conditions the plates are held at a constant temperature and are left undisturbed so the effect of advective forces would be negligible.

The primary reason for the minor discrepancy between the two models lies in the mathematical capability of the programs. Since Matlab is capable of high numbers of simultaneous calculations, it is possible for this program to solve

Equation 1, whereby gravitation settling and diffusion are calculated simultaneously for a single particle. In contrast, due to the computational limitations of Excel®, the gravitational effect and diffusion are applied separately on each particle and added together at the end. What is fascinating, is the particle size polydispersity dependency in the differences between the EXCEL and ISDD models. This polydisperisty of particle size distribution leads to the variance observed in the EXCEL predicted deposited dose. Taking the polydispersity into account the EXCEL predicted delivered dose as percentage of ISDD predicted dose show little discrepencey PS 50 (129% ± 23), PS 100 (90% ± 6), PS 200 (79% ± 6), PS 700 (130% ± 32) and PS 1000 (140% ± 36) which shows that the EXCEL predicted delivered dose values are approximately equal to the ISDD predicted delivered dose values. Does this factor make the EXCEL better or equivalent to ISDD? Yes, to a certain extent, the EXCEL model is equivalent, as the EXCEL predicted deliverd dose is equivalent to the ISDD predicted delivered dose values. However, the differences between the two programs are insignificant when put into the context of the comparisons to administered dose values. According to Khanbeigi *et al*. (169), ISDD predicts that ~8-15% of the administered dose of polystyrene beads 50-1000 nm actually reached the cell layer over the course of a 4 h incubation time period. With EXCEL this value range becomes ~7-21%. Thus, it may be clearly seen that researchers unable to access Matlab® to run ISDD predictions of the delivered dose would benefit from normalizing their data to the delivered dose using the EXCEL program, despite its limitations.

A drawback of the ISDD program is the reliance on mean hydrodynamic diameters, which can vary considerably depending on the selected measurement technique and conditions. The EXCEL program developed here takes into consideration the polydisperisty index of the particles in the relevant medium. Thus, the characterization of particle size in cell culture medium was important as the hydrodynamic diameter of the particle in the relevant medium was required to run both the models. The particle size measurements showed that there was a large increase in size for the 50 and 100 nm particles (Figure 3-9) as compared to the increase in size of 200, 700 and 1000 nm particles. This phenomenon may be explained by widespread particle aggregation for the 50 nm particles and limited aggregation for the 100 nm particles. Further, there is evidence for all particles that

formation of protein corona had occurred which causes stearic hindrance thus preventing the aggregation of particles (42, 177, 178). However, since the protein corona will affect the colloidal behaviour of the particles, it is very important to measure the hydrodynamic diameter in cell culture medium and use this diameter for input into particokinetic models of the delivered dose.

Some engineered nanomaterials may not necessarily undergo widespread aggregation, but may nonetheless show significant polydispersity. It was identified in this study that the ability to model the delivered dose for a non-aggregated, but polydisperse particle sample would increase the accuracy of the predicted delivered dose. This can be achieved using both programs by dividing the particle size distribution data into a frequency histogram. The corresponding delivered dose values can then be calculated separately for each fraction of the total particle population with a given particle size (following the size distribution curve; see Figure 3-12) and summated manually at the end. Using ISDD, this is a lengthy, multiple-step process. The advantage of the EXCEL program is that this process can be automated, whereby the operator only has to input the particle size distribution data.

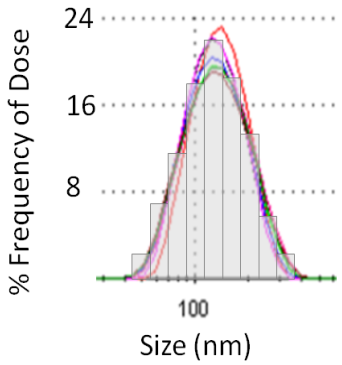

Class	Size (nm)	% of Dose	Delivered Dose (#/cm2)
1	75	2.0	1.5×10^{7}
2	80	7.3	9.8×10^{7}
3	92	12.4	1.4×10^{8}
4	101	19.0	5.5×10^{8}
5	143	23.8	3.4×10^{10}
6	162	17.2	1.2×10^{10}
7	205	10.3	6.6×10^{9}
8	250	7.0	1.2×10^{9}
9	308	1.0	7.5×10^{8}

Final Delivered Dose (#/cm2): 5.5×10^{10}

Figure 3-12: Corresponding delivered dose values calculated separately for each fraction of the total particle population with a given particle size following the size distribution curve.

As per recommendation of the examiners both data setsbased on gravity only and gravity + diffusion modelling of particle behavious in suspension are presented below (Figure 3-13) for comparison – the data from the original model which modelled the particle movement based on both gravity and diffusion and the new model as per examiner's recommendation which models the movement of particle based on gravity only.

Gravity Only vs. Gravity + Diffusion

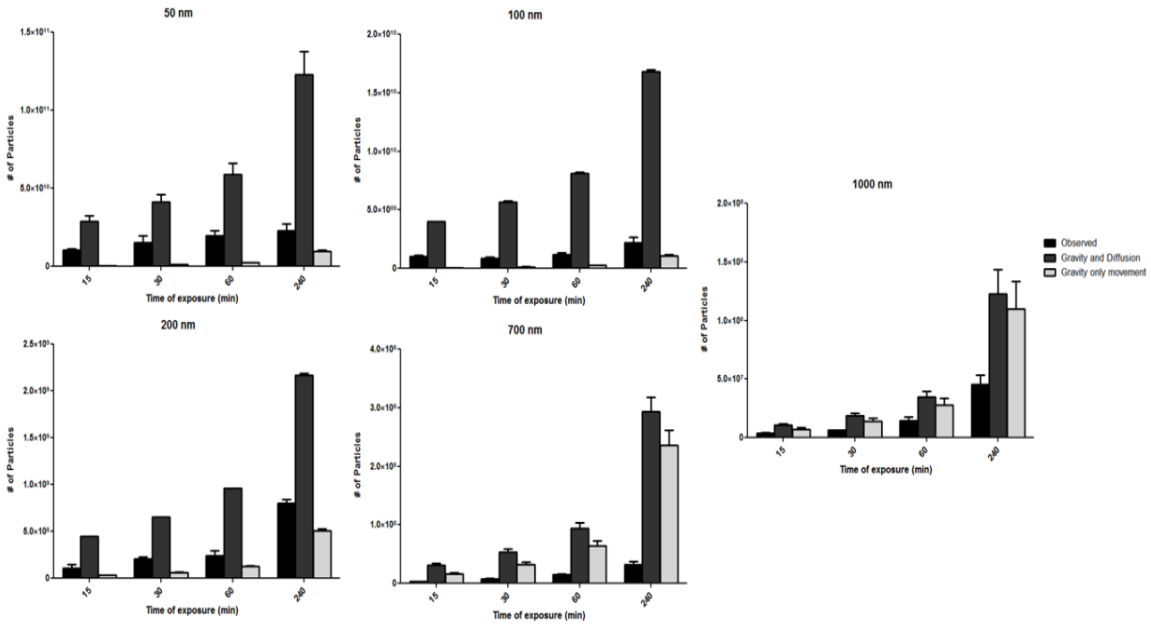

Figure 3-13: The graph shows a comparison of the measured particle uptake in J774.1 macrophage cells (black bars), the predicted delivered dose based on gravity + diffusion (dark grey bars) and the predicted delivered dose based on gravity only (light grey bar) of PS 50, PS 100, PS 200, PS 700 and PS 1000 nm particles at four different total exposure times of 15, 30, 60 and 240 minutes. The error bars on the observed data indicate mean ± SD of n = 6 individual experiments. The error bars on the modelled data represent the range of deposited dose obtained from three different particle size distribution data (obtained from particle characterization studies) input into the modelling program.

The graphs in Figure 3-13 depict two different models (Gravity + Diffusion vs. Gravity Only) for calculating a delivered dose value and compare these with measured particle uptake in macrophage cells. A discrepancy between the two models is observed, whereby the delivered dose value calculated by the Gravity Only model is lower than that of the Gravity + Diffusion model. The discrepancy between

the two model outputs is greater for smaller nanoparticles (i.e. PS 50, PS 100 and PS 200 nm) than for larger particles (700 and 1000 nm). The Stoke's Law of Sedimentation shows that sedimentation velocity is proportional to the square of the particle radius, meaning that the larger the particle, the greater number will sediment to the bottom of the cell culture dish within a given time period (e.g. 1-4 h in this study). Thus, the model of Gravity Only is suitable for particles with a large radius, a high density and longer incubation periods, as particle movement to the cell layer is defined primarily by sedimentation alone.

Table 3:3: Calculation of the percentage particle uptake in cells of PS 50 nm when normalised to delivered dose values calculated by two different methods: Gravity + Diffusion and Gravity Only

Exposure Time (min)	# of Particles Measured as Cellular Dose	# of Particles Predicted as Delivered Dose (Gravity + Diffusion)	# of Particles Predicted as Delivered Dose (Gravity Only)	% Uptake Normalised to Delivered Dose (Gravity + Diffusion)	% Uptake Normalised to Delivered Dose (Gravity Only)
15	1.03×10^{10}	2.88×10^{10}	6.14×10^{8}	36	1677
30	1.51×10^{10}	4.11×10^{10}	1.23×10^{9}	37	1227
60	1.95×10^{10}	5.88×10^{10}	2.45×10^{9}	33	796
240	2.28×10^{10}	1.23×10^{11}	9.82×10^{9}	18	232

Figure 3-13 and Table 3:3 show that cells exposed to 50, 100, and 200 nm particles took up a significantly higher number of particles than the Gravity Only delivered dose value predicted would reach the cell layer. Therefore, one or more further transport processes must be enabling small, low density particles to reach the cell layer during the short time periods covered in this study. For the purposes of this thesis, it was hypothesized that the published models (89, 90, 168) for delivered dose calculations, which incorporated gravity + diffusion, provide a good working approximation of a more accurate delivered dose value when compared to the Gravity Only delivered dose (and certainly when compared to the administered dose). Although these published models require assumptions to be made regarding particle diffusion, as discussed in (89, 90, 168), independent experimental evidence for the role of diffusion in small nanoparticle uptake into cells was provided by a recent study in *Nature – 'The effect of sedimentation and diffusion on cellular uptake of gold nanoparticles'* (179). In this study, the authors cultured the cells in two

different configurations – upright position which is what we commonly use in cell culture studies and inverted position (Figure 3-14).

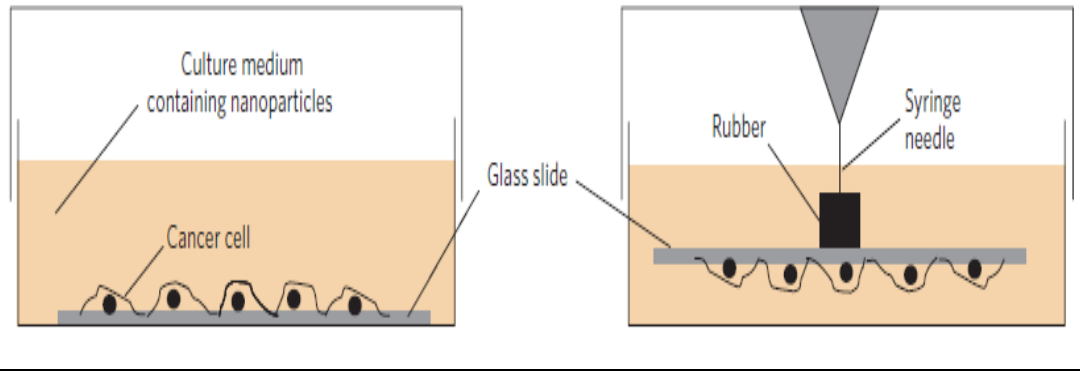

Figure 3-14: Schematic of upright (left) and inverted (right) configurations for measuring cellular uptake of gold nanoparticles as used by Cho *et al.* Image reproduced from Cho *et al.* (179).

The hypothesis of the authors was that cells in an inverted position would only take up gold nanoparticles (15, 54, and 100 nm) which would reach the cells by the process of diffusion. They found that while more NPs were taken up in the traditional configuration as compared to the inverted configuration, uptake was still observed in the inverted position. Notably, the uptake value of 15 nm gold nanoparticles was essentially the same for both configurations, which means that the transport of NP was predominantly diffusion driven. They also showed that increasing particle size from 15 nm to 54 nm to 100 nm led to an increase in disparity in particle uptake in the two positions. This disparity was thought to be due to the increased number of particles reaching the cell surface through sedimentation in the traditional upright well position. The disappointing aspect of this very creative approach, was that the authors did not try to predict the delivered dose in both configurations and evaluate the correlation with their experimental data.

Thus, comparison of our own uptake and modelling data with that reported in the relevant literature (89, 90, 168, 169, 179-181), indicates that the movement of particles in cell culture medium is governed by a transport process additional to gravity only movement.

3.6 Conclusion

In summary, this chapter describes the development of an EXCEL model to demonstrate that this predicts the deposited dose comparable to the ISDD model. Further refinements in the EXCEL model may be possible to improve it. However, this does not mean that the model in its current form cannot be used. Compared to the discrepancies with the administered dose values (especially for small or low density NPs), the deviations between the EXCEL and ISDD programs are very small. Since it is an easy and flexible program it can be more widely accessible to researchers and allow for greater variety of use, such as the easy calculation of delivered doses from non-aggregated, polydisperse particle size distribution data. The application of the particokinetics principal *in vitro* would give us a better understanding of the actual amount of NPs coming into contact with the cells and causing an effect. Just like physiologically-based pharmacokinetic modeling has led to better understanding of biological and toxicological effects of a drug and helped in promoting more accurate study design through better interpretation of data, particokinetics could lead to a better interpretation of toxicological data and the identification of the true biologically relevant dose of the particles coming in contact with the cell surface. This could improve the accuracy and scalability of *in vitro* systems. It might also lead to better correlation between *in vitro* and *in vivo* data thus reducing the animal use and reducing the cost of hazard screening of new materials.

Chapter 4

In vitro nanoparticle toxicology incorporating particokinetic modelling of dose

4.1 Introduction

There has been a rapid growth in the application of nanotechnology to consumer products which according to one estimate is projected to grow from $18 billion industry in 2008 to a $3 trillion industry by 2015 (5). Due to the special properties namely size, surface area and chemical reactivity; nanoparticles have been shown to be more toxic than their counter bulk materials. These findings have been reviewed in numerous publications (16, 28, 42, 161, 182). The traditional approach of using whole animal exposure models to assess the safety of all nanomaterials via all exposure routes will not be feasible given the rapid rate of development in the materials science sector (69, 70). Instead, the development of predictive *in vitro* models of nanotoxicology based on robust paradigms linking nanoparticle (NP) physicochemical properties and *in vivo* outcomes is the way forward to avoid the backlog. A number of studies (56, 61, 183, 184) have tried to develop inexpensive toxicological screening tools to correlate nanoparticle properties such as size, shape and surface area to biological activity observed *in vivo*. However, as outlined in a review article in *Nature* by Thomas Hartuang the most important point for any alternative (non animal based) testing method is the predictive power, reliability and the usefulness of these model systems (69). Despite all the research going on in the area of nanomaterial toxicity no conclusive information can be drawn. For example a search on PubMed for 'carbon AND nanotube AND toxicity' gave 664 results (PubMed accessed on 17th July 2012). A recent review by Kaiser *et al.* (185) performed a similar search and then analysed the paper identified according to their rigour. The results demonstrated a high number of publications with either incomplete information or contradictory results. It was highlighted that this was due

to lack of material characterization in many studies, different methods for preparations of nanomaterial suspensions, different duration of assays, different assay design, just to name a few factors. Importantly, it is often observed that crucial information regarding the applied concentrations is often missing which is important to reproduce the experiments in another laboratory. Thus, there is an obvious need for harmonization in characterization, suspension, application and assay of test particles.

4.2 Importance of particle characterization

A number of reviews have concluded that pulmonary exposures in rats to ultrafine/nanoparticles (i.e., defined here as <100 nm) produce enhanced lung toxicity when compared to equivalent mass doses of larger particle types of similar or identical composition (186, 187). In support of this hypothesis, one can compare the results of two 90-day inhalation studies that were conducted in three rodent species using pigment grade/fine (particle size ~380 nm; surface area = 6 m^2/g) or ultrafine/nano (particle size reported as 25 nm; 53 m^2/g) titanium dioxide particle-types. In the first study, rats, mice, and hamsters were exposed to fine TiO_2 particles at aerosol concentrations of 10, 50, or 250 mg/m^3 (188). In a second study, the same rodent species were exposed to ultrafine (i.e., nano) TiO_2 particulates at exposure concentrations of 0.5, 2, or 10 mg/m^3 (189) and evaluated at several time points postexposure. The results of the two studies demonstrated that (1) rats were the most sensitive rodent species for lung effects and (2) the effects measured at 250 mg/m^3 in the fine particle study were not dissimilar from those observed at 10 mg/m^3 in the ultrafine/nanoscale TiO_2 study. Accordingly, comparing the results of both studies would suggest that, on a mass basis, the effects measured following ultrafine/nanoscale TiO_2 exposures were ~25 times greater than those observed for the fine/pigment-grade TiO_2 particle types. However, a number of other factors require consideration before drawing this conclusion. These include the following issues:

(1) Surface area indices of the ultrafine/nanoscale TiO_2 particle-types were significantly greater compared to the fine-sized TiO_2 particulates used in the study (53 m^2/g vs 6 m^2/g).

(2) The crystal structure of the ultrafine/nano TiO_2 particles was composed of 80% anatase and 20% rutile, whereas the fine TiO_2 samples were 100% rutile.

(3) The measured surface reactivity index (i.e., delta b* -using the vitamin C assay) of the nanoscale TiO_2 particle types was substantially enhanced compared to the pigment-grade TiO_2 samples (delta b* values of 23.8 vs 0.4, (190)).

This is just one example to demonstrate the importance of robust particle characterization in correct interpretation of toxicology data obtained from both *in vitro* and *in vivo* studies. In an interesting article by Warheit *et al.* (86) the importance of particle characterization in the interpretation of nanotoxicity data obtained from *in vitro* or *in vivo* studies was further highlighted. In subsequent sections important particle characterization parameters raised in this article would be discussed.

4.2.1 Size

The effective size of the NP species becomes a crucial parameter in the lung because it directly influences their clearance and bio-distribution. It has been shown that the clearance by alveolar macrophages is dependent on particle size. Thus, when investigating size-dependent effects (191-193) the size distribution of the NPs in relevant biological media needs to be described (61, 193, 194). In a study investigating oxidative damage caused by TiO_2 particles on BEAS-2B cells by Gurr *et al.* (84) it was concluded that oxidative and genotoxic potential of nanoparticulate forms of TiO_2 was greater than that of their larger counterparts. The authors exposed BEAS-2B cells to 10, 20 and 200 nm anatase TiO_2 NPs. The results showed that 10 and 20 nm NPs in the absence of photoactivation induced oxidative DNA damage, lipid peroxidation, and micronuclei formation, and increased hydrogen peroxide and nitric oxide production in BEAS-2B cells, whereas 200 nm particles did not induce any oxidative damage in the absence of photoactivation. The authors concluded that the smaller the particle, the higher potency it had to induce oxidative stress in the absence of photoactivation. However, there was no particle characterization performed in this study. The authors only mentioned that TiO_2 NPs had an approximate size of 200 nm from the information supplied by the manufacturers. It is

a known fact that particles seldom retain their 'original' size in dry state when they are put in cell culture medium (195). In the study by Murdock *et al.* it was observed that the size of 10 nm and 16 nm TiO_2 particles in medium without serum was 1790 nm and 1810 nm. This size was similar to the aggregate size of 100 nm TiO_2 particles in medium without serum (2500 nm). This agglomeration in biologically relevant medium raises concern about concluding size- or surface area-dependent toxicity *in vitro*. One of the most commonly used particle size analysis techniques is dynamic light scattering (DLS) also known as photon correlation spectroscopy. It is a non-invasive, useful technique to evaluate particle size and size distribution of NPs in solution. However, DLS cannot distinguish between mixed particle population nad is biased towards larger size as the amount of light diffracted from a larger particle will be considerably more. These shortcomings have been highlighted by Filipe *et al.* (196) who used polystyrene beads of 100 and 400 nm mixed in different proportions (3:1, 6:1, 15:1, 150:1 and 300:1) to demonstrate that DLS was unable to resolve peaks of polydisperse samples and it was not possible by DLS to separate the two bead sizes. Another relevant technique used for particle size analysis is nanoparticle tracking analysis (NTA) which was compared against DLS by Filepe *et al.* (196) to demonstrate the better resolution power of NTA when polydisperse samples are being analyzed. However, the analysis by NTA is dependent upon the ability to resolve the video and track each particle individually. This usually means that a NTA could be used for low concentrations of particle suspension as for the study by Filepe *et al.* the PS 100 nm supplied by the manufacturer had to be diluted 1:100,000. In case of characterizing particles prior to *in vitro* toxicity testing it would be more relevant to measure particle size at a concentration corresponding to that applied on the cells. Other relevant techniques are scanning electron microscopy, transmission electron microscopy and atomic force microscopy. However, manual measurements from thousands of micrographs need to be done before gaining statistically significant information. Another limitation is the extensive preparation and fixation which could result in morphological change in the nature of the particle also this preparation may not represent the true state of particle in a biologically relevant medium.

4.2.2 Surface area

The choice of dose metric (mass dose, surface area dose or number dose) has been under debate as highlighted by Oberdorester *et al.* (197). In a study by Oberdorster *et al.* (166) the authors exposed rats for 24 h to fine (~ 250 nm) and ultrafine (~20 nm) TiO_2 NPs by intratracheal instillation and the results demonstrated the significantly greater inflammatory potency (as measured by polymorphic nuclear cell (PMN) recruitment) by of the ultrafine particles. The same group analysed the data in a subsequent study (165) and expressed the PMN recruitment in terms of particle surface area. When the instilled doses were expressed in terms of surface area the responses of the ultrafine and fine TiO_2 particles fell on the same dose-response curve as seen in Figure 3-1.

In another study by Hohr *et al.* (198) the authors exposed rats for 16 h to fine (180 nm) and ultrafine (20-30 nm) TiO_2 NPs by intratracheal instillation at four different surface area dose of 100, 500, 600 and 3000 cm^2 and equivalent mass dose of 1 or 6 mg. The surfaces of the particles were modified by methylation to achieve a hydrophobic surface or left unmodified and hydrophilic. The acute inflammatory response in the rat lung was measuring the PMN recruitment in the brochoalveolar lavage fluid. The results showed that PMN influx correlated with the surface area dose. It also showed that at low doses (1mg or < 500 cm^2) methylation (hydrophobic surface) seemed to suppress inflammatory activation although this was not statistically significant. The authors concluded that surface area of the instilled TiO_2 NPs determined the acute pulmonary inflammation. However, it must be noted that the authors did not present any experimental data to confirm the surface modification.

4.2.3 Surface charge/ zeta potential

In a recent study by Ruenraroengsak *et al.* (65) the authors exposed human alveolar epithelial type-1 cells for 4 h or 24 h to polystyrene NPs of 50 nm and 100 nm. The surface of these particles were amine modified (positively charged), carboxyl modified (negatively charged) or unmodified. The amine modified 50 nm particles were found to be consistently more cytotoxic followed by unmodified and then carboxyl modified particles. The cytotoxicity was measured by MTT assay,

LDH release, Capsase-3/7 activation and activation of cytokine release (IL-6). The authors suggested that the increased cell death and apoptosis observed in TT1 cells exposed to 50 nm amine-modified NPs in the present study may be due to increased depletion of significant medium nutrients. A unique finding was that the toxic effect of the amine-modified nanoparticles was associated with severe membrane damage and the formation of holes in the alveolar epithelial cells. The authors suggested that the alteration in cell membrane structure may be caused by electrostatic attraction between amino surface groups of the particles and phospholipids of cell membranes, possibly causing transformation of the lipid bilayer of the cell to the liquid phase.

However, in another study by Mura *et al.* (199) the authors exposed Calu-3 cells to surface modified (positive using chitosan, neutral using PVA or negative using PF68 stabilizer) PLGA NPs for 4 and 24 h. The particles were characterized for their size and zeta potential in serum supplemented cell culture medium. The cell viability and cytokine release from the Calu-3 cells were used as cytotoxicity markers. The authors found no influence of surface chemistry or surface charge on the cytotoxicity of PLGA NPs. It must be noted that the particle used by Mura *et al.* (197) was manufactured using poly(lactic-co-glycolic acid) (PLGA) and chitosan coating was applied for providing the particle with a positive charge whereas Ruenraroengsak *et al.* (65) used amine modified polystyrene particles to provide the positive charge with no chitosan coating. This difference in the nature of the particles does nto allow for direct comparison between the results of the two studies.

4.2.4 Surface reactivity

Recently Sayes *et al.* (200) studied the catalytic properties of anatase and rutile nano-TiO_2 and correlated these properties to the *in vitro* cytotoxic responses of different nano-TiO_2 crystal structures on both human dermal fibroblasts and human lung carcinoma cells using various biochemical endpoints (MTT, LDH, IL-8 production). These investigators concluded that nano-TiO_2 particles in the anatase crystal phase were superior catalysts, generators of reactive species, and more cytotoxic when compared to the rutile particle-types tested. The investigators determined the reactive species formation *ex vivo* by two different methods – first the chemiluminescence of luminol was used to qualitatively probe the production of reactive species over 20 min and second the decay of photograde organic dye Congo

Red was followed via absorption spectroscopy and correlated to rate constants for radical production in water. The differences in the cytotoxic response of the nano-TiO_2 tested were due to the anatase nano-TiO_2 being more reactive as measured by the production of reactive species *ex vivo*, and not because of differences in surface area. However, since the particles aggregated increasingly in the cell culture medium as suggested by the investigators, size of the particle influencing the cytotoxic endpoints measured cannot be completely ruled out. In another study by Warheit *et al.* (190) the authors exposed rats to three different types of ultrafine TiO_2 particles. UF-1 and UF-2 were rutile type and differed in the surface coating. UF-1 was coated with alumina where as UF-2 was coated with silica and alumina. The third type designated as UF-3 consisted of 80% anatase/20% rutile and were not coated with anything. The particle sizes as determined in a 0.1% tetrasodium pyrophosphate buffer using DLS of UF-1, UF-2 and UF-3 were 136, 149.4 and 129.4 nm respectively. The average surface areas in dry state as determined by BET of UF-1, UF-2 and UF-3 were 18, 35.7 and 53.0 m^2/g respectively. The chemical reactivity of the samples was measured using an ascorbic acid depletion assay. This assay measures the chemical reactivity of the sample toward an anti-oxidant, specifically ascorbic acid. With greater chemical reactivity, the yellowing of the test sample will increase providing a higher surface reactivity index (Δb^*). The chemical reactivity order of the three particle type was UF-3>UF-1>UF-2. The authors examined BAL fluid after intratracheal instillation of the particles for PMN influx, LDH and microprotein value (as an indicator of enhanced cellular permeability) after 24 h, 1 week, 1 month and 3 months post exposure. Further cell proliferation and histopathological examination was carried out on the rat lungs. UF-1 or UF-2 did not produce sustained adverse pulmonary effects in any of the endpoints utilized in this study. However, exposures to uf-3 TiO_2 particles produced inflammation and cytotoxicity responses through 1 month post-exposure as well as enhanced cell proliferative labeling and histopathologically adverse lung tissue effects when compared to PBS vehicle controls. The authors suggested the difference in chemical reactivity to be the reason behind this observation. The chemical reactivity assay basically represents an indirect measure of the number of active sites (sites on the particle's surface which can initiate the chemical transformation of molecules). Given this reactivity, UF-3 TiO_2 particles are likely to produce more reactive species than

either of the UF-1 or UF-2 TiO_2 particle-types, thus possibly contributing to the sustained *in vivo* cytotoxicity and inflammation measured through 1 month post-exposure. However, the authors have not taken into account the measured difference in the specific surface areas of the three particles. For the same mass of particles the UF-3 type has almost 3 times the surface area of UF-1 and 1.5 times the surface area of UF-2. Given this difference in surface area, it would be difficult to conclude if surface reactivity was the only contributing factor towards the difference seen in cytotoxicity.

The above mentioned examples highlight the importance of particle characterization in correct interpretation of *in vivo* toxicity and *in vitro* cytotoxicity data. Thus one of the aims of this chapter was to rigorously characterize the panel of model nanomaterials prior to cytotoxicity testing.

4.3 Need for nanoparticle toxicity testing

In 1990 two important papers were published in the *Journal of Aerosol Science* demonstrating on a mass for mass basis, titanium dioxide and aluminum dioxide NPs eliciting a significantly greater inflammatory response in the lungs of rats as compard to larger particles with the same chemical composition (201, 202). These two studies challenged the long held assumption that response to particulate exposure could be understood in terms of chemical composition and suggested unusual biological activity associated with NPs. As research began to focus on the potential risk associated with NP, the term ‘nanotoxicology’ was formalized in an editorial in *Occupational and Environmental Medicine* by Donaldson *et al.* (19).

4.3.1 Cell-based assays for evaluating nanotoxicology

There are many assays used *in vitro* for evaluating the toxicity of NP. The assays used for assessing cell viability are MTT (3-(4,5-dimethylthiazol-2-yl)-2,5-diphenyltetrazolium bromide) assay (203) and variations of of this assay (e.g. MTS, XTT, WST-1, etc.). These assays principally determine cell viability through determination of mitochondrial function by measuring the activity of mitochondrial enzymes such as succinate dehydrogenase. Another equally common measure of cytotoxicity is the lactate dehydrogenase (LDH) assay. LDH is an enzyme that is

normally found within the cell cytoplasm. Reduced cell viability leads to an increase in the leakiness of the plasma membrane and therefore release of the LDH enzyme into the cell culture medium. Trypan Blue exclusion has been used in a small number of studies to assess the toxicity induced by particles. Trypan Blue is a large negatively charged molecule. Cells with an intact cell membrane are able to prevent Trypan Blue uptake and therefore appear clear by light microscopy. In contrast, dead cells, which are unable to maintain an intact plasma membrane, are colored blue within seconds of exposure to the dye. The fluorescent dye propidium iodide (PI) works in a similar way to Trypan Blue, staining the DNA/nucleus of dead cells due to the heightened plasma membrane permeability. This staining is used as an indicator of cell death via necrosis. It is relatively common to combine PI staining with annexin V–FITC (fluorescein isothiocyanate). Annexin V (AV) binds to phosphatidyl serine on the surface of apoptotic cells. Using flow cytometry of dual-stained cells allows the identification of both apoptotic and necrotic cell death within the same cell population. Another way of assessing cytotoxicity is by the assessment of cellular adenosine triphosphate (ATP) content. This is a relatively sensitive assessment of cell viability and kits using luminescence to assess the ATP content of cell extracts are available, and the assay can be conducted in a 96-well plate format.

Apart from cell viability the toxicity from NP can also be quatified using assays to measure oxidative stress in the cells. The fluorescent dye 2,7-dichlorofluorescin (DCFH) or dihydrorhodamine-123 can be used to measure ROS inside the cells after exposure to NP and the fluorescence can be measured by fluorimetric or by flow-cytometric techniques. Other method for measuring oxidative stress is to measure redox sensitive antioxidants such as glutathuione (GSH) using the *o*-phthalaldehyde (OPA) method (204) where the GSH in the cellular extract forms a fluorescent GSH-OPA adduct that can be quantified by fluorimetry. Measurement of mRNA expression changes of oxidative stress-dependent genes has also been put forward as a sensitive marker of oxidative stress induced by particles and nanoparticles; among these, the best-described is heme oxygenase-1 (HO-1) (38).

Another way to quantify NP toxicity is to measure inflammatory cytokine and chemokine release from the cells after exposure to NP. Examples of cytokines and chemokines associated with inflammation include tumour necrosis factor alpha

(TNFα), interleukin (IL)-IL8, IL1α, IL1β and IL6. After exposure to NP the cells release cytokine protein into the cell culture medium. The medium can then be extracted, and centrifuged to remove cellular debris and particles, and then the cytokine protein content assessed by enzyme linked immunosorbent assay (ELISA). ELISA techniques are well-established, reliable, and usually relatively sensitive. Alternatively, cytokine mRNA expression can be measured as an indicator of alterations at the gene expression level.

4.3.1.1 MTT assay

The MTT assay (203) is a colorimetric assay which is used to measure the metabolic activity of the cells. The mitochondrial reductase enzyme reduces the yellow MTT salt to formazan dye which has a purple colour. This allows the investigator to assess the viability and proliferation of cells. In this case, it is used to determine the cytotoxicity of nanoparticles, since these nanoparticles are thought to interfere with cell viability and growth. MTT (3-(4,5-dimethylthiazol-2-yl)-2,5-diphenyltetrazolium bromide), a yellow tetrazole, forms purple formazan when it is reduced in living cell). Sodium dodecyl sulphate (SDS), a solubilising agent, is then used to dissolve the insoluble purple formazan, which yields a coloured solution. A spectrophotometer is then used to measure the absorbance of this coloured solution at 570 nm.

Although this is one of the most commonly used assays for cell viability it is important to include appropriate controls to prevent the interference of particles or cell debris from spectrophotometric analysis. In the final stage of MTT assay the cells are solubilised using SDS or DMSO which generates a suspension containing cell debris, NP and formazan. It has been suggested by Stone *et al.* (205) to centrifuge the test plate, transfer the supernatant into another test plate for measurement of absorbance. Another possible problem may be the interaction of NP with the dye as demonstrated in the cytotoxicity evaluation of single-walled carbon nanotubes (SWCNTs) by Worle-Knirsch *et al.* (206). The authors showed that the SWCNTs attached to the MTT-formazan crystals that were formed after the reduction of MTT and stabilized their chemical structure so that the crystals were not soluble in the solvents used to dissolve the MTT-formazan, such as 2-propanol,

hydrochloric acid, sodium dodecylsulfate or acetone. As a result, reduced cell viability was observed in the MTT test.

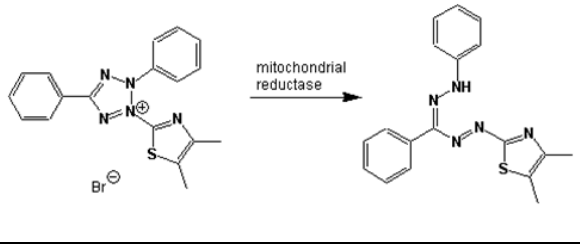

Figure 4-1: Schematics of MTT reaction (207).

4.3.1.2 LDH assay

Cell death or cytotoxicity is classically evaluated by the quantification of cell membrane damage. The LDH assay is based on the measurement of activity of lactate dehydrogenase (LDH) released from damaged cells. LDH is a stable cytoplasmic enzyme present in all cells and rapidly released into the cell culture supernatant upon damage of the plasma membrane. The loss of intracellular LDH and its release into the culture medium is an indicator of irreversible cell death due to cell membrane damage. This assay, therefore, is a measure of the membrane integrity. LDH activity can be determined by a coupled enzymatic reaction: LDH oxidizes lactate to pyruvate which then reacts with tetrazolium salt INT to form formazan. The increase in the amount of formazan produced in culture supernatant directly correlates to the increase in the number of lysed cells. The water-soluble formazan dye is detected by spectrophotometry (490 nm).

However, as with MTT assay NPs could interfere with the LDH assay. In a recent study by Han *et al.* (208) copper (Cu-40, 40nm), silver (Ag-35, 35nm; Ag-40, 40nm), and titanium dioxide (TiO_2-25, 25nm) NPs were examined for their potential to interact with LDH assay. The authors found that Cu NP and Ag NP interacted with LDH assay by inactivating LDH and caused a decrease in LDH activity over time whereas TiO_2 NP did not inactivate LDH.

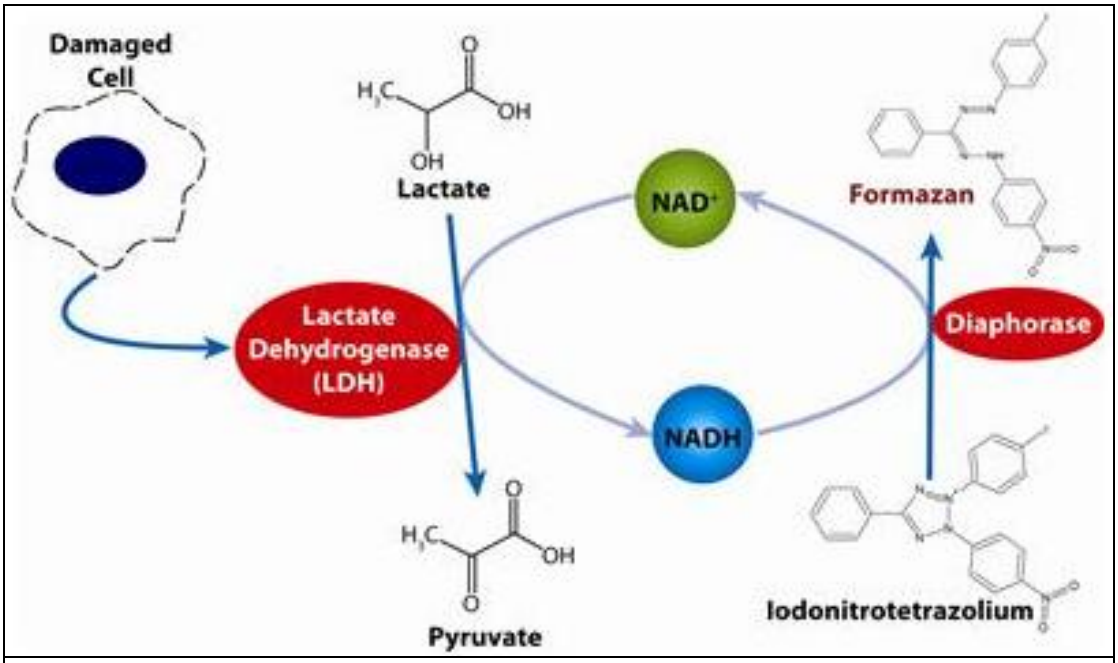

Figure 4-2: Schematics of LDH reaction (209).

The choice for the use of a particular cytotoxicity assay is dependent upon the toxic effect of interest. Apart from choosing the correct assay one has to take into account all the potential interferences to avoid obtaining false-positive or false-negative results. If these potential interferences are controlled for, the MTT or LDH assay can be used successfully to address nanoparticle-induced toxicity (210).

For the present work MTT assay and LDH assay were chosen and the experiments were performed according to the plate design shown in Figure 4-3. These assays have been widely used, sample preparation is not tedious, are quick and inexpensive. In contrast, the cost of screening six different NPs on two different cell lines using two different exposure times using a more sensitive assay such as PI staining with annexin V, inflammatory cytokine and chemokine analysis and oxidative stress generated was beyond the budget of the project.

Row/Column	1	2	3	4	5	6	7	8
A	Cells Media	Cells Sample 1 Dilution 1	Cells Sample 1 Dilution 2	Cells Sample 1 Dilution 3	Cells Sample 1 Dilution 4	Cells Sample 1 Dilution 5	Cells Sample 1 Dilution 6	Cells Triton X 1%
B	Cells Media	Cells Sample 1 Dilution 1	Cells Sample 1 Dilution 2	Cells Sample 1 Dilution 3	Cells Sample 1 Dilution 4	Cells Sample 1 Dilution 5	Cells Sample 1 Dilution 6	Cells Triton X 1%
C	Cells Media	Cells Sample 1 Dilution 1	Cells Sample 1 Dilution 2	Cells Sample 1 Dilution 3	Cells Sample 1 Dilution 4	Cells Sample 1 Dilution 5	Cells Sample 1 Dilution 6	Cells Triton X 1%
D	Media	Media Sample 1 Dilution 1	Media Sample 1 Dilution 2	Media Sample 1 Dilution 3	Media Sample 1 Dilution 4	Media Sample 1 Dilution 5	Media Sample 1 Dilution 6	Media Triton X 1%

Figure 4-3: Plate design for NP toxicity testing experiments. The row D of the 96-well plate contained no cells and helped in accounting for interaction between NP and dye.

Thus MTT and LDH assay were used with appropriate controls to assess the toxicity of NPs.

4.4 Aims and objectives

The aim of this chapter was to apply particokinetic modelling (developed in Chapter 3) to the assessment of *in vitro* cytotoxicity of rigorously characteried reference metal oxide nanoprticles, reference drug delivery like polystyrene nanoparticles and in-house developed lipid nanocapsules (LNCs) on the human alveolar epithelial cell line, A549, and the human nasal epithelial cell line, RPMI 2650.

4.5 Materials and methods

4.5.1 Nanomaterials

Polystyrene microsphere aqueous suspensions (Thermoscientific; 1% solids by weight and a density of 1.06 g/mL) were purchased with manufacturer reported

diameters of 50 and 200 nm. Reference metal oxide nanoparticles composed of CuO and TiO_2 were purchased from NanoScale Material Inc., USA with manufacture reported properties shown in Table 4-1.

Table 4-1: Properties of CuO and TiO_2 NP as supplied by manufacturer

Properties	NanoActive Copper Oxide	NanoActive Titanium Oxide
Appearance/Color	Black Powder	White Powder
Specific Surface Area(BET) (m^2/g)	≥ 65	≥ 500
Crystallite Size (nm)	≤ 8	Amorphous
Average Pore Diameter (Å)	85	32
Total Pore Volume (cc/g)	≥ 0.1	≥ 0.4
Bulk Density (g/cc)	1.65	0.6
True Density (g/cc)	5.7	3.7
Mean Aggregate Size, d0.5 (μm)	6	5
Moisture Content (%)	≤ 4	≤ 4
Loss on Ignition (%)	≤ 4	≤ 12
Content (Based on Metal) (%)	> 99.6	> 99.999

LNCs were prepared at two sizes (50 and 150 nm) by Dr. Marie-Christine Jones using a phase-inversion process developed by Heurtault *et al*. (211). In brief, Labrafac (Gattefossé, Saint-Priest, France), Lipoid S75-3 (Lipoid, Ludwigshafen, Germany), Solutol HS15 (BASF, Ludwigshafen, Germany) and a 3% w/w NaCl solution were stirred at room temperature (for composition see Table 4-2). The resulting coarse emulsion was heated to 85˚C under constant stirring then cooled back to 60˚C. This heating-cooling cycle was repeated twice more (85-60-85) before adding ice cold water to the emulsion maintained at 72˚C. The LNCs were then left under stirring at room temperature for 5-10 minutes. Excess Solutol HS15 was removed from LNC preparations using dialysis in combination with BioBeads® (BioRad Laboratories, USA) until the residual concentrations were: LNC 50 1.5 mg/mL and LNC 150 <0.5 mg/mL.

Table 4-2: Composition of LNC 50 and LNC 150					
Particles	Labrafac (%w/w)	Lipoid (%w/w)	Solutol HS15* (%w/w)	3% Saline (%w/w)	Water
LNC 50	17	1.75	17	64.25	2x volume
LNC 150	25	1.5	8.5	65	3.5x volume

*Prior to purification

4.5.2 Methods

4.5.2.1 Cell culture medium (CCM) and respiratory tract lining fluid (RTLF) characterization

Total Protein Content: RTLF samples were kindly provided by Dr Anders Blomberg of the University Hospital, Umea. Ethical approval for the study examining different modes of airway sampling was provided by the local research Ethics Committee (University of Umea), in accordance with the Declaration of Helsinki, and the written informed consent of all volunteers. These samples were generated form large volume BAL-fluid samples obtained from each of the subjects and concentrated using both 9K iCON and 3K microcon protein concentrators. RTLF and CCM were characterized by measurement of total protein content using the method of Smith *et al.*, 1985 adapted for use on a microplate reader. Briefly, total protein was measured by reaction with bicinchoninic acid and 4% copper (II) sulphate, following the method of Smith *et al*., 1985.

Dynamic Viscosity: The viscosity of RTLF and CCM supplemented with 2% FBS was measured at 37°C using an AMVn Automated Micro Viscometer (Anton Parr). Briefly, the samples were loaded into the microcapillary and the viscosity was determined in triplicate according to Höppler's falling ball principle.

4.5.2.2 Particle size measurement in water, CCM and RTLF

Particle size was measured in four different medium – water, CCM without serum, CCM with 2% serum and concentrated (1.2 mg/ml total protein) human RTLF. The particles were prepared at a concentration of 0.17 mg/ml in the respective medium and probe sonicated at 40Hz for 5 min to break up any aggregates. The particle size was then measured using dynamic light scattering (ZetasizerNano,

Malvern, UK), every 30 minutes, at 37°C for a period of 6 h. The samples were prepared in water, CCM without phenol red supplemented with 2% (v/v) FBS, 1% (v/v) non-essential amino acids, 0.1% (v/v) gentamicin, and 1% (v/v) L-glutamine ($CCM_{FBS2\%}$) and CCM without phenol red supplemented with 1% (v/v) non-essential amino acids, 0.1% (v/v) gentamicin, and 1% (v/v) L-glutamine (CCM) at a concentration of 0.17 mg/ml. The instrument parameters used for measurements in cell culture media were: refractive index of $CCM_{FBS2\%}$ = 1.337 (176), temperature = 37°C, dynamic viscosity of $CCM_{FBS2\%}$= $0.734x10^{-3}$ Pa s.

4.5.2.3 Zeta potential measurement in water and CCM

The zeta potential of particle was measured in water and CCM supplemented with 2% v/v serum. The particles were suspended in the respective medium at a concentration of 0.17 mg/ml and the zeta potential was measured using laser Doppler anemometry (ZetasizerNano, Malvern, UK) at 37°C. Zetasizer Software 6.20 was used to analyse the data.

4.5.2.4 Oxidative potential measurement

Preparation of chelex – resin treated water: 60g of Chelex® 100 sodium form were mixed in 2L of 18.2Ω ultra-water, covered and stirred at room temperature. The contaminated Chelex®-resin was removed by vacuum filtration through a Wattman 0.45 µm cellulose nitrate membrane and the water adjusted to pH7 with 1M HCl. To avoid further metal contamination which is likely to occur during the use of laboratory glassware the treated water was routinely stored in a sealable plastic container and finally stored in the fridge for up to 1 month.

NP dilution: NP stock solutions were prepared at 150 µg/ml in 5% MeOH in chelex water pH7 and vortexed for 10 minutes and probe-sonicated for 30 seconds. Then the solutions were diluted with Chelex water to a concentration of 12.5 µg/ml.

Ascorbate solution preparation: A concentrated 2mM ascorbate solution was prepared by the addition of 70.44mg of ascorbate to 180ml of Chelex®-treated water, pH7. The pH of the solution was then adjusted to pH7 with the use of 1M NaOH. The solution was then made up to a final volume of 200ml with Chelex®-

treated water (pH7) using a volumetric flask. Aliquots of 2.5ml were then stored at –80°C until day of exposure.

NPs exposures: All NPs exposures were performed in triplicate in UV-transparent 96 well flat-bottomed plates (Greiner bio-one) at a final volume of 200 µl. 160 µl of the diluted NP suspensions (12.5 µg/ml) were added to the plate in triplicate and a further 20 µl of Chelex-treated water was added to each. Immediately prior to the addition of the ascorbate to each assay well, the plate was pre-incubated for 10 minutes at 37°C in a plate reader (Spectra Max 190) and during the exposure the plate was maintained at this temperature. Exposure was initiated by the addition of 20 µl of the ascorbate stock (2mM) into each well of NP, giving a final concentration of 200 µM ascorbate and 10 µg/ml NPs. After addition of ascorbate, the concentration remaining in each well was monitored and recorded every 2 minutes for a period of two hours by measuring the absorbance at 265nm with the use of Softmax Pro software. The rate of ascorbic acid depletion was then determined by performing a linear regression through the initial part of a concentration verses time plot using Prism (version 5.0). This was performed for each of the triplicates and the rate of ascorbic acid depletion was finally expressed as mean mol s^{-1} x 10^{-9} depletion of ascorbate ± standard deviation.

AA depletion assay using inhibitors: The mechanisms driving the oxidative activity can also be examined by use of the ascorbate depletion assay by the addition of the transition metal chelators and free radical scavengers.

All NP exposures with inhibitors are performed in triplicate in **UV** 96 well flat-bottomed plates (Greiner bio-one) at a final volume of 200 µl. 160 µl of the diluted PM suspensions are added to the plate in triplicates. NP samples are pre-incubated in the presence or absence of inhibitor by the addition of 20 µl of 2mM DTPA inhibitor stock to one set of triplicates. Immediately prior to the addition of the ascorbate to each assay well, the plate was pre-incubated for 10 minutes at 37°C in a plate reader (Spectra Max 190) and during the exposure the plate was maintained at this temperature. Exposures were initiated by the addition of 20 µl of the ascorbate stock (2mM) into each well NP, giving a final concentrations of 200 µM ascorbate and 10µg/ml NP and final concentrations of inhibitors of 200 µM DTPA. The rate of ascorbate depletion was determined as above.

4.5.2.5 Culture of A549 and RPMI 2650

Human alveolar epithelial cells (A549, ATCC, USA) and human nasal epithelial cells (RPMI-2650, ATCC, USA) were cultured in $CCM_{FBS10\%}$ in a humidified incubator at 37°C and 95% air and 5% CO_2. All experiments were performed on cells seeded at a density of 30,000 cells/cm^2 in $CCM_{FBS2\%}$.

4.5.2.6 Nanoparticle preparation and exposure

For all cell culture experiments, particles were sterilized by dry heat sterilization at 180°C for 20 minutes (Memmert, Schwabach, Germany) and then suspended at 1.7 mg/mL in $CCM_{FBS2\%}$. The suspension was sonicated for five minutes using a probe sonicator at 40 Hz (Vibra Cell Sonics Material Inc. Danbury, CT, USA) and immediately diluted with $CCM_{FBS2\%}$ to the desired administration dose. The choice of mass-based administration dose range (0.00526, 0.0526, 0.526, 5.26 and 52.6 µg/cm^2 ≈ 0.0017 to 17 µg/100 µl corresponds to the following theoretical particle surface area (administered) doses: 0.0002 - 10 cm^2/cm^2 depending on particle type. These concentrations were chosen based on the findings of Faux and co-workers (73) who demonstrated that 1 cm^2/cm^2 is a critical threshold dose at which particle-induced inflammation occurs in both *in vitro* systems (as IL-8 production) and *in vivo* systems (as neutrophil recruitment). Although pro-inflammatory outcomes are not measured in this study, the use of this dosing scheme will allow for direct comparison of the study results with the wider nanotoxicology literature.

4.5.2.7 Cell viability assay using MTT

MTT Calibration Curve: The MTT assay was used to assess the effects of exogenously applied compounds on the cell layer metabolism. To compare the metabolic activity of cells seeded in 10% FBS supplemented CCM and 2% FBS supplemented medium, RPMI-2650 and A549 cells were plated at a range of seeding densities from 150 to 40,000 cells/well in two the two different cell culture medium in a 96-well plate and MTT assay was performed. The plates were incubated for 24h under standard conditions. After 24h, the cell culture medium was removed and replaced with fresh cell culture medium and 50 µl of MTT solution (5 mg/ml in PBS)

was added to each well. After 4h this medium was removed by gentle inversion and tapping onto paper. Any formazan crystals generated within the adherent cell layers were solublised with 100 µl of a surfactant solution (10% v/v SDS in DMF:water (1:1)). Upon complete solubilization of the crystals after incubating overnight under standard conditions, the absorbance of each well was measured by spectrophotometry using a wavelength of 570 nm and correcting for background absorbance using a wavelength of 650 nm. A calibration curve was produced using absorbance as a function of cell number/well and the calibration curve obtained from cells seeded under two different cell culture medium conditions were compared and the metabolic activity of cells grown in both the conditions was found to be similar.

Cytotoxicity: Nanoparticle toxicity as measured by a reduction in metabolic activity was assessed using the 3-(4,5-dimethylthiazol-2-yl)-2,5-diphenyltetrazolium bromide (MTT) assay. Cells were seeded in a 96-well plate and, after 24 h, were exposed to 100 µL of particles suspended in $CCM_{FBS2\%}$ at concentrations of 52.6, 5.26, 0.526, 0.0526 and 0.00526 µg/cm^2 or $CCM_{FBS2\%}$ alone (negative control) and incubated for 6 and 24 h. After the exposure period, the particle suspensions were aspirated and replaced by 200 µL fresh $CCM_{FBS2\%}$. 50 µL MTT (5 mg/mL) was then added to the wells and the plate was incubated for a further 4 h. The medium was then removed and the resulting intracellular formazan crystals were dissolved over 24 h in 100 µL of 10% SDS prepared in 1:1 water:DMF, after which the absorbance from the solubilized formazan was measured spectrophotometrically (SpectraMax, UK) at an absorbance wavelength of 560nm.

The relative cell viability (% viability) was calculated as follows:

$$Viability\ (\%) = \frac{A - S}{CM - S} \times 100$$

Equation 4-1

Where A is the absorbance obtained for each concentration of the test substance, S is the absorbance obtained for positive control (1% v/v Triton-X) and CM is the absorbance obtained for untreated cells (incubated with CCMFBS2% alone). The latter reading was defined as 100% cell viability.

4.5.2.8 Membrane damage study using LDH

Cells were seeded in a 96-well plate and, after 24 h, were exposed to 100 µL of particles suspended in $CCM_{FBS2\%}$ at concentrations of 52.6, 5.26, 0.526, 0.0526 and 0.00526 µg/cm^2 or $CCM_{FBS2\%}$ alone (negative control) and incubated for 6 and 24 h. LDH assay was performed according to manufacturer's guidelines (Cytoscan-LDH assay kit was purchased from G-Biosciences, Maryland, USA). Briefly, after the exposure period, 50 µl of supernatant from each exposure well was removed into a new 96-well plate and 50 µl of reconstituted reaction mixture was immediately added to each well. The plate was covered in foil and put on a shaker for thorough mixing at 37°C. After mixing for 20 minutes, the plate was removed and 50 µl of stop solution was added to all wells. The absorbance of the wells was measured by spectrophotometry (SpectraMax, UK) at an absorbance wavelength of 490 nm, using a reference wavelength of 680 nm.

All samples, positive, negative, and media controls are run in triplicate. The relative cell LDH release (% LDH release) was calculated as follows:

$$LDH\ release\ (\%) = \frac{A - CM}{S - CM} \times 100$$

Equation 4-2

Where A is the absorbance obtained for each concentration of the test substance, CM is the absorbance obtained for untreated cells (incubated with $CCM_{FBS2\%}$ alone) and S is the absorbance obtained for positive control (1% v/v Triton-X). The latter reading was defined as 100% LDH release.

4.5.2.9 Conventional Cytotoxicity vs. Particokinetics and Cytotoxicity

The particokinetic modelling program, EXCEL developed in Chapter 3 was applied to calculate the amount of particles reaching the cells. Cytotoxicity of the particles calculated from administered surface area dose was reanalysed and the cytotoxicity was recalculated using the delivered surface area dose. The half-maximal effective concentration derived from the administered surface area dose and delivered surface area dose were compared.

4.6 Results

4.6.1 CCM and RTLF characterization

Total Protein Content: The RTLF obtained from healthy human lungs and concentrated had the total protein content of 1.2 mg/ml and the total protein content in cell culture medium supplemented with 2% v/v FBS was determined as 0.8± mg/ml using BCA assay.

Dynamic Viscosity: The dynamic viscosity of the RTLF and cell culture medium supplemented with 2%FBS at 37°C was 0.696±0.039 mPa.s and 0.734±0.002 mPa.s.

4.6.2 Particle size in water, CCM and RTLF

Size in Water: The size of the NPs was measured in water every 30 minutes for a period of 6 hours as seen in Figure 4-4 A. The size of LNC 50 and LNC 150 remained stable over 6 h with the average size being 68 and 147 nm respectively. The size of PS 50 and PS 200 remained stable over 6 h with the average size being 57 and 248 nm respectively. The size of CuO NP increased from 850 ± 290 nm at t=0 h to >1500 nm at t=6 h. The size of TiO_2, NP remained over 1500 nm for the whole duration of particle size measurement.

Size in CCM: All the particles showed some degree of aggregation in CCM without serum as seen in Figure 4-4 B. The size of LNC 50 increased from 76 ± 2 nm at t=0 h to 113 ± 4 nm at t=6 h. The size of LNC 150 increased from 150 ± 3 nm at t=0 h to 157 ± 2 nm at t=6 h. The size of PS 50 increased from 205 ± 75 nm at t=0 h to 1127 ± 380 nm at t=6 h. The size of PS 200 increased from 254 ± 8 nm at t=0 h to > 1500 nm nm at t=6 h. The size of CuO and TiO_2 NP started at around 750 nm at t=0 but increased rapidly (within 1 h) to over 1500 nm and remained so for the remaining duration of particle size measurement.

Size in $CCM_{FBS2\%}$: The particles remained stable in $CCM_{FBS2\%}$ as seen in the size distribution profile in Figure 4-4 C. The size of LNC 50, LNC 150, PS 50, PS 200, CuO and TiO_2, remained stable over the period of 6 h with the average size being 91 ± 17, 162 ± 3, 95 ± 8, 243 ± 8, 267 ± 13 and 356 ± 90nm respectively.

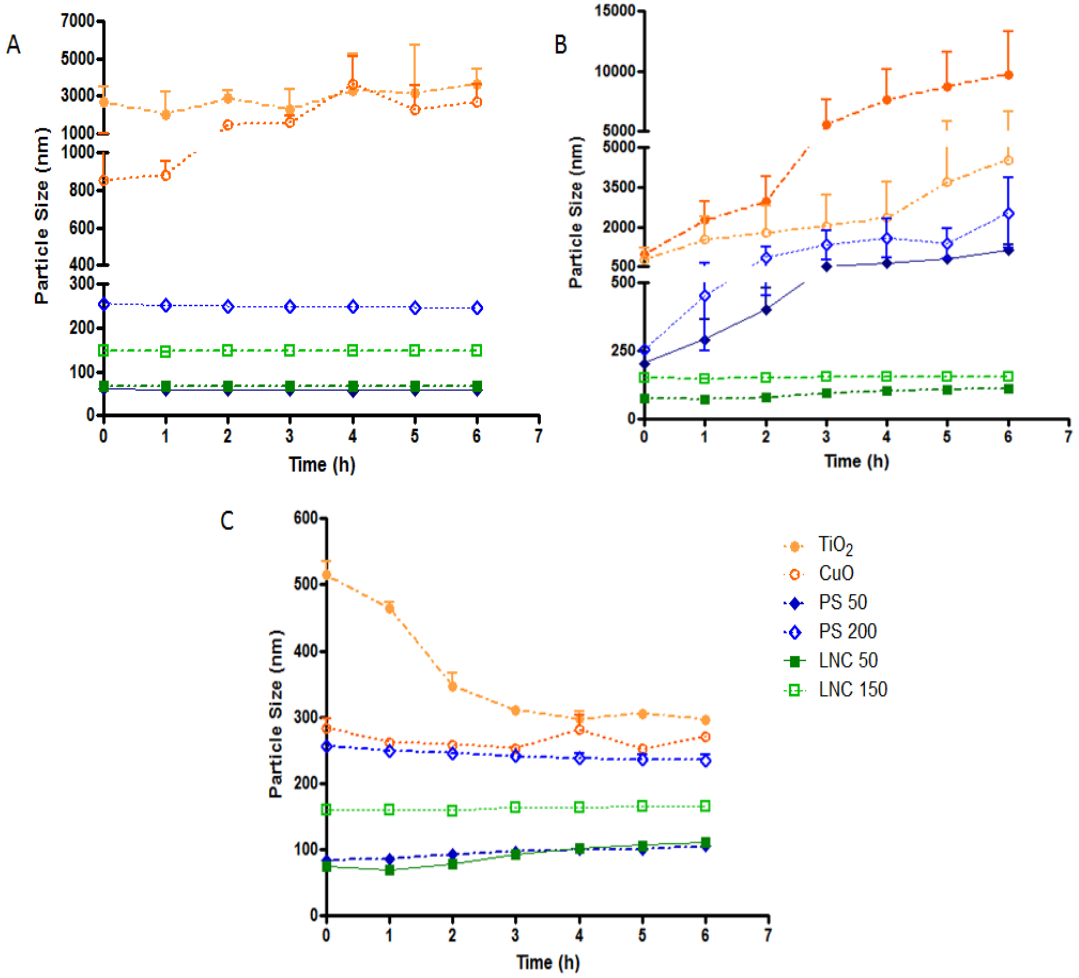

Figure 4-4: Particle size measurements of TiO_2, CuO, PS 50, PS 200, LNC 50 and LNC 150 in ultrapure water (A), CCM (B) and CCMFBS2% (C) over 6 h. All values listed represent the mean ± SD of n=3 experiments.

The data in Figure 4-4 show average particle size values of n=3 measurements at each hour over 6 h. The values are based on calculated Z-average values obtained from the Zetasizer Nano; however it can also be informative to look at the intensity distribution graphs of the particles suspended in different media. Figure 4-5 shows that the LNC 50 and PS 50 suspended in CCM gave a multi-modal particle size distribution, which is indicative of particle agglomeration.

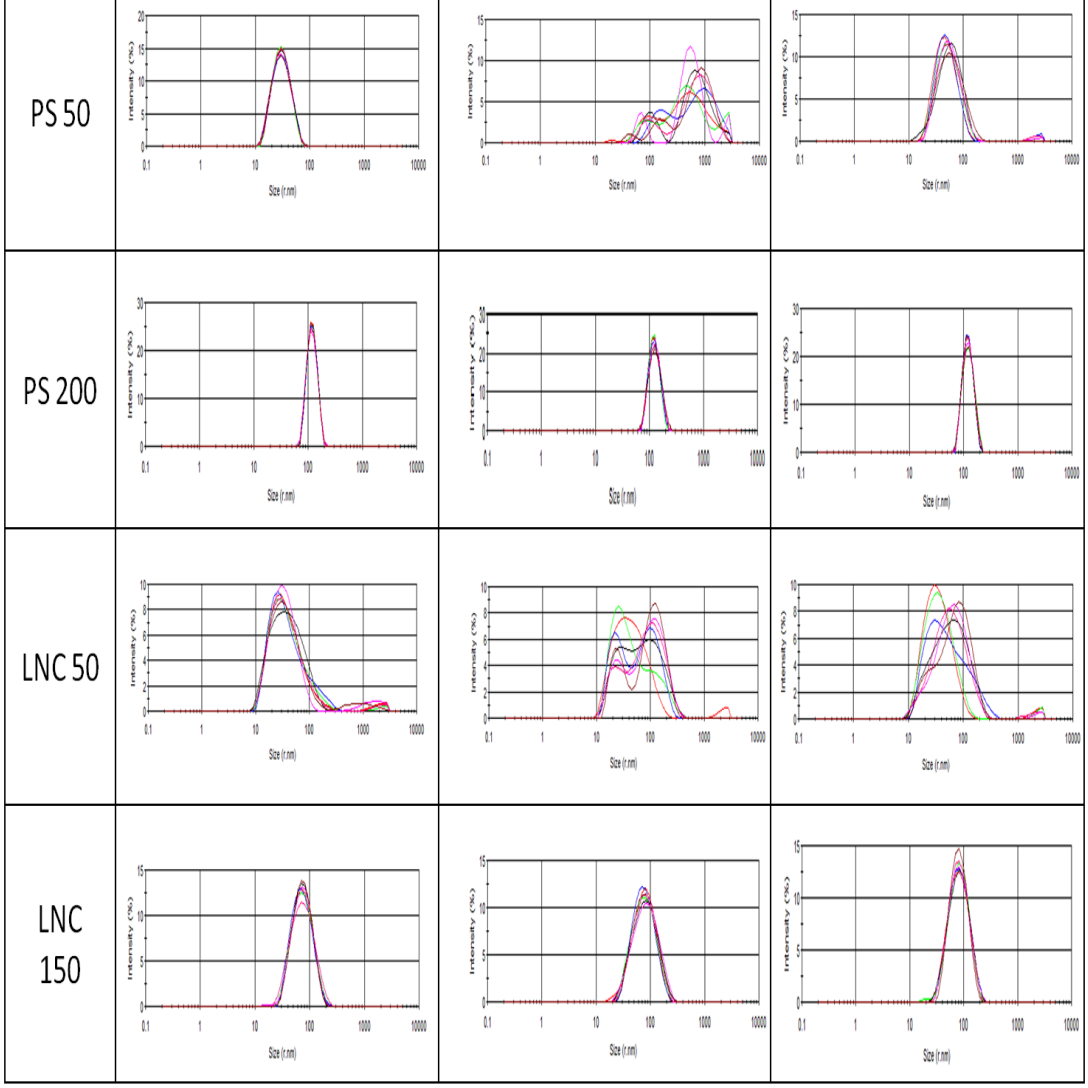

Figure 4-5: Particle size measurements PS 50, PS 200, LNC 50 and LNC 150 in ultrapure water, CCM and $CCM_{FBS2\%}$ over 6 h based on intensity distribution obtained from Zetasizer Nano.

Size in RTFL: The amount of RTLF available was very limited so all the particles could not be measured in RTLF. With future studies in mind, a decision was made to characterize CuO particles in RTLF. A look at size based on intensity distribution gives a better picture of the protein and particle agglomerate size in the system. The graphs in Figure 4-6 show that (a) $CCM_{FBS2\%}$ blank has peak intensity at 173 nm whereas (b) RTLF blank has peak intensity at 408 nm and (c) CuO NPs are

suspended in RTLF the peak intensity reduced to 237 nm. However, a look at time course of particle size in Figure 4-6 D shows that RTLF blank had a consistent size of about 300 nm where as the particle size of CuO decreased from 400 nm at t =0 h to 150 nm at t=6 h.

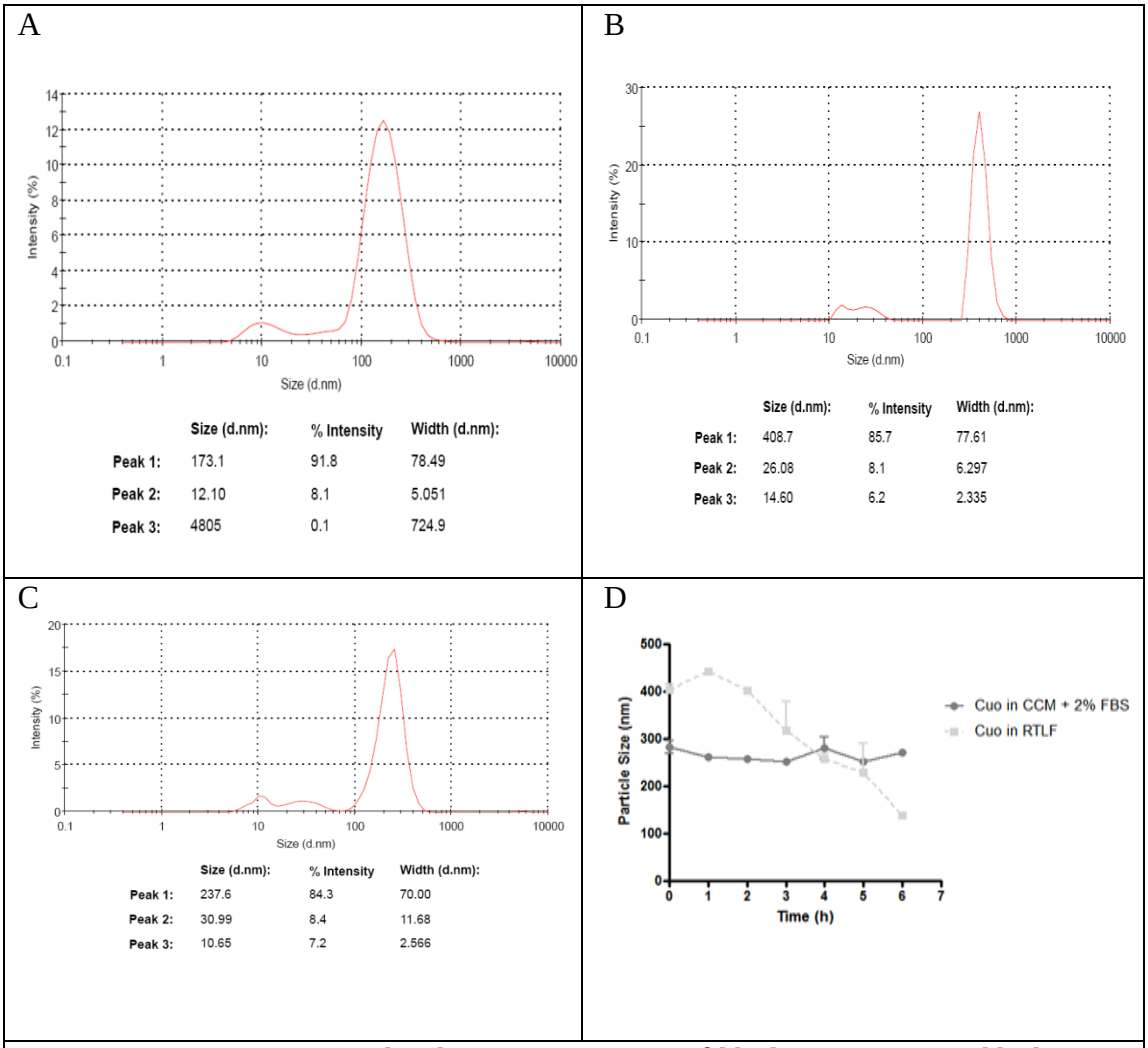

Figure 4-6: Average intensity distribution measurement of blank $CCM_{FBS2\%}$ (A), blank RTLF (B), CuO (0.017 mg/ml) in RTLF (C) and size of blank RTLF and CuO in RTLF (D) as measured by dynamic light scattering over a period of 6 h at 37°C.

4.6.3 Zeta potential in water and $CCM_{FBS2\%}$

The zeta potential of particles was measured at 37°C in water and $CCM_{FBS2\%}$. All the particles had negative zeta potential in water. In $CCM_{FBS2\%}$ all the particles except LNC 50 and LNC 150 seems to have approximately the same zeta potential of about -12 ± 2 mV (Figure 4-7). LNC 50 and LNC 150 had a ZP of -3 and -2.6

respectively. The ZP should ideally be measured in low ionic salt solutions line (10 nM NaCl) instead of water as measurement in water would lead to increase in the thickness of double layer due to lack of ions in the solution.

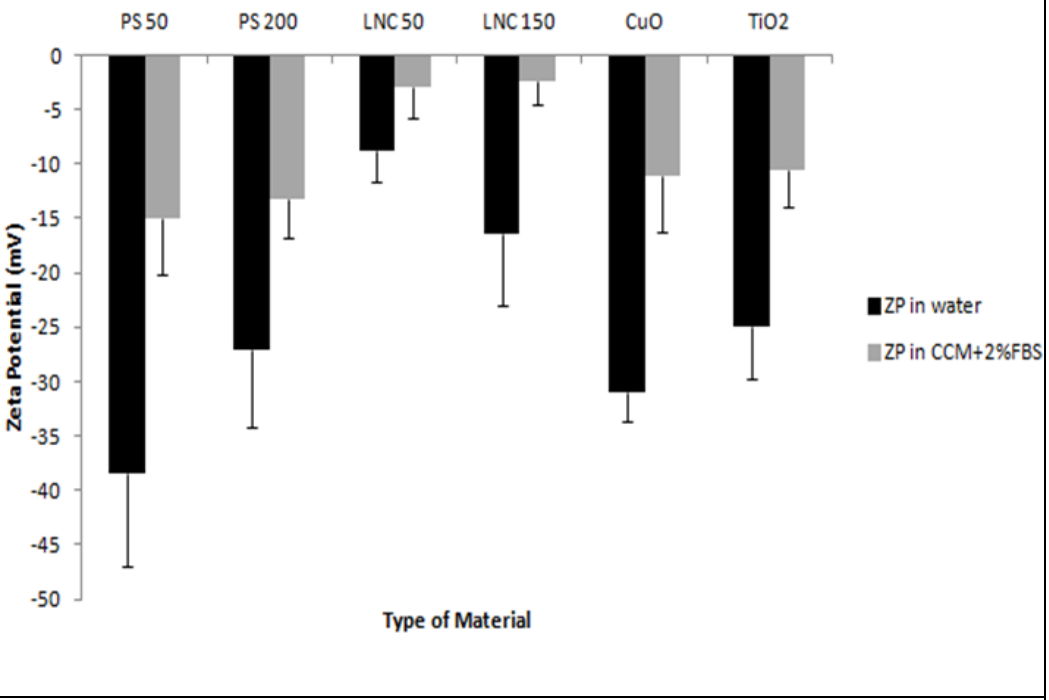

Figure 4-7: Zeta potential of particles in water and $CCM_{FBS2\%}$. The data represent mean ± SD; n=3.

4.6.4 Oxidative potential in water

Only copper oxide particles had a biologically significant oxidative potential, with an initial ascorbic acid depletion rate of 11.1 ± 0.7 nM/sec. All the other nanoparticles tested had a similar oxidative potential to that of water (initial ascorbic acid depletion rate) 1.4 nM/sec. In the presence of metal chelator DTPA the ascorbic acid depletion rate of CuO was similar to that of water (Figure 4-8).

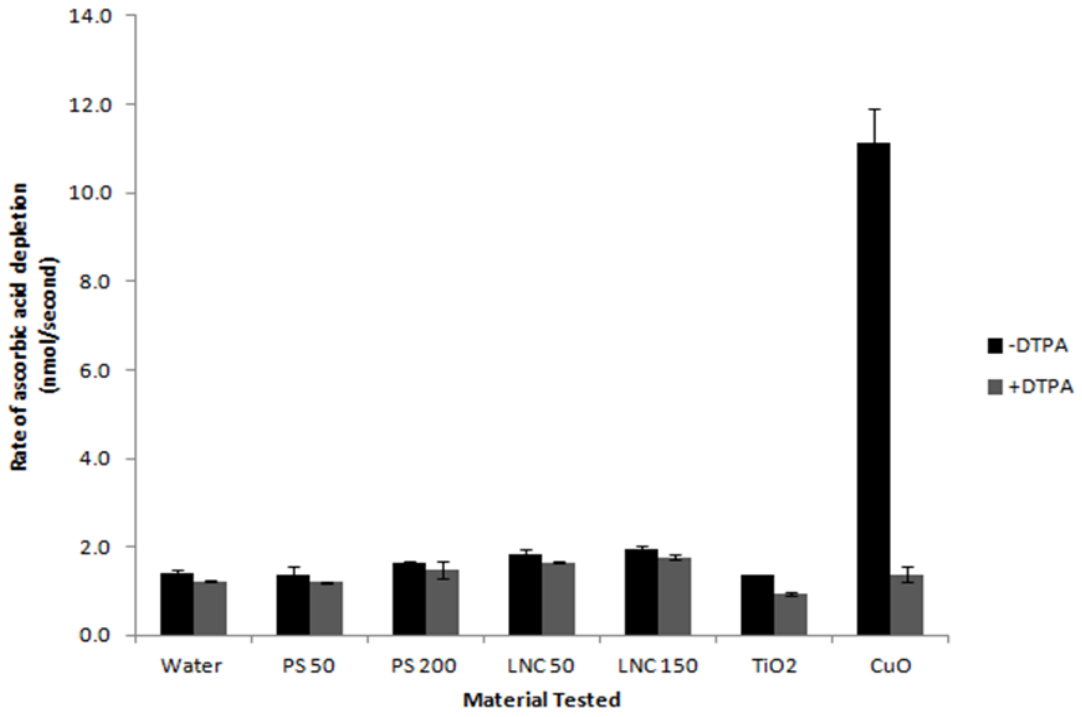

Figure 4-8: Rate of ascorbic acid depletion in presence of PS 50, PS 200, LNC 50, LNC 200, TiO_2 and CuO at pH=7 at 37°C. Depletion was determined in the absence and presence of metal chelator DTPA spectrophotometrically at a wavelength of 265 nm for 2 hours and readings taken at intervals of 2 minutes. The data represents the mean ± SD; n=3.

4.6.5 Culture of A549 and RPMI 2650 – MTT calibration

MTT Calibration Curve: The metabolic activity of A549 cells in CCM supplemented with 2% FBS was compared to the metabolic activity of RPMI 2650 after 24h incubation. A linear relationship was found for absorbance vs. cell number over the range of 1250 -40,000 cells/well, indicating seeding density over this range did not affect the rate of uptake or biotransformation of the MTT salt by individual cells. The coefficient of variation (R^2) value for both the calibration curves was greater than 0.97 (Figure 4-9). This allowed for the accurate analysis of loss in cell viability in subsequent experiments where cells were seeded at a density of 10,000 cells/well.

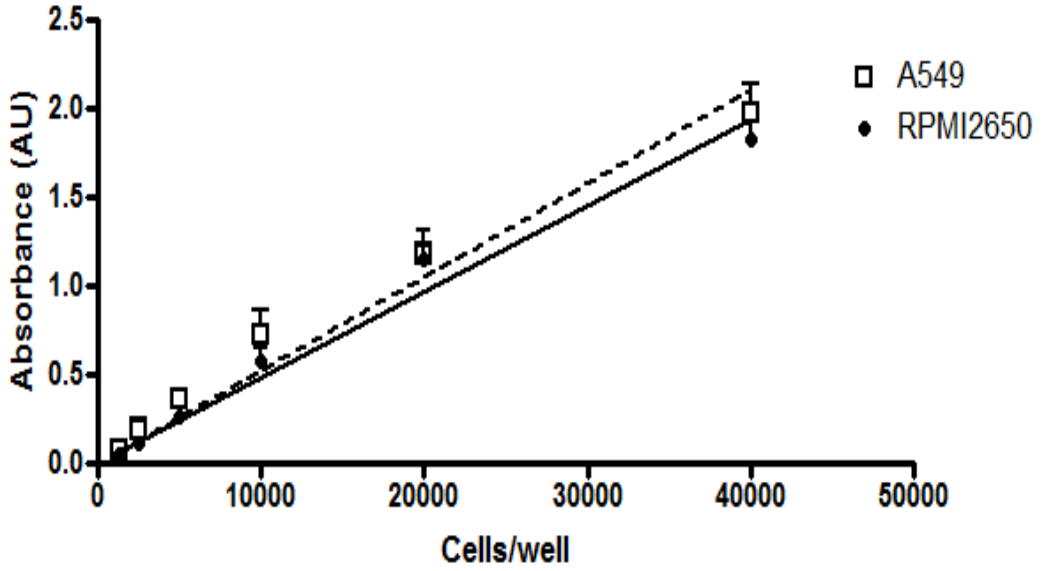

Figure 4-9: Calibration curve of A549 and RPMI 2650 cell number vs. absorbance after incubation with MTT for 4 h. The data represent mean ± SD of n=3 (3 different passages); each experiment performed in triplicate.

4.6.6 Cell viability and membrane damage

First the reference metal oxide nanoparticles were tested on A549 and RPMI 2650 cells for cytotoxicity and the particokinetics principal was applied to see if re-interpretation of data based on delivered dose made a difference in the cytotoxicity profile of the particles. In further tests more pharmaceutically relevant carrier systems were tested for cytotoxicity.

4.6.7 Reference CuO and TiO_2 metal oxide nanoparticle cytotoxicity

The reference metal oxide nanoparticles showed a dose and time dependent toxicity profile. The delivered dose was ~50% of the administered dose value for CuO NP after 3 h (Table 4-3) where as for TiO_2 NP all the administered particleshad reached the cells. This is due to the fact the TiO_2 has more density and a bigger particle size compared to CuO so the particles reach the cells primarily by gravitation. At 6 h and 24 h time points the delivered dose value for both the NP was the same as the administered dose value (Table 4-4). In the MTT assay the CuO

particles produced a greater inhibition of cellular metabolism than TiO_2 which only impaired cell activity at the overload concentration. In both the cases of copper oxide and titanium dioxide nanoparticle the delivered surface area dose was equal to the nominal surface area dose as these particles are heavy and almost all the particles (>97%) reach the bottom of the 96-well plate in 6 h. Hence no difference in nominal and delivered surface area dose was observed. The measurement of lactate dehydrogenase release after particle exposure could not be performed for CuO NPs as the particles interfered with LDH positive control supplied by the manufacturers (Figure 4-12). However, TiO_2 particles did not interfere with the LDH assay and the results of LDH release correlated will with MTT data.The cytotoxicity testing on RPMI 2650 indicated similar results. The metal oxide particles showed dose and time dependent toxicity. CuO NP showed more toxicity than TiO_2 NP at all the time points tested. In comparison the TiO_2 NPs did not show as much toxicity as the CuO particles (Figure 4-10 and Figure 4-11).

Table 4-3: Administered and delivered dose values of CuO and TiO_2 NP after 3 h exposure.

CuO Administered SA Dose (cm^2/cm^2)	CuO Delivered SA Dose (cm^2/cm^2)	TiO_2 Administered SA Dose (cm^2/cm^2)	TiO_2 Delivered SA Dose (cm^2/cm^2)
0.020	0.009	0.016	0.016
0.101	0.048	0.083	0.083
0.202	0.096	0.167	0.167
1.012	0.484	0.837	0.837
2.025	0.969	1.675	1.675
10.129	4.846	8.375	8.375

However, for 6 h and 24 h exposure different NP concentrations were used.

Table 4-4: Administered and delivered dose values of CuO and TiO_2 NP after 6 h exposure. The administered dose was equal to the delivered dose after 24 h exposure.

CuO Administered SA Dose (cm^2/cm^2)	CuO Delivered SA Dose (cm^2/cm^2)	TiO_2 Administered SA Dose (cm^2/cm^2)	TiO_2 Delivered SA Dose (cm^2/cm^2)
0.0002	0.0002	0.0001	0.0001
0.0020	0.0018	0.0016	0.0016
0.0208	0.018	0.016	0.016
0.104	0.094	0.083	0.083
0.208	0.189	0.167	0.167
2.080	1.890	1.675	1.675

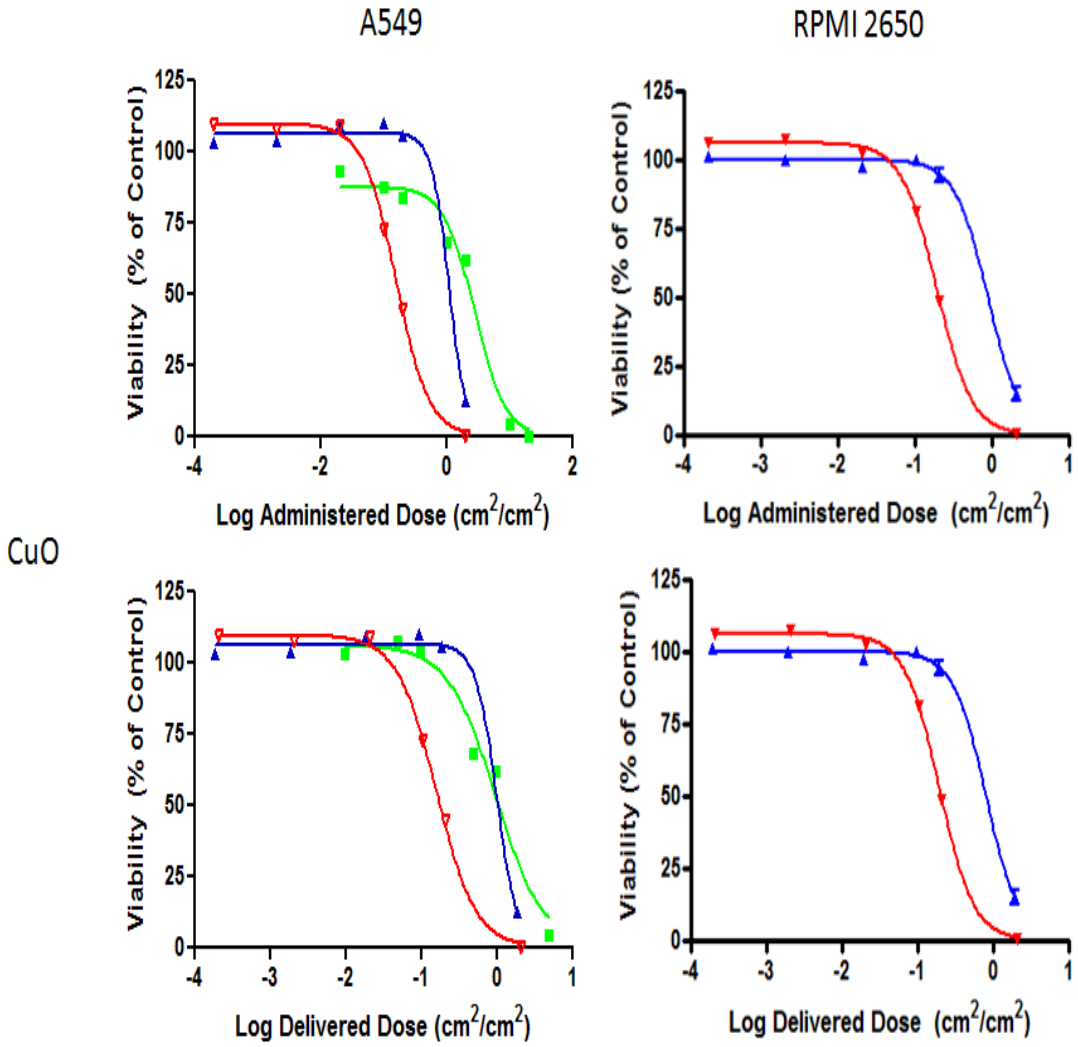

Figure 4-10: The effect of copper oxide on A549 and RPMI 2650 cell lines after 3 (green), 6 (blue) and 24 h (red) exposure. Cellular metabolic activity was measured spectrophotometrically at 570 nm and viability calculated as a percentage of the control (assay medium alone) over a particle concentration range. Effect of particles on cell viability as determined by conventional cytotoxicity (administered dose) was compared to effect of particles on cell viability after applying partico-kinetics principles (delivered dose). The data represent the mean ± SD; n=3

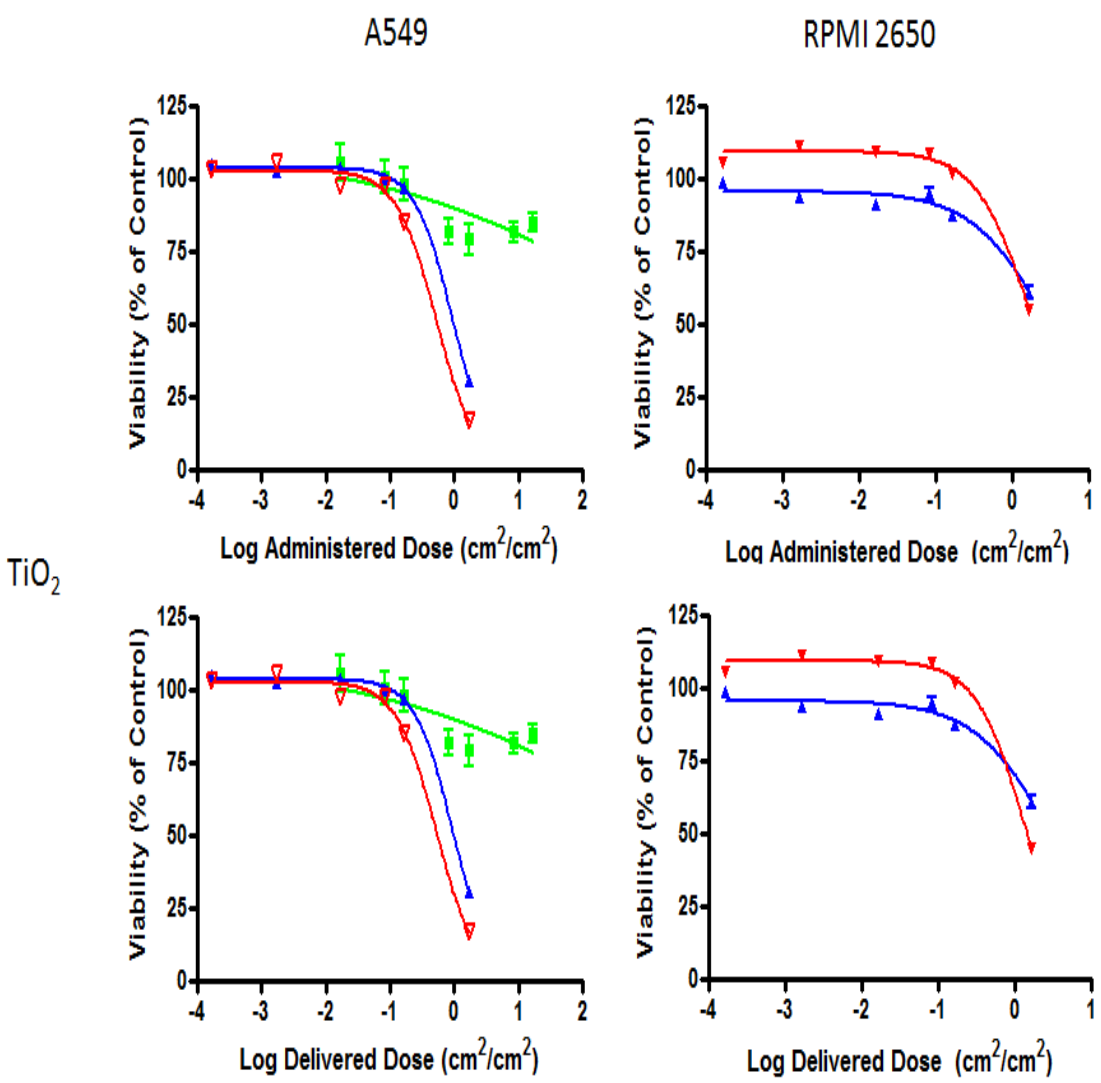

Figure 4-11: The effect of titanium dioxide on A549 for 3 (green), 6 (blue) and 24 h (red) and on RPMI 2650 cell lines after 6 (blue) and 24 h (red) exposure. Cellular metabolic activity was measured spectrophotometrically at 570 nm and viability calculated as a percentage of the control (assay medium alone) over a particle concentration range. Effect of particles on cell viability as determined by conventional cytotoxicity (administered dose) was compared to effect of particles on cell viability after applying partico-kinetics principles (delivered dose). The data represent the mean ± SD; n=3

The LDH assay was unavailable for the CuO particles as the test material interfered with the assay, but LDH release after exposure to TiO_2 showed a negative correlation with effects in the MTT assay with Pearson's correlation coefficient of value -0.94 (Figure 4-12).

CuO Interference with LDH	Pearson Corelation for TiO_2
A 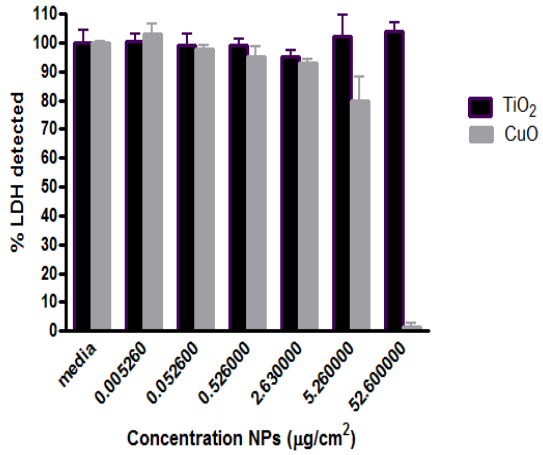	B 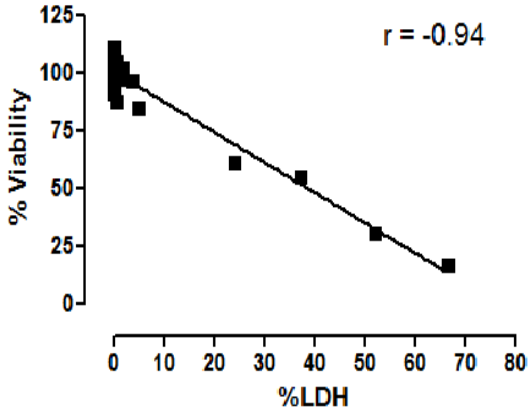

Figure 4-12: The effect of copper oxide and titanium dioxide on LDH positive control (A) and the correlation between cellular metabolic acitivity and lactate dehydrogenase release from the A549 and RPMI 2650 cell lines after exposure to TiO_2 NP for 6 and 24 h (B). The data represent the mean ± SD; n=3

4.6.8 PS 50 and PS 200 Cytotoxicity

Polystyrene nanoparticles did not show any toxicity in any of the cell lines tested at 6 h or 24 h. LDH release could not be measured at any of the particle concentration tested. The maximum LDH release was 5% of the control after exposure of A549 cells for 24 h to PS 50 at the maximum concentration. The particles were tested for interference with LDH using the standard LDH supplied by the manufacturer and showed no interference. This might mean that the particles were not membrane active. The effect of polystyrene nanoparticles on the viability of cell in the two cell lines tested A549 and RPMI 2650 were similar (Figure 4-13). None of the particles at any given concentration reduced the cell viability by less than 50% of control.

	A549	RPMI 2650
PS 50	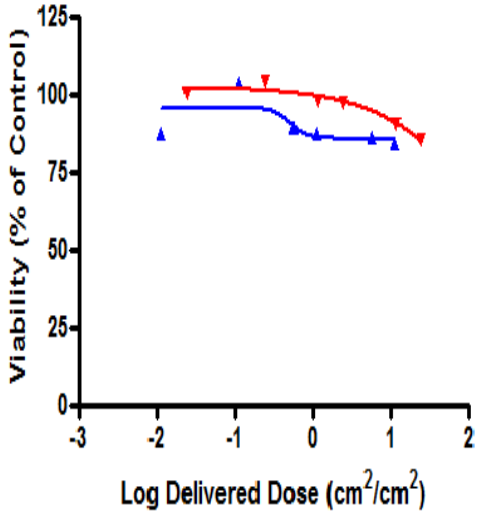	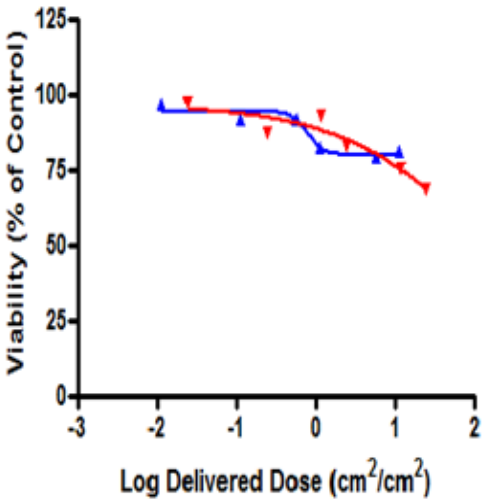
PS 200	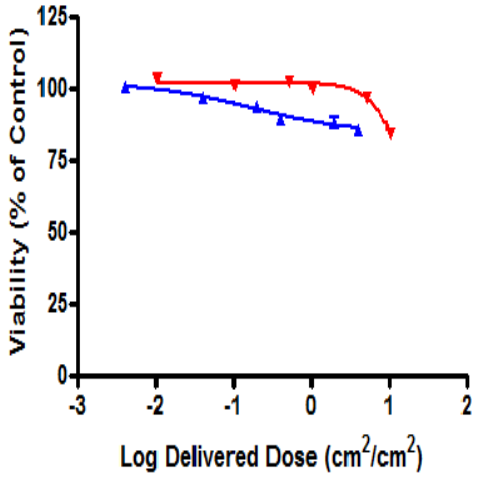	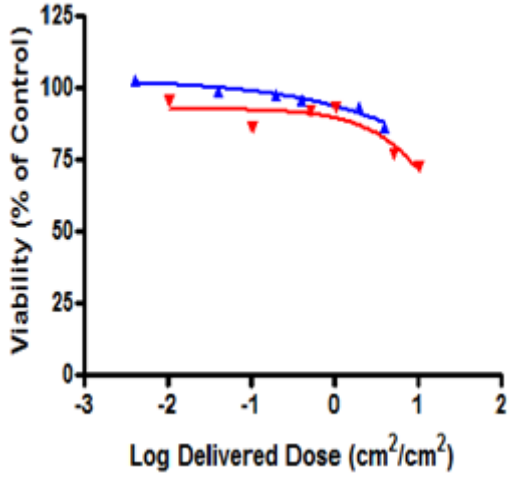

Figure 4-13: The effect of PS 50 and PS 200 on A549 and RPMI 2650 cell lines after 6 (blue) and 24 h (red) exposure. Cellular metabolic activity was measured spectrophotometrically at 570 nm and viability calculated as a percentage of the control (assay medium alone) over a particle concentration range. Effect of particles on cell viability as determined by conventional cytotoxicity was compared to effect of particles on cell viability after applying portico-kinetics principles. The data represent the mean ± SD; n=3

4.6.9 LNC 50 and LNC 150 Cytotoxicity

The in-house developed lipid nanocapsules (LNC 50 and LNC 150) of 50 and 150 nm showed a time and dose-dependent toxicity. The effects of LNC 50 and LNC

150 were similar in both cell lines. The administered surface area doses of LNCs were much higher than those tested for CuO and TiO_2 NP because these particles have been prepared for incorporation of pharmaceutically active molecule in them and they will be inhaled deliberately which might lead to higher deposited dose in lungs *in vivo*. The administered surface area concentration of LNC 50 ranged between 3300 cm^2/cm^2 to 0.33 cm^2/cm^2 and that of LNC 150 ranged between 1966 cm^2/cm^2 to 0.1966 cm^2/cm^2(Table 4-5 and Table 4-6).

Table 4-5: Administered and delivered dose values of LNC 50 and LNC 150 NP after 6 h exposure.

LNC 50 Administered SA Dose (cm^2/cm^2)	LNC 50 Delivered SA Dose (cm^2/cm^2)	LNC 150 Administered SA Dose (cm^2/cm^2)	LNC 150 Delivered SA Dose (cm^2/cm^2)
0.33	0.012	0.196	0.005
1.65	0.060	0.98	0.029
3.3	0.121	1.9	0.058
16.5	0.605	9.8	0.29
33	1.21	19.6	0.58
165	6.05	98	2.9
330	12.1	197	5.8
3300	121	1966	58

Table 4-6: Administered and delivered dose values of LNC 50 and LNC 150 NP after 24 h exposure.

LNC 50 Administered SA Dose (cm^2/cm^2)	LNC 50 Delivered SA Dose (cm^2/cm^2)	LNC 150 Administered SA Dose (cm^2/cm^2)	LNC 150 Delivered SA Dose (cm^2/cm^2)
0.33	0.025	0.196	0.013
1.65	0.125	0.98	0.068
3.3	0.25	1.9	0.136
16.5	1.25	9.8	0.68
33	2.5	19.6	1.4
165	12.5	98	6.8
330	25	197	13.6
3300	252	1966	136

The results show that particles only showed toxicity only at overload dose concentration (Figure 4-14 and Figure 4-15).This overload concentrations is based on the findings of Faux and co-workers (73) who demonstrated that 1 cm^2/cm^2 is a critical threshold dose at which particle-induced inflammation occurs in both *in vitro* systems (as IL-8 production) and *in vivo* systems (as neutrophil recruitment).

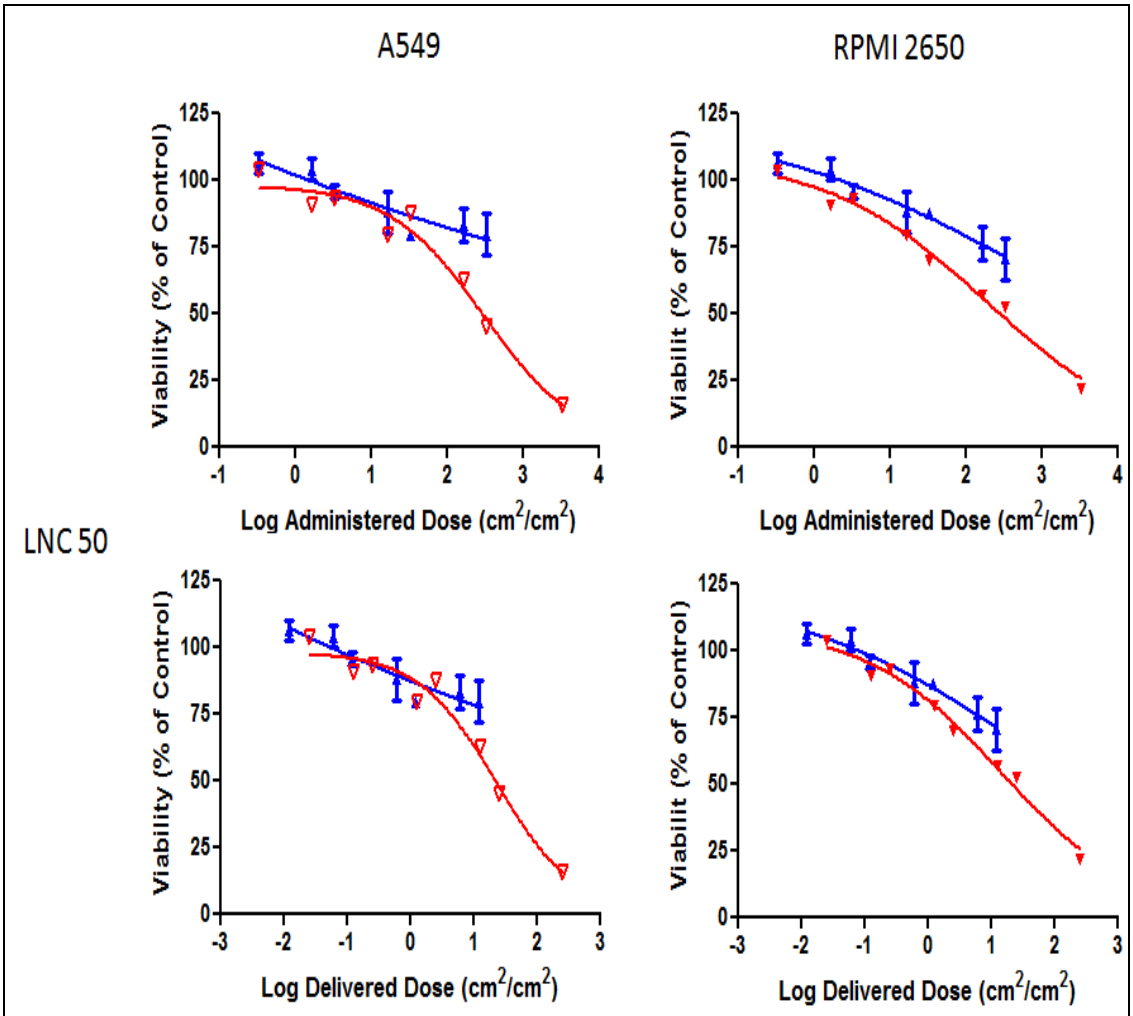

Figure 4-14: The effect of LNC 50 on A549 and RPMI 2650 for 6 (blue) and 24 h (red). Cellular metabolic activity was measured spectrophotometrically at 570 nm and viability calculated as a percentage of the control (assay medium alone) over a particle concentration range. Effect of particles on cell viability as determined by conventional cytotoxicity (administered dose) was compared to effect of particles on cell viability after applying partico-kinetics principles (delivered dose). The data represent the mean ± SD; n=3

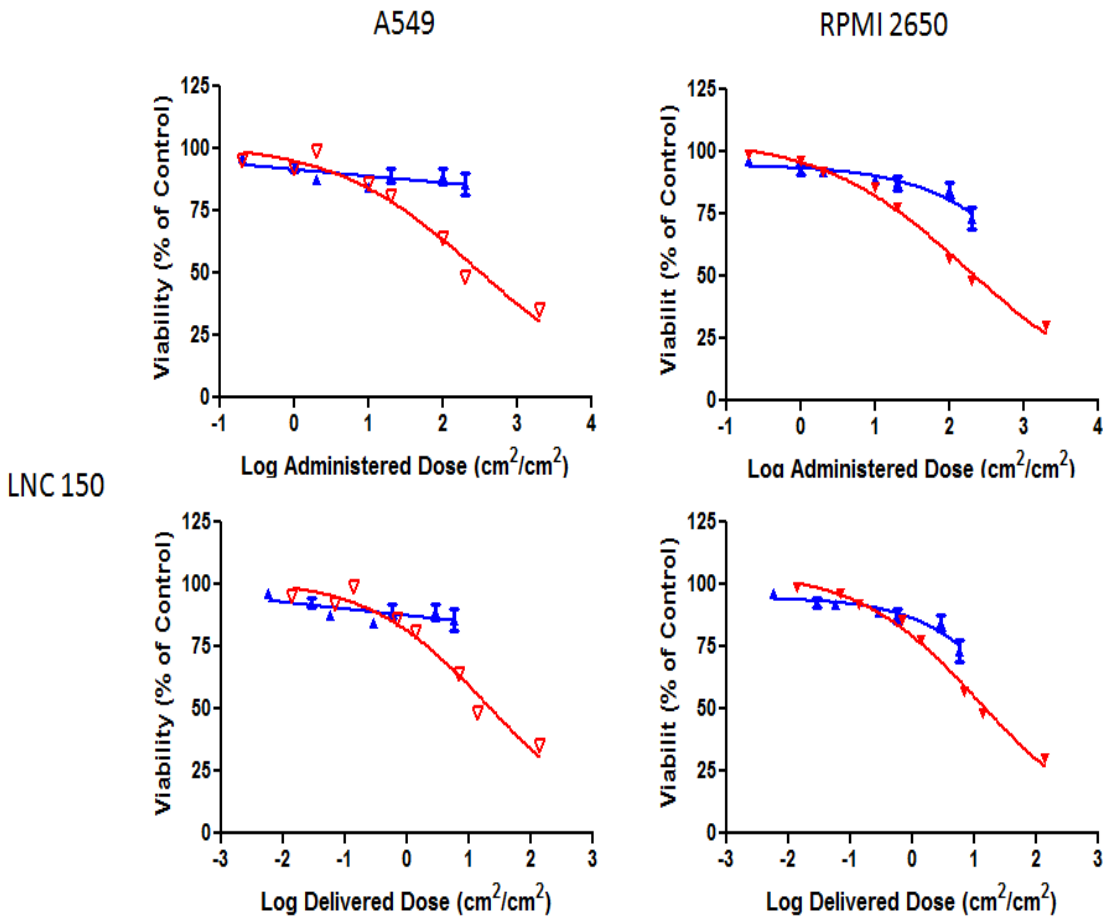

Figure 4-15: The effect of LNC 150 on A549 and RPMI 2650 for 6 (blue) and 24 h (red). Cellular metabolic activity was measured spectrophotometrically at 570 nm and viability calculated as a percentage of the control (assay medium alone) over a particle concentration range. Effect of particles on cell viability as determined by conventional cytotoxicity (administered dose) was compared to effect of particles on cell viability after applying partico-kinetics principles (delivered dose). The data represent the mean ± SD; n=3.

LDH release after exposure to LNC 50 and LNC 150 did not show a good negative correlation with effects in the MTT assay with Pearson's correlation coefficient of value -0.91 (Figure 4-16). This means that cytotoxicity of the LNC has a different mechanism of action rather than membrane disruption. However, our experiments did not provide us with a good hypothesis for this mechanism.

Further the data showed that LNC 50 caused more LDH release as compared to LNC 150 after 24 h exposure (Figure 4-17). At 6 h both LNC 50 and LNC 150 showed LDH release which was less than 10% of control in both the cell lines. However, at

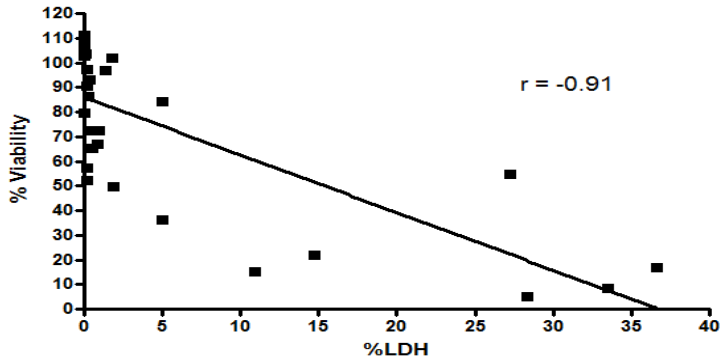

Figure 4-16: The correlation between cellular metabolic acitivity and lactate dehydrogenase release from the A549 and RPMI 2650 cell lines after exposure to LNC 50 and LNC 150 NP for 6 and 24 h (b). The data represent the mean ± SD; n=3.

24 h the LDH release from both the cell lines after exposure to LNC 50at delivered dose concentration of 25 cm^2/cm^2 was 28% (A549) and 33% (RPMI) of control. The cell viability after 24 h exposure at the same delivered dose concentration was 45% (A549) and 52% (RPMI) of control. LNC 150 even at the heighest tested concentration of 13 cm^2/cm^2 did not give more than 10% (of control) LDH release.

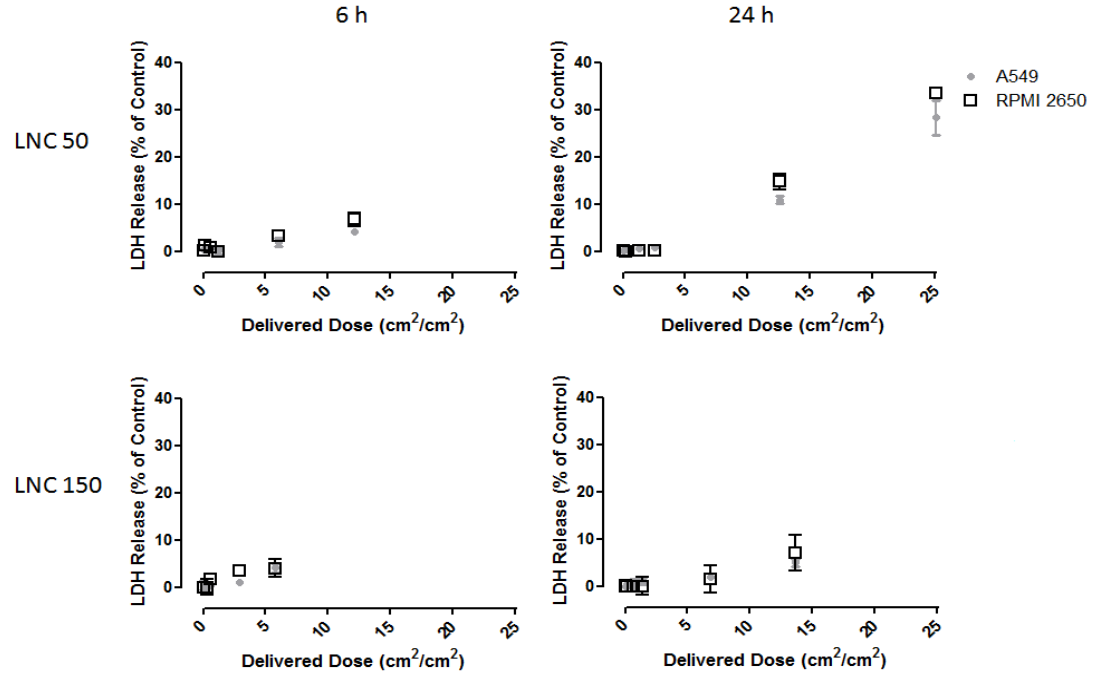

Figure 4-17: LDH release from the A549 (grey) and RPMI 2650 (black) cell lines after exposure to LNC 50 and LNC 150 NP for 6 and 24 h. The data represent the mean ± SD; n=3.

4.6.10 Re-calculation of response based on delivered dose and comparison to administered dose

The half-maximal effective concentration (EC_{50}) values were calculated using a sigmoidal dose-response curve. The EC_{50} values were calculated for both administered and delivered surface area doses. The EC_{50} value for PS 50 and PS 200 could not be calculated as the particles did not reduce the viability below 80% at any of the tested concentration. Similarly, the EC_{50} value for 6 h exposure could not be calculated for LNC 50 and LNC 150 as not even at the heighest administered concentration the cell viability was reduced below 50% of control. The administered SA dose EC_{50} was usually lower than the delivered SA dose EC_{50} except for CuO and TiO_2 NP. Comparison of IC_{50} value of LNC 50 and LNC 150 value showed that there was no size dependency of toxicity. In case of CuO and TiO_2 all the particles reached the bottom of the well by the end of 24 h so the administered dose was equal to the delivered dose. However, in case of LNC 50 and LNC 150 less than 10% of the particles administered reached the bottom of the well so the delivered dose was less than 10% of the administered dose. This is in agreement with findings of Khanbeigi *et al.* who found that for low density particles such as polystyrene beads less than 0.3% of the particles administered were able to interact with the cells.

Table 4-7: EC_{50} values for nanoparticles exposed to A549 cells for 24 h calculated using conventional nominal surface area dose and after applying particokinetics to calculate delivered surface area dose.

Particle Type	Administered SA EC_{50} (cm^2/cm^2)	Delivered SA EC_{50} (cm^2/cm^2)
CuO	1.60	1.60
TiO_2	5.09	5.09
Purified LNC 50	289.70	13.86
Purified LNC 150	266.90	11.78

4.7 Discussion

In order to understand the interaction of nanomaterials with biological systems it is essential to systematically and accurately define particle characteristics (212). In the present study the size of particles was measured using dynamic light

scattering over a period of 6 h in four different media – water, CCM without serum, CCM with 2% v/v serum and in reconstituted concentrated RTLF. The results in Figure 4-4 indicate that particles aggregate in water and CCM without serum and this aggregation is a dynamic process. Coating of the particles with stabilizers such as poly(vinyl alcohol), Tween-80, Fluonic 127, Fluonic 68, Solutol® HS 15 etc. prevents this aggregation by adhering to the nanoparticle surface and causing stearic hinderance (213-217). However, particles remained stable in CCM supplemented with serum (Figure 4-4) which may be due to opsonisation of serum protein onto the surface of the particles which provide steric hinderance and thus prevent the particles from agglomeration. These results are in agreement with reports from Murdock *et al.* (195), Allouni *et al.* (177) and Ji *et al.* (218) who have also observed aggregation of particles in water and non-supplemented cell culture medium. They also observed size stabilization in cell culture medium supplemented with serum. Murdock *et al.* tested the particle size in F-12K and RPMI-1640 media supplemented with either 10% (v/v) or 20% (v/v) FBS, Allouni *et al.* measured TiO_2 size in RPMI-1640 supplemented with 10% (v/v) FBS and Ji *et al.* used six different types of cell culture medium each supplemented with a range (0.5% to 10% v/v) of FBS to measure the particle size of TiO_2.

To understand the colloidal stabilisation of particles suspended in supplemented media we have to consider the forces operating at the nanoparticle and liquid interface. Typical forces operating between the particles suspended in a liquid would be van der Waal's (VDW), electrostatic interactions, steric interactions and solvation forces (219). Typically in water the particles have a net attractive VDW force and a repulsive electrostatic force. The balance between the attractive and repulsive forces would determine the aggregation of particles. The zeta potential of a particle is the potential difference between the stationary layer of fluid attached to the particle and the dispersion medium (220). A value of 25 mV (negative or positive) can be considered an arbitrary value that separates the low-charged surfaces particles from the high-charged surface particles (American Standard, 1985). Nanoparticles with a high zeta potential are electrically stabilised due to the repulsion between adjacent and similarly charged particles. So the non-aggregation of PS 50 and PS 200 particles in water can be explained by the high zeta potential of the particles measured in water (-58.5 mV and -27.1 mV, respectively). For LNC 50 and LNC

150, the size stability in most media can be explained by steric stabilization of the particles conferred by the polyethylene glycol (600 Da) component of the particle shell, which is composed of Solutol® HS15 (polyethylene glycol (600)-hydroxystearate).

When the particles are suspended in cell culture medium without serum we observed an aggregation of particles. The CCM is highly ionic due to presence of a number of salts with an ionic strength usually greater than 100 mM (218). According to Derjaguin, Landau, Verwey, and Overbeek (DLVO) theory, the stability of a colloidal suspension is based on the net balance of two forces: the electrostatic repulsion which prevents aggregation and a universal attractive van der Waals force which acts to bind particles together (219). In dilute electrolyte solutions, the counterion zone formed around the charged surface of nanoparticles extends causing interaction between the double layers of the two particles at long range. The van der Waals attraction is calculated by:

$$V_A = -A/12\pi D^2$$

Equation 4-3

where V_A is van der Waal's attractive force (Newton), A is the Hamaker constant (Joule) and D is the particle separation (meters). Since V_A is inversely proportional to distance between the particles, it is relatively weak at long-range, hence electrostatic repulsion between the double layer dominates and a stable nanoparticle suspension results. However, high ionic strength compresses the electrical double layer and the magnitude of the repulsive barrier decreases, thereby van der Waals attraction dominates. Therefore, the net interaction potential becomes purely attractive leading to nanoparticle agglomeration as observed in the CCM. The zeta potential of the particles in $CCM_{FBS2\%}$ was approximately the same for CuO, TiO_2, PS 50 and PS 200 which may be due to the adsorption of albumin from the FBS onto the surface of the particles. This result is in agreement with the results from other authors who have observed similar trend for metal oxide NPs (168, 177, 218). The study by Limbach *et al.*(168) investigated the changes to zeta potential values of metal oxide NPs (SiO_2, TiO_2, Fe_2O_3, CuO, Al_2O_3, ZrO_2, CeO_2) of 20-70 nm in water and cell culture medium with 10% FBS. In pure water, the zeta-potential measurements of oxide dispersions cover a wide range from -25 to 55 mV. Once these dispersions were mixed with cell

culture medium, protein adsorption strongly affected the surface charge distribution of oxides and shifted the zeta potential to around -18 mV. The zeta potential of LNC's was much lower compared to other particles tested in $CCM_{FBS2\%}$ which might mean that due to PEG coating of the LNC's the adsorption of serum around the particles is not the same which may explain the deviation from the trend.

For nanoparticles that are inhaled, the respiratory tract lining fluid (RTLF) is the first physical interface between the body and the outside environment, with a crucial physiological and protective role for the underlying epithelial cells from nasal to alveolar passages. The understanding of the interactions between/coating of inhaled particles that deposit in the lung with the RTLF is important in understanding the interactions between particles with respiratory cells. This is why the colloidal stability of nanoparticles in RTLF was investigated in this study. The major protein constituents of the RTLF are albumin, transferrin, lysozyme and immunoglobulins A, G, M and surfactant protein A, which constitute more than 75% of the total protein component of RTLF (221). In comparison, the primary constituents of FBS are albumin and alpha globulins (Supplier Information). In this study, the total protein content measured in $CCM_{FBS2\%}$ and RTLF was 0.8 mg/ml and 1.2 mg/ml, respectively. It should be noted that the concentrations in these samples are not as high as the total protein content in RTLF *in vivo* (17.9 ± 8.6 mg/ml) (219); however, inherent limitations of dynamic light scattering techniques limit the ability to generate useful particle size data in media with high protein concentrations due to significant background scattering caused by biomolecule agglomerates. Particle tracking analysis is a more robust technique for polydisperse suspensions or particle suspension in biological medium (222), but was not available during this study. The measurement of blank $CCM_{FBS2\%}$ and RTLF showed interesting differences in the protein agglomeration profiles (Figure 4-6). In $CCM_{FBS2\%}$ there is an initial peak between 8 to 20 nm which is representative of un-agglomerated albumin and over time (approximately 3 h) it agglomerates and stabilizes at about 150 nm. However, for blank RTLF there are peaks at ~20 nm and ~400 nm which might be representative of the respective protein aggregates and lung surfactant-containing liposomes formed in RTLF after lavage. The particle size measurements of CuO NPs in different media revealed that they aggregated in water and CCM without serum, but remained stable in $CCM_{FBS2\%}$ and RTLF. This might be due to opsonization of

proteins onto the surface of the particles. The increase in particle size from dry state to the size measured in $CCM_{FBS2\%}$ and in RTLF might be attributed to the opsonization of proteins on the particle surface. The decrease in particle size observed in RTLF might be attributed to the fact that at the beginning some agglomerates of both particles and large surfactant containing liposomes might cause a bias of intensity distribution towards large particles due to their scattering thousands of times more light than smaller particles (85). Over the period of time these particle agglomerates settle down and are not present in suspension any more to cause the bias thus causing the decrease in particle size over time.

Importance of measuring reactive oxygen species *ex vivo*: In a study by Sayes *et al.* (200) the authors showed that simple *ex vivo* tests of nanotitania photoactivity could thus prove useful as a comparative screen for cytotoxicity in this important class of materials. The authors measured the reactive oxygen species generation *ex vivo* of nano-TiO_2 (dry state size 3-10 nm, anatase, rutile and anatase/rutile 60/40) and measured the cytotoxicity in human dermal fibroblasts and human lung carcinoma cells using various biochemical endpoints (MTT, LDH, IL-8 production). The investigators determined the reactive species formation *ex vivo* by two different methods – first the chemiluminescence of luminol was used to qualitatively probe the production of reactive species over 20 min and second the decay of photograde organic dye Congo Red was followed via absorption spectroscopy and correlated to rate constants for radical production in water. The differences in the cytotoxic response of the nano-TiO_2 tested were due to the anatase nano-TiO_2 being more reactive as measured by the production of reactive species *ex vivo*, and not because of differences in surface area. The authors found that the differences in the cytotoxic response of the nano-TiO_2 tested were due to the anatase nano-TiO_2 being more reactive as measured by the production of reactive species *ex vivo*, and not because of differences in surface area.

Ascorbic acid depletion as a valid model for assessing oxidative potential *ex vivo*:Nanoparticle toxicity in many cases has been attributed (35-38, 223) to their capacity to generate oxidative stress due to the production of reactive oxygen species (ROS). The characterization of NPs by measurement of their oxidative potential was performed using a well established method of ascorbic acid depletion. This method was described systematically by Seiffert and co-workers (224) in her doctoral thesis.

Basically, ascorbic acid can be oxidised in the presence of redox metal ions (Fe^{3+}, Cu^{2+}) with the subsequent formation of superoxide ($\bullet O_2^-$) and redox cycling (224). The rate of ascorbic acid oxidisation can be measured and provides an indirect value for the oxidative potential of the sample. Figure 4-8 shows that CuO NP had the highest oxidative potential (as measured by ascorbic acid depletion rate), which might be due to the CuO being highly redox active metal. This result is agreement with the findings of Seiffert and co-workers (224) who found similar ascorbic acid depletion rates for CuO and TiO_2 NPs. The lack of oxidative potential of LNC's affirmed that the in-house manufacturing process did not contaminate the surfaces of these particles with reactive species, as the components of the LNC are not expected to be reactive in themselves (unless degraded).

A comparison of nanoparticle cytotoxicity covering a wide range of materials, as conducted in this study, showed very interesting results. First, it should be mentioned that a true comparison of cytotoxicity for these different nanomaterials may only be performed when the cell viability and membrane integrity assay results are normalized to the delivered dose (modeled using EXCEL as discussed in Chapter 3). The reason for this is that the different nanoparticle properties, especially particle size distribution, aggregation potential and density, will mean that each particle type will exhibit a very different colloidal behavior during particle exposure. Thus, if cells are exposed to particle suspensions at similar administered doses (as was done in this study), particle-specific colloidal behavior will dictate that delivered dose values will differ by order of magnitude for the same exposure times.

In this study, CuO NP proved to be most toxic as compared to other NPs, as expected. This can be explained by the high oxidative potential of CuO. These results are in agreement with Karlsson *et al.* (225) who tested different metal oxide particles (CuO, TiO_2, ZnO, $CuZnFe_2O_4$, Fe_3O_4, Fe_2O_3) and multiwalled carbon nanotubes on A549 cells. Cytotoxicity was analysed using trypan blue assay. DNA damage and oxidative lesions were determined using the comet assay and intracellular production of reactive oxygen species (ROS) was measured using the oxidation-sensitive fluoroprobe 2',7'-dichlorofluorescin diacetate (DCFH-DA). CuO nanoparticles were most potent regarding cytotoxicity and DNA damage, and were the only particles to induce significant increase in intracellular ROS generation. Interestingly, it should be noted that, due to the high density of CuO, the administered and delivered dose

values are very similar, especially after 24 h exposure time. Interesting differences can be seen when the same delivered doses came into contact with the cells, yet different cytotoxicity outcomes were achieved because the overall incubation times are different. This might be due to a longer accumulative intracellular residence time. If we compare the cytotoxicity of TiO_2 with PS 200 then at a similar delivered dose levels (1.67 cm^2/cm^2 for TiO_2 and 1.97 cm^2/cm^2 for PS 200 after 6 h exposure) we can see that the cell viability in case of TiO_2 was reduced to 30% of control in contrast to 97% cell viability for PS 200 particles. This may be partly explained by the fact that TiO_2 particles being heavier will reach the cells faster and in effect the cumulative cell surface residence time of TiO_2 particles will be much greater than the cumulative cell surface residence time of PS 200 particles. This means that more TiO_2 could be internalised as compared to PS 200 particles. This also shows that the particokinetic model can be further improved such that it reflects the cumulative cellular surface residence time.

The assessment of cytotoxicity of LNC 50 and LNC 150 showed that particle size did not influence toxicity, when similar surface area doses are administered (Figure 4-14, Figure 4-15 and Table 4-5). This is in agreement with the results obtained by Oberdorester *et al.* (165) (Figure 3-1).It should be noted that the toxicity of LNC particles when compared to PS particles at similar delivered dose levels was greater (Figure 4-13, Figure 4-14 and Figure 4-15). This was unexpected as the LNC's are manufactured from biocompatible components for drug delivery applications. One reason might be that there is still some excess surfactant stabilizer, Solutol HS15, present in the particle suspension which may be causing this toxicity. Indeed, previous studies showed that LNC particles which are not subjected to a rigorous purification procedure exhibited IC_{50} values similar to copper oxide nanoparticles (data not shown). Thus, the residual surfactant stabiliser is likely to play a role in cytotoxicity observed in this study.

4.8 Conclusion

The application of particokinetic model to normalise the results to delivered dose values allowed for a highly robust comparison of nanoparticle cytotoxicity. This is in agreement with Teeguarden *et al. (90)* who described a model of colloidal behaviour whereby the fractions of the administered dose calculated to sediment and

diffuse towards the cell layer were summated to obtain a single delivered dose value for any given set of experimental conditions. By applying the particokinetic model *post hoc* to an experimental data set examining nanoparticle influence on membrane integrity (i.e. half-maximal effective concentrations (EC_{50}) for lactate dehydrogenase release (91), Teeguarden *et al.* were able to show that the EC_{50} values reported (normalized to the administered dose) were 150-1200 fold higher than the values obtained when the results were normalized *post hoc* to the particokinetic derived delivered dose. In this study, the differences in EC_{50} values for cell viability (comparison administered vs. delivered dose) were not as drastic, but still showed at least one order of magnitude difference for the LNC particles. In this study particokinetic modelling was applied to cytotoxicity studies to determine the impact of dosimetry on common cytotoxicity values such as cell viability and membrane integrity. The differences in nominal and delivered dose EC_{50} values for LNC 50 and LNC 150 demonstrates that normalization of *in vitro* results to administered dose values may lead to reporting of effective toxic or minimum active doses that are artificially higher than they should be in safety studies. This study thus provides an example of using particokinetic modeling in designing *in vitro* cell-based assays that more accurately assess dose-response effects of nanoparticle systems.

Chapter 5

Standard cell culture conditions promote hyperoxia-induced cellular adaptations that mask the true toxicity of nanoparticles in *in vitro* screens

5.1 Introduction

One of the primary drivers for the growth in nanotoxicology research is the rapid expansion of engineered nanomaterials designed for use in consumer products. According to the Project on Emerging Nanotechnologies, there are currently more than 1300 consumer products that incorporate nanomaterials and this number is expected to grow to 10^4 materials within a decade (6). The traditional approach of using whole animal exposure models to assess the safety of all nanomaterials via all exposure routes will not be feasible given the rapid rate of development in the materials science sector (69, 70). Instead, the development of predictive models of nanotoxicology based on robust paradigms linking nanoparticle (NP) physicochemical properties and *in vivo* outcomes is underway. The enhanced surface reactivity of NP and their related ability to generate oxidative stress is one of the principal mechanisms hypothesized to drive both NP-induced inflammation and cellular damage (reviewed by (35, 36)). Based on this paradigm, cell cultures in which reactive oxygen species (ROS) production and the generation of oxidative stress can be quantified are regarded as valid assay systems for comparing the toxicity of manufactured or ambient NP (35, 36, 38, 43, 58). A hierarchical model for NP-induced oxidative stress has been proposed, in which cells undergo graded or tiered responses ind response to increased insults: Tier 1) upregulation of adaptive antioxidant defences, Tier 2) inflammation and Tier 3) cell death (Figure 1-3; (38, 43, 58)).

For the evaluation of ROS production in the presence of cells, various methods are available – using fluorescent probes like 2',7'-dichlorfluorescein-diacetate (DCFH-DA), dihydrorhodamine-123, dihydroethidium or using electroparamagnetic resonance. Each method has its advantages and disadvantages which have been reviewed here (226). What has been overlooked, however, is the fact that standard cell culture practices use atmospheric oxygen (i.e. 150 mm Hg, ~21%, O_2) concentrations that constitutes an hyperoxic environment. With the exception of the cornea, epidermis and respiratory tract epithelial layer, cells *in vivo* typically experience 1-10 mmHg oxygen pressure (equating to ~ 1-5% O_2). In the respiratory tract, small airway epithelial cells and alveolar cells experience approximately 100 mm Hg oxygen (~ 13% O_2) (92). Despite this, most mammalian cells are cultured using 21% O_2,which promotes increased intracellular production of ROS (93, 94). Cultured cells that fail to adapt to this oxidative environment fail to thrive, thus leaving only cells that have adopted an adaptive phenotype (94-97). Cellular adaptation to the oxidative stress, sometimes termed 'culture shock', involves enhancement of antioxidant defenses (e.g. upregulation of superoxide dimustases, increased glutathione (GSH) synthesis etc.), downregulation of ROS-generating enzymes (e.g. cytochrome *c* oxidase (98)) or alteration of cellular targets of oxidative damage (replacement of fumarase A and B with fumarase C in *E. Coli (99)* and loss of aconitase in primates (100)). Logically, this process of adaptation may be anticipated to mute oxidative responses in cells

cultured using 21% O_2, thereby masking NP toxicity when measured using oxidative stress-related endpoints and making such systems poor predictors of *in vivo* toxicity outcomes.

The implications of 'culture shock' for the *in vitro* assessment of nanoparticle-induced generation of intracellular ROS, especially as such studies are under investigation as predictors of *in vivo* outcomes, must be carefully considered. If standard cell culture conditions are exposing cells to artificially high oxygen levels thus forcing adaptation in surviving cells, such adaptive mechanisms may mask the true toxicity of nanomaterials under investigation and result in poor correlations to *in vivo* results. Therefore, the aim of this study was to investigate whether standard culture conditions in atmospheric oxygen (21% O_2; termed hyperoxia in this study)

produce adaptation to oxidative stress compared to cells cultured at 13% O_2 (termed normoxia in this study). Further, the impact of hyperoxia vs. normoxia on the results of standard *in vitro* nanoparticle toxicity assays (i.e. generation of ROS, intracellular glutathione and cell metabolism) were evaluated to assess the importance of this parameter for the robust interpretation of *in vitro* nanotoxicity data.

5.2 Materials and methods

5.2.1 Materials

5.2.1.1 Test materials and cell culture media

Reference nanocomposite copper oxide (CuO) particles (nanocrystallite form with a diameter of 2-10 nm according to the manufacturer's data) were procured from NanoScale Material Inc. (USA). Physicochemical characterization of the particles in suspension was carried out in house as described below.

Three variations of cell culture media were used in the study. Cell culture media without FBS (CCM_{FBS-}) was used in selected physicochemical characterisation experiments and was comprised of minimum essential medium (phenol red-free) supplemented with 10% v/v fetal bovine serum (FBS), 1% v/v non-essential amino acids (NEAA), 1% v/v L-glutamine (L-Glu) and 0.1% v/v gentamicin (all from Sigma Aldrich, UK). Cell culture media with 10% FBS ($CCM_{FBS10\%}$) was used to culture cells and was comprised of minimum essential medium (with phenol red) supplemented with 10% v/v FBS, 1% v/v NEAA, 1% v/v L-Glu and 0.1% v/v gentamicin. Cell culture media with 2% FBS ($CCM_{FBS2\%}$) was used for selected assays and was comprised of minimum essential medium (phenol red-free) supplemented with 10% v/v FBS, 1% v/v NEAA, 1% v/v L-Glu and 0.1% v/v gentamicin.

5.2.2 Methods

5.2.2.1 Nanoparticle characterization

The particle size of a 0.017 mg/mL suspension was characterized over 6h in three different media, deionised water, CCM_{FBS-} and $CCM_{FBS2\%}$ using dynamic light

scattering. Measurements were taken every 30 min with a Zetasizer Nano ZS (Malvern, Worcestershire, UK). The zeta potential was also measured in deionised water and $CCM_{FBS2\%}$ at the same particle concentration using the same instrument. All measurements were carried out at 37°C.

5.2.2.2 Nanoparticle dispersion and dosing scheme

For all cell culture experiments, particles were sterilized by dry heat sterilization at 180°C for 20 minutes (Memmert, Schwabach, Germany) and then suspended at 1.7 mg/mL in $CCM_{FBS2\%}$. The suspension was sonicated for five minutes using a probe sonicator at 40 Hz (Vibra Cell Sonics Material Inc. Danbury, CT, USA) and immediately diluted with $CCM_{FBS2\%}$ to the desired administration dose. The choice of administration dose range (0.00526, 0.0526, 0.526, 5.26 and 52.6 $\mu g/cm^2$) corresponds to the following theoretical particle surface area doses: 0.0002, 0.002, 0.02, 0.2 and 2 cm^2/cm^2. These concentrations were chosen based on the findings of Faux and co-workers (227) who demonstrated that 1 cm^2/cm^2 is a critical threshold dose at which particle-induced inflammation occurs in both *in vitro* systems (as IL-8 production) and *in vivo* systems (as neutrophil recruitment). Although pro-inflammatory outcomes are not measured in this study, the use of this dosing scheme is will allow for direct comparison of the study results with the wider nanotoxicology literature.

5.2.2.3 Respiratory epithelial cell culture

Human alveolar epithelial cells (A549, ATCC, USA) were cultured in an oxygen cabinet (Don Whitely Scientific, UK) under normoxic conditions (13% O_2) and in a separate standard incubator under hyperoxic conditions (21% O_2). The cells were cultured in $CCM_{FBS10\%}$ in a humidified incubator at 37°C and 5% CO_2. The cells were thawed and cultured at 21% O_2 for at least two passages. Cells were then transferred and cultured at their respective pO_2 (13% or 21%) for 72 h before being trypsinization and plating. All experiments were performed on cells seeded at a density of 30,000 cells/cm^2 in $CCM_{FBS2\%}$ and between passage number 90 and 110.

5.2.2.4 Measurement of endogenous glutathione level

The original method described by Neuschwander-Tetri *et. al.* (204) was modified for measurement of intracellular GSH (extraction of GSH was done in 13%). The flask of cells were transferred to 13% oxygen chamber and left for 72 h and then trypsinized and were seeded in 6-well plates. They were left in the 6-well plate for 24 h for the cells to adhere and were then exposed to 1) $CCM_{FBS2\%}$ (baseline GSH control), 2) 100 µM (final concentration) diethylmaleate (DEM; Sigma Aldrich, UK) or 3) CuO nanosuspension (52.6 to 0.00526 µg/cm^2 equivalent to 2 to 0.0002 cm^2/cm^2). Cells exposed to the positive control, DEM, were incubated for 2, 4 or 8 h with the compound, after which the supernatant was removed and the cells washed twice with ice cold PBS before addition of 6.5% v/v trichloroacetic acid (TCA) for 10 min on ice. The TCA extract was collected for glutathione (GSH) measurement, mixed with *O*-phthaldialdehyde (OPA) and the fluorescence from the GSH-OPA adduct was measured using a Hidex Chameleon fluorometer (Hidex, Turku, Finland) at a $\lambda_{excitation}$ of 350nm and $\lambda_{emission}$ of 420nm. The cells were then lysed by incubation with 0.5M sodium hydroxide (NaOH) for 1 h at room temperature and the NaOH extract was collected for total protein measurement. Total protein was measured using the bicinchoninic acid method (228). The fluorescence per mg protein was calculated and the results were plotted as nmol intracellular GSH per mg protein.

Intracellular glutathione levels were determined at 2, 4, and 8 h following exposure to 0.02 cm^2/cm^2 CuO nanoparticle suspension. Intracellular glutathione levels were also determined at 6 h following exposure to 0.0002 cm^2/cm^2 to 2 cm^2/cm^2 of CuO nanoparticle suspension. At each time point, cells were processed as described above and also plotted as nmol intracellular GSH per mg protein.

5.2.2.5 Measurement of intracellular reactive oxygen species

Dihydrorhodamine-123, a redox-sensitive probe, was used to determine intracellular ROS generation induced by either hydrogen peroxide (positive control) or CuO nanoparticles. The methods described by Henderson *et al*. and Royall *et al*. (229, 230) were used in a slightly modified format. The flask of cells were transferred to 13% oxygen chamber and left for 72 h and then trypsinized and were seeded in a clear-bottom black 96-well plate. They were left in the 96-well plate for 24 h for the cells to adhere and after 24 h the cells were loaded dihydrorhodamine-

123 at a final concentration of 20 µM (DHR-123 Sigma Aldrich, UK) prepared in Hank's balanced salt solution (HBSS). After 30 min incubation with DHR-123 the cells were washed twice with cell culture medium. The cells were then exposed to hydrogen peroxide (H_2O_2; 2.5, 25, 250 and 500 µM), CuO nanoparticles (2, 0.2, 0.02, 0.002 and 0.0002 cm^2/cm^2) or $CCM_{FBS2\%}$ (negative control) for 1, 2, 3 and 4 h. Live cell fluorescence was measured using an atmospheric controlled fluorescence plate reader (BMG Labtech, Aylesbury, UK) every hour at a $\lambda_{excitation}$ of 490nm and $\lambda_{emission}$ of 530nm. The cells were then lysed by incubation with 0.5M sodium hydroxide (NaOH) for 1 h at room temperature and the NaOH extract was collected for total protein measurement. Total protein was measured using the bicinchoninic acid method (228). The fluorescence per mg protein was calculated and the results were presented as % ROS generated relative to the medium control for each concentration of H_2O_2 and CuO. The area under curve (AUC) of each graph was calculated using GraphPad Prism software to provide a single value reflective of the cumulative % ROS generated over the exposure period of 4 h at different concentrations of challenge.

5.2.2.6 Measurement of metabolic activity using the MTT assay

Nanoparticle toxicity as measured by a reduction in metabolic activity was assessed using the 3-(4,5-dimethylthiazol-2-yl)-2,5-diphenyltetrazolium bromide (MTT) assay (203). The flask of cells was transferred to 13% oxygen chamber and left for 72 h and then trypsinized and were seeded in a 96-well plate. They were left in the 96-well plate for 24 h for the cells to adhere and after 24 h, were exposed to 100 µL CuO particles suspended in $CCM_{FBS2\%}$ at concentrations of 2, 1, 0.2, 0.1 and 0.02 cm^2/cm^2 or $CCM_{FBS2\%}$ alone (negative control) and incubated at hyperoxia or normoxia for 24 h. After the exposure period, the particle suspensions were aspirated and replaced by 200 µL fresh $CCM_{FBS2\%}$. 50 µL MTT (5 mg/mL) was then added to the wells and the plate was incubated for a further 4 h. The medium was then removed and the resulting intracellular formazan crystals were dissolved over 24 h in 100 µL of 10% SDS prepared in 1:1 water:DMF, after which the absorbance from the solubilized formazan was measured spectrophotometrically (SpectraMax, UK) at an absorbance wavelength of 560nm.

The relative cell viability (% viability) was calculated as follows:

$$Viability\ (\%) = \frac{A - S}{CM - S} \times 100$$

Eq.: 5:3

Where A is the absorbance obtained for each concentration of the test substance, S is the absorbance obtained for positive control (1% v/v Triton-X) and CM is the absorbance obtained for untreated cells (incubated with $CCM_{FBS2\%}$ alone). The latter reading was defined as 100% cell viability.

5.2.2.7 Data analysis

A Student's *t*-test and one-way ANOVA were used to perform the statistical analysis. All analyses were performed using GraphPad Prism statistical program (Version 4, GraphPad Software, USA).

5.3 Results

5.3.1 Test material characterization

CuO nanoparticles could only be dispersed as large aggregates in deionized water and CCM_{FBS-}, with both suspensions increasing steadily in agglomerate size over the 6 h measurement period (Figure 4-4A, 4-4B). Dispersion in $CCM_{FBS2\%}$ showed an initial particle size of ~280 nm and remained stable in size over the same measurement period (Figure 4-4C). A look at the particle size distribution by intensity (Figure 5-1) shows that particle size remained stable with peak intensity of ~242 nm. The zeta potential of CuO particles in media without serum supplementation was highly negative (-31±3 mV), which was reduced to only a moderately negative charge of -11±1 mV in the presence of 2% serum.

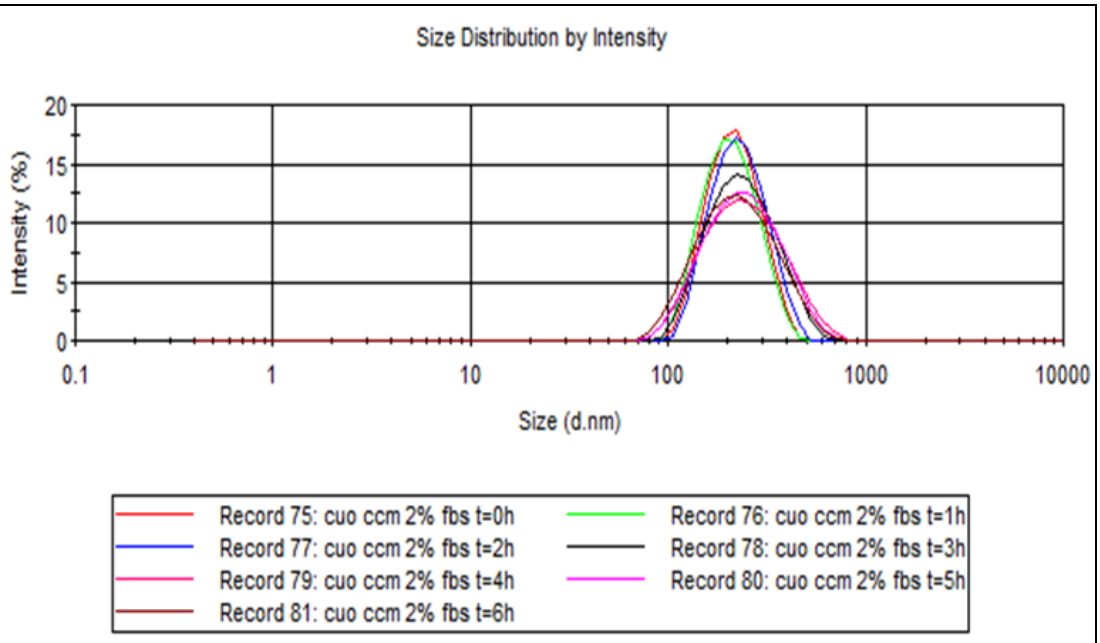

Figure 5-1: Particle size measurements CuO in $CCM_{FBS2\%}$ over 6 h based on intensity distribution obtained from Zetasizer Nano.

5.3.2 GSH levels in A549 cells cultured in 21% oxygen and 13% oxygen

Intracellular GSH levels measured over 8 h in A549 cells cultured at 21% O_2 were on average 81% higher than those measured in cells cultured at 13% O_2 (47 ± 2 versus 26 ± 7 nmol GSH/mg protein, respectively; Figure 5-2).

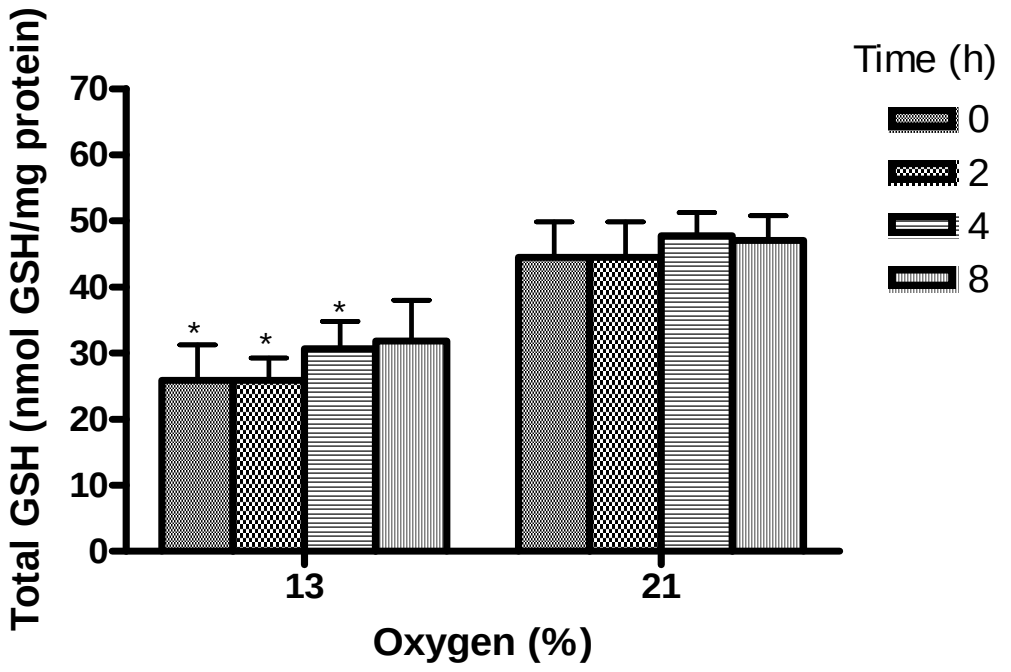

Figure 5-2: Intracellular glutathione (GSH) levels in cells cultured under physiological versus standard atmospheric conditions, 13% and 21% oxygen (O_2) concentration, respectively. GSH in cells cultured under 13% O_2 for 0, 2 and 4 h (* $P < 0.05$ compared to 21% O_2) was significantly lower compared to cells cultured at 21% O_2. Data represent mean ± SEM, n = 4.

The exposure of A549 cells cultured at 13% O_2 to 100 μM DEM reduced GSH levels by approximately 30% during the first 2 h of exposure followed by a rebound phase during which GSH levels steadily increased to baseline concentration level (Figure 5-3a). In contrast, cells cultured at 21% O_2 exhibited no change in GSH levels in response to DEM (Figure 5-3b). Particles with a surface area dose of 0.02 cm^2/cm^2 (0.526 μg CuO/cm^2) resulted in a time-dependent decrease in GSH (26 ± 10 nmol GSH/mg protein at t=0 h and 17 ± 3 nmol GSH/mg protein at t=8 h in cells cultured in 13% O_2, but no change in cells cultured at 21% O_2 (Figures 5-3a and 5-3b). This dose was chosen because no reduction in GSH level was seen at 21% when cell were exposed to CuO NP in a dose-dependent manner. The reduction in GSH in cells exposed to CuO NP was dose-dependent in cells cultured in 13% O_2 (Figure 5-3c), but only apparent at the highest concentration of CuO (2.0 cm^2/cm^2) in cells cultured at 21% O_2 (Figure 5-3d).

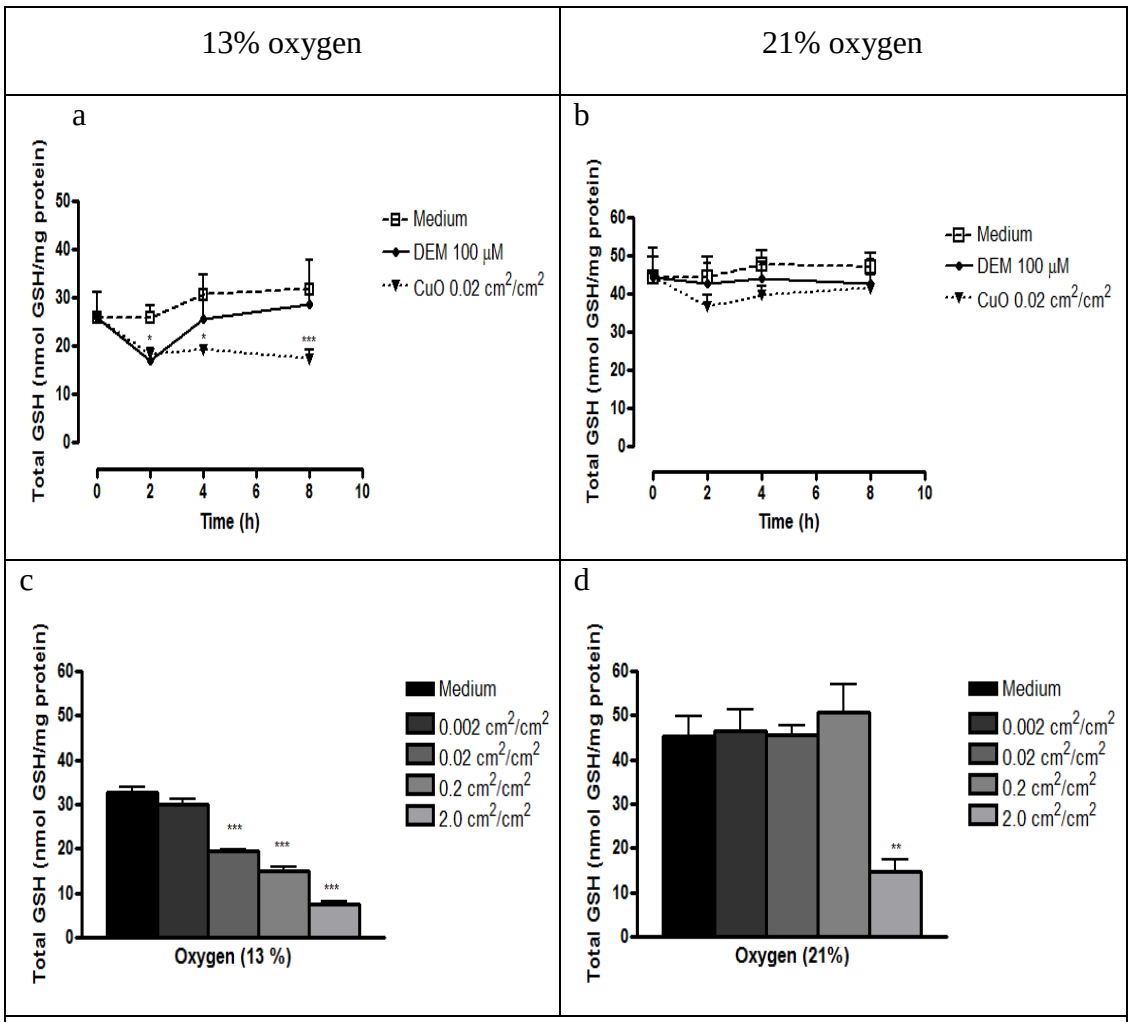

Figure 5-3: Change in intracellular glutathione (GSH; nmol per mg protein) levels in A549 cells cultured under oxygen concentrations of 13% (left) and 21% (right) when challenged by (a & b) DEM 100 µM and copper nanoparticles 0.02 cm^2/cm^2 data represent the mean ± SEM (n = 4 with each experiment performed in duplicate). (c & d) Exposure to CuO nanoparticles at 0.002, 0.02, 0.2 and 2.0 cm^2/cm^2 for 6 h; data represent the mean ± sd (n = 3). (* P < 0.05, ** P < 0.01, *** P < 0.001).

5.3.3 Intracellular ROS formation in A549 cells cultured in 21% oxygen and 13% oxygen

Intracellular ROS is reported as an area under the curve (AUC; % h) of increased ROS generation over 4 h (illustrated in Figure 5-4a and 5-4b; see appendix for full data set). Each experiment consisted of ROS quantification every 60 min (n=3) over 4 h at each H_2O_2 or CuO NP concentration and was performed in duplicate or triplicate. Thus the data illustrated in Figure 5-4a and 5-4b represent 30-45 individual measurements and contributes to a single robust data point in the

analysis of ROS generation over time (% h) versus H_2O_2 or CuO NP concentration (µM or cm^2/cm^2) under *physiological* and atmospheric oxygen levels (Figure 5-4c and 5-4d). These results indicate that at low concentrations of H_2O_2 (2.5 µM) the

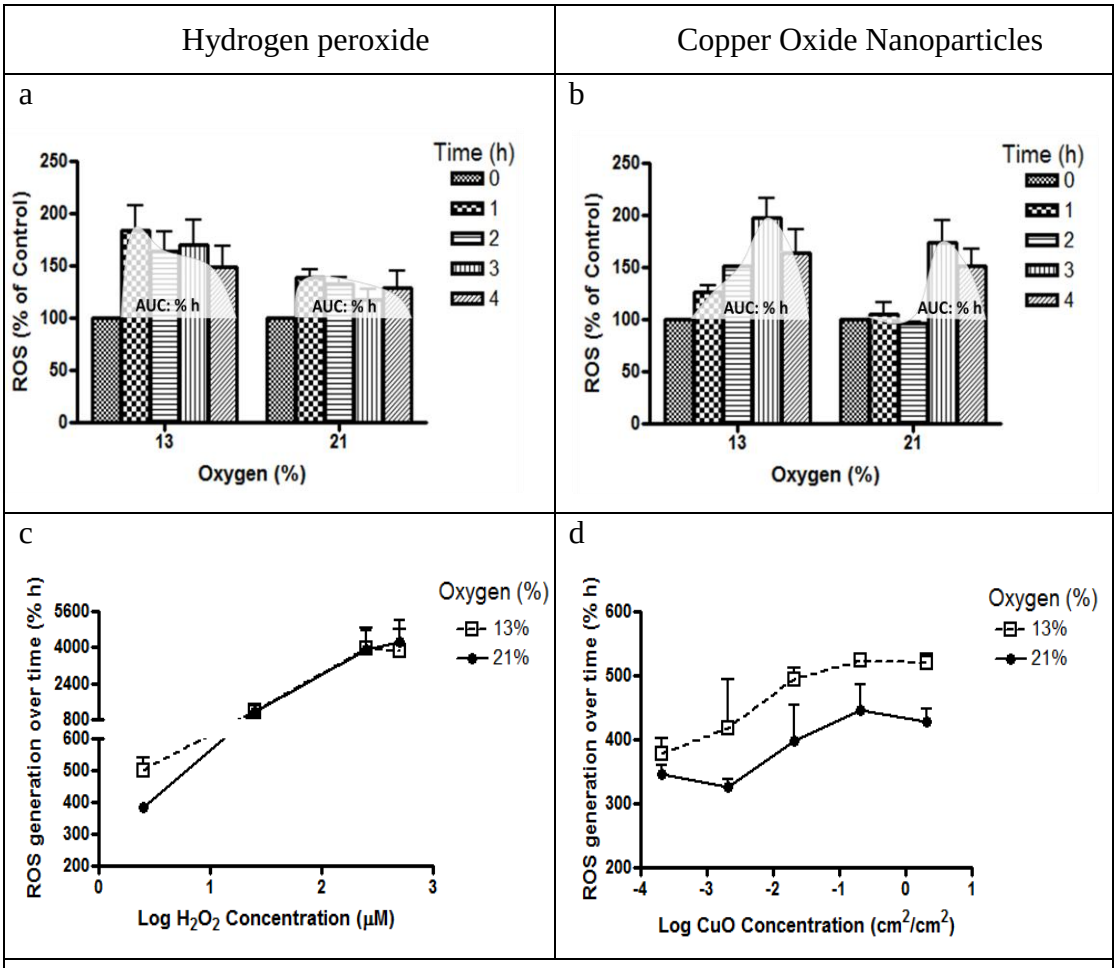

Figure 5-4: Top panel: Representative figures to illustrate the effect of different culture conditions on ROS generation in A549 cells over 4 h exposure to (a) H_2O_2 2.5 µM (b) CuO nanoparticles 0.02 cm^2/cm^2. The data represent duplicate experiments of n = 3 and the shaded areas illustrate how the AUC values were determined for each plot. Bottom panel: The area under the response curve (AUC; % h) of four or five such plots (see appendix Figure S1 and S2) was used to generate each data point in the evaluation of the effect of atmospheric vs. physiological oxygen levels on ROS generation over time (% h) in response to (c) H_2O_2, 2.5 µM to 500 µM and (d) CuO nanoparticles, 0.0002 to 2 cm^2/cm^2.

AUC of ROS production over 4 h in cells cultured under physiological O_2 levels was 32% greater compared to cells cultured in 21% O_2 (185 ± 40 versus 138 ± 14 % h; Figure 5-4c). At higher concentrations of H_2O_2, cells cultured at both oxygen levels produced equivalent quantities of ROS over time. Although a strong positive dose

response was observed between 2.5 to 250 µM H_2O_2, no increase in ROS production was observed at concentrations above 250 µM in both culture conditions. As NP-induced ROS generation is a significant driver of NP toxicity, we examined whether cells cultured under physiological oxygen levels would be more sensitive to ROS generated from CuO NP using a similar study design and data analysis to that described above. ROS elevation was measured at five CuO particle surface area doses (representative results in Figure 5-4b; full data in appendix) and the AUC (% h) was calculated to show the effect of ROS elevation over 4 h in cells cultured under atmospheric or *physiological* oxygen. The AUC of values of the cells cultured at 13% were on average 19% lower at each concentration bar the lowest (Figure 5-4d). A review of the literature failed to find any studies reporting *in vitro* ROS production or nanotoxicity using cells cultured in physiological oxygen levels.

A549 cells cultured under hyperoxic conditions show a reduced dose-dependent sensitivity to nanoparticle-induced stress than those cultured under normoxia.

The MTT assay was used to evaluate the effect of CuO NP on cell viability when cultured under different oxygen pressures (Figure 5-5). No significant difference was seen in the half-maximal effective concentration (EC_{50}) of cells cultured at 13% oxygen compared to 21% oxygen after exposure to CuO particles for 24 h. The EC_{50} value in 13% oxygen was 23% lower than EC_{50} value in 21% (0.7 cm^2/cm^2 versus 0.9 cm^2/cm^2, P = 0.06).

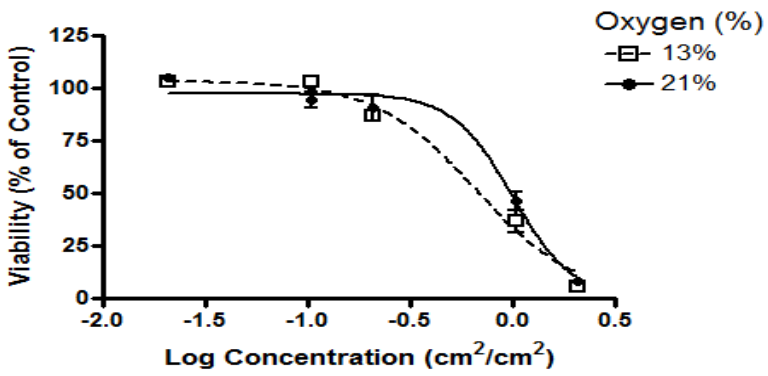

Figure 5-5: The effect of CuO nanoparticles on the viability of A549 cells after 24 h exposure to different oxygen levels. Cellular metabolic activity was measured spectrophotometrically at 560 nm and viability calculated as a percentage of the control (assay medium alone) over a particle concentration range of 0.02, 0.1, 0.2, 1 and 2 cm^2/cm^2. The data represent the mean ± SD of n = 3; each experiment performed in triplicate.

5.4 Discussion

We demonstrated that when the human alveolar epithelial-derived A549 cell line is cultured under atmospheric oxygen (21%) oxidative stress responses of the cells to NP challenge are diminished. We showed that cells exhibiting this impairment have elevated GSH levels, which presumably act as a protective mechanism against copper oxide (CuO) NP-induced oxidative stress (Figure 5-2). A549 cells cultured at 13% oxygen (i.e., the *physiological* oxygen level reflecting an oxygen pressure comparable to that in the lung) possess lower GSH levels and are more responsive to NP challenge.

The unique properties such as increased surface area, reactivity, solubility and oxidative potential conferred upon the materials at nanoscale which makes them interesting for consumer and health products also raises concern regarding their safety for human health and the environment (223, 231). Inhaled nanoparticles have been known to produce inflammation and have been linked with chronic effects such as lung fibrosis and cancer (232). Nanoparticles have also been linked with oxidative damage (DNA damage, mitochondria damage) due to production of oxidative stress (233). Nanoparticles can generate free radicals and these radicals upon interaction with cellular proteins and fatty acids can produce oxidative stress (94). The oxidative stress mechanism is probably the most well developed paradigm for explaining nanoparticle toxicity. A number of *in vitro* models have shown a clear link between nanoparticle exposure and the generation of oxidative stress (35-38, 42, 50, 54, 55, 78, 161, 223, 234-237).

Intracellular GSH levels measured over 8 h in A549 cells cultured at 21% O_2 were on average 81% higher than those measured in cells cultured at 13% O_2 (47 ± 2 versus 26 ± 7 nmol GSH/mg protein, respectively; Figure 5-2). In comparison, GSH values measured in lung biopsies of 24 healthy volunteers were found to be 11.2 ± 0.6 nmol GSH/mg protein (238). Compared to this value, which may not be reflective of the alveolar environment, A549 cells cultured under atmospheric oxygen exhibited a 5-fold upregulation of baseline GSH synthesis which can be attributed to the higher oxygen pressure and other oxidative stress-inducing artefacts *in vitro*, e.g. cell culture medium can itself generate ROS upon exposure to high oxygen levels (239). This response was only partially attenuated under *physiological* culture conditions of 13% oxygen.

The proposed mechanism of adaptive upregulation of GSH in response to elevated oxygen pressure is outlined in Figure 5-6 below. GSH is synthesized from three amino acids: L-γ-glutamate, L-cysteine, and L-glycine. The availability of intracellular L-cysteine is low, therefore uptake into the cell is proposed to be the rate-limiting step for GSH synthesis (240). To be transported into the cell, extracellular L-cysteine undergoes auto-oxidation to the disulfide L-cystine, which is a substrate of the Na^+-independent anionic amino acid transport system $^- x_c^-$, which exchanges cystine for intracellular L-glutamate (35). Once in the cell, the disulfide form of L-cystine is reduced to L-cysteine, which becomes available for GSH synthesis or is transported out of the cell by neutral amino acid transporters. The cystine-cysteine exchange cycle operates continuously (241) with the availability of L-cystine providing the driving force. Increasing the concentration of extracellular oxygen accelerates the formation of L-cystine (241) thus leading to enhanced GSH synthesis.

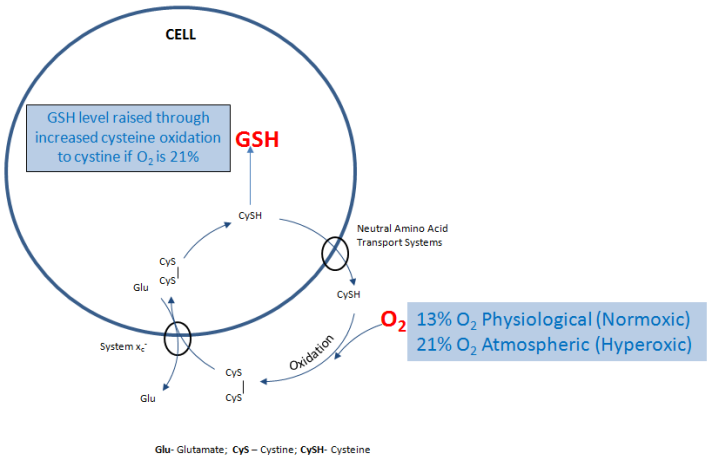

Figure 5-6: Proposed mechanism for elevation of intracellular GSH concentration via alteration of environmental O_2 concentration.

The electrophile diethylmaleate (DEM) depletes GSH by direct interaction with reactive cysteine sulfhydryl groups to form a stable adduct (242). GSH depletion leads to activation of the redox sensitive transcription factor Nuclear Factor-E2-Related Factor 2 (Nrf2), which is thought to stimulate pathways resulting in an increased influx of cystine via the cystine-glutamate exchanger resulting in a compensatory stimulation of GSH synthesis (242). Under this mechanism, exposure

to DEM depletes GSH levels initially followed by a rebound phase of increased GSH synthesis. This is consistent with the temporal profile of intracellular GSH production reported by Sato and co-workers for pancreatic cell lines and islet cell lines after challenge with 100 µM DEM (243). They showed that GSH levels decreased initially, followed by a 2-fold increase above control level after 24 h.

The exposure of A549 cells cultured at 13% O_2 to 100 µM DEM reduced GSH levels by approximately 30% during the first 2 h of exposure followed by a rebound phase during which GSH levels steadily increased to baseline concentration level (Figure 5-3a). In contrast, cells cultured at 21% O_2 exhibited no change in GSH levels in response to DEM (Figure 5-3b). The absence of any change of GSH in cells cultured under atmospheric conditions is in agreement with the work of Horton *et al.* (244) and Yang *et al.* (245) who reported no change in GSH level in A549 cells when they were challenged with 125 µM and 250 µM DEM. The mechanism underlying the lack of response to DEM in A549 cells cultured 21% O_2 is not known, although we postulate that adaptive increases in GSH are masked by the high basal GSH levels measured at atmospheric oxygen levels. Thus, low concentrations of DEM do not deplete GSH levels sufficiently to activate Nrf2 leading to an upregulation of GSH synthesis.

Our GSH measurements indicate that the cells cultured under the hyperoxic conditions adapt to oxidative stress via an increase in baseline GSH levels. These results are in agreement with the findings of Atkuri and co-workers (246), who investigated the effect of atmospheric oxygen level on the intracellular redox state in cultures of primary T cells. By measuring the GSH/GSSG ratio they concluded that culturing T cells under 21% O_2 leads to the development of highly oxidative intracellular environment (intra-cellular nitric oxide and intra-cellular ROS were 1.5 to 2 times higher ($p<0.001$)) in comparison to cells cultured under a physiological oxygen level of 5% O_2.

To investigate the differences in adaption to oxidative stress we measured the amount of reactive oxygen species (ROS) generated after the cells were challenged with hydrogen peroxide. Hydrogen peroxide is a known radical generator which causes the generation of oxidative stress. Dihydrorhodamine-123 is a redox sensitive dye which passively enters the living cells where it binds to the mitochondria upon oxidation to rhodamine-123 by ROS. Our results indicate that at low concentrations

of H_2O_2 (2.5 µM) the cells cultured under normoxia produce 30% more ROS as compared to cells cultured hyperoxia. To ensure that the fluorescence generated was from the ROS and DHR-123 interaction, we incubated the cells with radical scavenger PEG-catalse. Upon incubation with PEG-catalase the ROS levels stayed similar to the medium control (data not shown) in both the culture conditions. To ensure that this was not an artefact we performed live cell fluorescence studies using atmospheric controlled plate reader (BMG Labtech) so as not to compromise the normoxic state by exposing the plate to 21% atmospheric oxygen while reading the plate.

As NP-induced ROS generation is a significant driver of NP toxicity, we examined whether cells cultured under physiological oxygen levels would be more sensitive to ROS generated from CuO NP using a similar study design and data analysis to that described above. ROS elevation was measured at five CuO particle surface area doses (representative results in Figure 5-4b; full data in the appendix) and the AUC (% h) was calculated to show the effect of ROS elevation over 4 h in cells cultured under atmospheric or *physiological* oxygen. The exposure of A549 cells cultured at 21% O_2 to copper oxide (CuO) nanoparticles (a nanomaterial known to induce cytotoxicity via oxidative stress pathways) showed decreased intracellular reactive oxygen species (ROS) levels compared to cells cultured at 13% O_2 (Figure 5-4d), supporting the hypothesis that key indicators of toxicity, such as ROS generation, may be suppressed *in vitro* by cellular adaption to culture conditions.

Although no significant difference was seen in the half-maximal effective concentration (EC_{50}) of cells cultured at 13% oxygen compared to 21% oxygen after exposure to CuO particles for 24 h. The EC_{50} value in 13% oxygen was 23% lower than EC_{50} value in 21% (0.7 cm^2/cm^2 versus 0.9 cm^2/cm^2, P = 0.06). Interestingly, in a study by Kang and co-workers (247), much greater reduction in GSH (to 10% of control) was used to produce a 50% reduction in EC_{50} values using the MTT assay (untreated cells EC_{50}=31 µM, DEM 500 µM treated cells EC_{50}=15 µM) to measure the cytotoxic effect of Cd++ on A549 cells. It may be that cellular compensation mechanisms designed to withstand acute oxidative stress make the widely used MTT assay a low sensitivity end-point for nanotoxicology.

Our findings that cells with elevated GSH levels are also less sensitive to GSH disrupting agents and are protected from oxidative stress are consistent with our

hypothesis that cells adapt to hyperoxic conditions (summarised in Figure 5-7) rendering them less sensitive to the NP toxicity endpoints advocated under the oxidative stress paradigm for nanotoxicology screening (35, 36, 38, 43, 58).

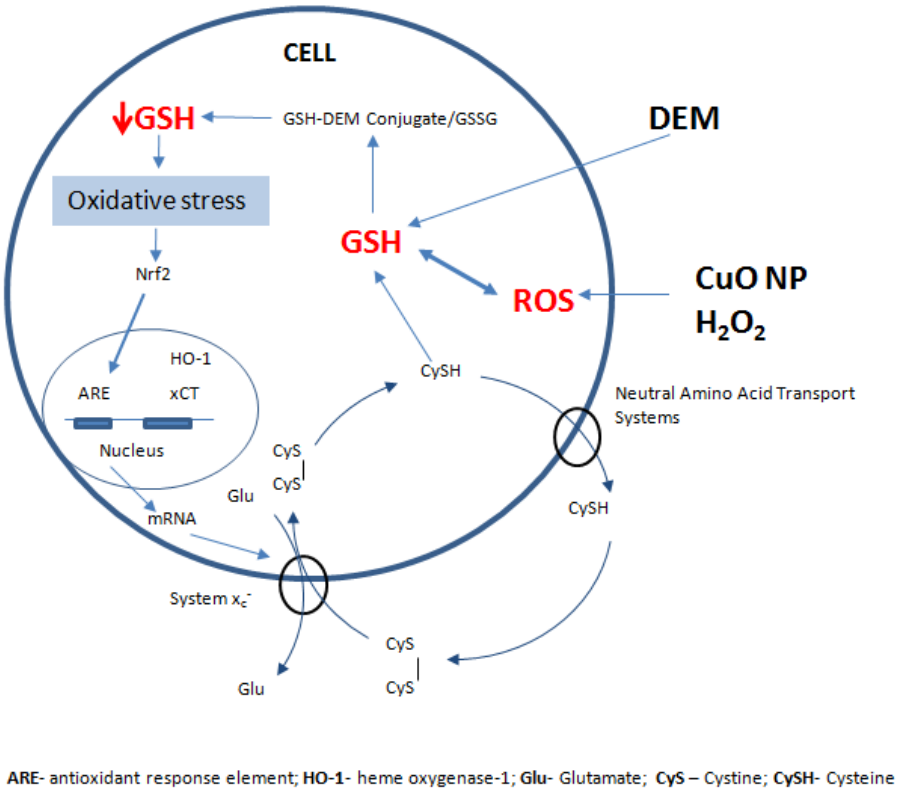

Figure 5-7: Summary of the effects of DEM, CuO nanoparticles and hydrogen peroxide on intracellular GSH and ROS levels adapted from Bannani *et al.* (241). Cells cultured under atmospheric oxygen concentrations adapt to hyperoxic conditions by generating higher intracellular GSH levels. Challenge with 100 µM DEM only affects cells cultured in physiological oxygen conditions under which the lower level of GSH undergoes a characteristic depletion followed by a rebound as the System X_c transporter mechanism is activated (Figure 5-3a). GSH levels in unadapted cells were reduced by CuO nanoparticles in a time dependent (Figure 5-3a) and dose dependent (Figure 5-3c) manner. The adapted cells are not sensitive to DEM challenge (Figure 5-3b) and cellular GSH concentration was only reduced by the highest dose of CuO nanoparticles (Figure 5-3d). Challenge with hydrogen peroxide produced a dose response in intracellular ROS, with the effect of the adaptation to the oxidative environment only conferring protection against the lowest dose used (Figure 5-4c). Cellular ROS was elevated in non-adapted cells after exposure to copper NP across the entire dosage range, 0.0002 - 2 cm^2/cm^2 (Figure 5-4d).

5.5 Conclusion

We have demonstrated that A549 cells cultured using an atmospheric oxygen concentration (21%) adapt to hyperoxia by producing higher levels of the antioxidant GSH. Cells featuring this adaptation were less susceptible to interference with their antioxidant balance by DEM or CuO NP. Furthermore, intracellular ROS generation after challenge with hydrogen peroxide (2.5 µM) or CuO NP (0.002 - 2 cm^2/cm^2) was attenuated. This is consistent with the hypothesis that generation of intracellular ROS will be subject to altered sensitivity in cells cultured under different oxygen tension.

Oxidative stress is proposed as an early indicator of nanotoxicity (tier 1 under the three tier model of Xiao *et al*. (38, 43, 58)). In contrast to the sensitivity of oxidative stress markers (ROS generation and GSH depletion) to oxygen potential, the MTT assay results indicated that despite the EC_{50} value of cells cultured at 13% oxygen being 23% lower that of cells cultured at 21% oxygen, cells cultured under physiological conditions were not significantly more sensitivity in terms of this tier 3 toxicological endpoint. Further work will determine whether tier 2 markers (e.g. activation of inflammatory cytokines and chemokines) are affected by the cellular responses to hyperoxic culture that we report. A much bigger question is to what extent these findings can be generalised across different cell types and nanotoxicity endpoints. We raise important concerns regarding the impairment of oxidative stress responses in cells cultured at 21% oxygen. The data provided herein leads us to caution that cells used under standard protocols for nanotoxicology screening may be limited in their ability to report biological mechanisms related to oxidative stress.

Chapter 6

Discussion

6.1 Current state of nanotoxicology

In 2004, the Royal Society and the Royal Academy of Engineering published a key review of the opportunities and uncertainties associated with nanotechnology applications, which was a key report highlighting the potential environmental and human health risk issues of NPs (3). Since then, more than 50 reviews carried out by governmental and international organizations, industry associations and research institutes have considered NP risk issues, concluding that multiple deficiencies of toxicity and exposure data make it impossible to perform sound risk assessment of NPs (248).

A recent review by Hristozov *et al.* (249) of available data discussed the state of the art in the area of NP risk assessment. The authors surveyed 42 environmental, health and safety databases including NAPIRhub, Hazardous Substances Data Bank, Chemical Safety Data Searcher etc. for seven engineered NP including: carbon nanotubes (CNTs), C_{60} fullerene, titanium dioxide (TiO_2), silver (Ag), zinc oxide (ZnO), iron (III) oxide (Fe_2O_3) and silica (SiO_2) NP. All the records were counted and categorised into: (1) manufacture, use and disposal; (2) physical and chemical properties; (3) environmental fate and pathways; (4) ecotoxicological information; (5) toxicological information; and (6) guidance on safe use. The authors found that majority of information obtained concerned TiO_2, followed by ZnO and Fe_2O_3 and most of them were situated in toxicological information category. The authors found that for TiO_2 of the 302 data records in toxicological information (Figure 6-1 top panel) section only 99 records (33%) were usable and out of 44 data records in physical and chemical category only 5 records (12%) were usable (Figure 6-1 bottom panel).

This search was not exhaustive as data in scientific literature including journal articles, books, conference proceedings and reports were not included due to large number of publications. A search with the key string ((nanoparticle OR nanomaterial OR nano) AND (toxicity OR ecotoxicity OR exposure OR health effect

OR medicine OR drug)) in the 'topic' section of ISI Web of Knowledge article database on 28 June 2012 returned 51,861 articles (approximately). A further modification to narrow the search to inhalation related toxicity with the key string

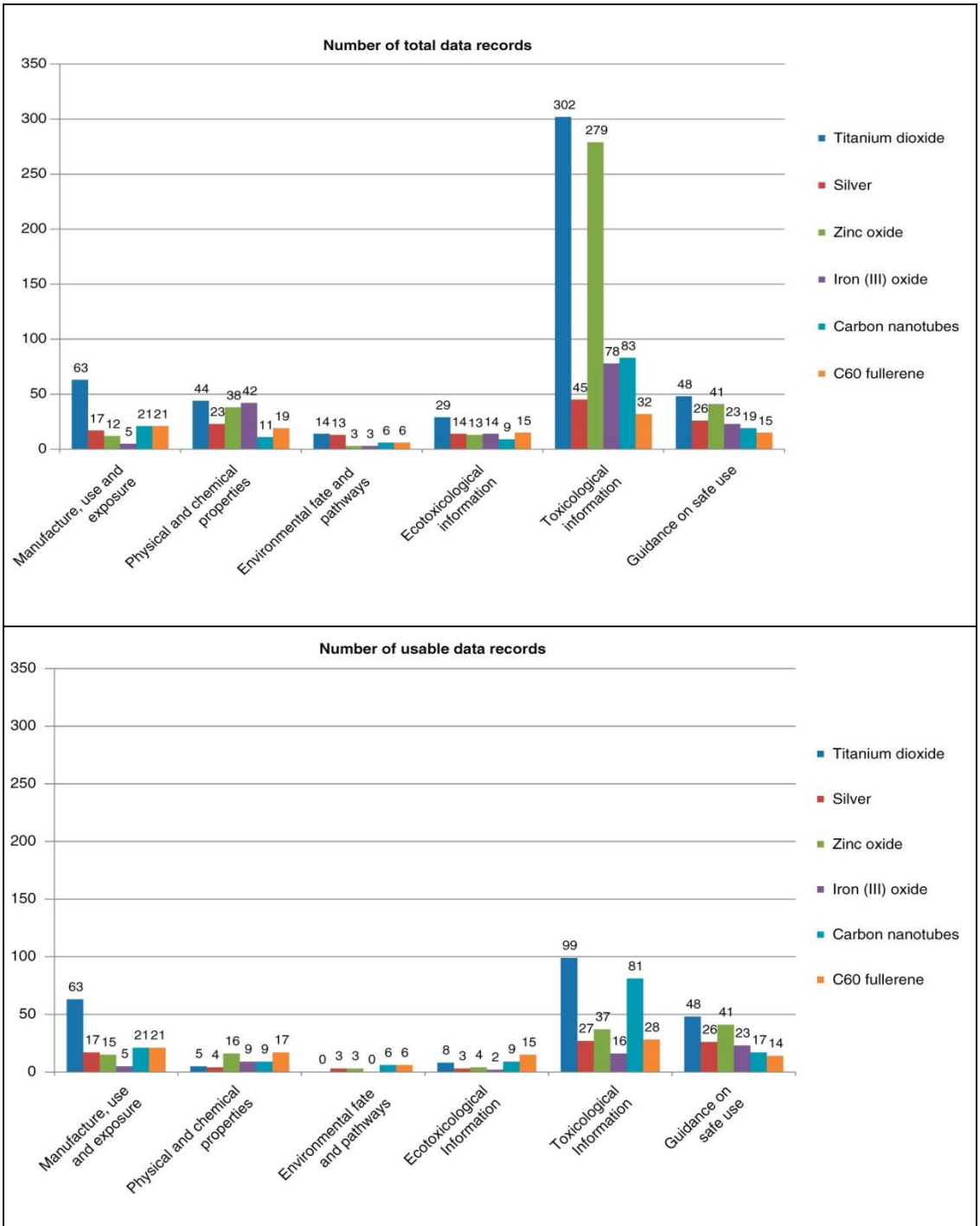

Figure 6-1: Distribution of total data records (top panel) and usable data (bottom panel) records for six different NPs in all the databases; titanium dioxide (dark blue), silver (red), zinc oxide (green), iron(III) oxide (purple), carbon nanotubes(light blue), C60 fullerene (orange) (adapted from Hristozov *et al.* (249)).

((nanoparticle OR nanomaterial OR nano) AND (toxicity OR ecotoxicity OR exposure OR health effect OR medicine OR drug) AND (lung OR airway OR respiratory OR pulmonary)) in the 'topic' section of ISI Web of Knowledge article database on 28 June 2012 returned 2,366 articles. A look at the distribution of these published articles published every year from 2000 till 2011 indicates an increasing interest in the respiratory effects of nanomaterials (Figure 6-2).

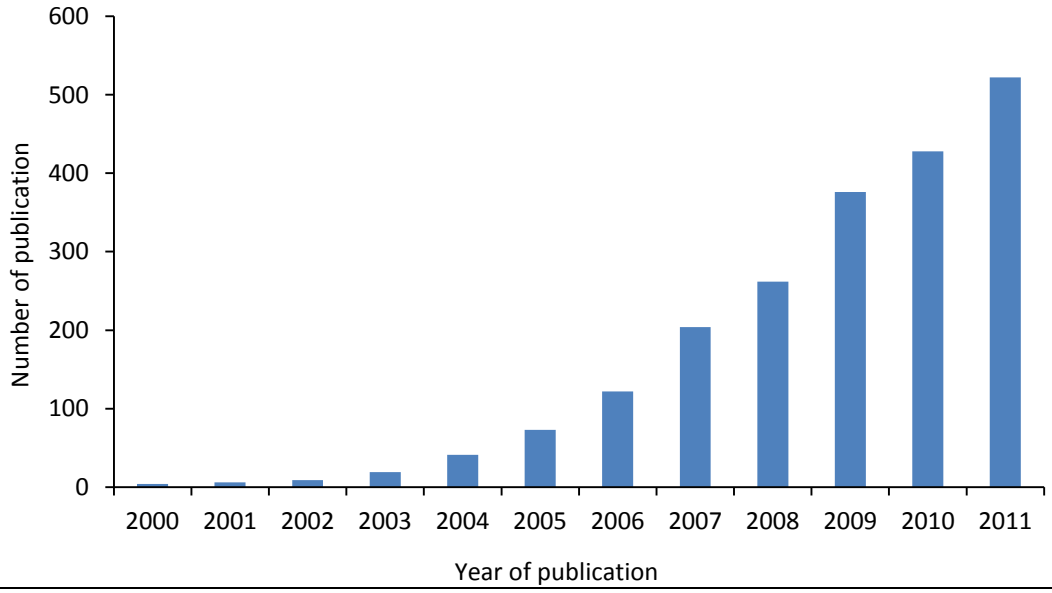

Figure 6-2: Distribution of number of publications per year published between the years 2000 till 2011. Search was made on ISI Web of Knowledge database on 28 June 2012. The following search string was used within the 'topic' field of the database search engine: ((nanoparticle OR nanomaterial OR nano) AND (toxicity OR ecotoxicity OR exposure OR health effect OR medicine OR drug) AND (lung OR airway OR respiratory OR pulmonary)).

Figure 6-2 shows a snapshot of the current state of research and assuming that the distribution of usable data across scientific literature amongst various categories may be similar to the data set reviewed by Hristozov *et al.* (249) then the opportunity to utilize the nanotechnology sector to its fullest would be difficult.

6.2 Redefining nanotoxicity research protocols

The body of literature (42, 77, 80, 85, 86, 161, 236, 250) confirms the essential role which NP characterization plays in identifying the key physico-chemical characteristics of NP with regard to assessing the potential toxicity of NP in

biological systems. It is important to characterize the test material as thoroughly as possible, especially in biologically relevant systems, to ensure the results are reproducible and also to provide the basis for understanding the properties of NP that determine their biological effects. With respect to particle characterization in biologically relevant media it has been demonstrated how serum (177, 218) (commonly used supplement in cell culture medium) often affects the dispersion (aggregation/agglomeration) profile of NP in suspension. Further it has been shown how the adsorption of cell culture medium components on the surface of NP affects the cellular impact of NP (251, 252), usually providing the cells with some protection from the cytotoxic effect of NPs. Another discrepancy highlighted when reviewing the literature is the usage of high dosage/concentrations and the dose metrics used for expressing the concentration of particles exposed to cells or animals. For example, a study by Yokohira *et al.* (253) tested the carcinogenicity of TiO_2 (80 nm) by instilling 0.5 mg/rat lung of NP in F344 male rats and upon hisopathological examination concluded that there were no lung lesions i.e. theTiO_2 NPs were non-carcinogenic. However, in another study by Roller *et a.l* (254) TiO_2 (25 nm) were instilled in rats at 15, 30 and 60 mg/rat lung dose and the authors found that the TiO_2 NPs clearly showed carcinogenicity. There is a basic error in both these studies and that is their use of dose metrics. A study by Bellmann *et al.* (255) identified that particle overload occurred at a lung burden of 3 mg/rat lung (material: test toner) as identified by number of PMNs in BALF and the clearance of gamma labelled tracer particles. In contrast, at a lung burden of 0.4 mg/rat lung the alveolar clearance rate was not significantly impaired. In light of this information the first study by Yokohira *et al.* uses a very low dose whereas the study by Roller *et al.* uses an extremely high dose. Another example cited by Oberdorester *et al.* (161) points to the high-bolus type dose used in *in vivo* studies which can be misinterpreted by the popular non-scientific press. The case in point is a study by Wang *et al.* (256) who instilled 7.5 mg nano-TiO_2 intranasally in mice which resulted in significant oxidative stress and inflammation in the brain. However, Oberdörster points out that the dose in this case was the equivalent of intranasally instilling ~17.5 g of the material into a human subject.

It is not only *in vivo* studies which get the dosage wrong, but also *in vitro* studies. A study by Long *et al.* (257) demonstrated oxidative stress induction by

microglia cells caused by doses of well characterized nano TiO_2 at 25 μg/ml and higher. It has been argued that 'whilst this result represents an interesting hypothesis forming finding, an extrapolation to real-world exposure scenarios is not possible given that the dose administered to the microglia cells was already greater than will be received by alveolar macrophages in the lung following 24 h of inhalation at a high concentration of 1 mg m^{-3} (258). Considering that only 1% or 2% of the NPs deposited in the lung may translocate to the blood circulation, and of that none or <1%, may translocate to the CNS (24), the relevancy of results from unrealistic high *in vitro* doses for real-world *in vivo* conditions should be seriously questioned.

Apart from dosage/concentration issues, the debate regarding the units used (surface area, mass, number of NP) has been discussed previously in Chapter 1 and Chapter 3. There is a growing understanding of NP behaviour in suspension and it is not only low density drug delivery NPs for which the delivered dose *in vitro* is a concern but also high density particles like gold NP as demonstrated by Cho *et al.* (179). Even after using well characterized NPs, a biologically relevant dose metric and considering particokinetics *in vitro,* it may be possible to make methodological errors thus leading to misinterpretation of results. In developing a cell-based safety screening programme it is generally recommended that more than one cell type is utilised in conjunction with standardised assays that are sensitive, predictive and robust (259). However, the literature indicates that NP toxicity studies are often performed and reported using single cell line.

The issue of choosing the correct controls can also be problematic. For example, it has been discovered that some particles display a high intracellular dissolution rate (example: zinc oxide). Often the toxicity associated with these NP is due to the dissolution of ions either in the cell or in suspension (260). Therefore, it is important in such cases to use Zn ions (such as $ZnCl_2$) as a control to truly understand the mechanisms of toxicity.

Apart from the lack of controls, a common methodological error has been to culture cells under atmospheric oxygen condition. One of the proposed paradigms for nanotoxicity is the generation of oxidative stress (35-38, 42, 50, 54, 55, 78, 161, 223, 234-236). What has been overlooked, however, is the fact that standard cell culture practices use atmospheric oxygen (i.e. 150 mm Hg, ~21%, O_2) which in itself constitutes a hyperoxic environment. With the exception of the cornea, epidermis and

respiratory tract epithelial layer, cells *in vivo* typically experience 1-10 mmHg oxygen pressure (equating to ~ 1-5% O_2). In the respiratory tract, small airway epithelial cells and alveolar cells experience approximately 100 mm Hg oxygen (~ 13% O_2) (92). Despite this, most mammalian cells are cultured using 21% O_2 which exposes them to elevated levels of ROS (93, 94).

In the present work the shortcomings discussed above in the *in vitro* nanotoxicity methods were addressed by trying to develop, standardize and validate *in vitro* cytotoxicity tests so that the methods are more robust, reliable and reproducible. In Chapter 2 a novel primary cell culture method was developed to harvest primary human nasal epithelial cell in a pain free way. The method is non-invasive, self administered and permits repeated isolation from the same source. The cell viability of the lavaged cells was approximately 50% and more than 90% of the cells were epithelial in nature. In the freshly lavaged cells sometimes ciliated cells (with live beating cilia) could also be seen under the microscope. Although the cells were healthy and viable, they did not proliferate and were thus not well suited for NP toxicity screening. However, this method has other possible advantages, as it could be beneficial in performing geno-toxicity studies across higher numbers of volunteers. For example, it is envisioned that one could fill a 96-well plate with samples from a diverse range of subjects, including diseased and non-diseased groups.

As demonstrated in Chapter 3, the choice of dose metric is very important in cytotoxicity studies as particle behaviour in suspension is very different to behaviour of soluble chemicals. An Excel®-based particokinetics program (EXCEL) was written to model the movement of particles in suspension due to gravitation and diffusion. The model results of calculated delivered dose values were compared to experimental uptake data from Khanbeigi *et al.* (169) and as well as delivered dose values generated by the ISDD program developed by Hindergarten *et al*. (89). EXCEL results showed a reasonable correlation with both the experimental data and ISDD values over a wide variety of particle sizes and exposure times. The EXCEL program differs from ISDD in the aspect that it may double count some particles, dependent upon particle size and density, leading to a slightly over-estimated delivered dose value. On the other hand, the program's flexibility allows it to compute the delivered dose from a particle size distribution curve (instead of a

simple mean particle size value) thus allowing it to take into consideration non-agglomerated particle size polydispersity. The results in Chapter 3 led to the conclusion that *in vitro* particle-cell interaction data should be reported in terms of the delivered dose metric as opposed to the commonly used administered dose. This would help us in making valid comparisons of NP toxicity across different nanoparticle sizes and material types.

It is increasingly recignised that NP characterization plays an essential role in identifying the key physico-chemical characteristics of NP with regard to assessing the potential toxicity of NP in biological systems. In Chapter 4, NPs were characterized in terms of size and zeta potential in both water and more importantly in a biologically relevant medium. It was found that NPs remained stable in serum-supplemented cell culture medium compared to aggregation in serum depleted medium and water. Thus it is important to report physicochemical properties of nanoparticles such as size as they would manifest the experiment. Further, an ascorbic acid depletion assay was used to determine the *ex vivo* oxidative potential of NPs. It was found that CuO NP had the highest oxidative potential and this correlated well with CuO showing the highest cytotoxicity in two cell lines compared to all the other particles tested. The cytotoxcity data was normalised to delivered dose values using the EXCEL program developed in Chapter 3 and the differences in EC_{50} values for cell viability (comparison administered vs. delivered dose) showed that there was one order of magnitude difference for the LNC particles. The differences in nominal and delivered dose EC_{50} values for LNC 50 and LNC 150 demonstrated that normalization of *in vitro* results to administered dose values may lead to reporting of effective toxic or minimum active doses that are artificially higher than they should be in safety studies. This study thus ilustrated how using particokinetic modeling in designing *in vitro* cell-based assays can lead to more accurately assess most of dose-response effects of nanoparticle systems.

In Chapter 5, the commonly overlooked flaw of using atmospheric oxygen (i.e. 150 mm Hg, ~21%, O_2) to culture cells, was explored. Since generation of oxidative stress due to NP-cell interactions has been highlighted as an important paradigm for certain types of NP toxicity, the oxidative environment generated by atmospheric culture conditions may induce a protective response mechanism in cultured cells, rendering them less sensitive to nanoparticle-induced oxidative stress.

In Chapter 5 we tested this hypothesis and showed that (i) the culture of respiratory epithelial cells in a hyperoxic environment produces an adaptation in terms of increased GSH levels, (ii) the adapted cells were less sensitive in terms of nanotoxicity assay end-points, particularly ROS production and altered GSH synthesis interference. This work may explain, in part, why *in vitro-in vivo* correlation is often poor and raises questions regarding the physiological relevance of studies conducted with epithelial cells cultured under hyperoxic conditions. We conclude that the adaptation demonstrated herein by cells cultured in 21% O_2 renders these assay systems inappropriate for studies where sensitivity to oxidative stress is necessary and question whether this may be the case for the majority of *in vitro* nanotoxicity assay systems.

6.3 Future work

Approximately €10 billion are spent on animal experimentation worldwide every year, out of which ~€2 billion is for toxicological studies. Given that more than 100 million experimental animals are used and that products worth €5.6 trillion are regulated by such testing (69), the usage of *in vitro* assays becomes more and more important. In a Nature review article, Thomas Hartung proposed that the crux of the matter is the predictive power, reliability and usefulness of these model systems (69). The aim of this work was to address some shortcomings in the current practice of *in vitro* NP toxicity testing. However, more work remains to be done in end of these study areas to make the current *in vitro* tests reliable.

To culture the primary human nasal epithelial cells successfully, further modifications need to be made to the culturing techniqueand further characterisation is required. For example, culturing cells in bronchial epithelial growth medium (BEGM – Lonza, UK) supplemented with BEGM SingleQuot Kit Supplement & Growth Factors (Lonz, UK) including insulin, hydrocortisone, transferrin, choleratoxin, T3, EGF and retinoic acid, may be one method to improve conditions such that growth, expansion, and viability of the primary human nasal epithelial cells is achieved (145, 261). Further, the nasal cells still require characterisation, for example with antibody staining of cytokeratins 4, 5, 6, 8, 10, 13 and 18, as well as epithelial cell specific markers.

The particokinetic model reported in Chapter 3 can be further improved by taking into account the cumulative cell surface residence time. It could also be possible to modify the ISDD program so that it takes into account a non-aggregated, but polydisperse particle sample. Currently such analysis has to be performed manually using ISDD, whereas in the EXCEL program this process has been automated. In Chapter 4 it could be seen that the application of the particokinetic model to normalise the results to delivered dose values allowed for a highly robust comparison of nanoparticles of different properties. To expand upon this, particle characterization in RTLF could be performed using the technique developed by Braeckmans *et al.* (222) fluorescence single particle tracking coupled with maximum entropy doconvolution method. It would be highly interesting to compare the properties of the particles in cell culture medium and RTLF. Further it has been shown that protein corona formed around the particle influences the particle-cell interaction (262, 263) so it would be interesting to investigate which nanoparticle physicochemical characteristics, especially size and surface chemistry, will dictate the type and amount of protein and phospholipid adsorption to the particle surface (i.e. the macromolecule corona). This in turn will influence the particokinetics and toxicity profile of the particles in the nose and lung. Further, a comparison of the different proteins adsorbed onto the particles suspended in cell culture medium could be made to the ones adsorbed onto the particle suspended in RTLF. These studies would significantly advance our understanding of particle interactions at the air-lung interface, informing our understanding of bio-persistence and potential toxicity. Furthermore, such studies would generate insightful information which may help to guide the design of safer engineered particles for such purposes as inhalation drug delivery.

In terms of toxicity testing it would be helpful to perform cytotoxicity testing using live-dead cell staining, GSH depletion, intra-cellular ROS generation and cytokine release. This might help in comparing particokinetics-normalised results to *in vivo* studies where PMN recruitment and inflammatory cytokine released are usually reported in BAL samples.

In Chapter 5 we demonstrated that standardised cell culture conditions are inappropriate for assessing toxicity arising from oxidative stress, because culturing cells at atmospheric oxygen pressure (150 mm Hg or ~21% O_2) results in phenotypic

adaptations to the hyperoxic environment that mask toxicity. These observations have significant repercussions in predictive toxicology, not only for novel engineered and environmental nanoparticles, but also in non-particulate drug safety testing. However, further work is required to elaborate fully the nature of the cellular adaption occurring under atmospheric oxygen tension and the extent to which this desensitises cell models to the induction of inflammation and cell injury/death. To do this we propose to investigate (1) the pathways upregulating intracellular GSH in response to hyperoxia, e.g. increased cystiene import versus de novo synthesis and (2) how cellular adaptation to hyperoxia influences the regulation of chemical- and particle-induced inflammatory pathways and cytotoxicity (apoptosis and necrosis). To address the transition from protective adaptation to inflammation and ultimately cell death, we will examine the expression of a panel of genes under the regulation of Nrf2 (including glutamate cysteine ligase), AP1, NFκB and p53, parallel to transcription factor binding assays in detailed dose response experiments. Further we could include chemicals (TCDD (2,3,7,8-tetra-chlorodibenzo-p-dioxin) an arylhydrocarbon receptor agonist) and particles (TiO_2 NP) which are known not to cause oxidative stress and compare it to the results obtained from challenges of H_2O_2, DEM and CuO NP and this will help to determine the extent to which cell adaptations to culture conditions attenuate or mediate the response of the cells to a chemical or particle challenge. Preparation of a comprehensive database of *in vivo* respiratory toxicity measurements (including biochemical readouts, inflammation and tissue histology) compiled from the literature for the relevant panel of toxicants over an equivalent dose range, would allow data to be compared with results generated as discribed above to assess whether dose-response effects in cells cultured at physiological oxygen tension correlate better with dose-responses measured *in vivo* than data produced in cells cultured at atmospheric oxygen tension. Such a study could be extended to examine the behaviour of primary airway epithelial cells in the different oxygen environment and use some of the advanced *in vitro* cultures such as biculture systems (264-266) or a triple co-culture system consisting of epithelial cells, human monocyte-derived macrophages and dendritic cells simulating the epithelail airways (267, 268). Further, the application of IVIVC (*in vitro-in vivo correlation*) analysis to the entire hierarchy of responses to toxicity (i.e. cellular adaption, inflammation, cell injury and cell death) will also make it possible to

distinguish between cellular responses that are influenced to a greater or lesser extent by the incubator oxygen tension.

In vitro assays based on cell cultures are widely used, but their implementation is limited by poor predictive capacity, especially for particle testing. In response, the National Academy of Science, *Toxicity Testing in the 21st Century* (81) has set forth a vision of the paradigm shift needed in toxicity screening of nanoparticles. This vision rests on a comprehensive suite of *in vitro* assays in human cells and cell lines enabling identification of perturbations of toxicity pathways. The reliance on toxicity pathway perturbations as the basis for human health risk assessment will require sufficient understanding of such pathways to permit the shift away from animals to occur with confidence (43). To achieve this, we must address one of the major shortcomings of *in vitro* cell models, which is the inconsistency in transcriptional regulation of toxicity pathways *in vitro* as compared to that which occurs *in vivo.* These differences result from the difference in microenvironment, lack of multicellular interactions and inadequate or inappropriate metabolism. The toxicokinetic work presented here provides solutions to some of these critical limitations and may provide important stepping stones towards a breakthrough in the acceptance of *in vitro* testing methods and the replacement of animal models in toxicity screening.

APPENDIX

Intracellular ROS reflect differences in protective GSH levels

Intracellular ROS levels were measured using dihydrorhodamine-123 (DHR-123, non-fluorescent), a redox sensitive dye which passively enters living cells where it binds to the mitochondria upon oxidation by ROS to the fluorescent, rhodamine-123 (R-123). R-123 fluorescence was measured in live cells using an atmospheric controlled plate reader (BMG Labtech) so as not to alter oxygen levels while reading the plate.

Each experiment consisted of 4 measurements over 4 h at each H_2O_2 and nanoparticle concentration and was performed in triplicate on two occasions and these data (Figure S1 a - d and Figure S2 a-e) were used to generate an area under the curve (AUC) of the increase in ROS (Figure 5-4c, 5-4d).

Hydrogen Peroxide

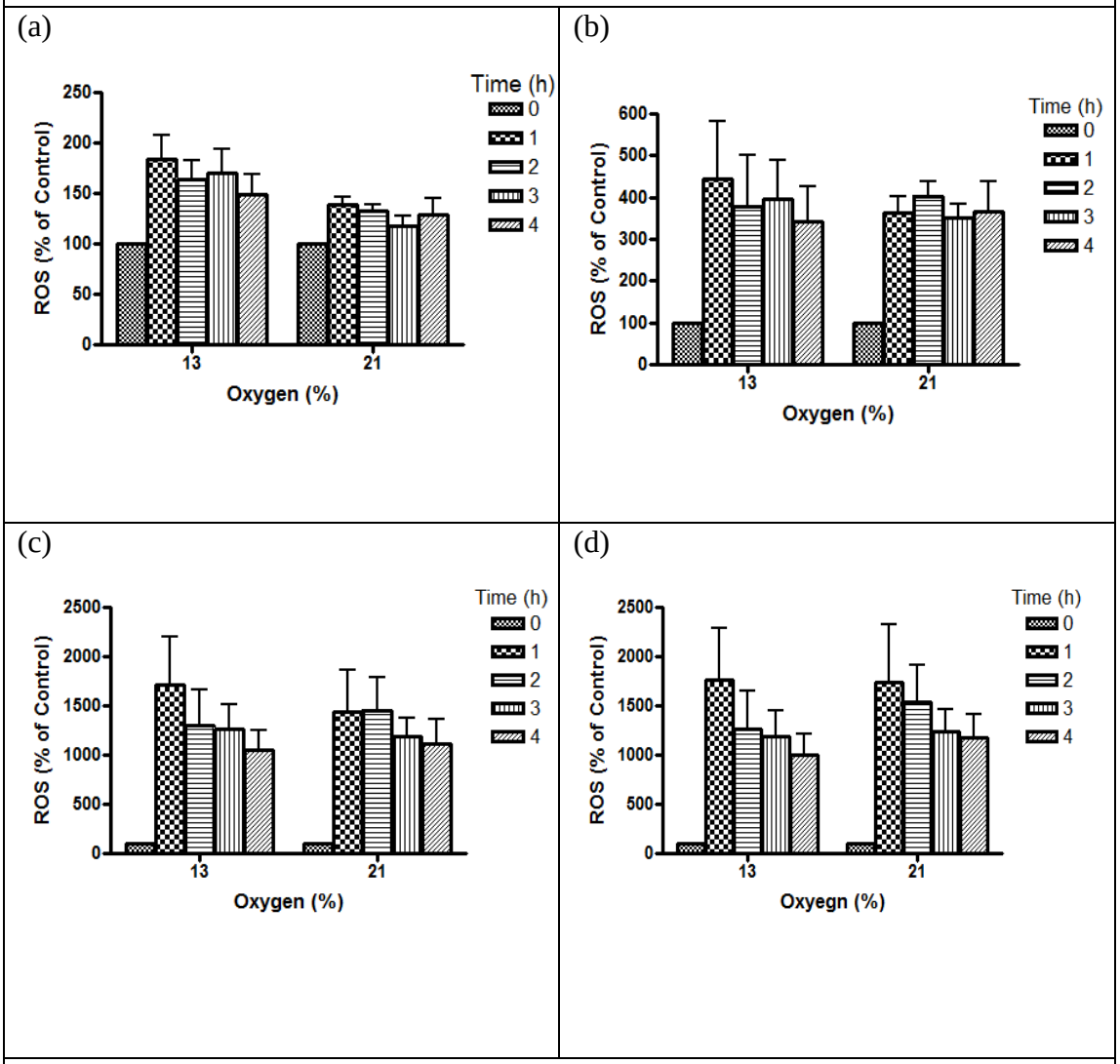

Figure S 1: Representative figures to illustrate the effect of different culture conditions on ROS generation in A549 cells after 1-4 h exposure to hydrogen peroxide (a) 2.5, (b) 25, (c) 250 and (d) 500 µM. The data represent duplicate experiments of n=3 and the area under the response curve of these plots was used to generate each data point in the evaluation of the effect of atmospheric vs. physiological oxygen levels on ROS generation in A549 (AUC % h; increase compared to control) 1-4 h exposure H_2O_2, 2.5 to 500 µM (Figure 3c). The fluorescence was measured at an Ex of 490 nm and Em of 530 nm in an atmosphere-controlled plate reader.

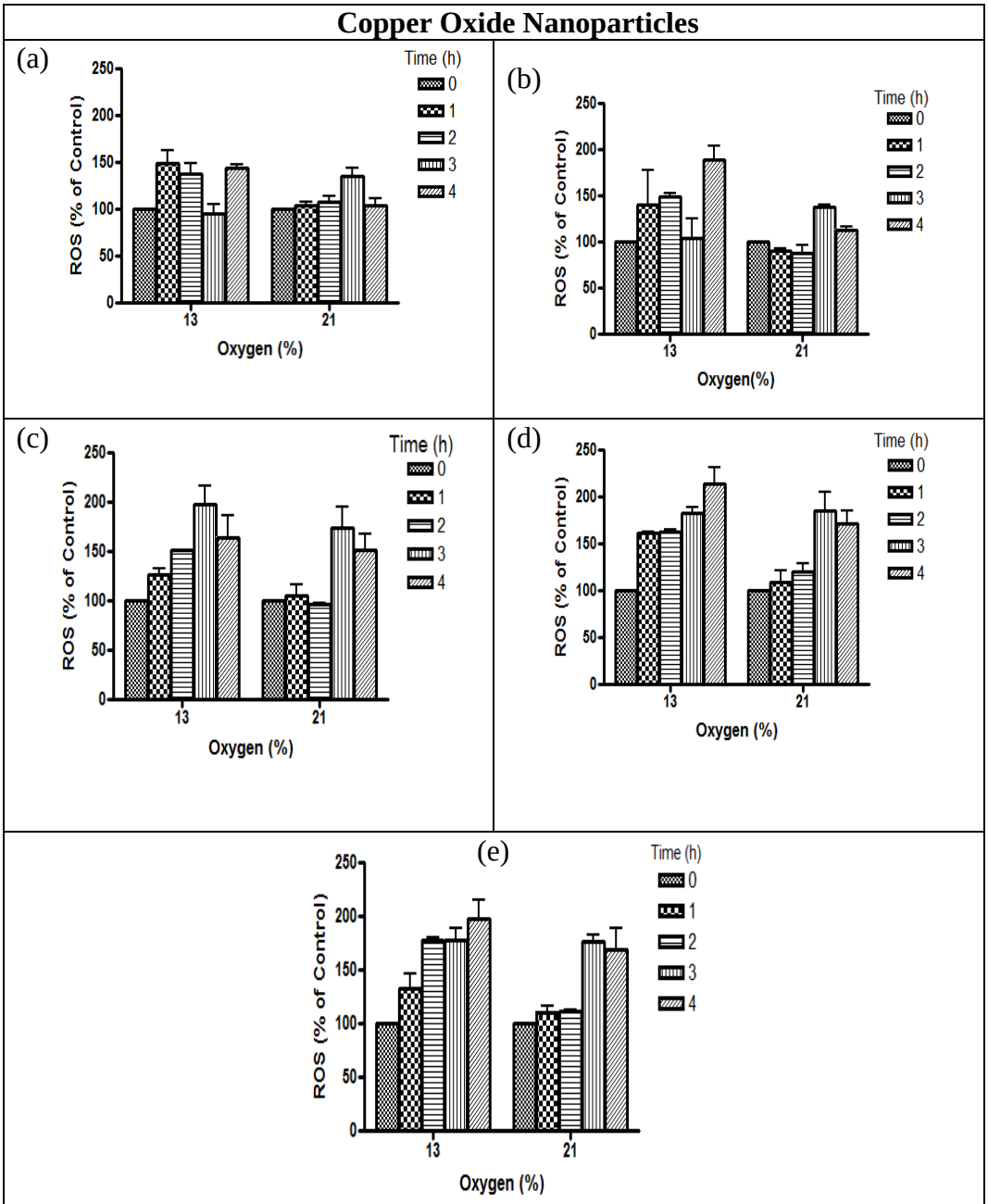

Figure S 2: Representative figures to illustrate the effect of different culture conditions on ROS generation in A549 cells after 1-4 h exposure to CuO nanoparticles (a) 0.0002, (b) 0.002, (c) 0.02, (d) 0.2 and (e) 2 cm^2/cm^2. The data represent duplicate experiments of n=3 and the area under the response curve of these plots was used to generate each data point in the evaluation of the effect of atmospheric vs. physiological oxygen levels on ROS generation in A549 (AUC % h; <u>increase</u> compared to control) 1-4 h exposure CuO nanoparticles, 0.0002 to 2 cm^2/cm^2 (figure 3d). The fluorescence was measured at an Ex of 490 nm and Em of 530 nm in an atmosphere-controlled plate reader.

Reference List

1. Feynman R P. There's Plenty of Room at the Bottom. *Engineering and Science* 1960;23:22-36.

2. Tata Swach Nanotech Water Purifier.; 2012.

3. The Royal Society and the Royal Academy of Engineering (UK) Nanoscience and Nanotechnologies: Opportunities and Uncertainties.; 2004.

4. Nijhara R, Balakrishnan K. Bringing Nanomedicines to Market: Regulatory Challenges, Opportunities, and Uncertainties. *Nanomedicine* 2006;2:127-136.

5. Lux Research. The Nanotech Report, 4th Edition.: Lux Research Inc., New York, NY; 2006.

6. Nanotechnology Consumer Product Inventory Washington DC: Project on Emerging Nanotechnology.: Woodrow Wilson International Center for Scholars; 2011.

7. Abbott LC, Maynard AD. Exposure Assessment Approaches for Engineered Nanomaterials. *Risk Anal* 2010;30:1634-1644.

8. Byrne JD, Baugh JA. The Significance of Nanoparticles in Particle-Induced Pulmonary Fibrosis. *Mcgill J Med* 2008;11:43-50.

9. Zanobetti A, Schwartz J, Samoli E, Gryparis A, Touloumi G, Peacock J, Anderson RH, Le TA, Bobros J, Celko M, et al. The Temporal Pattern of Respiratory and Heart Disease Mortality in Response to Air Pollution. *Environ Health Perspect* 2003;111:1188-1193.

10. Brunekreef B, Beelen R, Hoek G, Schouten L, Bausch-Goldbohm S, Fischer P, Armstrong B, Hughes E, Jerrett M, van den Brandt P. Effects of Long-Term Exposure to Traffic-Related Air Pollution on Respiratory and Cardiovascular Mortality in the Netherlands: the NLCS-AIR Study. *Res Rep Health Eff Inst* 2009:5-71.

11. Tsai DH, Wang JL, Chuang KJ, Chan CC. Traffic-Related Air Pollution and Cardiovascular Mortality in Central Taiwan. *Sci Total Environ* 2010;408:1818-1823.

12. Dockery DW, Pope CA, III, Xu X, Spengler JD, Ware JH, Fay ME, Ferris BG, Jr., Speizer FE. An Association Between Air Pollution and Mortality in Six U.S. Cities. *N Engl J Med* 1993;329:1753-1759.

13. Eisen EA, Dockery DW, Speizer FE, Fay ME, Ferris BG, Jr. The Association Between Health Status and the Performance of Excessively Variable Spirometry Tests in a Population-Based Study in Six U.S. Cities. *Am Rev Respir Dis* 1987;136:1371-1376.

14. Brouwer D. Exposure to Manufactured Nanoparticles in Different Workplaces. *Toxicology* 2010;269:120-127.

15. Warheit DB. Debunking Some Misconceptions About Nanotoxicology. *Nano Lett* 2010.

16. Xia T, Li N, Nel AE. Potential Health Impact of Nanoparticles. *Annu Rev Public Health* 2009;30:137-150.

17. SCENIHR. Risk Assessment of Products of Nanotechnologies.: Scientific Committee on Emerging and Newly Identified Health Risks; 2009.

18. National Nanotechnology Initiative. Environmental, Health, and Safety Research Needs for Engineered Nanoscale Materials.: Nanoscale Science,Engineering and Technology; 2006.

19. Donaldson K, Stone V, Tran CL, Kreyling W, Borm PJ. Nanotoxicology. *Occup Environ Med* 2004;61:727-728.

20. Choudhury AH, Gordian ME, Morris SS. Associations Between Respiratory Illness and PM10 Air Pollution. *Arch Environ Health* 1997;52:113-117.

21. Kreyling WG, Semmler M, Erbe F, Mayer P, Takenaka S, Schulz H, Oberdorster G, Ziesenis A. Translocation of Ultrafine Insoluble Iridium Particles From Lung Epithelium to Extrapulmonary Organs Is Size Dependent but Very Low. *J Toxicol Environ Health A* 2002;65:1513-1530.

22. Oberdorster G, Sharp Z, Atudorei V, Elder A, Gelein R, Lunts A, Kreyling W, Cox C. Extrapulmonary Translocation of Ultrafine Carbon Particles Following Whole-Body Inhalation Exposure of Rats. *J Toxicol Environ Health A* 2002;65:1531-1543.

23. Warheit DB, Overby LH, George G, Brody AR. Pulmonary Macrophages Are Attracted to Inhaled Particles Through Complement Activation. *Exp Lung Res* 1988;14:51-66.

24. Kreyling WG, Semmler M, Erbe F, Mayer P, Takenaka S, Schulz H, Oberdorster G, Ziesenis A. Translocation of Ultrafine Insoluble Iridium Particles From Lung Epithelium to Extrapulmonary Organs Is Size Dependent but Very Low. *J Toxicol Environ Health A* 2002;65:1513-1530.

25. Oberdorster G, Ferin J, Morrow PE. Volumetric Loading of Alveolar Macrophages (AM): a Possible Basis for Diminished AM-Mediated Particle Clearance. *Exp Lung Res* 1992;18:87-104.

26. Oberdorster G, Finkelstein JN, Johnston C, Gelein R, Cox C, Baggs R, Elder AC. Acute Pulmonary Effects of Ultrafine Particles in Rats and Mice. *Res Rep Health Eff Inst* 2000:5-74.

27. Semmler M, Seitz J, Erbe F, Mayer P, Heyder J, Oberdorster G, Kreyling WG. Long-Term Clearance Kinetics of Inhaled Ultrafine Insoluble Iridium Particles From the Rat Lung, Including Transient Translocation into Secondary Organs. *Inhal Toxicol* 2004;16:453-459.

28. Oberdorster G, Oberdorster E, Oberdorster J. Nanotoxicology: an Emerging Discipline Evolving From Studies of Ultrafine Particles. *Environ Health Perspect* 2005;113:823-839.

29. Hoet PH, Bruske-Hohlfeld I, Salata OV. Nanoparticles - Known and Unknown Health Risks. *J Nanobiotechnology* 2004;2:12.

30. Ferin J, Oberdorster G, Penney DP. Pulmonary Retention of Ultrafine and Fine Particles in Rats. *Am J Respir Cell Mol Biol* 1992;6:535-542.

31. Hamilton RF, Buford MC, Wood MB, Arnone B, Morandi M, Holian A. Engineered Carbon Nanoparticles Alter Macrophage Immune Function and Initiate Airway Hyper-Responsiveness in the BALB/c Mouse Model. *Nanotoxicology* 2007;1:104-117.

32. Song Y, Li X, Du X. Exposure to Nanoparticles Is Related to Pleural Effusion, Pulmonary Fibrosis and Granuloma. *Eur Respir J* 2009;34:559-567.

33. SCENIHR. The Appropriateness of Existing Methodologies to Assess the Potential Risks Associated With Engineered and Adventitious Products of Nanotechnologies.; 2006.

34. Splettstoesser WD, Schuff-Werner P. Oxidative Stress in Phagocytes--"the Enemy Within". *Microsc Res Tech* 2002;57:441-455.

35. Nel A, Xia T, Madler L, Li N. Toxic Potential of Materials at the Nanolevel. *Science* 2006;311:622-627.

36. Stone V, Donaldson K. Nanotoxicology: Signs of Stress. *Nat Nanotechnol* 2006;1:23-24.

37. Xia T, Kovochich M, Brant J, Hotze M, Sempf J, Oberley T, Sioutas C, Yeh JI, Wiesner MR, Nel AE. Comparison of the Abilities of Ambient and Manufactured Nanoparticles to Induce Cellular Toxicity According to an Oxidative Stress Paradigm. *Nano Lett* 2006;6:1794-1807.

38. Xiao GG, Wang M, Li N, Loo JA, Nel AE. Use of Proteomics to Demonstrate a Hierarchical Oxidative Stress Response to Diesel Exhaust Particle Chemicals in a Macrophage Cell Line. *J Biol Chem* 2003;278:50781-50790.

39. Klotz LO. Oxidant-Induced Signaling: Effects of Peroxynitrite and Singlet Oxygen. *Biol Chem* 2002;383:443-456.

40. Xue C, Wu J, Lan F, Liu W, Yang X, Zeng F, Xu H. Nano Titanium Dioxide Induces the Generation of ROS and Potential Damage in HaCaT Cells Under UVA Irradiation. *J Nanosci Nanotechnol* 2010;10:8500-8507.

41. Li N, Sioutas C, Cho A, Schmitz D, Misra C, Sempf J, Wang M, Oberley T, Froines J, Nel A. Ultrafine Particulate Pollutants Induce Oxidative Stress and Mitochondrial Damage. *Environ Health Perspect* 2003;111:455-460.

42. Nel A, Xia T, Madler L, Li N. Toxic Potential of Materials at the Nanolevel. *Science* 2006;311:622-627.

43. Meng H, Xia T, George S, Nel AE. A Predictive Toxicological Paradigm for the Safety Assessment of Nanomaterials. *ACS Nano* 2009;3:1620-1627.

44. Johnson F, Giulivi C. Superoxide Dismutases and Their Impact Upon Human Health. *Mol Aspects Med* 2005;26:340-352.

45. del Rio LA, Sandalio LM, Palma JM, Bueno P, Corpas FJ. Metabolism of Oxygen Radicals in Peroxisomes and Cellular Implications. *Free Radic Biol Med* 1992;13:557-580.

46. Teixeira HD, Schumacher RI, Meneghini R. Lower Intracellular Hydrogen Peroxide Levels in Cells Overexpressing CuZn-Superoxide Dismutase. *Proc Natl Acad Sci U S A* 1998;95:7872-7875.

47. Lin SJ, Shyue SK, Shih MC, Chu TH, Chen YH, Ku HH, Chen JW, Tam KB, Chen YL. Superoxide Dismutase and Catalase Inhibit Oxidized Low-Density Lipoprotein-Induced Human Aortic Smooth Muscle Cell Proliferation: Role of Cell-Cycle Regulation, Mitogen-Activated Protein Kinases, and Transcription Factors. *Atherosclerosis* 2007;190:124-134.

48. Nel AE, Diaz-Sanchez D, Ng D, Hiura T, Saxon A. Enhancement of Allergic Inflammation by the Interaction Between Diesel Exhaust Particles and the Immune System. *J Allergy Clin Immunol* 1998;102:539-554.

49. Karin M, Gallagher E. From JNK to Pay Dirt: Jun Kinases, Their Biochemistry, Physiology and Clinical Importance. *IUBMB Life* 2005;57:283-295.

50. Li N, Xia T, Nel AE. The Role of Oxidative Stress in Ambient Particulate Matter-Induced Lung Diseases and Its Implications in the Toxicity of Engineered Nanoparticles. *Free Radic Biol Med* 2008;44:1689-1699.

51. Rahman I, MacNee W. Oxidative Stress and Regulation of Glutathione in Lung Inflammation. *Eur Respir J* 2000;16:534-554.

52. Albrecht C, Borm PJ, Unfried K. Signal Transduction Pathways Relevant for Neoplastic Effects of Fibrous and Non-Fibrous Particles. *Mutat Res* 2004;553:23-35.

53. Beck-Speier I, Dayal N, Karg E, Maier KL, Schulz H, Schumann G, Ziesenis A, Heyder J. Formation of Prostaglandin E2, Leukotriene B4 and 8-Isoprostane in Alveolar Macrophages by Ultrafine Particles of Elemental Carbon. *Adv Exp Med Biol* 2003;525:117-120.

54. Beck-Speier I, Dayal N, Karg E, Maier KL, Schumann G, Schulz H, Semmler M, Takenaka S, Stettmaier K, Bors W, et al. Oxidative Stress and Lipid Mediators Induced in Alveolar Macrophages by Ultrafine Particles. *Free Radic Biol Med* 2005;38:1080-1092.

55. Dick CA, Brown DM, Donaldson K, Stone V. The Role of Free Radicals in the Toxic and Inflammatory Effects of Four Different Ultrafine Particle Types. *Inhal Toxicol* 2003;15:39-52.

56. Sayes CM, Reed KL, Warheit DB. Assessing Toxicity of Fine and Nanoparticles: Comparing in Vitro Measurements to in Vivo Pulmonary Toxicity Profiles. *Toxicol Sci* 2007;97:163-180.

57. Brown DM, Donaldson K, Borm PJ, Schins RP, Dehnhardt M, Gilmour P, Jimenez LA, Stone V. Calcium and ROS-Mediated Activation of Transcription Factors and TNF-Alpha Cytokine Gene Expression in Macrophages Exposed to Ultrafine Particles. *Am J Physiol Lung Cell Mol Physiol* 2004;286:L344-L353.

58. Xia T, Kovochich M, Brant J, Hotze M, Sempf J, Oberley T, Sioutas C, Yeh JI, Wiesner MR, Nel AE. Comparison of the Abilities of Ambient and Manufactured Nanoparticles to Induce Cellular Toxicity According to an Oxidative Stress Paradigm. *Nano Lett* 2006;6:1794-1807.

59. Shukla A, Jung M, Stern M, Fukagawa NK, Taatjes DJ, Sawyer D, Van HB, Mossman BT. Asbestos Induces Mitochondrial DNA Damage and Dysfunction Linked to the Development of Apoptosis. *Am J Physiol Lung Cell Mol Physiol* 2003;285:L1018-L1025.

60. Wang L, Liu Y, Li W, Jiang X, Ji Y, Wu X, Xu L, Qiu Y, Zhao K, Wei T, et al. Selective Targeting of Gold Nanorods at the Mitochondria of Cancer Cells: Implications for Cancer Therapy. *Nano Lett* 2011;11:772-780.

61. George S, Xia T, Rallo R, Zhao Y, Ji Z, Lin S, Wang X, Zhang H, France B, Schoenfeld D, et al. Use of a High-Throughput Screening Approach Coupled With in Vivo Zebrafish Embryo Screening to Develop Hazard Ranking for Engineered Nanomaterials. *ACS Nano* 2011;5:1805-1817.

62. Limbach LK, Wick P, Manser P, Grass RN, Bruinink A, Stark WJ. Exposure of Engineered Nanoparticles to Human Lung Epithelial Cells: Influence of Chemical Composition and

Catalytic Activity on Oxidative Stress. *Environmental Science and Technology* 2007;41:4158-4163.

63. Park EJ, Yi J, Kim Y, Choi K, Park K. Silver Nanoparticles Induce Cytotoxicity by a Trojan-Horse Type Mechanism. *Toxicol In Vitro* 2010;24:872-878.

64. Lubick N. Nanosilver Toxicity: Ions, Nanoparticles--or Both? *Environmental science & technology* 2008;42:8617.

65. Ruenraroengsak P, Novak P, Berhanu D, Thorley AJ, Valsami-Jones E, Gorelik J, Korchev YE, Tetley TD. Respiratory Epithelial Cytotoxicity and Membrane Damage (Holes) Caused by Amine-Modified Nanoparticles. *Nanotoxicology* 2011.

66. Illum L. Nasal Delivery. The Use of Animal Models to Predict Performance in Man. *J Drug Target* 1996;3:427-442.

67. Harkema JR Comparative Structure, Function, and Toxicity of the Nasal Airways. Predicting Human Effects From Animal Studies. Washington, DC: Taylor and Francis; 1999. p. 55-83.

68. Werner U, Kissel T. Development of a Human Nasal Epithelial Cell Culture Model and Its Suitability for Transport and Metabolism Studies Under in Vitro Conditions. *Pharmaceutical Research* 1995;12:565-571.

69. Hartung T. Toxicology for the Twenty-First Century. *Nature* 2009;460:208-212.

70. Service RF. Nanotechnology. Can High-Speed Tests Sort Out Which Nanomaterials Are Safe? *Science* 2008;321:1036-1037.

71. Sayes CM, Reed KL, Warheit DB. Assessing Toxicity of Fine and Nanoparticles: Comparing in Vitro Measurements to in Vivo Pulmonary Toxicity Profiles. *Toxicol Sci* 2007;97:163-180.

72. Warheit DB, Sayes CM, Reed KL. Nanoscale and Fine Zinc Oxide Particles: Can in Vitro Assays Accurately Forecast Lung Hazards Following Inhalation Exposures? *Environ Sci Technol* 2009;43:7939-7945.

73. Faux S P. In Vitro Determinants of Particulate Toxicity: The Dose-Metric for Poorly Soluble Dusts. Research Report 154. Norwich, Great Britain: Institute of Occupational Medicine for the Health and Safety Executive; 2003.

74. Tran CL, Buchanan D, Cullen RT, Searl A, Jones AD, Donaldson K. Inhalation of Poorly Soluble Particles. II. Influence Of Particle Surface Area on Inflammation and Clearance. *Inhal Toxicol* 2000;12:1113-1126.

75. Oberdorster G, Ferin J, Lehnert BE. Correlation Between Particle Size, in Vivo Particle Persistence, and Lung Injury. *Environ Health Perspect* 1994;102 Suppl 5:173-179.

76. Dolmetsch RE, Xu K, Lewis RS. Calcium Oscillations Increase the Efficiency and Specificity of Gene Expression. *Nature* 1998;392:933-936.

77. Rivera GP, Oberdorster G, Elder A, Puntes V, Parak WJ. Correlating Physico-Chemical With Toxicological Properties of Nanoparticles: the Present and the Future. *ACS Nano* 2010;4:5527-5531.

78. Meng H, Xia T, George S, Nel AE. A Predictive Toxicological Paradigm for the Safety Assessment of Nanomaterials. *ACS Nano* 2009;3:1620-1627.

79. Donaldson K, Borm PJ, Castranova V, Gulumian M. The Limits of Testing Particle-Mediated Oxidative Stress in Vitro in Predicting Diverse Pathologies; Relevance for Testing of Nanoparticles. *Part Fibre Toxicol* 2009;6:13.

80. Warheit DB. Debunking Some Misconceptions About Nanotoxicology. *Nano Lett* 2010.

81. National Research Council. Toxicity Testing in the 21st Century: A Vision and a Strategy.: National Academy Press: Washington, DC; 2007.

82. Rothen-Rutishauser B, Muhlfeld C, Blank F, Musso C, Gehr P. Translocation of Particles and Inflammatory Responses After Exposure to Fine Particles and Nanoparticles in an Epithelial Airway Model. *Part Fibre Toxicol* 2007;4:9.

83. Warheit DB. How Meaningful Are the Results of Nanotoxicity Studies in the Absence of Adequate Material Characterization? *Toxicol Sci* 2008;101:183-185.

84. Gurr JR, Wang AS, Chen CH, Jan KY. Ultrafine Titanium Dioxide Particles in the Absence of Photoactivation Can Induce Oxidative Damage to Human Bronchial Epithelial Cells. *Toxicology* 2005;213:66-73.

85. Murdock RC, Braydich-Stolle L, Schrand AM, Schlager JJ, Hussain SM. Characterization of Nanomaterial Dispersion in Solution Prior to in Vitro Exposure Using Dynamic Light Scattering Technique. *Toxicol Sci* 2008;101:239-253.

86. Warheit DB. How Meaningful Are the Results of Nanotoxicity Studies in the Absence of Adequate Material Characterization? *Toxicol Sci* 2008;101:183-185.

87. Semmler-Behnke M, Kreyling WG, Lipka J, Fertsch S, Wenk A, Takenaka S, Schmid G, Brandau W. Biodistribution of 1.4- and 18-Nm Gold Particles in Rats. *Small* 2008;4:2108-2111.

88. Limbach LK, Li Y, Grass RN, Brunner TJ, Hintermann MA, Muller M, Gunther D, Stark WJ. Oxide Nanoparticle Uptake in Human Lung Fibroblasts: Effects of Particle Size, Agglomeration, and Diffusion at Low Concentrations. *Environ Sci Technol* 2005;39:9370-9376.

89. Hinderliter PM, Minard KR, Orr G, Chrisler WB, Thrall BD, Pounds JG, Teeguarden JG. ISDD: A Computational Model of Particle Sedimentation, Diffusion and Target Cell Dosimetry for in Vitro Toxicity Studies. *Part Fibre Toxicol* 2010;7:36.

90. Teeguarden JG, Hinderliter PM, Orr G, Thrall BD, Pounds JG. Particokinetics in Vitro: Dosimetry Considerations for in Vitro Nanoparticle Toxicity Assessments. *Toxicol Sci* 2007;95:300-312.

91. Hussain SM, Hess KL, Gearhart JM, Geiss KT, Schlager JJ. In Vitro Toxicity of Nanoparticles in BRL 3A Rat Liver Cells. *Toxicol In Vitro* 2005;19:975-983.

92. Ward JP. Oxygen Sensors in Context. *Biochim Biophys Acta* 2008;1777:1-14.

93. de GH, Littauer A. Hypoxia, Reactive Oxygen, and Cell Injury. *Free Radic Biol Med* 1989;6:541-551.

94. Halliwell B, Gutteridge JMC. Free Radicals in Biology and Medicine, 3 ed. Oxford Oxford University Press; 1999.

95. Halliwell B. The Antioxidant Paradox. *Lancet* 2000;355:1179-1180.

96. Free Radicals, Proteins and DNA: Oxidative Damage Versus Redox Regulation. *Biochem Soc Trans* 1996;24:1023-1027.

97. Aerts C, Wallaert B, Voisin C. In Vitro Effects of Hyperoxia on Alveolar Type II Pneumocytes: Inhibition of Glutathione Synthesis Increases Hyperoxic Cell Injury. *Exp Lung Res* 1992;18:845-861.

98. Campian JL, Qian M, Gao X, Eaton JW. Oxygen Tolerance and Coupling of Mitochondrial Electron Transport. *J Biol Chem* 2004;279:46580-46587.

99. Liochev SI, Fridovich I. Modulation of the Fumarases of Escherichia Coli in Response to Oxidative Stress. *Arch Biochem Biophys* 1993;301:379-384.

100. Morton RL, Ikle D, White CW. Loss of Lung Mitochondrial Aconitase Activity Due to Hyperoxia in Bronchopulmonary Dysplasia in Primates. *Am J Physiol* 1998;274:L127-L133.

101. Dai YT, Juang YJ, Wu Yy, Breysse PN, Hsu DJ. In Vivo Measurements of Inhalability of Ultralarge Aerosol Particles in Calm Air by Humans. *Journal of Aerosol Science* 2006;37:967-973.

102. Harrington JB, Jr., Metzger K. Ragweed Pollen Density. *American Journal of Botany* /7;50:532-539.

103. Gizurarson Sr. The Relevance of Nasal Physiology to the Design of Drug Absorption Studies. *Advanced Drug Delivery Reviews* 1993;11:329-347.

104. Jones N. The Nose and Paranasal Sinuses Physiology and Anatomy. *Adv Drug Deliv Rev* 2001;51:5-19.

105. Illum L. Nasal Drug Delivery--Possibilities, Problems and Solutions. *J Control Release* 2003;87:187-198.

106. Mygind N, Dahl R. Anatomy, Physiology and Function of the Nasal Cavities in Health and Disease. *Advanced Drug Delivery Reviews* 1998;29:3-12.

107. Ugwoke MI, Agu RU, Verbeke N, Kinget R. Nasal Mucoadhesive Drug Delivery: Background, Applications, Trends and Future Perspectives. *Adv Drug Deliv Rev* 2005;57:1640-1665.

108. Cheng YS, Yamada Y, Yeh HC, Swift DL. Diffusional Deposition of Ultrafine Aerosols in a Human Nasal Cast. *Journal of Aerosol Science* 1988;19:741-751.

109. Cheng KH, Cheng YS, Yeh HC, Guilmette RA, Simpson SQ, Yang YH, Swift DL. In Vivo Measurements of Nasal Airway Dimensions and Ultrafine Aerosol Deposition in the Human Nasal and Oral Airways. *Journal of Aerosol Science* 1996;27:785-801.

110. Wang SM, Inthavong K, Wen J, Tu JY, Xue CL. Comparison of Micron- and Nanoparticle Deposition Patterns in a Realistic Human Nasal Cavity. *Respiratory Physiology & Neurobiology* 2009;166:142-151.

111. Sunderman FW, Jr. Nasal Toxicity, Carcinogenicity, and Olfactory Uptake of Metals. *Ann Clin Lab Sci* 2001;31:3-24.

112. Badder EW. Chronic Cadmium Poisoning. *Industrial medicine & surgery* 1952;21:427-430.

113. Elder A, Gelein R, Silva V, Feikert T, Opanashuk L, Carter J, Potter R, Maynard A, Ito Y, Finkelstein J, et al. Translocation of Inhaled Ultrafine Manganese Oxide Particles to the Central Nervous System. *Environ Health Perspect* 2006;114:1172-1178.

114. Hernandez-Escobar SA, Avila-Casado MC, Soto-Abraham V, Lopez Escudero OL, Soto ME, Vega-Bravo ML, van der Goes TF, Reyes-Maldonado E. Cytological Damage of Nasal Epithelium Associated With Decreased Glutathione Peroxidase in Residents From a Heavily Polluted City. *Int Arch Occup Environ Health* 2009;82:603-612.

115. Merkle HP, Ditzinger G, Lang SR, Peter H, Schmidt MC. In Vitro Cell Models to Study Nasal Mucosal Permeability and Metabolism. *Adv Drug Deliv Rev* 1998;29:51-79.

116. Wadell C, Bj÷rk E, Camber O. Nasal Drug Delivery - Evaluation of an in Vitro Model Using Porcine Nasal Mucosa. *European Journal of Pharmaceutical Sciences* 1999;7:197-206.

117. Schmidt D, Hubsch U, Wurzer H, Heppt W, Aufderheide M. Development of an in Vitro Human Nasal Epithelial (HNE) Cell Model. *Toxicol Lett* 1996;88:75-79.

118. Kissel T, Werner U. Nasal Delivery of Peptides: an in Vitro Cell Culture Model for the Investigation of Transport and Metabolism in Human Nasal Epithelium. *J Control Release* 1998;53:195-203.

119. Ugwoke MI, Agu RU, Jorissen M, Augustijns P, Sciot R, Verbeke N, Kinget R. Nasal Toxicological Investigations of Carbopol 971P Formulation of Apomorphine: Effects on Ciliary Beat Frequency of Human Nasal Primary Cell Culture and in Vivo on Rabbit Nasal Mucosa. *Eur J Pharm Sci* 2000;9:387-396.

120. Agu RU, Jorissen M, Willems T, Augustijns P, Kinget R, Verbeke N. In-Vitro Nasal Drug Delivery Studies: Comparison of Derivatised, Fibrillar and Polymerised Collagen Matrix-Based Human Nasal Primary Culture Systems for Nasal Drug Delivery Studies. *J Pharm Pharmacol* 2001;53:1447-1456.

121. Lin H, Yoo JW, Roh HJ, Lee MK, Chung SJ, Shim CK, Kim DD. Transport of Anti-Allergic Drugs Across the Passage Cultured Human Nasal Epithelial Cell Monolayer. *Eur J Pharm Sci* 2005;26:203-210.

122. Auger F, Gendron MC, Chamot C, Marano F, Dazy AC. Responses of Well-Differentiated Nasal Epithelial Cells Exposed to Particles: Role of the Epithelium in Airway Inflammation. *Toxicol Appl Pharmacol* 2006;215:285-294.

123. McDougall CM, Blaylock MG, Douglas JG, Brooker RJ, Helms PJ, Walsh GM. Nasal Epithelial Cells As Surrogates for Bronchial Epithelial Cells in Airway Inflammation Studies. *Am J Respir Cell Mol Biol* 2008;39:560-568.

124. Mosler K, Coraux C, Fragaki K, Zahm JM, Bajolet O, Bessaci-Kabouya K, Puchelle E, Abely M, Mauran P. Feasibility of Nasal Epithelial Brushing for the Study of Airway Epithelial Functions in CF Infants. *J Cyst Fibros* 2008;7:44-53.

125. Harder SPDBKHSDRB. Comparison of Nasal Lavage Techniques for Analysis of Nasal Inflammation. *Am J Respir Crit Care Med* 1994;151:A565.

126. Lechner J. A Serum-Free Method for Culturing Normal Human Bronchial Epithelial Cells at Clonal Density. *Methods in Cell Science* 1985;9:43-48.

127. Cornaz AL, Buri P. Nasal Mucosa As an Absorption Barrier. *European Journal of Pharmaceutics and Biopharmaceutics* 1994;40:261-270.

128. Wu R, Yankaskas J, Cheng E, Knowles MR, Boucher R. Growth and Differentiation of Human Nasal Epithelial Cells in Culture. Serum-Free, Hormone-Supplemented Medium and Proteoglycan Synthesis. *Am Rev Respir Dis* 1985;132:311-320.

129. Pipkorn U, Karlsson G. Methods for Obtaining Specimens From the Nasal Mucosa for Morphological and Biochemical Analysis. *European Respiratory Journal* 1988;1:856-862.

130. Pipkorn U, Karlsson G, Enerback L. A Brush Method to Harvest Cells From the Nasal Mucosa for Microscopic and Biochemical Analysis. *Journal of Immunological Methods* 1988;112:37-42.

131. Boucher RC, Yankaskas JR, Cotton CU, Knowles MR, Stutts MJ. Cell Culture Approaches to the Investigation of Human Airway Ion Transport. *European Journal of Respiratory Diseases* 1987;71:59-67.

132. Mullol J, Raphael GD, Lundgren JD, Baraniuk JN, Merida M, Shelhamer JH, Kaliner MA. Comparison of Human Nasal Mucosal Secretion in Vivo and in Vitro. *Journal of Allergy and Clinical Immunology* 1992;89:584-592.

133. Farr B, Hackett SF, Winther B, Hendley JO. A Method for Measuring Polymorphonuclear Leukocyte Concentrations in Nasal Mucus. *Acta Oto-Laryngologica* 1984;98:15-18.

134. Bisgaard H, Krogsgaard OW, Mygind N. Measurement of Secretion in Nasal Lavage. *Clinical Science* 1987;73:217-222.

135. Bascom R, Wachs M, Naclerio RM, Pipkorn U, Galli SJ, Lichtenstein LM. Basophil Influx Occurs After Nasal Antigen Challenge: Effects of Topical Corticosteroid Pretreatment. *Journal of Allergy and Clinical Immunology* 1988;81:580-589.

136. Bascom R, Pipkorn U, Lichtenstein LM, Naclerio RM. The Influx of Inflammatory Cells into Nasal Washings During the Late Response to Antigen Challenge. Effect of Systemic Steroid Pretreatment. *American Review of Respiratory Disease* 1988;138:406-412.

137. Prat J, Xaubet A, Mullol J, Plaza V, Maso M, Lleonart R, Picado C. Immunocytologic Analysis of Nasal Cells Obtained by Nasal Lavage: a Comparative Study With a Standard Method of Cell Identification. *Allergy* 1993;48:587-591.

138. Prat J, Xaubet A, Mullol J, Plaza V, Picado C. Cell Content and Albumin Concentration in Nasal Lavage From Patients With Rhinitis. *Annals of Allergy* 1993;70:175-178.

139. Park WH. **NASAL BACTERIA IN HEALTH.** *The Journal of Laryngology* 1882:124-130.

140. Hoang VD, Uchenna AR, Mark J, Renaat K, Norbert V. Characterization of Human Nasal Primary Culture Systems to Investigate Peptide Metabolism. *Int J Pharm* 2002;238:247-256.

141. Gruenert DC, Finkbeiner WE, Widdicombe JH. Culture and Transformation of Human Airway Epithelial Cells. *American Journal of Physiology - Lung Cellular and Molecular Physiology* 1995;268.

142. Yankaskas JR, Cotton CU, Knowles MR. Culture of Human Nasal Epithelial Cells on Collagen Matrix Supports. A Comparison of Bioelectric Properties of Normal and Cystic Fibrosis Epithelia. *American Review of Respiratory Disease* 1985;132:1281-1287.

143. Steele VE, Arnold JT. Isolation and Long-Term Culture of Rat, Rabbit, and Human Nasal Turbinate Epithelial Cells. *In Vitro* 1985;21:681-687.

144. Boucher RC, Yankaskas JR, Cotton CU, Knowles MR, Stutts MJ. Cell Culture Approaches to the Investigation of Human Airway Ion Transport. *European Journal of Respiratory Diseases* 1987;71:59-67.

145. Mattinger C, Nyugen T, Schafer D, Hormann K. Evaluation of Serum-Free Culture Conditions for Primary Human Nasal Epithelial Cells. *Int J Hyg Environ Health* 2002;205:235-238.

146. Rechler MM, Nissley SP. The Nature and Regulation of the Receptors for Insulin-Like Growth Factors. *Annu Rev Physiol* 1985;47:425-442.

147. Froesch ER, Schmid C, Schwander J, Zapf J. Actions of Insulin-Like Growth Factors. *Annu Rev Physiol* 1985;47:443-467.

148. Kahn CR. The Molecular Mechanism of Insulin Action. *Annu Rev Med* 1985;36:429-451.

149. Straus DS. Growth-Stimulatory Actions of Insulin in Vitro and in Vivo. *Endocr Rev* 1984;5:356-369.

150. Green H. Cyclic AMP in Relation to Proliferation of the Epidermal Cell: a New View. *Cell* 1978;15:801-811.

151. COHEN S. Isolation of a Mouse Submaxillary Gland Protein Accelerating Incisor Eruption and Eyelid Opening in the New-Born Animal. *J Biol Chem* 1962;237:1555-1562.

152. Gospodarowicz D, Greenburg G, Bialecki H, Zetter BR. Factors Involved in the Modulation of Cell Proliferation in Vivo and in Vitro: the Role of Fibroblast and Epidermal Growth Factors in the Proliferative Response of Mammalian Cells. *In Vitro* 1978;14:85-118.

153. Krane JF, Murphy DP, Carter DM, Krueger JG. Synergistic Effects of Epidermal Growth Factor (EGF) and Insulin-Like Growth Factor I/Somatomedin C (IGF-I) on Keratinocyte Proliferation May Be Mediated by IGF-I Transmodulation of the EGF Receptor. *J Invest Dermatol* 1991;96:419-424.

154. Gutteridge JMC, Smith A. Antioxidant Protection by Haemopexin of Haem-Stimulated Lipid Peroxidation. *Biochemical Journal* 1988;256:861-865.

155. Lavrovsky Y, Song CS, Chatterjee B, Roy AK. Age-Dependent Increase of Heme Oxygenase-1 Gene Expression in the Liver Mediated by NF+¦B. *Mechanisms of Ageing and Development* 2000;114:49-60.

156. Balla J, Balla G, Jeney V, Kakuk G, Jacob HS, Vercellotti GM. Ferriporphyrins and Endothelium: A 2-Edged Sword - Promotion of Oxidation and Induction of Cytoprotectants. *Blood* 2000;95:3442-3450.

157. Wagener FADT, Feldman E, De Witte T, Abraham NG. Heme Induces the Expression of Adhesion Molecules ICAM-1, VCAM-1, and E Selectin in Vascular Endothelial Cells. *Experimental Biology and Medicine* 1997;216:456-463.

158. Letarte PB, Lieberman K, Nagatani K, Haworth RA, Odell GB, Duff TA. Hemin: Levels in Experimental Subarachnoid Hematoma and Effects on Dissociated Vascular Smooth-Muscle Cells. *Journal of Neurosurgery* 1993;79:252-255.

159. Vincent SH. Oxidative Effects of Heme and Porphyrins on Proteins and Lipids. *Seminars in Hematology* 1989;26:105-113.

160. Schmitt TH, Frezzatti J, Schreier S. Hemin-Induced Lipid Membrane Disorder and Increased Permeability: A Molecular Model for the Mechanism of Cell Lysis. *Archives of Biochemistry and Biophysics* 1993;307:96-103.

161. Oberdorster G. Safety Assessment for Nanotechnology and Nanomedicine: Concepts of Nanotoxicology. *J Intern Med* 2010;267:89-105.

162. Donaldson K, Stone V, Gilmour PS, Brown DM, MacNee W. Ultrafine Particles: Mechanisms of Lung Injury. *Philosophical Transactions of the Royal Society of London Series A: Mathematical, Physical and Engineering Sciences* 2000;358:2741-2749.

163. Duffin R, Tran CL, Clouter A, Brown DM, MacNee W, Stone V, Donaldson K. The Importance of Surface Area and Specific Reactivity in the Acute Pulmonary Inflammatory Response to Particles. *Annals of Occupational Hygiene* 2002;46:242-245.

164. Stoeger T, Reinhard C, Takenaka S, Schroeppel A, Karg E, Ritter B, Heyder J, Schulz H. Instillation of Six Different Ultrafine Carbon Particles Indicates a Surface Area Threshold Dose for Acute Lung Inflammation in Mice. *Environ Health Perspect* 2006;114:328-333.

165. Oberdorster G. Pulmonary Effects of Inhaled Ultrafine Particles. *Int Arch Occup Environ Health* 2001;74:1-8.

166. Oberdorster G, Gelein R, Johnston C, Mercer P, Finkestein JN Ambient Ultrafine Particles: Inducers of Acute Lung Injury? In: Dungworth DL, editor. Relationships Between Respiratory Disease and Exposure to Air Pollution Washington: ILSI Press; 1998. p. 216-229.

167. Wittmaack K. In Search of the Most Relevant Parameter for Quantifying Lung Inflammatory Response to Nanoparticle Exposure: Particle Number, Surface Area, or What? *Environ Health Perspect* 2007;115:187-194.

168. Limbach LK, Li Y, Grass RN, Brunner TJ, Hintermann MA, Muller M, Gunther D, Stark WJ. Oxide Nanoparticle Uptake in Human Lung Fibroblasts: Effects of Particle Size, Agglomeration, and Diffusion at Low Concentrations. *Environ Sci Technol* 2005;39:9370-9376.

169. Khanbeigi RA, Kumar A, Sadouki F, Lorenz C, Forbes B, Dailey LA, Collins H. The Delivered Dose: Applying Particokinetics to In Vitro Investigations of Nanoparticle Internalization by Macrophages. *J Control Release* 2012.

170. Ayuyan AG, Cohen FS. Raft Composition at Physiological Temperature and PH in the Absence of Detergents. *Biophys J* 2008;94:2654-2666.

171. Iversen TG, Skotland T, Sandvig K. Endocytosis and Intracellular Transport of Nanoparticles: Present Knowledge and Need for Future Studies. *Nano Today* 2011;6:176-185.

172. Smoluchowski M. Drei Vorträge Über Diffusion, Brownsche Molekularbewegung Und Koagulation Von Kolloidteilchen. *Physik Zeit* 1916;17:557-585.

173. Mason M, Weaver W. The Settling of Small Particles in a Fluid. *Phys Rev* 1924;23:412-426.

174. Clift MJ, Rothen-Rutishauser B, Brown DM, Duffin R, Donaldson K, Proudfoot L, Guy K, Stone V. The Impact of Different Nanoparticle Surface Chemistry and Size on Uptake and Toxicity in a Murine Macrophage Cell Line. *Toxicol Appl Pharmacol* 2008;232:418-427.

175. Cussler E.L. Diffusion-Mass Transfer in Fluid Systems, 2nd ed. Cambridge University Press; 1997.

176. Gu JJ, Yu FY, Li PE, Ng HS, Yap HP, Zhou QX, Cheng HT, Liu QA Real-Time Measurement of Cellular Refractive Index and Thickness Using Cell Culture Chip. Twelfth International Conference of Miniaturized Systems for Chemistry and Life Sciences, San Diego, CA; 2008.

177. Allouni ZE, Cimpan MR, Hol PJ, Skodvin T, Gjerdet NR. Agglomeration and Sedimentation of TiO2 Nanoparticles in Cell Culture Medium. *Colloids Surf B Biointerfaces* 2009;68:83-87.

178. Ji Z, Jin X, George S, Xia T, Meng H, Wang X, Suarez E, Zhang H, Hoek EM, Godwin H, et al. Dispersion and Stability Optimization of TiO2 Nanoparticles in Cell Culture Media. *Environ Sci Technol* 2010;44:7309-7314.

179. Cho EC, Zhang Q, Xia Y. The Effect of Sedimentation and Diffusion on Cellular Uptake of Gold Nanoparticles. *Nat Nanotechnol* 2011;6:385-391.

180. Cohen J, Deloid G, Pyrgiotakis G, Demokritou P. Interactions of Engineered Nanomaterials in Physiological Media and Implications for in Vitro Dosimetry. *Nanotoxicology* 2012.

181. Lison D, Thomassen LC, Rabolli V, Gonzalez L, Napierska D, Seo JW, Kirsch-Volders M, Hoet P, Kirschhock CE, Martens JA. Nominal and Effective Dosimetry of Silica Nanoparticles in Cytotoxicity Assays. *Toxicol Sci* 2008;104:155-162.

182. Maynard AD, Warheit DB, Philbert MA. The New Toxicology of Sophisticated Materials: Nanotoxicology and Beyond. *Toxicol Sci* 2011;120 Suppl 1:S109-S129.

183. Han X, Corson N, Wade-Mercer P, Gelein R, Jiang J, Sahu M, Biswas P, Finkelstein JN, Elder A, Oberdorster G. Assessing the Relevance of in Vitro Studies in Nanotoxicology by Examining Correlations Between in Vitro and in Vivo Data. *Toxicology* 2012;297:1-9.

184. Rushton EK, Jiang J, Leonard SS, Eberly S, Castranova V, Biswas P, Elder A, Han X, Gelein R, Finkelstein J, et al. Concept of Assessing Nanoparticle Hazards Considering Nanoparticle Dosemetric and Chemical/Biological Response Metrics. *J Toxicol Environ Health A* 2010;73:445-461.

185. Kaiser JP, Roesslein M, Buerki-Thurnherr T, Wick P. Carbon Nanotubes - Curse or Blessing. *Curr Med Chem* 2011;18:2115-2128.

186. Donaldson K, Stone V, Clouter A, Renwick L, MacNee W. Ultrafine Particles. *Occup Environ Med* 2001;58:211-6, 199.

187. Oberdorster G. Toxicology of Ultrafine Particles: in Vivo Studies. *Philosophical Transactions of the Royal Society of London Series A: Mathematical, Physical and Engineering Sciences* 2000;358:2719-2740.

188. Bermudez E, Mangum JB, Asgharian B, Wong BA, Reverdy EE, Janszen DB, Hext PM, Warheit DB, Everitt JI. Long-Term Pulmonary Responses of Three Laboratory Rodent Species to Subchronic Inhalation of Pigmentary Titanium Dioxide Particles. *Toxicol Sci* 2002;70:86-97.

189. Bermudez E, Mangum JB, Wong BA, Asgharian B, Hext PM, Warheit DB, Everitt JI. Pulmonary Responses of Mice, Rats, and Hamsters to Subchronic Inhalation of Ultrafine Titanium Dioxide Particles. *Toxicol Sci* 2004;77:347-357.

190. Warheit DB, Webb TR, Reed KL, Frerichs S, Sayes CM. Pulmonary Toxicity Study in Rats With Three Forms of Ultrafine-TiO2 Particles: Differential Responses Related to Surface Properties. *Toxicology* 2007;230:90-104.

191. Chithrani BD, Chan WC. Elucidating the Mechanism of Cellular Uptake and Removal of Protein-Coated Gold Nanoparticles of Different Sizes and Shapes. *Nano Lett* 2007;7:1542-1550.

192. Jin H, Heller DA, Sharma R, Strano MS. Size-Dependent Cellular Uptake and Expulsion of Single-Walled Carbon Nanotubes: Single Particle Tracking and a Generic Uptake Model for Nanoparticles. *ACS Nano* 2009;3:149-158.

193. Jamison JA, Krueger KM, Yavuz CT, Mayo JT, LeCrone D, Redden JJ, Colvin VL. Size-Dependent Sedimentation Properties of Nanocrystals. *ACS Nano* 2008;2:311-319.

194. Maiorano G, Sabella S, Sorce B, Brunetti V, Malvindi MA, Cingolani R, Pompa PP. Effects of Cell Culture Media on the Dynamic Formation of Protein-Nanoparticle Complexes and Influence on the Cellular Response. *ACS Nano* 2010;4:7481-7491.

195. Murdock RC, Braydich-Stolle L, Schrand AM, Schlager JJ, Hussain SM. Characterization of Nanomaterial Dispersion in Solution Prior to in Vitro Exposure Using Dynamic Light Scattering Technique. *Toxicol Sci* 2008;101:239-253.

196. Filipe V, Hawe A, Jiskoot W. Critical Evaluation of Nanoparticle Tracking Analysis (NTA) by NanoSight for the Measurement of Nanoparticles and Protein Aggregates. *Pharm Res* 2010;27:796-810.

197. Oberdorster G, Oberdorster E, Oberdorster J. Concepts of Nanoparticle Dose Metric and Response Metric. *Environ Health Perspect* 2007;115:A290.

198. Hohr D, Steinfartz Y, Schins RP, Knaapen AM, Martra G, Fubini B, Borm PJ. The Surface Area Rather Than the Surface Coating Determines the Acute Inflammatory Response After Instillation of Fine and Ultrafine TiO2 in the Rat. *Int J Hyg Environ Health* 2002;205:239-244.

199. Mura S, Hillaireau H, Nicolas J, Le DB, Gueutin C, Zanna S, Tsapis N, Fattal E. Influence of Surface Charge on the Potential Toxicity of PLGA Nanoparticles Towards Calu-3 Cells. *Int J Nanomedicine* 2011;6:2591-2605.

200. Sayes CM, Wahi R, Kurian PA, Liu Y, West JL, Ausman KD, Warheit DB, Colvin VL. Correlating Nanoscale Titania Structure With Toxicity: a Cytotoxicity and Inflammatory Response Study With Human Dermal Fibroblasts and Human Lung Epithelial Cells. *Toxicol Sci* 2006;92:174-185.

201. Ferin J, Oberd+¦rster G, Penney DP, Soderholm SC, Gelein R, Piper HC. Increased Pulmonary Toxicity of Ultrafine Particles? I. Particle Clearance, Translocation, Morphology. *Journal of Aerosol Science* 1990;21:381-384.

202. Oberdorster G, Ferin J, Finkelstein G, Wade P, Corson N. Increased Pulmonary Toxicity of Ultrafine Particles? II. Lung Lavage Studies. *Journal of Aerosol Science* 1990;21:384-387.

203. Mosmann T. Rapid Colorimetric Assay for Cellular Growth and Survival: Application to Proliferation and Cytotoxicity Assays. *J Immunol Methods* 1983;65:55-63.

204. Neuschwander-Tetri BA, Roll FJ. Glutathione Measurement by High-Performance Liquid Chromatography Separation and Fluorometric Detection of the Glutathione-Orthophthalaldehyde Adduct. *Anal Biochem* 1989;179:236-241.

205. Stone V, Johnston H, Schins RP. Development of in Vitro Systems for Nanotoxicology: Methodological Considerations. *Crit Rev Toxicol* 2009;39:613-626.

206. Worle-Knirsch JM, Pulskamp K, Krug HF. Oops They Did It Again! Carbon Nanotubes Hoax Scientists in Viability Assays. *Nano Lett* 2006;6:1261-1268.

207. MTT Assay.; 2012.

208. Han X, Gelein R, Corson N, Wade-Mercer P, Jiang J, Biswas P, Finkelstein JN, Elder A, Oberdorster G. Validation of an LDH Assay for Assessing Nanoparticle Toxicity. *Toxicology* 2011;287:99-104.

209. A Colorimetric Assay for Cellular Cytotoxicity - CytoScan LDH Assay Kit.; 2012.

210. Stone V, Shaw J, Brown DM, MacNee W, Faux SP, Donaldson K. The Role of Oxidative Stress in the Prolonged Inhibitory Effect of Ultrafine Carbon Black on Epithelial Cell Function. *Toxicol In Vitro* 1998;12:649-659.

211. Heurtault B, Gentine P, Thomann JS, Baehr C, Frisch B, Pons F. Design of a Liposomal Candidate Vaccine Against Pseudomonas Aeruginosa and Its Evaluation in Triggering Systemic and Lung Mucosal Immunity. *Pharm Res* 2009;26:276-285.

212. Hood E. Nanotechnology: Looking As We Leap. *Environ Health Perspect* 2004;112:A740-A749.

213. Dailey LA, Jekel N, Fink L, Gessler T, Schmehl T, Wittmar M, Kissel T, Seeger W. Investigation of the Proinflammatory Potential of Biodegradable Nanoparticle Drug Delivery Systems in the Lung. *Toxicol Appl Pharmacol* 2006;215:100-108.

214. Gul MO, Jones SA, Dailey LA, Nacer H, Ma Y, Sadouki F, Hider R, Araman A, Forbes B. A Poly(Vinyl Alcohol) Nanoparticle Platform for Kinetic Studies of Inhaled Particles. *Inhal Toxicol* 2009;21:631-640.

215. Nassimi M, Schleh C, Lauenstein HD, Hussein R, Hoymann HG, Koch W, Pohlmann G, Krug N, Sewald K, Rittinghausen S, et al. A Toxicological Evaluation of Inhaled Solid Lipid Nanoparticles Used As a Potential Drug Delivery System for the Lung. *Eur J Pharm Biopharm* 2010;75:107-116.

216. Harush-Frenkel O, Bivas-Benita M, Nassar T, Springer C, Sherman Y, Avital A, Altschuler Y, Borlak J, Benita S. A Safety and Tolerability Study of Differently-Charged Nanoparticles for Local Pulmonary Drug Delivery. *Toxicol Appl Pharmacol* 2010;246:83-90.

217. Jones MC, Kumar A, Spina D, Forbes B, Page C, Dailey LA. In Vivo Safety and Particokinetics of Inhaled Nanomedicines. *J Drug Deliv Sci Tech* 2011;21:339-346.

218. Ji Z, Jin X, George S, Xia T, Meng H, Wang X, Suarez E, Zhang H, Hoek EM, Godwin H, et al. Dispersion and Stability Optimization of TiO2 Nanoparticles in Cell Culture Media. *Environ Sci Technol* 2010;44:7309-7314.

219. Derjaguin BV, Landau LD. Theory of the Stability of Strongly Charged Lyophobic Sols and of the Adhesion of Strongly Charged Particles in Solutions of Electrolytes. *Acta Physicochim URSS* 1941:733-762.

220. An Introduction to Zeta Potential.; 2012.

221. Elif Melis Bicer, Benjamin Forbes, Graham Somers, Ian Mudway The Design and Evaluation of Simulated Human Lung Lining Fluids. London, UK: King's College London; 2011.

222. Braeckmans K, Buyens K, Bouquet W, Vervaet C, Joye P, De VF, Plawinski L, Doeuvre L, Angles-Cano E, Sanders NN, et al. Sizing Nanomatter in Biological Fluids by Fluorescence Single Particle Tracking. *Nano Lett* 2010;10:4435-4442.

223. Nel AE, Madler L, Velegol D, Xia T, Hoek EM, Somasundaran P, Klaessig F, Castranova V, Thompson M. Understanding Biophysicochemical Interactions at the Nano-Bio Interface. *Nat Mater* 2009;8:543-557.

224. J M Seiffert Assessing the Oxidative Potential of Manufactured Nanoparticles.: King's College London; 2008.

225. Karlsson HL, Cronholm P, Gustafsson J, Moller L. Copper Oxide Nanoparticles Are Highly Toxic: a Comparison Between Metal Oxide Nanoparticles and Carbon Nanotubes. *Chem Res Toxicol* 2008;21:1726-1732.

226. Halliwell B, Whiteman M. Measuring Reactive Species and Oxidative Damage in Vivo and in Cell Culture: How Should You Do It and What Do the Results Mean? *Br J Pharmacol* 2004;142:231-255.

227. Faux SP, Tran CL, Miller BG, Jones AD, Monteiller C, Donaldson K. In Vitro Determinants of Particulate Toxicity: The Dose-Metric for Poorly Soluble Dusts.: Institute of Occupational Medicine; 2003.

228. Smith PK, Krohn RI, Hermanson GT, Mallia AK, Gartner FH, Provenzano MD, Fujimoto EK, Goeke NM, Olson BJ, Klenk DC. Measurement of Protein Using Bicinchoninic Acid. *Anal Biochem* 1985;150:76-85.

229. Henderson LM, Chappell JB. Dihydrorhodamine 123: a Fluorescent Probe for Superoxide Generation? *Eur J Biochem* 1993;217:973-980.

230. Royall JA, Ischiropoulos H. Evaluation of 2',7'-Dichlorofluorescin and Dihydrorhodamine 123 As Fluorescent Probes for Intracellular H2O2 in Cultured Endothelial Cells. *Arch Biochem Biophys* 1993;302:348-355.

231. Warheit DB. Assessing Health Risks of Inhaled Nanomaterials: Development of Pulmonary Bioassay Hazard Studies. *Anal Bioanal Chem* 2010;398:607-612.

232. Lee KP, Trochimowicz HJ, Reinhardt CF. Pulmonary Response of Rats Exposed to Titanium Dioxide (TiO2) by Inhalation for Two Years. *Toxicol Appl Pharmacol* 1985;79:179-192.

233. Li JJ, Muralikrishnan S, Ng CT, Yung LY, Bay BH. Nanoparticle-Induced Pulmonary Toxicity. *Exp Biol Med (Maywood)* 2010;235:1025-1033.

234. Donaldson K, Borm PJ, Castranova V, Gulumian M. The Limits of Testing Particle-Mediated Oxidative Stress in Vitro in Predicting Diverse Pathologies; Relevance for Testing of Nanoparticles. *Part Fibre Toxicol* 2009;6:13.

235. Hussain S, Boland S, Baeza-Squiban A, Hamel R, Thomassen LC, Martens JA, Billon-Galland MA, Fleury-Feith J, Moisan F, Pairon JC, et al. Oxidative Stress and Proinflammatory Effects of Carbon Black and Titanium Dioxide Nanoparticles: Role of Particle Surface Area and Internalized Amount. *Toxicology* 2009;260:142-149.

236. Maynard AD, Warheit DB, Philbert MA. The New Toxicology of Sophisticated Materials: Nanotoxicology and Beyond. *Toxicol Sci* 2011;120 Suppl 1:S109-S129.

237. Unfried K, Albrecht C, Klotz LO, Von Mikecz A, Grether-Beck S, Schins RPF. Cellular Responses to Nanoparticles: Target Structures and Mechanisms. *Nanotoxicology* 2007;1:52-71.

238. Cook JA, Pass HI, Iype SN, Friedman N, DeGraff W, Russo A, Mitchell JB. Cellular Glutathione and Thiol Measurements From Surgically Resected Human Lung Tumor and Normal Lung Tissue. *Cancer Res* 1991;51:4287-4294.

239. Grzelak A, Rychlik B, Bartosz G. Light-Dependent Generation of Reactive Oxygen Species in Cell Culture Media. *Free Radic Biol Med* 2001;30:1418-1425.

240. Bannai S, Tateishi N. Role of Membrane Transport in Metabolism and Function of Glutathione in Mammals. *J Membr Biol* 1986;89:1-8.

241. Bannai S, Sato H, Ishii T, Sugita Y. Induction of Cystine Transport Activity in Human Fibroblasts by Oxygen. *J Biol Chem* 1989;264:18480-18484.

242. Bannai S. Induction of Cystine and Glutamate Transport Activity in Human Fibroblasts by Diethyl Maleate and Other Electrophilic Agents. *J Biol Chem* 1984;259:2435-2440.

243. Sato H, Kuriyama-Matsumura K, Siow RC, Ishii T, Bannai S, Mann GE. Induction of Cystine Transport Via System X-c and Maintenance of Intracellular Glutathione Levels in Pancreatic Acinar and Islet Cell Lines. *Biochim Biophys Acta* 1998;1414:85-94.

244. Horton ND, Biswal SS, Corrigan LL, Bratta J, Kehrer JP. Acrolein Causes Inhibitor KappaB-Independent Decreases in Nuclear Factor KappaB Activation in Human Lung Adenocarcinoma (A549) Cells. *J Biol Chem* 1999;274:9200-9206.

245. Yang X, Wu X, Choi YE, Kern JC, Kehrer JP. Effect of Acrolein and Glutathione Depleting Agents on Thioredoxin. *Toxicology* 2004;204:209-218.

246. Atkuri KR, Herzenberg LA, Niemi AK, Cowan T, Herzenberg LA. Importance of Culturing Primary Lymphocytes at Physiological Oxygen Levels. *Proc Natl Acad Sci U S A* 2007;104:4547-4552.

247. Kang YJ, Enger MD. Effect of Cellular Glutathione Depletion on Cadmium-Induced Cytotoxicity in Human Lung Carcinoma Cells. *Cell Biol Toxicol* 1987;3:347-360.

248. Stone V, Hankin S, Aitkin RJ, Achberger K, Baun A, Christensen F, Fernandes T. Engineered Nanomaterials: Review of Health and Environmental Safety (ENRHES).; 2010.

249. Hristozov D, Gottardo S, ritto A, arcomini A. Risk Assessment of Engineered Nanomaterials: a Review of Available Data and Approaches From a Regulatory Perspective. *Nanotoxicology* 2012.

250. Rogers NJ, Franklin NM, Apte SC, Batley GE. The Importance of Physical and Chemical Characterization in Nanoparticle Toxicity Studies. *Integr Environ Assess Manag* 2007;3:303-304.

251. Maiorano G, Sabella S, Sorce B, Brunetti V, Malvindi MA, Cingolani R, Pompa PP. Effects of Cell Culture Media on the Dynamic Formation of Protein-Nanoparticle Complexes and Influence on the Cellular Response. *ACS Nano* 2010;4:7481-7491.

252. Tedja R, Lim M, Amal R, Marquis C. Effects of Serum Adsorption on Cellular Uptake Profile and Consequent Impact of Titanium Dioxide Nanoparticles on Human Lung Cell Lines. *ACS Nano* 2012;6:4083-4093.

253. Yokohira M, Hashimoto N, Yamakawa K, Suzuki S, Saoo K, Kuno T, Imaida K. Lung Carcinogenic Bioassay of CuO and TiO(2) Nanoparticles With Intratracheal Instillation Using F344 Male Rats. *J Toxicol Pathol* 2009;22:71-78.

254. Roller M. Carcinogenicity of Inhaled Nanoparticles. *Inhal Toxicol* 2009;21 Suppl 1:144-157.

255. Bellmann B, Muhle H, Creutzenberg O, Mermelstein R. Irreversible Pulmonary Changes Induced in Rat Lung by Dust Overload. *Environ Health Perspect* 1992;97:189-191.

256. Wang J, Liu Y, Jiao F, Lao F, Li W, Gu Y, Li Y, Ge C, Zhou G, Li B, et al. Time-Dependent Translocation and Potential Impairment on Central Nervous System by Intranasally Instilled TiO(2) Nanoparticles. *Toxicology* 2008;254:82-90.

257. Long TC, Saleh N, Tilton RD, Lowry GV, Veronesi B. Titanium Dioxide (P25) Produces Reactive Oxygen Species in Immortalized Brain Microglia (BV2): Implications for Nanoparticle Neurotoxicity. *Environ Sci Technol* 2006;40:4346-4352.

258. OberdÃ¶rster G, Yu CP. The Carcinogenic Potential of Inhaled Diesel Exhaust: a Particle Effect? *Journal of Aerosol Science* 1990;21, Supplement 1:S397-S401.

259. BeruBe K, Aufderheide M, Breheny D, Clothier R, Combes R, Duffin R, Forbes B, Gaca M, Gray A, Hall I, et al. In Vitro Models of Inhalation Toxicity and Disease. The Report of a FRAME Workshop. *Altern Lab Anim* 2009;37:89-141.

260. Buerki-Thurnherr T, Xiao L, Diener L, Arslan O, Hirsch C, Maeder-Althaus X, Grieder K, Wampfler B, Mathur S, Wick P, et al. In Vitro Mechanistic Study Towards a Better Understanding of ZnO Nanoparticle Toxicity. *Nanotoxicology* 2012.

261. Sachs LA, Finkbeiner WE, Widdicombe JH. Effects of Media on Differentiation of Cultured Human Tracheal Epithelium. *In Vitro Cell Dev Biol Anim* 2003;39:56-62.

262. Lynch I, Cedervall T, Lundqvist M, Cabaleiro-Lago C, Linse S, Dawson KA. The Nanoparticle-Protein Complex As a Biological Entity; a Complex Fluids and Surface Science Challenge for the 21st Century. *Adv Colloid Interface Sci* 2007;134-135:167-174.

263. Lynch I, Salvati A, Dawson KA. Protein-Nanoparticle Interactions: What Does the Cell See? *Nat Nanotechnol* 2009;4:546-547.

264. Diabate S, Mulhopt S, Paur HR, Krug HF. The Response of a Co-Culture Lung Model to Fine and Ultrafine Particles of Incinerator Fly Ash at the Air-Liquid Interface. *Altern Lab Anim* 2008;36:285-298.

265. Mogel M, Kruger E, Krug HF, Seidel A. A New Coculture-System of Bronchial Epithelial and Endothelial Cells As a Model for Studying Ozone Effects on Airway Tissue. *Toxicol Lett* 1998;96-97:25-32.

266. Wottrich R, Diabate S, Krug HF. Biological Effects of Ultrafine Model Particles in Human Macrophages and Epithelial Cells in Mono- and Co-Culture. *Int J Hyg Environ Health* 2004;207:353-361.

267. Lehmann AD, Daum N, Bur M, Lehr CM, Gehr P, Rothen-Rutishauser BM. An in Vitro Triple Cell Co-Culture Model With Primary Cells Mimicking the Human Alveolar Epithelial Barrier. *Eur J Pharm Biopharm* 2011;77:398-406.

268. Rothen-Rutishauser BM, Kiama SG, Gehr P. A Three-Dimensional Cellular Model of the Human Respiratory Tract to Study the Interaction With Particles. *Am J Respir Cell Mol Biol* 2005;32:281-289.